

On Development of Some Soft Computing Based Multiuser Detection Techniques for SDMA–OFDM Wireless Communication System

Kala Praveen Bagadi



**Department of Electrical Engineering
National Institute of Technology Rourkela
Rourkela – 769008, India**

On Development of Some Soft Computing Based Multiuser Detection Techniques for SDMA–OFDM Wireless Communication System

A Thesis submitted in partial fulfillment of the requirements for the degree of

Doctor of Philosophy

in

Electrical Engineering

by

Kala Praveen Bagadi

(Roll: 509EE101)

Under the supervision of

Dr. Susmita Das

Associate Professor



Department of Electrical Engineering

National Institute of Technology

Rourkela–769008, India

2014



Department of Electrical Engineering
National Institute of Technology Rourkela
Rourkela – 769008, Odisha, India

CERTIFICATE

This is to certify that the thesis titled “**On Development of Some Soft Computing Based Multiuser Detection Techniques for SDMA–OFDM Wireless Communication System**”, submitted to the National Institute of Technology Rourkela by **Mr. Kala Praveen Bagadi**, Roll No. **509EE101** for the award of Doctor of Philosophy in Electrical Engineering, is a bona fide record of research work carried out by him under my supervision and guidance.

The candidate has fulfilled all the prescribed requirements.

The research is based on candidate's own work and has not submitted elsewhere for a degree/diploma to the best of my knowledge and belief.

In my opinion, the thesis is of standard required for the award of a Doctor of Philosophy degree in Electrical Engineering.

Date: March 2014

Dr. Susmita Das
Associate Professor
Department of Electrical Engineering
National Institute of Technology
Rourkela, India



Department of Electrical Engineering
National Institute of Technology Rourkela
Rourkela – 769008, Odisha, India

DECLARATION OF ORIGINALITY

I hereby declare that the work which is being presented in the thesis entitled “**On Development of Some Soft Computing Based Multiuser Detection Techniques for SDMA–OFDM Wireless Communication System**”, in partial fulfillment of the requirements for the award of the degree of Doctor of Philosophy, submitted to the Department of Electrical Engineering of National Institute of Technology, Rourkela, is an authentic record of my own work under the supervision of Prof. Susmita Das, Department of Electrical Engineering. I have not submitted the matter embodied in this thesis for the award of any other degree or diploma of the university or any other institute.

26/3/14

Date: March 2014

Kala Praveen Bagadi
Department of Electrical Engineering
National Institute of Technology
Rourkela, India

ACKNOWLEDGMENT

I would like to express my sincere gratitude to my supervisor Prof. Susmita Das, for her guidance, encouragement, and support throughout the course of this work. It was a precious learning experience for me and I am proud to be one of her students. In fact, she taught me the essence of the principles of research. I have gained not only extensive knowledge, but also creative research thoughts, while working with her.

I am very much thankful to Prof. A. K. Panda, Head, Department of Electrical Engineering, for his constant support. Also, I am indebted to him for providing me the official and laboratory facilities.

I am grateful to my Doctoral Scrutiny Members, Prof. S. K. Patra, Prof. P. K. Sahu and Prof. D. P. Mohapatra, for their valuable suggestions and comments during the course of work.

I am especially thankful to my friends, research scholars in the Signal Processing and Communication group Mr. Kiran Kumar Gurralla and Mr. Deepak Kumar Rout, who helped me a lot through their creative suggestions. I would also thank my beloved friend, Dr. Y. Suresh for his constant encouragement especially at times when life was tough. I am obliged to Prof. K. R. Subhashini for her comments and advice. I also express special thanks to all my friends, colleagues and seniors who have inspired me all along and made my stay at NIT Rourkela pleasant and enjoyable.

I am highly indebted to the authorities of NIT, Rourkela for providing me various infrastructures like library, computational facility and Internet access, which have been very useful.

Lastly, with deepest love, I am grateful to my beloved father Mr. B. Sree Rama Murthy, mother Mrs. B. Padmavathi and brother Mr. B. Pradeep Chandra who supported and encouraged me all the time, no matter what difficulties are encountered.

Kala Praveen Bagadi

Dedicated to My Family

ABSTRACT

Space Division Multiple Access (SDMA) based technique as a subclass of Multiple Input Multiple Output (MIMO) systems achieves high spectral efficiency through bandwidth reuse by multiple users. On the other hand, Orthogonal Frequency Division Multiplexing (OFDM) mitigates the impairments of the propagation channel. The combination of SDMA and OFDM has emerged as a most competitive technology for future wireless communication system. In the SDMA uplink, multiple users communicate simultaneously with a multiple antenna Base Station (BS) sharing the same frequency band by exploring their unique user specific-special spatial signature. Different Multiuser Detection (MUD) schemes have been proposed at the BS receiver to identify users correctly by mitigating the multiuser interference. However, most of the classical MUDs fail to separate the users signals in the over load scenario, where the number of users exceed the number of receiving antennas. On the other hand, due to exhaustive search mechanism, the optimal Maximum Likelihood (ML) detector is limited by high computational complexity, which increases exponentially with increasing number of simultaneous users. Hence, cost function minimization based Minimum Error Rate (MER) detectors are preferred, which basically minimize the probability of error by iteratively updating receiver's weights using adaptive algorithms such as Steepest Descent (SD), Conjugate Gradient (CG) etc.

The first part of research proposes Optimization Techniques (OTs) aided MER detectors to overcome the shortfalls of the CG based MER detectors. Popular metaheuristic search algorithms like Adaptive Genetic Algorithm (AGA), Adaptive Differential Evolution Algorithm (ADEA) and Invasive Weed Optimization (IWO), which rely on an intelligent search of a large but finite solution space using statistical methods, have been applied for finding the optimal weight vectors for MER MUD. Further, it is observed in an overload SDMA-OFDM system that the channel output phasor constellation often becomes linearly non-separable. With increasing the number of users, the receiver weight optimization task turns out to be more difficult due to the exponentially increased number of dimensions of the weight matrix. As a result, MUD becomes a challenging multidimensional optimization problem. Therefore, signal classification requires a nonlinear solution. Considering this, the second part of research work suggests Artificial Neural Network (ANN) based MUDs on the standard Multilayer Perceptron (MLP) and Radial Basis Function (RBF) frameworks for

SDMA–OFDM system as the ANNs are well known non-linear classifiers. It is observed that, ANN detectors can provide additional complexity gain as they approximate the channel state information in training phase before detecting the signals in testing phase. Moreover, multiuser detection process becomes more challenging when the users are transmitting high order modulated signals because the signal processing has to be accomplished in a complex multidimensional space. Hence, the research work exploits new complex valued NN based MUDs to overcome the limitations of real-valued NN models. It is observed that the complex valued RBF MUD provides near optimal performance at a significantly lower complexity especially under high user loads. In view of obtaining an improved mapping of input and outputs, new activation functions have been incorporated. Suitable modifications of conventional Back Propagation (BP) and Gradient Descent (GD) training algorithms have been done for complex NN training. Extensive simulation studies are made in MATLAB environment to prove the efficacy of the proposed MUD schemes for SDMA–OFDM system considering standard wireless channel models. Further, detection of images over wireless link, when several users are transmitting simultaneously sharing the same spectral resource is investigated. Significant performance improvement over classical Minimum Mean Square Error (MMSE), complexity gain over ML and sustenance in the overload scenario are the significant achievements of the proposed soft computing based MUDs.

Key words: *Space Division Multiple Access, Orthogonal Frequency Division Multiplexing, Multiuser Detection, Bit Error Rate, Minimum Mean Square Error, Maximum Likelihood, Minimum Bit Error Rate, Minimum Symbol Error Rate, Conjugate Gradient, Optimization techniques, Adaptive Genetic Algorithm, Adaptive Differential Evolution Algorithm, Invasive Weed Optimization, Neural Networks, Multilayer Perceptron, Radial Basis Function.*

CONTENTS

Certificate	iii
Declaration of Originality	iv
Acknowledgment	v
Abstract	vii
Contents	ix
List of Figures	xi
List of Tables	xv
Abbreviations	xvii
Notations	xix
1. Introduction	1
1.1 Literature review	3
1.2 Motivation of the thesis	7
1.3 Contribution of the thesis	9
1.4 Thesis layout	12
2. Introduction to SDMA–OFDM System and Comparison of Classical MUD Schemes	14
2.1 Multiple Input Multiple Output (MIMO) system	15
2.1.1 Space Division Multiplexing (SDM)	15
2.1.2 Space Division Multiple Access (SDMA)	16
2.2 Orthogonal Frequency Division Multiplexing (OFDM) technique	17
2.2.1 Need for multicarrier transmission	17
2.2.2 Importance of being orthogonal	18
2.2.3 Cyclic prefix	19
2.2.4 OFDM modulation and demodulation	19
2.3 Overview of SDMA–OFDM system model	21
2.4 MIMO channel characteristics	24
2.4.1 Design of MIMO channels	24
2.4.2 MIMO channel capacity	25
2.4.3 Empirical MIMO channel models	27
2.5 MIMO–OFDM channel estimation, a brief overview	28
2.5.1 Least Square (LS) estimator	29
2.5.2 Minimum Mean Square Error (MMSE) estimator	30
2.6 Classical Multiuser Detection (MUD) schemes	31
2.6.1 Zero Forcing (ZF) MUD	32
2.6.2 Minimum Mean Square Error (MMSE) MUD	32
2.6.3 Maximum Likelihood (ML) MUD	33
2.6.4 Ordered Successive Interference Cancellation (OSIC) MUD	34
2.6.5 QR Decomposition–M (QRD–M) MUD	35

2.6.6	Minimum Bit Error Rate (MBER) MUD	37
2.6.7	Minimum Symbol Error Rate (MSER) MUD	39
2.7	Simulation study and performance analysis	41
2.8	Summary	46
3.	Proposed Metaheuristic Optimization Techniques Aided Minimum Error Rate MUD	
	Schemes	47
3.1	Adaptive Genetic Algorithm (AGA) aided MER MUD	49
3.2	Adaptive Differential Evolution Algorithm (ADEA) aided MER MUD	53
3.3	Invasive Weed Optimization (IWO) aided MER MUD	57
3.4	Simulation study and performance analysis	60
3.4.1	Results and discussion for OTs aided MBER MUD	62
3.4.1.1	Selection of control parameters	62
3.4.1.2	Performance analysis	70
3.4.1.3	Convergence speed	75
3.4.1.4	Complexity	76
3.4.2	Results and discussion for OTs aided MSER MUD	78
3.4.2.1	Performance analysis	78
3.4.2.2	Convergence speed	83
3.4.2.3	Complexity	84
3.5	Summary	86
4.	Proposed Neural Network Based Adaptive MUD Schemes	88
4.1	Neural network as multiuser detector for the SDMA–OFDM system	90
4.2	Multilayer Perceptron (MLP) based MUD scheme	92
4.2.1	Network training procedure for MLP MUD	94
4.3	Radial Basis Function (RBF) based MUD scheme	95
4.3.1	Network training procedure for RBF MUD	96
4.4	Necessity of complex valued neural networks	97
4.5	Complex MLP (CMLP) based MUD scheme	98
4.5.1	Development of complex BP algorithm for CMLP network training	100
4.5.2	Network training procedure for CMLP MUD	103
4.6	Complex RBF (CRBF) based MUD scheme	104
4.6.1	Development of complex GD algorithm for CRBF network training	105
4.6.2	Network training procedure for CRBF MUD	108
4.7	Simulation study and performance analysis	109
4.7.1	Results and discussion for real valued NN based MUDs.....	109
4.7.1.1	Performance analysis	110
4.7.1.2	Convergence speed	114
4.7.1.3	Complexity	115
4.7.2	Results and discussion for complex valued NN based MUDs	116
4.7.2.1	Performance analysis	117

4.7.2.2	Convergence speed	120
4.7.2.3	Complexity	121
4.8	Summary	122
5.	Progressive Image Transmission and Detection Using Proposed MUD Schemes	124
5.1	SPIHT image coding for progressive image transmission	126
5.1.1	Coefficient ordering for progressive image transmission	126
5.1.2	Features of set partitioning	128
5.1.3	Set partitioning rules	129
5.1.4	SPIHT encoding and decoding	130
5.2	Proposed SDMA–OFDM system model for image transmission	131
5.3	Statistical parameters for image quality analysis	133
5.4	Simulation study and performance analysis	135
5.4.1	Results and discussion for gray scale image transmission	135
5.4.2	Results and discussion for color image transmission	144
5.5	Summary	152
6.	Conclusions and Future Scope of Research	154
6.1	Summary of the thesis	155
6.2	Limitations and future scope of research.....	158
	Dissemination of Work.....	159
	References	161
	Appendix	171

LIST OF FIGURES

Figure 2.1	SDM system model	16
Figure 2.2	SDMA uplink system model	17
Figure 2.3	Comparison of OFDM band spectrum with FDM	18
Figure 2.4	Consecutive OFDM subcarriers in time domain	18
Figure 2.5	Spectrum of an OFDM signal	19
Figure 2.6	Representation of cyclic prefix in the OFDM symbols	19
Figure 2.7	Schematic diagram of: (a) OFDM modulator (b) OFDM demodulator	20
Figure 2.8	Block diagram of the SDMA–OFDM system with L users and P receiving antennas	22
Figure 2.9	SDMA–OFDM frame structure	23
Figure 2.10	Capacity versus E_b/N_o for different antenna configurations	26
Figure 2.11	Frequency response of channel link between User-1 and Receiving Antenna-1 under various channel conditions (a) MIMO Rayleigh fading (b) SUI (c) SWATM	28
Figure 2.12	Frequency response of the SUI channel link between User-1 and Receiving Antenna-1 using: (a) LS estimator (b) MMSE estimator	31
Figure 2.13	Classification of MUD schemes	32
Figure 2.14	Tree structure of QRD-M ($M = 4$) algorithm for 4×4 SDMA–OFDM system with 4-QAM	37
Figure 2.15	Average BER performance of all users using various classical MUDs under different channel conditions (a) MIMO fading (b) SUI (c) SWATM	42
Figure 2.16	Average BER performance of all users using QRD–M detector communicating over the SWATM channel for different number of branches (M)	43
Figure 2.17	Comparison of the average BER performance of all users using MBER MUD with respect to MMSE and ML detectors under MIMO fading channel model	44
Figure 2.18	Average BER performance of all users using the MMSE and CG MBER MUDs in the SDMA–OFDM system equipped with $L = 4$ while varying the numbers of users under the SUI channel condition (a) MMSE MUD (b) CG MBER MUD	45
Figure 3.1	Flowchart of the working principle for an adaptive genetic algorithm	49
Figure 3.2	Flowchart of working principle for an adaptive differential evolution algorithm	54
Figure 3.3	Flowchart of working principle for an invasive weed optimization algorithm	58
Figure 3.4	Seed reproduction in a weed colony	59
Figure 3.5	Simulation model of the SDMA–OFDM system for multiuser detection using proposed OTs aided MER schemes	61
Figure 3.6	Performance comparison between GA and AGA aided MBERMUDs (a) BER performance (b) Convergence speed	62
Figure 3.7	BER performance comparison of AGA MBER MUD while varying N_g and G_g at 15 dB E_b/N_o	63
Figure 3.8	BER performance comparison of the ADEA MBER MUD while varying C_p and F at 15 dB E_b/N_o	64

Figure 3.9	Convergence speed comparison of ADEA MBER MUD while varying C_p and F at 15 dB E_b/N_o	64
Figure 3.10	Performance comparison between DEA and ADEA MBERMUDs (a) BER performance (b) Convergence speed	65
Figure 3.11	BER performance comparison of ADEA MBER MUD while varying N_d and G_d at 15 dB E_b/N_o	66
Figure 3.12	Convergence speed comparisons of IWO MBER MUD for different combinations of initial and final standard deviations	68
Figure 3.13	BER performance comparison of IWO MBER MUD while varying N_l and I_{max} at 15 dB E_b/N_o	68
Figure 3.14	Rate of change in (a) Standard deviation (b) Cost value, for different valued of nonlinear modulation index 'r' while varying number of iterations	69
Figure 3.15	Average BER performance of all users using MMSE, OTs aided MBER and ML MUDs under different channel conditions (a) MIMO Rayleigh fading (b) SUI (c) SWATM	71
Figure 3.16	Average BER performance of all users using MMSE, OTs aided MBER and ML MUDs under load conditions (a) Under Load ($L=3, P=4$) (b) Full Load ($L=P=4$) (c) Over Load ($L=6, P=4$)	72
Figure 3.17	Estimated symbol distribution of User-1 from noise less received symbols using various MUD schemes for the case of $L=6$ and $P=4$ when User-1 is always transmitting +1 (a) MMSE (b) AGA MBER (c) ADEA MBER (d) IWO MBER	73
Figure 3.18	Figure 3.18: Estimated symbol distribution of User-1 using various MUD schemes for the case of $L=6$ and $P=4$ (a, b) MMSE at $E_b/N_o = 5, 20$ dB (c, d) AGA MBER at $E_b/N_o = 5, 20$ dB (e, f) ADEA MBER at $E_b/N_o = 5, 20$ dB (g, h) IWO MBER at $E_b/N_o = 5, 20$ dB	74
Figure 3.19	Convergence speed comparison of proposed OTs aided MBER MUDs at 15 dB E_b/N_o	75
Figure 3.20	Average BER performance of all users using MMSE, OTs aided MSER and ML MUDs under load conditions (a) Under Load ($L=3, P=4$) (b) Full Load ($L=P=4$) (c) Over Load ($L=6, P=4$)	79
Figure 3.21	Average BER performance of all users using MMSE, OTs aided MSER and ML MUDs in the SDMA-OFDM system transmitting 16-QAM signals	80
Figure 3.22	Estimated symbol distribution of User-1 from noise less received symbols using MMSE and OTs aided MSER MUDs for the case of $L=6$ and $P=4$ when User-1 is always transmitting $1+j$ (a) MMSE (b) AGA MSER (c) ADEA MSER (d) IWO MSER	81
Figure 3.23	Figure 3.23: Estimated symbol distribution of User-1 using MMSE and OTs aided MSER MUDs for the case of $L=6$ and $P=4$ (a, b) MMSE at $E_b/N_o = 5, 20$ dB (c, d) AGA MSER at $E_b/N_o = 5, 20$ dB (e, f) ADEA MSER at $E_b/N_o = 5, 20$ dB (g, h) IWO MSER at $E_b/N_o = 5, 20$ dB	82
Figure 3.24	Estimated symbol distribution of User-1 using MMSE and OTs aided MSER MUDs for the case of $L=P=4$ in the SDMA-OFDM system transmitting 16-QAM signals at 20 dB E_b/N_o (a) MMSE (b) AGA MSER (c) ADEA MSER (d) IWO MSER	83
Figure 3.25	Convergence speed comparison of proposed OTs aided MSER MUDs at 15 dB E_b/N_o	84
Figure 4.1	Classification mechanisms in two dimension space: (a) MLP network (b) RBF network	90

Figure 4.2	NN based multiuser detector for the SDMA–OFDM system with L number of users and P number of receiving antennas	92
Figure 4.3	Schematic diagram of proposed MLP based MUD scheme for the SDMA–OFDM system	94
Figure 4.4	Schematic diagram of proposed RBF based MUD scheme for the SDMA–OFDM system	95
Figure 4.5	Magnitude plot of activation functions used in different NN models (a) Real valued MLP (b) Complex valued MLP (c) Real valued RBF (d) Complex valued RBF	98
Figure 4.6	Schematic diagram of proposed CMLP based MUD scheme for the SDMA–OFDM system	99
Figure 4.7	Training model of CMLP network	100
Figure 4.8	Schematic diagram of proposed CRBF based MUD scheme for the SDMA–OFDM system	104
Figure 4.9	Average BER performance of NN model based MUDs for the case of $L = P = 4$ with a variable number of hidden neurons (a) MLP detector (b) RBF detector	110
Figure 4.10	Average BER performance of all users using MMSE, IWO aided MBER, NN model based and ML MUDs under different channel conditions (a) MIMO Rayleigh fading (b) SUI (c) SWATM	111
Figure 4.11	Average BER performance of all users using MMSE, IWO MBER and NNs MUD schemes in the SDMA–OFDM system with $P = 4$ and increasing L at 15 dB E_b/N_o	112
Figure 4.12	Estimated symbol distribution of User-1 from noise less received symbols using various MUD schemes for the case of $L = 6$ and $P = 4$ when User-1 is always transmitting +1 (a) IWO MBER (b) MLP (c) RBF	113
Figure 4.13	Estimated symbol distribution of User-1 using various MUD schemes for the case of $L = 6$ and $P = 4$ at 15 dB E_b/N_o (a) IWO MBER (b) MLP (c) RBF	114
Figure 4.14	Convergence speed comparison of NN based MUDs at 15 dB E_b/N_o	114
Figure 4.15	Average BER performance of all users using various MUDs, when the SDMA–OFDM with $L = P = 4$ is transmitting 4-QAM signals	117
Figure 4.16	Average BER performance of all users using various MUDs, when the SDMA–OFDM with $L = P = 4$ is transmitting 16-QAM signals	118
Figure 4.17	Average BER performance of all users using MMSE, IWO MSER and complex NN MUD schemes in the SDMA–OFDM system with $P = 4$ and increasing L at 15 dB E_b/N_o	118
Figure 4.18	Estimated symbol distribution of User-1 from noise less received symbols using various MUD schemes for the case of $L = 6$ and $P = 4$ when User-1 is always transmitting $1+j$ (a) IWO MSER (b) CMLP (c) CRBF	119
Figure 4.19	Estimated symbol distribution of User-1 using various MUDs for the case of $L = 6$ and $P = 4$ when User-1 is transmitting 4-QAM signals at 15 dB E_b/N_o (a) IWO MSER (b) CMLP (c) CRBF	119
Figure 4.20	Estimated symbol distribution of User-1 using various MUDs for the case of $L = 4$ and $P = 4$ when User-1 is transmitting 16-QAM signals at 15 dB E_b/N_o (a) IWO MSER (b) CMLP (c) CRBF	120

Figure 4.21	Convergence speed comparison of real and complex valued NN based MUDs at 15 dB E_b/N_o	120
Figure 5.1	Example of descendant trees in a three-level wavelet decomposition	129
Figure 5.2	Block diagram of the SDMA-OFDM system used for image transmission with $L = P = 4$	132
Figure 5.3	(a) RGB Image encoder (b) RGB Image decoder	133
Figure 5.4	256×256 pixel size gray scale test images transmitted through four different users in the SDMA-OFDM system (a) Kid (b) Lena (c) Cameraman (d) Peppers	135
Figure 5.5	Reconstructed Kid image using MMSE MUD at different values of E_b/N_o (a) $E_b/N_o = 10$ dB (b) $E_b/N_o = 15$ dB (c) $E_b/N_o = 20$ dB	136
Figure 5.6	PSNR of Kid image while varying bits per pixels at 15 dB E_b/N_o	137
Figure 5.7	Reconstructed Kid image using MMSE MUD at different compression rates (a) bpp = 0.5 (b) bpp = 2 (c) bpp = 8	137
Figure 5.8	Reconstructed Kid image using various MUDs (a) MMSE (b) AGA MBER (c) ADEA MBER (d) IWO MBER (e) MLP (f) RBF (g) ML	138
Figure 5.9	Reconstructed Lena image using various MUDs (a) MMSE (b) AGA MBER (c) ADEA MBER (d) IWO MBER (e) MLP (f) RBF (g) ML	139
Figure 5.10	Reconstructed Cameraman image using various MUDs (a) MMSE (b) AGA MBER (c) ADEA MBER (d) IWO MBER (e) MLP (f) RBF (g) ML	140
Figure 5.11	Reconstructed Peppers image using various MUDs (a) MMSE (b) AGA MBER (c) ADEA MBER (d) IWO MBER (e) MLP (f) RBF (g) ML	141
Figure 5.12	PSNR of reconstructed images using various MUDs for all four different users (a) Kid (b) Lena (c) Cameraman (d) Peppers	144
Figure 5.13	256×256 pixel size RGB test images transmitted through four different users in the SDMA-OFDM system (a) RGB Kid (b) RGB Lena (c) RGB Cameraman (d) RGB Peppers	145
Figure 5.14	Reconstructed RGB Kid image using various MUDs (a) MMSE (b) AGA MSER (c) ADEA MSER (d) IWO MSER (e) CMLP (f) CRBF (g) ML	146
Figure 5.15	Reconstructed RGB Lena image using various MUDs (a) MMSE (b) AGA MSER (c) ADEA MSER (d) IWO MSER (e) CMLP (f) CRBF (g) ML	147
Figure 5.16	The reconstructed RGB Cameraman image using various MUDs (a) MMSE (b) AGA MSER (c) ADEA MSER (d) IWO MSER (e) CMLP (f) CRBF (g) ML	148
Figure 5.17	Reconstructed RGB Peppers image using various MUDs (a) MMSE (b) AGA MSER (c) ADEA MSER (d) IWO MSER (e) CMLP (f) CRBF (g) ML	149
Figure 5.18	PSNR of reconstructed images using various MUDs for all four different users (a) RGB Kid (b) RGB Lena (c) RGB Cameraman (d) RGB Peppers	152

LIST OF TABLES

Table 2.1	Basic simulation parameters of the SDMA–OFDM with classical MUDs	41
Table 2.2	Complexity comparison between ML and QRD– M detectors	44
Table 3.1	Simulation parameters of AGA MBER MUD	63
Table 3.2	Simulation parameters of ADEA MBER MUD	66
Table 3.3	Effect of S_{max} on complexity and performance of the IWO MBER MUD at 15 dB E_b/N_o	67
Table 3.4	Simulation parameters of IWO MBER MUD	69
Table 3.5	Complexity comparison of OTs aided MBER and ML MUD schemes with respect to CF evaluations when $L = 6$ and $P = 4$	76
Table 3.6	Complexity comparison of MMSE, OTs aided MBER and ML MUD schemes with respect to number of computational operations when $L = 6$ and $P = 4$	77
Table 3.7	Complexity comparison of OTs aided MBER and ML MUD schemes with respect to CF evaluations while varying L keeping P fixed at four	77
Table 3.8	Performance and complexity comparisons of OTs aided MBER MUDs at E_b/N_o values 15 dB	78
Table 3.9	Complexity comparison of OTs aided MSER and ML MUD schemes with respect to CF evaluations when $L = 6$ and $P = 4$	85
Table 3.10	Complexity comparison of MMSE, OTs aided MSER and ML MUD schemes with respect to number of computational operations when $L = 6$ and $P = 4$	85
Table 3.11	Complexity comparison of OTs aided MSER and ML MUD schemes with respect to CF evaluations while varying L keeping P fixed at four	86
Table 3.12	Performance and complexity comparisons of OTs aided MSER MUDs at E_b/N_o values 15 dB	86
Table 4.1	Simulation parameters of NN based MUD schemes	110
Table 4.2	Complexity comparison of MMSE, IWO MBER, NN and ML MUD schemes with respect to number of computational operations when $L = 6$ and $P = 4$	115
Table 4.3	Complexity comparison of IWO MBER, NN and ML MUD schemes with respect to CF evaluations when $L = 6$ and $P = 4$	116
Table 4.4	Simulation parameters of complex valued NN based MUD schemes	116
Table 4.5	Complexity comparison of MMSE, IWO MSER, complex valued NN and ML MUD schemes with respect to number of computational operations when $L = 6$ and $P = 4$	121
Table 4.6	Complexity comparison of IWO MSER, complex valued NN and ML MUD schemes with respect to CF evaluations when $L = 6$ and $P = 4$	122
Table 5.1	Performance comparison of MMSE, OTs aided MBER, NN and ML MUD schemes based on statistical parameters while reconstructing Kid image	142
Table 5.2	Performance comparison of MMSE, OTs aided MBER, NN and ML MUD schemes based on statistical parameters while reconstructing Lena image	142
Table 5.3	Performance comparison of MMSE, OTs aided MBER, NN and ML MUD schemes based on statistical parameters while reconstructing Cameraman image	143

Table 5.4	Performance comparison of MMSE, OTs aided MBER, NN and ML MUD schemes based on statistical parameters while reconstructing Peppers image	143
Table 5.5	Performance comparison of MMSE, OTs aided MSER, complex valued NN and ML MUD schemes based on statistical parameters while reconstructing RGB Kid image	150
Table 5.6	Performance comparison of MMSE, OTs aided MSER, complex valued NN and ML MUD schemes based on statistical parameters while reconstructing RGB Lena image	150
Table 5.7	Performance comparison of MMSE, OTs aided MSER, complex valued NN and ML MUD schemes based on statistical parameters while reconstructing RGB Cameraman image	151
Table 5.8	Performance comparison of MMSE, OTs aided MSER, complex valued NN and ML MUD schemes based on statistical parameters while reconstructing RGB Peppers image	151
Table 6.1	Performance comparisons of OTs aided MER and NN MUDs in terms of E_b/N_o gain (in dBs)	157
Table 6.2	Complexity comparisons of OTs aided MER and NN MUDs in terms of computational operations	157

ABBREVIATIONS

ACTS	Advanced Communication Technologies and Services
ADEA	Adaptive Differential Evolution Algorithm
AGA	Adaptive Genetic Algorithm
ANN	Artificial Neural Network
AWGN	Additive White Gaussian Noise
BER	Bit Error Rate
BICM	Bit Interleaved Coded Modulation
BLAST	Bell Labs Layered Space Time
BP	Back Propagation
bpp	Bits Per Pixel
BPSK	Binary Phase Shift Keying
BS	Base Station
CC	Correlation Coefficient
CCI	Co-channel Interference
CDMA	Code Division Multiple Access
CF	Cost Function
CG	Conjugate Gradient
CIR	Channel Impulse Response
CMLP	Complex Multilayer Perceptron
COST	Cooperative for Scientific and Technical
CP	Cyclic Prefix
CRBF	Complex Radial Basis Function
CSI	Channel State Information
DAB	Digital Audio Broadcasting
DCT	Discrete Cosine Transforms
DEA	Differential Evolution Algorithm
DFT	Discrete Fourier Transform
DWT	Discrete Wavelet Transform
EZW	Embedded Zero tree Wavelet
FDM	Frequency division Multiplexing
FEC	Forward Error Correction
FFT	Fast Fourier Transform
GA	Genetic Algorithm
GD	Gradient Descent
GI	Guard Interval
ICI	Inter Carrier Interference
ISI	Inter Symbol Interference
IEEE	Institute of Electrical and Electronics Engineers
IFFT	Inverse Fast Fourier Transform
IWO	Invasive Weed Optimization
LAN	Local Area Network
LTE	Long Term Evolution

LIS	List of Insignificant Sets
LOS	Line of Site
LPI	List of Insignificant Pixels
LSP	List of Significant Pixels
MAI	Multiple Access Interference
MAP	Maximum a Posterior
MBER	Minimum Bit Error Rate
MER	Minimum Error Rate
MIMO	Multiple Input Multiple Output
ML	Maximum Likelihood
MLP	Multilayer Perceptron
MMSE	Minimum Mean Square Error
MS	Mobile Station
MSE	Mean Square Error
MSER	Minimum Symbol Error Rate
MUD	Multiuser Detection
MUI	Multiuser Interference
NN	Neural Network
OFDM	Orthogonal Frequency Division Multiplexing
OTs	Optimization Techniques
PAPR	Peak to Average Power Ratio
PDF	Probability Density Function
PIC	Parallel Interference Cancellation
PSNR	Peak Signal to Noise Ratio
PSO	Particle Swarm Optimization
QAM	Quadrature Amplitude Modulation
QPSK	Quadrature Phase Shift Keying
QRD	QR Decomposition
RBF	Radial Basis Function
RMSE	Root Mean Square Error
SD	Standard Deviation
SDD	Standard Deviation Difference
SDM	Space Division Multiplexing
SDMA	Space Division Multiple Access
SER	Symbol Error Rate
SIC	Successive Interference Cancellation
SISO	Single Input Single Output
SNR	Signal to Noise Ratio
SPIHT	Set Partitioning Hierarchical Tree
STBC	Space Time Block Codes
STTC	Space Time Trellis Codes
SUI	Stanford University Interim
SWATM	Shortened Wireless Asynchronous Transfer Mode
V-BLAST	Vertical BLAST
ZF	Zero Forcing

NOTATIONS

$(.)^*$	Complex conjugate
$(.)^H$	Hermitian transpose
$(.)^I$	Imaginary component
$(.)^R$	Real component
$(.)^T$	Transpose
$(.)^{-1}$	Inverse
$(.)^\dagger$	pseudo inverse
$\ \cdot\ ^2$	Euclidian Norm
μ	Learning rate parameter in MLP
μ_c	Center learning parameter
μ_s	Spread learning parameter
μ_v	Scaling factor's learning parameter
μ_w	Weight learning parameter
σ_f	Final standard deviation of IWO algorithm
σ_{iter}	Standard deviation of i^{th} iteration IWO algorithm
σ_h	Spread parameter of h^{th} hidden neuron of RBF
σ_i	Initial standard deviation of IWO algorithm
σ_n^2	Noise variance
τ_{\max}	Maximum delay spread
Ω	Unitary hierarchical sub band transformation
λ	Wavelength
η	Step size of CG algorithm
\Re	Real component
\Im	Imaginary component
ρ_r	Correlation coefficients at the receiver
ρ_t	Correlation coefficients at the transmitter
T	Sampling time
\mathbf{b}_l	l^{th} user's data bit stream
\mathbf{b}_l^c	l^{th} user's FEC coded data bit stream
B_C	Coherence bandwidth
B_S	Signal bandwidth
\mathbf{C}_h	$(P \times 1)$ complex-valued center
C_p	DEA cross-over probability
\mathbf{d}	$(L \times 1)$ desired response
E	Sum squared error
F	DEA mutation factor
G_d	ADEA generation count
G_g	GA generation count
\mathbf{H}	$(P \times L)$ MIMO channel matrix

$\hat{\mathbf{H}}$	$(P \times L)$ estimated channel matrix
H_N	Number of hidden neurons
\mathbf{H}_w	$(P \times L)$ fading channel with no spatial correlation
I_{\max}	Maximum number of iterations in the IWO algorithm
\mathbf{I}_P	$(P \times P)$ identity matrix
L	Number of users
m	Number of bits per symbol
M	Modulation order
\mathbf{n}	$(P \times 1)$ noise vectors
N_C	Number of subcarriers/IFFT length
N_{CM}	Average number of training symbols taken for CMLP
N_{CP}	Length of cyclic prefix
N_{CR}	Average number of training symbols taken for CRBF
N_d	ADEA population count
N_e	The size of encoded data stream from each SPIHT coder
N_F	Number of OFDM frames
N_g	AGA population count
N_I	Initial population of the IWO algorithm
N_M	Average number of training symbols taken for MLP
N_R	Number of receiving antennas
N_{RB}	Average number of training symbol taken for RBF
N_S	Maximum number of seeds in the IWO algorithm
N_T	Number of transmitting antennas
P	Number of receiving antennas
P_c	GA cross-over probability
P_m	GA mutation probability
\mathbf{Q}	$(P \times P)$ unitary matrix
r	Non-linear modulation index in the IWO algorithm
R	Data rate in bits/sec
\mathbf{R}	$(P \times L)$ upper triangular matrix
R_H	Auto covariance matrix of \mathbf{H}
R_y	Auto covariance matrix of \mathbf{y}
R_{yx}	Cross covariance of \mathbf{y} and \mathbf{x}
R_{Hy}	Cross covariance matrix between \mathbf{H} and \mathbf{y}
\mathbf{R}_r	Spatial correlations across the receiving antennas
\mathbf{R}_t	Spatial correlations across the transmitting antennas
\mathbf{V}_h	$(P \times 1)$ complex-valued scaling factor
\mathbf{w}	$(P \times L)$ dimension weight matrix
\mathbf{x}	$(L \times 1)$ transmitted vectors
$\bar{\mathbf{x}}$	$(L \times 1)$ noiseless transmitted vectors
$\hat{\mathbf{x}}$	$(L \times 1)$ estimated vectors
\mathbf{y}	$(P \times 1)$ received vectors
$\bar{\mathbf{y}}$	$(P \times 1)$ noiseless received vectors

Chapter 1

Introduction

Wireless communication has become gradually more important worldwide not only for professional applications but also for many fields in our daily routine. In early 90s, a mobile telephone was a quite expensive gadget, whereas today almost everyone has a personal mobile. A clear example of this may be found in the Indian telecom industry, which has a high pace of market liberalization and growth since 1990s and now it has become the world's most competitive telecom markets with the inclusion of 3G services. The average growth of this industry is around twenty five times in just ten years. The number of subscribers in the year of 2001 is under 37 million, and it has increased to 960.9 million by the year of 2012. India has the largest mobile phone user base and the annual income from it has is around USD 33,350 million. Nowadays, the mobile users use it not only for voice calls but also for high bandwidth applications such as, MMS services, video calling, accessing high speed internet support etc. The 4G technology is already developed to provide next generation internet support (IPv6, VOIP and Mobile IP), high capacity, seamless integrated services and coverage. With such an expansion in the mobile communication networks, the demand for design of robust communication system with high performance quality of service (QoS) increases.

Wireless channel is an unguided dielectric media and hence the frequency ranges it can support are ideally infinite. Still due to many reasons, full available spectrum cannot be utilized. Bandwidth limitations, propagation loss, noise and interference make the wireless channel a narrow pipe that does not readily accommodate rapid flow of data. The propagation conditions in such environments are frequency selective due to dispersive multipath nature of wireless channels and hence Inter Symbol Interference (ISI) is introduced. OFDM is a parallel transmission scheme that distributes a serial data stream with high data rate into a set of low data rate parallel sub streams by modulating with orthogonal subcarriers. As these low data rate symbols undergo flat fading in radio environment, the ISI effect of the channel can be mitigated. In this technique, though the spectra of the individual orthogonal subcarriers overlap, the information can be completely recovered without any interference from other subcarriers. OFDM is extensively utilized in many applications like European Digital Audio Broadcasting (DAB), 3GPP Long Term Evolution (LTE) system, Wireless Local Area Network (WLAN) of IEEE 802.11a/g standard and WiMAX of IEEE 802.16 standard. On the other hand, the ever increasing demand for wireless communication system requires a high spectral efficiency. As a subclass of MIMO arrangements, SDMA techniques allow sharing of frequency band simultaneously by many subscribers in different geographical locations.

This can overcome the scarcity of spectral resources of wireless communication systems. In SDMA system, each of the users is equipped with a single antenna and the base station is equipped with multiple antennas. Each user will have their own spatial signature, and by using this, the Base Station (BS) receiver can detect multiple user's signals. Generally, a multiuser system like SDMA suffers from the Multiuser Interference (MUI), whenever a receiver observes signals from multiple transmitters. Due to MUI, a strong user's signal source may influence the reception of weak one. This problem can be solved by incorporating Multiuser Detection (MUD) at the receiver. The MUD is one of the receiver design technology used for detecting desired user signal by eliminating interference from neighborhood user's signal. The detection problem in the SDMA system becomes more challenging as the complexity grows exponentially while increasing number of users. So research continues in this field to design better MUD schemes maintaining a tradeoff between complexity and performance.

This chapter begins with a brief literature survey on the development of the SDMA–OFDM system and existing MUD techniques as presented in Section 1.1. An exposition of the principal motivation behind the work undertaken in the thesis is discussed in Section 1.2. The research contributions have been outlined in Section 1.3. At the end, the layout of the thesis is presented in Section 1.4.

1.1 Literature review

The wireless channel is characterized by multipath propagation, where the transmitted signal arrives at the receiver using various paths of different lengths including Line of Sight (LOS) path. These multiple versions of the transmitted signals reach the receiver at different time instants. These reflected or delayed waves interfere with the direct wave and cause ISI, which results significant degradation of network performance. This problem can be solved by means of frequency diversity, which relies on the principle that signals are transmitted on different frequencies so that the multipath propagation in the media is exploited. Transmitting signals over different frequencies are referred as multicarrier transmission. One special case of multicarrier transmission is the OFDM scheme, which is first proposed by R. W. Chang [1]. However, this synthesis model using sinusoidal subcarrier generators and demodulators imposes high implementation complexity. As a design alternative, Weinstein and Ebert [2] suggested the OFDM modulation and demodulation processes using the Discrete Fourier Transform (DFT), which significantly reduces the implementation complexity of OFDM.

Since the development of OFDM, it has received a great interest by researchers and it is successfully incorporated in several applications like high-speed modems, digital mobile communications, high-density recording and so on [3, 4]. OFDM modulation technique is also adopted by IEEE 802.11a/g wireless LAN [5, 6]. The operation and detailed study about the OFDM is presented in several literatures [7–9].

In recent past, the MIMO technique has become potentially attractive for achieving high data rates in wireless communication systems. Among various contributions, a fundamental breakthrough for MIMO technology came in the late 1980's with a pioneer work presented by Winters [10, 11]. The MIMO system has significant advantages compared to Single Input Single Output (SISO) system, as it may provide either diversity gain or throughput gain. In the spatial diversity techniques, the Space Time Trellis Coding (STTC) proposed by Tarokh et al. [12] and the Space Time Block Coding (STBC) proposed by Alamouti [13] are well-accepted schemes. Compared to STTC, the structural complexity of STBC is less and it also provides full diversity gain. As the space time codes are basically intended for diversity gain, these don't offer any throughput gain with respect to a SISO system. Hence, these codes are excellent for improving the link quality by combating deep fades. The multiplexing gain can be improved by using Bell Labs Layered Space Time (BLAST) architectures. Foschini proposed Diagonal BLAST (D-BLAST) architecture by transmitting several independent data streams through different transmitting antennas [14]. This is further modified in Vertical BLAST (V-BLAST), by G. D. Golden [15]. Several important contributions on the properties of MIMO systems are made during the 1990's, and the area is still drawing considerable research attention [16–19]. Interestingly, as the OFDM provides resistance from ISI and the MIMO provide high system throughput, the combination of these two techniques has become a promising solution in 3G and 4G standards. This inspired numerous further contributions in the area of MIMO-OFDM system [20–24]. On the other hand, the SDMA system is a special architecture of MIMO that allows multiple users to share the same bandwidth simultaneously in different geographical locations. The multiple users of the system are distinguished by their unique user specific Channel Impulse Response (CIR), which solves the capacity problem of the SDMA-OFDM system [35–30].

At the receiving end of the SDMA-OFDM systems, estimating Channel State Information (CSI) is required for coherent demodulation and data detection. In order to obtain CSI, blind and training based channel estimation techniques can be applied. In blind channel estimation technique, CSI is estimated by channel statistics without any knowledge of the transmitted

data. But it suffers from slow convergence because of the time varying nature of channels [31–35]. In training based estimation techniques, training symbols that are also called as pilots are inserted in all of the subcarriers of OFDM symbols with specific period or inserted in each OFDM symbol [36–40]. Compared to blind estimation, pilot-based channel estimation techniques provide better performance in fast fading and time varying channels. Further, as the pilot tones directly affect the performance of channel estimation algorithms, several researches also concentrated on designing optimal training symbols [41–45]. Once the CSI is known at the receiver, the transmitted signals of all users can be detected using various MUD schemes. In recent past, there has been a significant attention paid towards developing efficient MUD techniques. The linear detectors like Zero Forcing (ZF) and Minimum Mean Square Error (MMSE) detect signals with the aid of a linear combiner [28, 46]. The linear detectors cannot mitigate the nonlinear degradation caused by the fading channel, because the channel's output phasor constellation often becomes linearly non-separable. Hence, these detectors result high residual error. On the other hand, the nonlinear and computationally intensive Maximum Likelihood (ML) detector is capable of achieving optimal performance through an exhaustive search, which prohibits its usage in practical systems [28, 46]. Considering the tradeoff between complexity and performance, some non-linear MUD techniques like Successive Interference Cancellation (SIC) [16, 47], Parallel Interference Cancellation (PIC) [28], Sphere Decoding (SD) [48–50] and QR Decomposition (QRD) [51–53] MUDs are introduced. Modifications of SD [54–57] and QRD [58–60] techniques are also proposed in several literatures. Among all these developments, the MMSE based QRDM technique is widely accepted as it exploits MMSE metric instead of the ML metric, which leads to enhanced performance with less complexity [60]. However, all these MUDs either fail to detect users in overload or rank deficient scenarios, where the number of users is more than the number of receiving antennas, or suffer from high complexity. Hence, S. Chen et al. proposed Minimum Bit Error Rate (MBER) MUD by minimizing BER directly rather than minimizing mean square error for CDMA system to support in overload condition [61]. Conjugate Gradient (CG) algorithm is used for updating receiver's adaptable weights [62]. However, it requires proper selection of initial solutions and differentiable cost functions. These drawbacks can be eliminated by incorporating metaheuristic Optimization Techniques (OTs), as they start the search process from random positions. M. Y. Alias et al. proposed Genetic Algorithm (GA) based MBER MUD and implemented it for the SDMA-OFDM system [63, 64]. Subsequently, the MBER MUD algorithm was modified using other well known OTs like Particle Swarm Optimization (PSO) [65, 66] and Differential Evolution

Algorithm (DEA) [67]. The MBER MUD technique is basically designed for Binary Shift Keying (BPSK) modulation scheme. As the next generation communication systems also require high throughput, the OTs are directly used for detection of higher order modulated signal using the ML cost function [68–70]. But these techniques result high complexity especially in block fading channels. Therefore, J. Zhang et al. proposed an another Minimum Error Rate (MER) detection technique depending on Minimum Symbol Error Rate (MSER) for detecting Quadrature Amplitude Modulation (QAM) signals [71, 72].

Most of the discussed classical detectors assume that the channel is perfectly known at the receiver's end, whereas practical systems need estimation of the channel state information, which imposes an additional complexity. This problem can be resolved directly by employing highly nonlinear classifiers such as Artificial Neural Networks (ANNs) [73–75]. During past decade, ANNs are extensively utilized as multiuser detectors for CDMA system [76–80], but these are not yet applied for the SDMA–OFDM system [30]. Among various ANNs, the Multilayer Perceptron (MLP) and the Radial Basis Function (RBF) are considered to be simple but powerful tools in the area of pattern classification. These models can perform complex mapping between its input and output space and are capable of forming decision regions separated by nonlinear decision boundaries. Generally, the real valued NN models fail to transfer the complete complex input information to the output layer. Therefore, subsequently several complex NN models are also developed. Especially, the complex valued MLP [81–83] and complex valued RBF [84–88] models are used for solving adaptive equalization problems when both input and desired signals are complex valued.

Progressive image transmission over noisy channel using image compression techniques is another active research area in recent past. For image compression, Embedded Zero Wavelet (EZW) coding proposed by Shapiro [89] can be used efficiently for fast execution. Later, Said and Pearlman modified the underlying principles of EZW technique and proposed Set Partitioning Hierarchical Tree (SPIHT) coding for achieving better results [90]. The SPIHT coding will convert a two dimensional image into compressed binary bit streams. As wireless channels often suffer from multipath fading, shadowing and ISI, the transmission of compressed image is a major concern due to error prone environment. The transmission error may lead to degrade the received image quality. By incorporating efficient MUD techniques, these degraded images can be recovered at the BS receiver. Such kind of progressive image transmission and detection analysis has been already studied for space time coded MIMO–OFDM system in the literatures [91, 92].

1.2 Motivation of the thesis

In a classical wireless transmission scenario, the transmitted signal arrives at the receiver using various paths of different lengths. If the maximum path delay is more than the symbol period, then ISI will occur. Since the multiple versions of the signal interfere with each other, it becomes extremely difficult to extract the original information. This problem can be solved by multicarrier transmission scheme like OFDM. OFDM generates orthogonal parallel symbols, whose delay spread is a significantly shorter fraction of a symbol period. As a result it is less sensitive from ISI [93]. On the other hand, the evolution of wireless communications from pure telephony to multimedia platforms offering high data rate applications led to the enhancement of early propagation models. This goal can be achieved by incorporating multiple antennas at both the transmitting and receiving ends, which is often called as MIMO system [94, 95]. As the OFDM and MIMO techniques have their own merits, the combination, that is MIMO–OFDM, can offer a reliable communication with high data rate [96–100]. Further, as the number of mobile users increasing drastically, bandwidth has become an extremely scarce resource. This emphasizes the need for transmission schemes offering high spectral efficiency. The spectral efficiency can be achieved by the SDMA based MIMO system, which allows multiple users to share a single frequency band simultaneously, where multiple users are distinguished by their own spatial signature. Hence, the SDMA–OFDM system results in highly efficient reliable data [101, 102]. The SDMA like multiuser systems often suffer from Multiuser Interference (MUI) also called as Multiple Access Interference (MAI). In a mobile cellular network system, MUI arises due to the sum of interference resulting from multiple transmissions in a cell or from neighboring cells. High capacity requirements by supporting more users need to be achieved suppressing the MUI. Such interference can be suppressed through Multiuser Detection (MUD). MUD technique jointly detects multiple users, which are transmitting simultaneously through the same wireless media.

During the past few decades, an extensive research has been carried out for designing efficient MUD techniques. Amongst those, the conventional linear detectors are simple but are interference limited. The linear detectors cannot mitigate the nonlinear degradation caused by the fading channel, hence these detectors result high residual error. In addition to that, as the number of users increases, the MUI also increases, which in turn degrades the Bit Error Rate (BER) performance of the receiver. Considering these points, the linear detectors cannot achieve the full potential of detection process. On the other hand, the optimal

nonlinear detectors possess high complexity, which restricts them in practical implementation. Hence, extensive research attention is drawn for designing efficient sub-optimal detection techniques with a trade-off between complexity and performance. However, most of the sub-optimal detectors fail to detect users in overload scenario. In such a case, the MIMO channel matrix becomes singular, and hence rendering the degree of freedom of the detector insufficiently high for detecting the signals of all the transmitters in its vicinity. This will drastically degrade the performance of various classical detectors. The prime objective of the present research is to minimize the Bit Error Rate (BER). However, the classical linear Minimum Mean Square Error (MMSE) detector minimizes Mean Square Error (MSE), which may not give guarantee that the BER also minimizes. By contrast, the MER MUDs like MBER and MSER directly minimize the probability of error by optimizing the receiver weights [64, 65]. Earlier, gradient descent algorithms are used for weight optimization of MER detectors, which have certain limitations. Considering all these issues, this research work is motivated towards the development of new improved MER MUDs, in which intelligent search algorithms will be utilized for locating optimal weights. Therefore, the improved MER MUDs can offer better performance with low computational complexity and also supports in overload conditions.

The process of the MUD can be basically considered as a pattern classification problem, where the optimal decision boundary is highly nonlinear. Taking this into consideration, Artificial Neural Network (ANN) or simply Neural Network (NN) models can offer a much better solution to MUD problem due to their highly nonlinear pattern classification capability. In recent past, NNs based MUD techniques have been applied successfully to the Code Division Multiple Access (CDMA) system achieving better performance than conventional linear techniques [103–105]. The ANNs are parallel distributed structures in which many simple interconnected elements (neurons) simultaneously process information and adapt themselves to learn from past patterns. Attractive properties of NNs relevant to the MUD problem are robustness, finite memory and nonlinear classification ability. With these motivations, the present work investigates the feasibility of employing the NNs especially Multilayer Perceptron (MLP) model and Radial Basis Function (RBF) models for solving the MUD problem in the SDMA–OFDM system.

Thus, the prime objective of the proposed work is to develop some soft computing based MUDs to achieve a near optimal performance considering the complexity and overload issues in a multiuser scenario of the SDMA–OFDM system.

1.3 Contribution of the thesis

The present work aims at developing efficient soft computing based MUD schemes with reduced computational complexity for the SDMA–OFDM system, which will be suitable for easier implementation in practical applications. The first part of the research focuses on proposing OTs aided Minimum Error Rate (MER) detectors with proper selection of control parameters. Second part of research introduces the development of NN based MUD schemes. Suitable modifications of the activation functions of neurons and training algorithms are incorporated considering the communication system parameters. Applications of the proposed detectors result near optimal performance at reduced complexity even in the critical overload scenario of an uplink SDMA–OFDM system. Further, for challenging multimedia applications limited by the fading channel conditions and spectrum allocation, the proposed MUDs prove to be successful in reconstruction of images when all the users are transmitting simultaneously. Details of the research contribution are discussed below.

Advantages and limitation of classical linear and nonlinear MUD schemes are analyzed through simulation based performance evaluations. Standard MIMO channel models representing indoor, outdoor and fixed wireless scenarios are considered to prove the robustness of the proposed MUD schemes. The classical MMSE detector minimizes the Mean Square Error (MSE), which may not give guarantee that the BER also minimizes. Also it fails to detect users in the overload scenario. So the CG based MER MUDs like MBER and MSER ones are preferred as they can directly minimize the probability of error by optimizing the receiver weights. In MER MUD schemes, global optimum solution needs to be found for receiver weights to achieve a near optimal performance. But as the higher the number of users to be supported, the optimization task becomes more challenging due to exponentially increased number of dimensions to be estimated. The higher computational complexity poses major problem. Hence, this research work suggests using popular metaheuristic OTs such as Adaptive Genetic Algorithms (AGA), Adaptive Differential Evolution Algorithm (ADEA) and Invasive Weed Optimization (IWO) for providing solution to this challenging multidimensional optimization problem. However, as the control parameters of these search algorithms greatly influence the system performance, selection of control parameters is suitably done based on system performance. Development of these OTs aided MER MUD schemes have been suggested with the following considerations:

- The classical GA uses fixed values of cross-over and mutation probabilities. If these values are low, then the GA search strategy requires large number of generations,

otherwise if these values are high it may cause the disruption of the near optimal solutions when a population is at the verge of approaching a globally optimal solution. So an adaptive GA is suggested which chooses lower values of cross-over and mutation probabilities for low fitness solutions and higher values for high fitness solutions. Thus, the high values help in faster convergence while the low values prevent the GA from getting stuck at a local optimum before approaching the global optimal solution.

- Unlike the classical DEA, the adaptive DEA uses a self-adaptive control mechanism, which changes the mutation factor and crossover probability during each evolution or generation in order to achieve improved performance with faster speed of convergence.
- The IWO allows all of the individuals to participate in the reproduction process. Sometimes, it is also possible that the individuals with the lower fitness carry more useful information compared to the fitter individuals. Hence, this algorithm, gives a chance to the less fit plants also to reproduce and if the seeds produced by them have good fitnesses in the colony, they can survive. Fitter individuals produce more seeds than less fit individuals, which tends to improve the convergence of the algorithm.

In the overload SDMA–OFDM system, the channel's output phasor constellation often becomes linearly non separable. Hence, application of Artificial Neural Networks (ANNs) is suggested for MUD at the BS receiver as these models are known as nonlinear classifiers and can exhibit massive parallelism. NNs size, weight matrix etc are defined based on the uplink SDMA system parameters. Besides that, most of the classical detectors assume that the channel dynamics are perfectly known at the receiver's end, whereas in practical systems, estimation of channel response imposes additional complexities. But, as the NN models approximate channel parameters in training phase and can subsequently detect signals in testing phase, these may become a good substitute for classical detectors. The developed NN based MUDs are adaptive in nature as they can adapt to unknown time varying channel conditions through training. The proposed NN based detectors have been designed on both standard Multilayer Perceptron (MLP) and Radial Basis Function (RBF) frameworks. Generally, as the response of the MLP and RBF models are always real valued, these models can be incorporated for detection of lower order modulated signals such as BPSK. However, as high throughput is also a major requirement, the transmission of higher order symbols such as M -Quadrature Amplitude Modulation (QAM) is essential. While transmitting such higher order modulated signals, the nonlinear channel degradation affects both the In-phase and Quadrature components of the transmitted symbols. In order to extend the NN models to

detect such signals, processing has to be done in a complex multidimensional space. Therefore, this research work significantly contributes to development of complex valued NNs, again on both MLP and RBF frame work changing the nonlinear activation functions of neuron nodes. The conventional BP and GD Algorithm cannot be directly applied for training free parameters of the proposed new NN models. Hence, suitable modifications have been included in those algorithms while estimating the local gradient of errors considering the complex output response. Development of the proposed complex valued NN detectors is based on the following considerations:

- The Complex MLP (CMLP) can be viewed as an extension to the MLP, which can process both real and imaginary components of the transmitted signals. The complex response can be achieved by expanding the sigmoid activation function into both real and imaginary components such that the function becomes analytic and bounded everywhere in the complex plane. With such modification, the CMLP is expected to a better nonlinear mapping between input and output when higher order signals are transmitted.
- The real valued RBF network uses Gaussian activation functions. The proposed complex valued RBF (CRBF) has replaced it with *sech* activation function, whose behavior is similar to Gaussian approximation but it is capable of generating complex response corresponding to complex input signals directly. Further, by splitting it into real and imaginary components, the error gradient computation can be made more economical.

As observed from the exhaustive simulation studies under taken in this research, the proposed NN based adaptive MUD schemes have resulted near optimal performances, a significant performance gain over classical MMSE, faster learning and low computational complexity. But it is observed that the gains obtained here are entirely channel dependent.

The task of image transmission in a SDMA–OFDM wireless communication system is really a challenging problem due to limited bandwidth, vulnerability of wireless links and noisy channel. As the SDMA–OFDM system doesn't provide any transmitting diversity, detection becomes a more difficult task when number of users interfering with each other increases. Hence, reliable image transmission through wireless channels has drawn considerable research attention. As an extension of this research work, the proposed soft computing based MUD schemes are utilized for image reconstruction when all users in the system are transmitting progressive images simultaneously. The techniques suggested here can be implemented for real time image traffic over a radio link in the SDMA–OFDM system.

1.4 Thesis layout

The rest of the thesis is organized as follows.

Chapter–2: Introduction to SDMA–OFDM System and Comparison of Classical MUD Schemes

This chapter introduces the basic SDMA–OFDM wireless communication system along with mathematical expressions for multiuser signal transmission and reception. As the mobile radio channel plays a major role in deciding the performance of the system, its statistical properties are analyzed and standard models for frequency selective wireless MIMO channels are presented. Afterwards, the operating principles of MUD and expressions for such detection process are discussed. Some of the classical linear and nonlinear MUD schemes with their merits and demerits have been explained. The probability of error functions for in both the basics of MBER and MSER MUDs are also derived, which form the basis of the following proposed MUD schemes. Performance comparisons of all classical MUDs are analyzed based on the simulation study.

Chapter–3: Proposed Metaheuristic Optimization Techniques Aided Minimum Error Rate MUD Schemes

This chapter discusses in detail about the applications of popular Metaheuristic OTs like Adaptive Genetic Algorithm (AGA), Adaptive Differential Evolution Algorithm (ADEA) and Invasive Weed Optimization (IWO) for determining the optimal solution in MER detection problems. A detail study on control parameters of OTs, which influence the performance of MBER/MSER MUDs, is included here and accordingly selection of control parameters is suggested. The chapter concludes with results of simulation study which includes the comparison of proposed OTs aided MER detectors with the classical MUD schemes based on Bit Error Rate (BER) performance, convergence analysis and computational complexity analysis.

Chapter–4: Proposed Neural Network Based Adaptive MUD Schemes

This chapter proposes efficient MUD schemes based on feed forward NN topologies (both MLP and RBF) and modification of existing training algorithms to faster adapt the network parameters. The fundamental concept of using NNs for MUD design has been described. The limitations of real valued NN models while detecting higher order modulated signals are discussed and the necessity of complex valued NN models for processing of such signals is

also explained. For the NN models, selection of number of nodes in input, hidden and output layers according to the order of SDMA–OFDM system is chosen based on BER performance and an empirical relationship between number of hidden nodes and number of users is established. Finally, the efficacy of the proposed NN based adaptive MUD schemes are proved through performance and complexity analysis using simulation based study.

Chapter–5: Progressive Image Transmission and Detection Using Proposed MUD Schemes

This chapter validates the proposed MUD schemes presented in Chapter–3 and Chapter–4 by successfully reconstructing images (both gray scale and colored), when all the users are transmitting different images simultaneously. The basic system model used to transmit images and the process of image coding and decoding by the SPIHT algorithm are explained in detail. The chapter ends with a comparison of all proposed MUD schemes (OTs aided MER and NN based MUDs) while visualizing the reconstructed images and calculating their statistical parameters. The widely used statistical parameters for an image quality analysis metrics are Bias, Standard Deviation Difference (SDD), Root Mean Square Error (RMSE), Peak Signal to Noise Ratio Correlation Coefficient (CC) and (PSNR), which are presented in a tabular form for comparative analysis.

Chapter–6: Conclusions and Future Scope of Research

This chapter summarizes the research work undertaken in the thesis. Limitations of the present work and a few points on future scope of research are presented at the end.

Chapter 2

Introduction to SDMA-OFDM System and Comparison of Classical MUD Schemes

Two major technical challenges in the design of wireless communication system are the impairments of the propagation channel and better spectral efficiency. OFDM, which transforms a frequency selective channel in a set of frequency flat channels, can mitigate the channel impairments [7–9]. On the other hand, SDMA based techniques as a subclass of MIMO systems enables multiple users to share the same bandwidth simultaneously. Thus SDMA technique has the advantages of improving the capacity of wireless systems with the expense of the requiring robust detection in the receiver. The SDMA can differentiate multiple users by exploiting their unique user specific spatial signature even when they are in the same frequency/time slots [25–30]. The spatial signature in a SDMA is like spreading code in the conventional CDMA. Multiuser Detection (MUD) techniques known from CDMA can be applied in SDMA–OFDM receivers to mitigate Multiple Access Interference (MAI), which causes performance degradation. MUD refers to the scenario in which a single receiver jointly detects multiple simultaneous transmissions. In MUD scheme, multiuser information available in the MAI term is used to demodulate the signal and will not be treated it like a noise term. This concept is similar to the exploiting multipath for diversity. In the recent past, designing efficient MUDs which have the property of minimizing the bit error probability while being realistic from the computational complexity point of view has attracted lot of attention amongst researchers. The overview of MUD schemes is presented by Sergio Verdu in the early 1980's [47].

This chapter introduces MIMO, OFDM and SDMA–OFDM, in Section 2.1, Section 2.2 and Section 2.3 respectively. The wireless MIMO channel characteristics and basic channel estimation techniques are briefed in Section 2.4 and Section 2.5 respectively. Some classical linear and nonlinear MUD schemes are discussed in Section 2.6 and their performances have been compared using simulation study as presented in Section 2.7. Finally, this chapter concludes with a summary as given in Section 2.8.

2.1 Multiple Input–Multiple Output (MIMO) system

Basically, the MIMO system has been categorized as Space Division Multiplexing (SDM) and Space Division Multiple Access (SDMA) for achieving different design goals in various wireless applications.

2.1.1 Space Division Multiplexing (SDM)

This system employs multiple antennas at both transmitting and receiving antennas as shown in Figure 2.1. The multiple transmitting antennas are used for either diversity gain or

throughput gain (data rate gain). In the context of diversity techniques, multiple replicas of the information are transmitted through different paths, hence the SDM system is capable of exploiting both transmitter and receiver diversity to achieve reliable communications. The antennas are spaced as far apart as possible, so that the signals transmitted to or received by the different antennas experience independent fading and hence the highest possible diversity gain can be attained. Space Time Trellis Coding (STTC) [12] and Space Time Block Coding (STBC) [13] techniques are widely used to achieve the maximum possible diversity gain. However, the BER performance improvement is often obtained at the expense of a data rate loss, since STBCs and STTCs may not result additional throughput gain. As a design alternative, a specific class of SDM system was developed for improving multiplexing gain by transmitting different signal streams independently over each of the transmit antennas. This class of MIMO techniques is renowned as the Bell Labs Layered Space-Time (BLAST) scheme [14, 15]. The BLAST architecture aims to increase the system throughput in terms of the data rate that can be transmitted in a limited bandwidth.

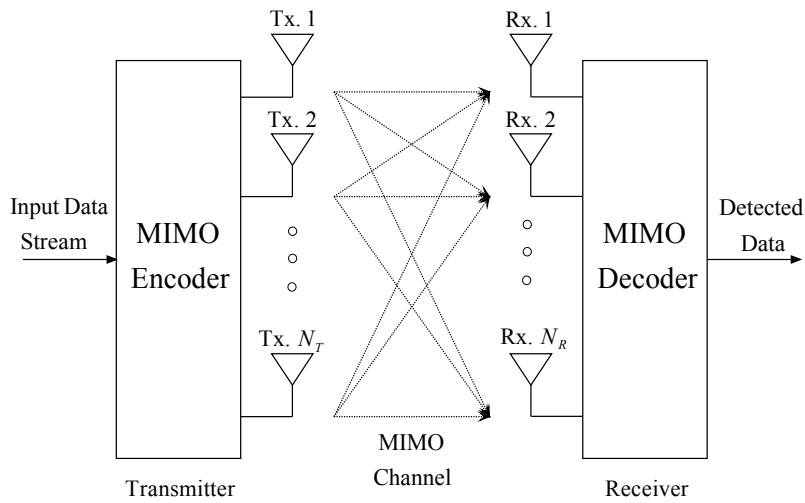


Figure 2.1: SDM system model

2.1.2 Space Division Multiple Access (SDMA)

In contrast to the multiplexing schemes, the SDMA employs multiple users each equipped with a single transmitting antenna and an array of base station antennas [30]. SDMA exploits the unique user specific spatial signature constituted by their channel transfer function or equivalently Channel Impulse Response (CIR) for separating user's signals. This allows the system to support multiple users within the same frequency band and/or time slot, given that their CIRs are sufficiently different and are accurately measured. Spatially separated user's data streams can simultaneously access the channel in the same frequency band, provided that

the locations of transmit and receive antennas are appropriately chosen. Figure 2.2 illustrates A SDMA uplink transmission scenario, where each of the L simultaneous users is equipped with a single transmissions antennas, while the receiver capitalizes on a P –element antenna front end.

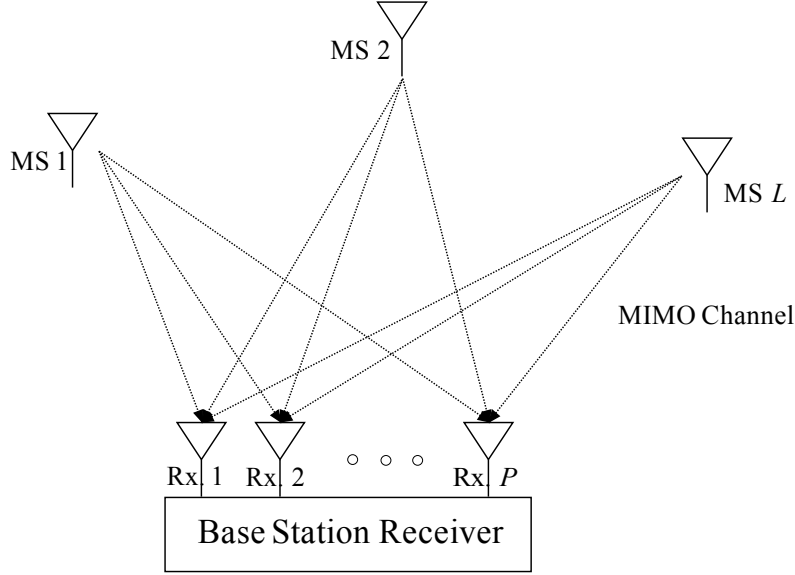


Figure 2.2: SDMA uplink system model

2.2 Orthogonal Frequency Division Multiplexing (OFDM) technique

2.2.1 Need for multicarrier transmission:

The system performance of high data rate wireless communication suffers from multipath propagation. The multipath fading is introduced due to the frequency selectivity when the signal bandwidth (B_S) is larger than the coherence bandwidth (B_C) of a channel. In a classical wireless transmission scenario, the transmitted signal arrives at the receiver using various paths of different lengths. These multiple versions of the signal interfere with each other and cause Inter Symbol Interference (ISI). If the system transmits information at discrete time intervals T and the maximum delay spread is τ_{\max} , then a received symbol can theoretically be influenced by τ_{\max}/T previous symbols [7]. Additionally, Doppler shift causing time selectivity occurs at the terminal due to its mobility in the environment. These problems can be solved by dividing the spectrum into small portions of available bandwidth, called sub channel. Such multicarrier systems are less sensitive to delay spread and yields flat fading response. This is the basic idea of the OFDM system. The OFDM has become a promising technique for high data rate wireless communication due to its robust nature against frequency selectivity and also for its better spectral efficiency.

2.2.2 Importance of being orthogonal:

The main concept of the OFDM technique depends on the orthogonality among the subcarriers. This orthogonality occurs when all these subcarriers have integer number of cycles over a symbol period. As all the carriers are sine/cosine waves, if the area under the product of two sinusoidal signals of different frequencies is zero then those two signals are orthogonal to each other. In such an orthogonal system, the spectrum of each subcarrier has a null at the center frequency of all other subcarriers, which results no interference between the subcarriers. This idea is the key idea behind OFDM [9]. Unlike Frequency Division Multiplexing (FDM), OFDM uses the spectrum much more efficiently by spacing the subchannels close together as shown in Figure 2.3. The orthogonality allows simultaneous transmission on a number of sub-carriers in a tight frequency space without interference from each other as seen in Figure 2.4.

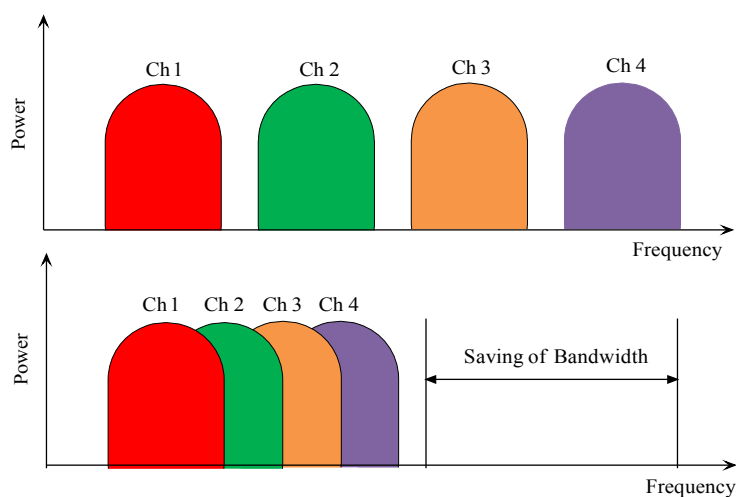


Figure 2.3: Comparison of OFDM spectrum with FDM

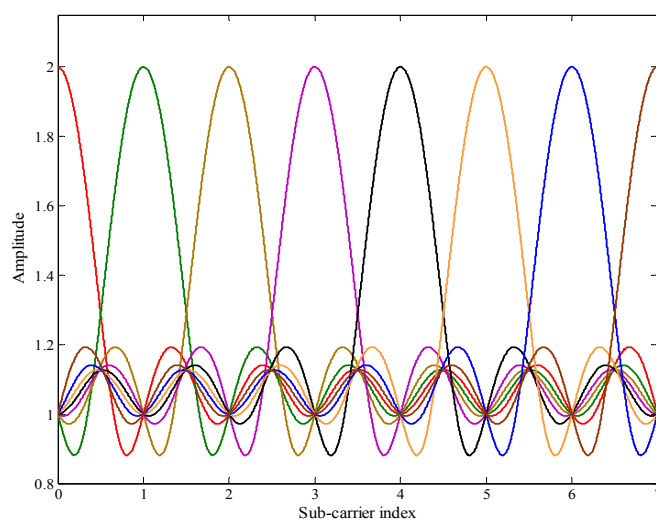


Figure 2.4: Consecutive OFDM subcarriers in time domain

Further, the simulated power spectrum of the OFDM signal is depicted in Figure 2.5, which is estimated over averaging 1000 frames each consisting 128 subcarriers with 1 MHz symbol rate. The signal mapper used in this simulation is 4–QAM. In this figure, we can observe that the peak power is comparatively high over the average power, which can be eliminated efficiently by using Peak to Average Power Ratio (PAPR) techniques [9].

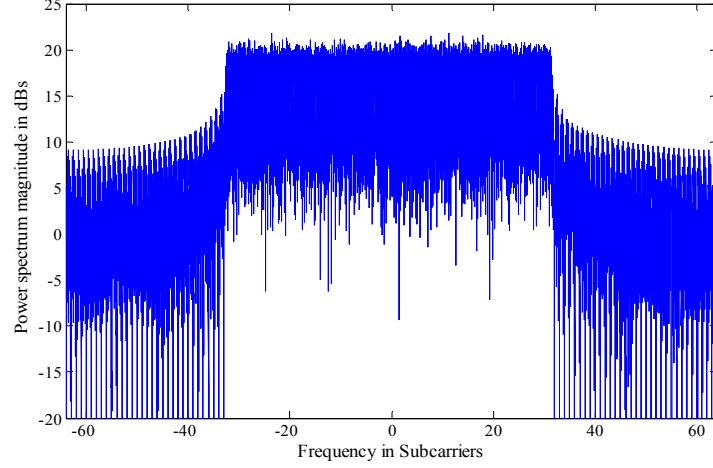


Figure 2.5: Spectrum of an OFDM signal

2.2.3 Cyclic prefix:

In OFDM system, the Cyclic Prefix (CP) is placed between two consecutive OFDM symbols to preserve the orthogonality of the sub-carriers. The duration of CP is selected to be larger than τ_{\max} to avoid interference of one OFDM symbol on the consecutive one, which is called as ISI [9]. As depicted in Figure 2.6, a copy of the end of the OFDM symbols (N_{CP}) is added before the data stream (N_C). The length of the CP should be adjustable and must be set for a bandwidth efficient system.

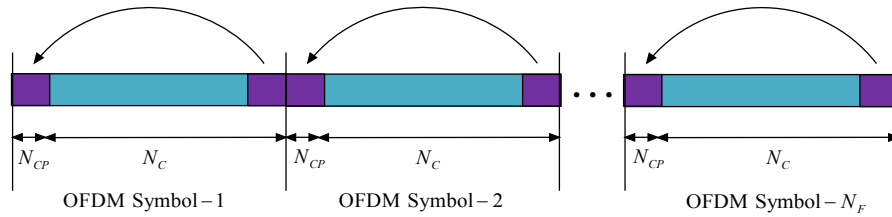


Figure 2.6: Representation of cyclic prefix in the OFDM symbols

2.2.4 OFDM modulation and demodulation:

The OFDM block diagram which includes a Cyclic Prefix (CP) to mitigate the impairment of multipath radio channels is given in Figure 2.7. In OFDM modulation, a large number of closely spaced orthogonal sub-carrier signals are used to carry data. The orthogonality between subcarriers must be carefully maintained to avoid Inter Carrier Interference (ICI).

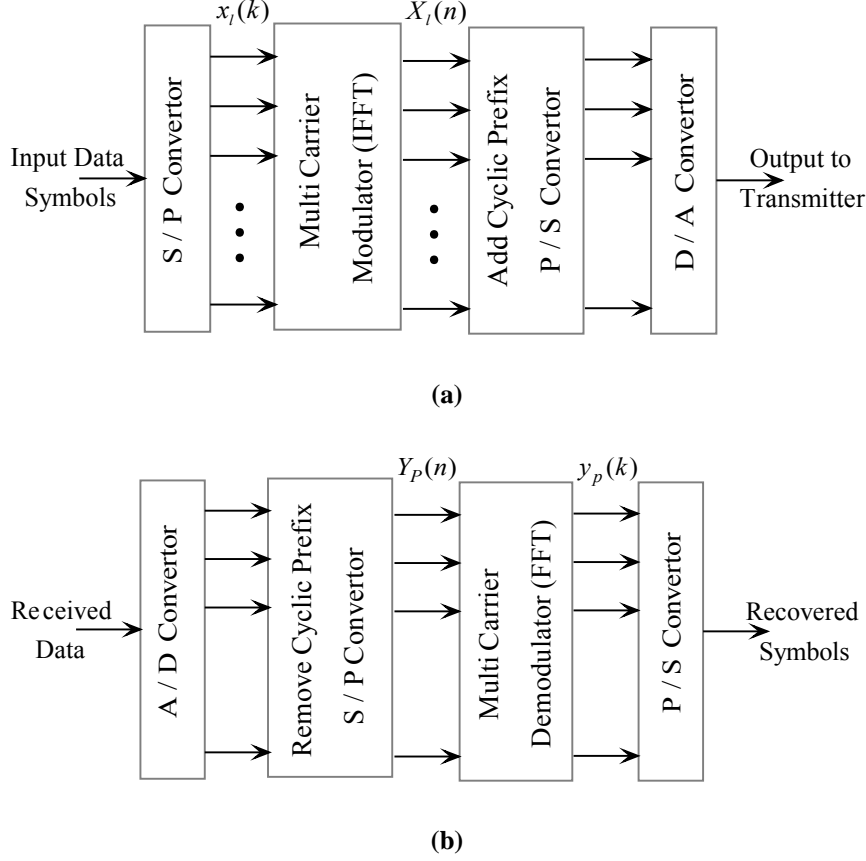


Figure 2.7: Schematic diagram of: (a) OFDM modulator (b) OFDM demodulator

Initially, the input binary serial data is encoded using any one conventional modulation techniques such as, BPSK, QPSK or QAM. While this binary data is transformed to a multilevel signal, the symbol rate is reduced to, $D = R / \log_2 M$ symbols/sec, where R refers to the bit rate of the data stream in bits/sec and M denotes the modulation order. When this serial data is converted to parallel, the data rate gets further reduced by N_C , where N_C is the number of parallel channels. So the parallel symbols are essentially low data rate symbols and since they are narrowband, they experience flat fading. This parallel data stream is then subjected to an Inverse Fast Fourier Transform (IFFT) to produce a time domain symbol $X_l(n)$. In OFDM, the time domain symbols appear as frequency spectrum because these symbols are modulated with multiple carrier frequencies. The OFDM modulated symbol $X_l(n)$ is represented mathematically as:

$$X_l(n) = IFFT\{x_l(k)\}, \quad k = 1, 2, \dots, N_C \quad (2.1)$$

$$= \sum_{k=0}^{N-1} x_l(k) e^{j(2\pi nk/N)} \quad (2.2)$$

After OFDM modulation, a CP is inserted to suppress ICI. The CP is a copy of the last part of the OFDM symbol, which is prepended to the OFDM symbol. This makes the symbol periodic and helps in identifying frames correctly. Then the parallel data is converted to serial data and transmitted through the wireless channel. At the receiver's end, the serial data is converted back to parallel form and CP is removed. Finally, the time domain received symbol $Y_p(n)$ is passed through the Fast Fourier Transform (FFT) block for extracting the frequency spectrum and then parallel data is converted back to serial form.

$$y_p(k) = FFT\{Y_p(n)\}, \quad n = 1, 2, \dots, N_C \quad (2.3)$$

2.3 Overview of SDMA–OFDM system model

Figure 2.8 demonstrates the uplink transmission of the SDMA–OFDM system model [74]. In this figure, each of the L simultaneous users is equipped with a single transmitting antenna and the base station is equipped with a P element antenna array. Each user accesses the entire frequency band with subcarrier spreading. This scenario can improve capacity of the system. The received signal ' $y[s, k]$ ' at the k^{th} subcarrier of the s^{th} OFDM block can be characterized by the super position of L independently transmitted user signals. The SDMA–OFDM frame structure consisting N_F number of OFDM frames, where each frame with $N_C + N_G$ subcarriers is shown in Figure 2.9. Thus, the received signal corrupted with Additive White Gaussian Noise (AWGN) and the noise less received signal at each frequency bin can be expressed respectively in vector form as:

$$\mathbf{y}[s, k] = \mathbf{H}[s, k]\mathbf{x}[s, k] + \mathbf{n}[s, k] \quad (2.4)$$

$$\bar{\mathbf{y}} = \mathbf{H}\mathbf{x} \quad (2.5)$$

Hereafter, the indices $[s, k]$ are omitted for the sake of notational convenience. In the above equation $\mathbf{y} = [y_1, y_2, \dots, y_P]^T \in \mathbb{C}^{P \times 1}$, $\mathbf{x} = [x_1, x_2, \dots, x_L]^T \in \mathbb{C}^{L \times 1}$ and $\mathbf{n} = [n_1, n_2, \dots, n_P]^T \in \mathbb{C}^{P \times 1}$ are the received, transmitted and the noise vectors respectively. The noise vector is assumed to be uncorrelated and exhibits zero mean and σ_n^2 variance. Hence, $E[n] = 0$, $E[n^2] = \sigma_n^2$ and the auto co-variance matrix $E[\mathbf{n}\mathbf{n}^H] = \sigma_n^2 \mathbf{I}_P$. The users are assumed to be located at a sufficiently large distance from each other, mostly at a distance of more than a typical spacing of 10λ , so that the transmitted signals of the different antennas experience independent fading.

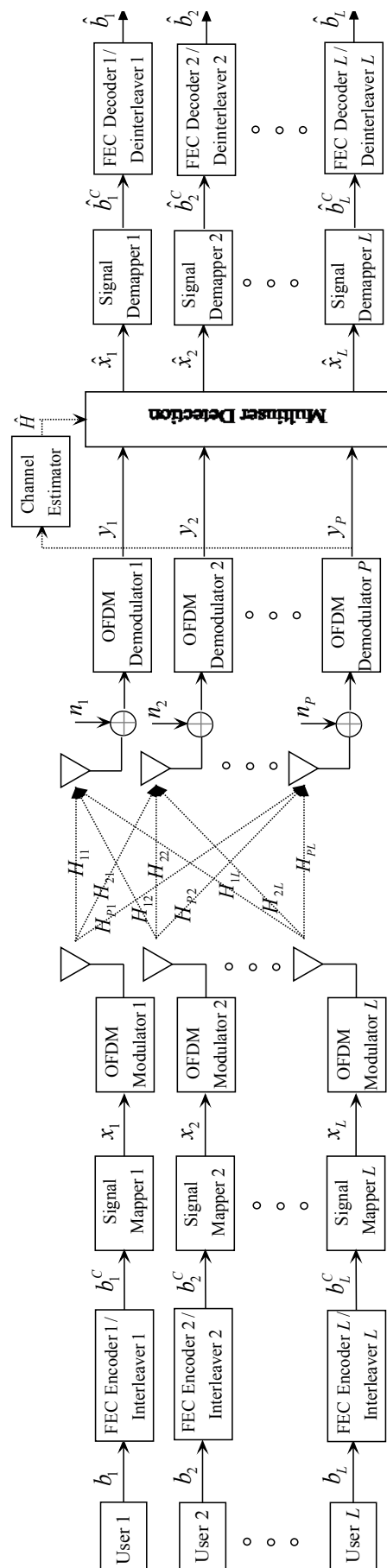


Figure 2.8: Block diagram of the SDMA–OFDM system with L users and P receiving antennas

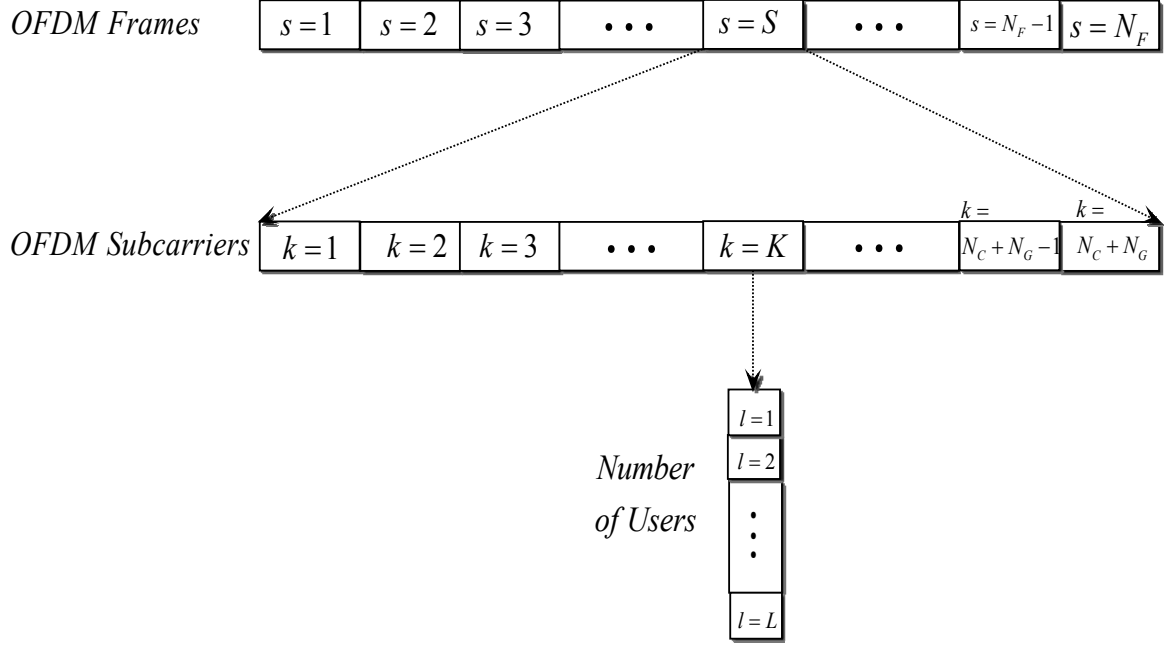


Figure 2.9: SDMA–OFDM frame structure

Further, in eq. (2.4), $\mathbf{H} \in \mathbb{C}^{P \times L}$ represents the frequency domain channel matrix, which is expressed as:

$$\mathbf{H} = \begin{bmatrix} H_{1,1} & H_{1,2} & \dots & H_{1,L} \\ H_{2,1} & H_{2,2} & \dots & H_{2,L} \\ \vdots & \vdots & \ddots & \vdots \\ H_{P,1} & H_{P,2} & \dots & H_{P,L} \end{bmatrix} \quad (2.6)$$

where $H_{P,L}$ is the channel gain between the P^{th} receiving antenna and L^{th} user link. The l^{th} ($l=1, 2, \dots, L$) column of channel matrix \mathbf{H} is often referred to as the spatial signature of the l^{th} user across the receive antenna array. Further, the channel link between p^{th} receiving antenna and l^{th} user at each sub-carrier in a multipath channel is expressed as:

$$H_{p,l} = \sum_{m=1}^M h_{p,l}(m) \exp\left(\frac{-i2\pi km}{N_C}\right), \quad k = 1, 2, \dots, N_C, \quad p = 1, 2, \dots, P, \quad l = 1, 2, \dots, L \quad (2.7)$$

where N_C represents the IFFT length, M is number of propagation paths and $h_{p,l}$ is time domain channel gain of link between p^{th} receiving antenna and l^{th} user. The data bit stream \mathbf{b}_l , $l = 1, 2, \dots, L$ of the L mobile users is then encoded by the L independent FEC encoders and interleavers. The resultant coded bit streams \mathbf{b}_l^c are then mapped to higher order modulation

symbols \mathbf{x}_l . The FEC encoder, Interleaver and signal mapper together can often called as Bit Interleaved Coded Modulation (BICM). The higher order symbols \mathbf{x}_l are then modulated by the IFFT based OFDM modulators and transmitted over the MIMO channel. At the receiving end, each of the received symbols (i.e. \mathbf{y}_p , $p=1,2,\dots,P$) is first demodulated using FFT based OFDM demodulator and then forwarded to the multiuser detection block to estimate transmitted symbols $\hat{\mathbf{x}}_l$. These estimated symbols are then converted to bit streams using the signal demapper. The detected bits $\hat{\mathbf{b}}_l^c$ are forwarded to the L independent bit interleavers and FEC decoders to produce detected bit streams $\hat{\mathbf{b}}_l$.

2.4 Wireless MIMO channel characteristics

In a classical wireless transmission scenario, the transmitted signal arrives at the receiver using various paths of different angles and/or different time delays and/or different frequencies. As a result, the received signal power changes in space (due to angle spread) and/or frequency (due to delay spread) and/or time (due to Doppler spread) through the random superposition of the impinging multi-path components. This random changes in signal level is known as multipath fading [93]. This multi-path fading effect predominantly impairs signal transmission in wireless medium and severely influence the quality and reliability of wireless communication. Additionally, the wireless channel is also subjected to some other losses like propagation loss, shadowing and Doppler spread [94]. Hence, designing a wireless channel model considering these affects is an extremely challenging task. Further, the constraints posed by limited power, scarce spectrum and the requirement of high data rate make the channel modeling more complex.

2.4.1 Design of MIMO channels

The design of channel matrix will play a major role to determine the performance of the communication system. Several methods could be considered to approximate the statistics of the channel matrix elements. One of them is to characterize the channel matrix based on geometrical structure of the arrays and the transmit environment. Another way is to use a statistical model of the channel parameters and geographical conditions. The second approach often results a more appropriate. The channel can be modeled in a point-to-point SDMA/MIMO system with L number of transmitting users and P number of receiving antennas under fading channels as [17, 19]:

$$\mathbf{H} = \mathbf{R}_r^{1/2} \mathbf{H}_w \mathbf{R}_t^{1/2} \quad (2.8)$$

\mathbf{H}_w denotes the i.i.d. fading channel with no spatial correlation. The components of \mathbf{H}_w are complex Gaussian random variables with zero mean and unit variance. \mathbf{R}_r and \mathbf{R}_t represent the spatial correlations across the receiving antennas and transmitting antennas respectively, which are modeled as:

$$\mathbf{R}_r = \begin{bmatrix} 1 & \rho_r & \rho_r^{2*} & \cdots & \rho_r^{L-1*} \\ \rho_r & 1 & \rho_r^* & \cdots & \rho_r^{L-2*} \\ \vdots & & \ddots & \ddots & \vdots \\ \rho_r^{L-1} & \rho_r^{L-2} & \rho_r^{L-3} & \cdots & 1 \end{bmatrix}$$

$$\mathbf{R}_t = \begin{bmatrix} 1 & \rho_t & \rho_t^{2*} & \cdots & \rho_t^{L-1*} \\ \rho_t & 1 & \rho_t^* & \cdots & \rho_t^{L-2*} \\ \vdots & & \ddots & \ddots & \vdots \\ \rho_t^{L-1} & \rho_t^{L-2} & \rho_t^{L-3} & \cdots & 1 \end{bmatrix}$$

where ρ_r and ρ_t ($0 \leq \rho_r, \rho_t \leq 1$) are the correlation coefficients at the receiver and the transmitter respectively.

When there is no spatial correlation, that is $\rho_r = \rho_t = 0$, then the resultant channel matrix \mathbf{H} become \mathbf{H}_w . Further, the Hermitian matrices $\mathbf{R}_r^{1/2}$ and $\mathbf{R}_t^{1/2}$ can be decomposed as:

$$\mathbf{R}_r^{1/2} = \mathbf{U}_r \mathbf{\Lambda}_r^{1/2} \mathbf{U}_r^*$$

$$\mathbf{R}_t^{1/2} = \mathbf{U}_t \mathbf{\Lambda}_t^{1/2} \mathbf{U}_t^*$$

where \mathbf{U}_r and \mathbf{U}_t are unitary matrices.

$\mathbf{\Lambda}_r$ and $\mathbf{\Lambda}_t$ are diagonal matrices with diagonal elements (Eigen values) denoted by λ .

2.4.2 MIMO channel capacity

When the channel is unknown at the receiving end with uniform power allocation across all the N_T number of transmitting antennas, then the MIMO channel capacity can be expresses as [21]:

$$C = \log \left| \mathbf{I} + \frac{SNR}{N_T} \mathbf{H} \mathbf{H}^* \right| \quad (2.9)$$

where SNR denotes the signal to noise ratio at the receiver, that is, the transmitter transmits under the constraint $E[\mathbf{x}^* \mathbf{x}] \leq SNR$.

The channel capacity under a uniform power constraint may be express from an Eigen value decomposition of $\mathbf{H}\mathbf{H}^* / N_T$, as:

$$C = \sum_{i=1}^{N_R} \log(1 + SNR \lambda_i) = C(\boldsymbol{\lambda})$$

where $\boldsymbol{\lambda} = [\lambda_1, \lambda_2, \dots, \lambda_{N_R}]$, $\lambda_1 \geq \lambda_2 \geq \dots \geq \lambda_{N_R}$ denotes the Eigen values of $\mathbf{H}\mathbf{H}^* / N_T$ and

N_R represents the number of receiving antennas.

The performance gains of MIMO technology at different antenna configurations with respect to the capacity in bits/s/Hz is shown in Figure 2.10 under Rayleigh fading channel. In this simulation, a highly scattered environment is considered. The Capacity of a MIMO channel with N_T transmit antenna and N_R receive antenna is analyzed. The power in parallel channel is distributed using water-filling algorithm. From this figure, it is observed that at a target receive E_b/N_o value of 15 decibels (dB) the conventional Single Input Single Output (SISO) system, that is, $N_T = 1$ and $N_R = 1$, can provide a data rate up to 5.681 bits/s/Hz. However, while considering $N_T = 4$ and $N_R = 4$, the capacity gets increased to 15.854 bits/s/Hz. This increase in capacity is realized for no additional power or bandwidth expenditure compared to a SISO system.

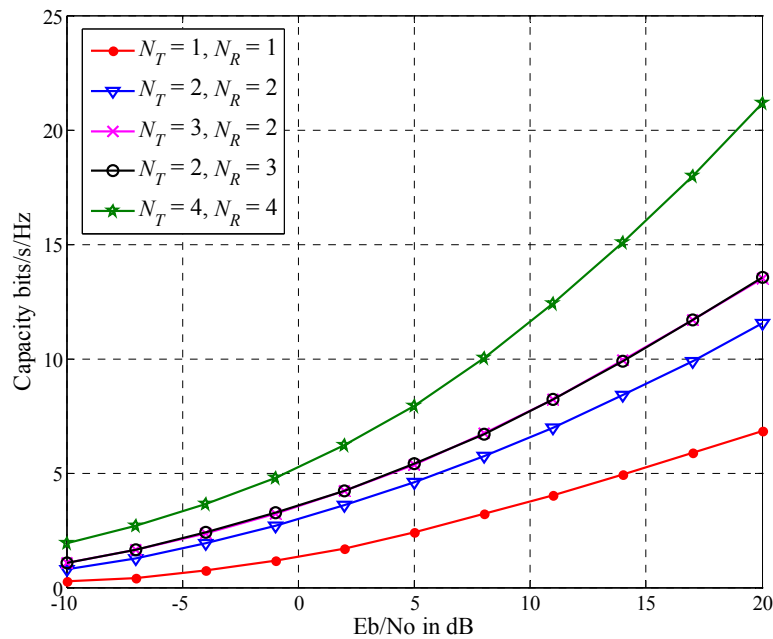


Figure 2.10: Capacity versus E_b/N_o for different antenna configurations

2.4.3 Empirical MIMO channel models

Actual wireless environments are too complex to model accurately. In practice, most simulation studies use empirical models that have been developed based on measurement data taken in various real environments. In order to design an accurate channel model, sufficient knowledge about the characteristics of reflectors, including their placement and movement, and the power of the reflected signal is essential. The channel model may also vary with the antenna configuration along with the number of transmitting and receiving antennas. Different channel models may be valid with respect to their applications in indoor and outdoor environment. Considering all these, several empirical channel models have been developed during the past few decades. Among various contributions, Okumura conducted extensive measurements and developed free space path loss based on the attenuation between base station and mobile stations [106]. This model is further improvised by Hata by means of some empirical data [107]. The Hata model can well approximates the Okumura model for distances greater than 1km. This model is basically proposed for large cells. However, both these models are intended for low frequency applications, that is 150–1500 MHz band. As the demand for high frequency applications is increasing, the European Cooperative for Scientific and Technical (COST) research extended the Hata model to 2 GHz frequency band in COST 231 Model [108]. Simultaneously, Ikegami [109] and Walfisch [110] designed some channel models for urban areas. Further, Erceg characterized channel model for macro cells at 1.9 GHz band [111]. Thus, depending upon channel conditions, different models have been developed.

Considering MIMO applications, in this research, three standard wireless channel models are used for the simulation studies. The channel models investigated throughout this research are MIMO Rayleigh fading [71, 72], Stanford University Interim (SUI) [112] and Shortened Wireless Asynchronous Transfer Mode (SWATM) [30], which are suitable for outdoor, fixed wireless and indoor applications respectively. The detail impulse responses and the statistical parameters of these channel models are discussed in Appendix A. The channel parameters of MIMO Rayleigh fading, SUI and SWATM are presented in Table A.1, Table A.2 and Table A. 3 respectively. Figure 2.11 (a), Figure 2.11 (b) and Figure 2.11 (c) show the frequency response of the channel link between User–1 and Receiving Antenna–1 during transmission of one OFDM frame including the guard symbols, for three different channel conditions. Here, it is shown that the SWATM channel has more deep fades compared to other two because it has more delay spread.

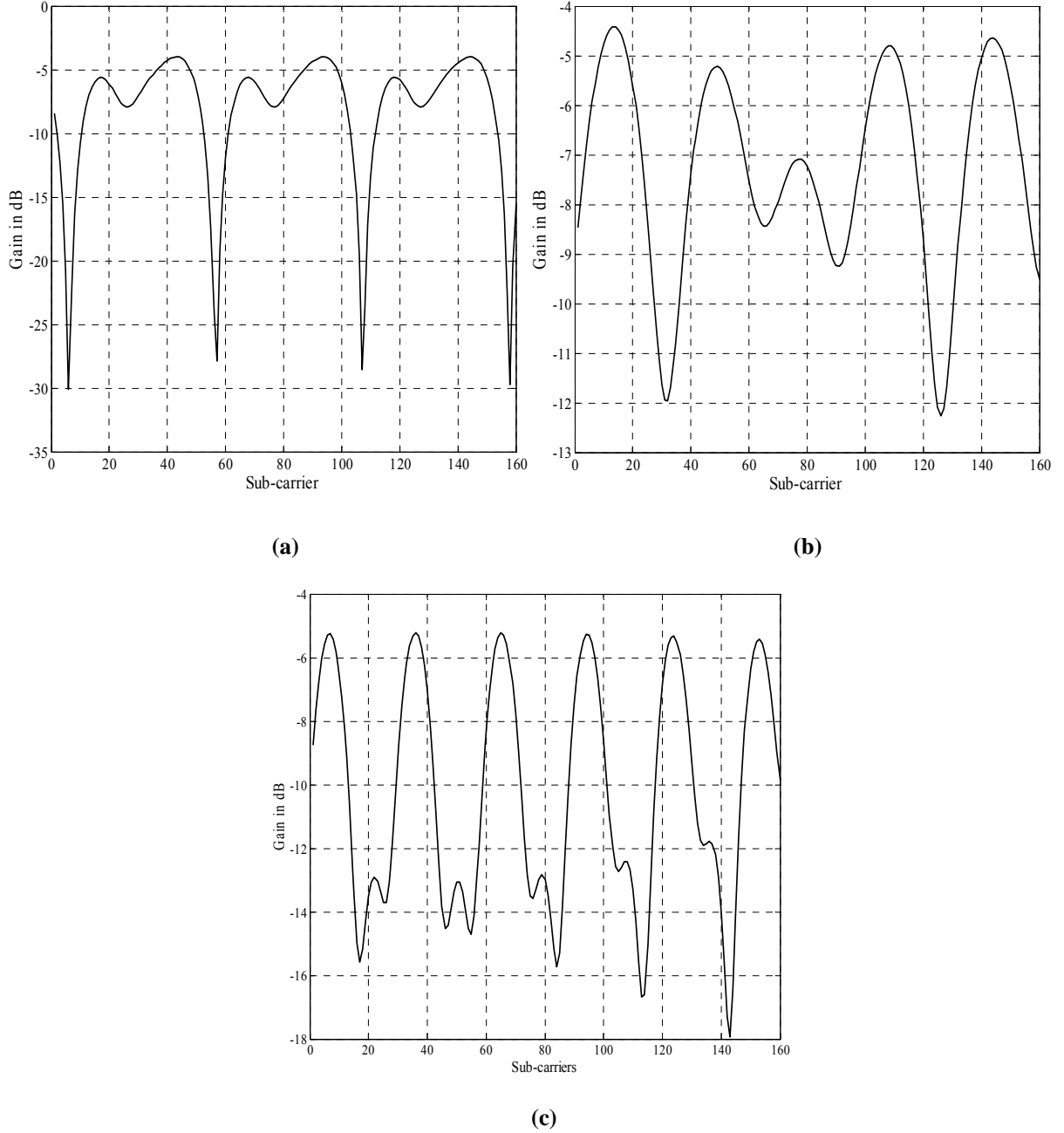


Figure 2.11: Frequency response of channel link between User-1 and Receiving Antenna-1 under various channel conditions (a) MIMO Rayleigh fading (b) SUI (c) SWATM

2.5 MIMO–OFDM channel estimation, a brief overview:

The channel state information can be obtained through training, blind and semi blind channel estimation techniques. The blind channel estimation is based on the statistical information of the channel and certain properties of the transmitted signals [31–35]. The training-based channel estimation is based on the training data (pilots) sent from the transmitter that is known *a priori* at the receiver [36–40]. Though the former has the advantage of not having overhead loss, it is only applicable to slow time-varying channels due to its need for a long

data record. In general, the mobile wireless applications are fast time-varying and hence the training based channel estimation is a preferable one. Further, the semi-blind channel techniques are hybrid of blind and training estimation techniques, which utilizes pilots and other natural constraints to perform channel estimation. This section introduces a brief description about training based channel estimation approach to the MIMO–OFDM system.

Estimation theory is a division of statistical signal processing, which approximates the channel parameters based on the measured data. In the channel estimation theory, as the channel matrix \mathbf{H} is unknown at the receiving end of the SDMA–OFDM system, it should be estimated with training symbols \mathbf{x}_t and its corresponding response symbols \mathbf{y}_t , where the response symbols can be expressed as:

$$\mathbf{y}_t = \mathbf{H}\mathbf{x}_t + \mathbf{n}_t \quad (2.10)$$

where \mathbf{x}_t is the $L \times T_N$ training matrix, \mathbf{n}_t is the $P \times T_N$ noise matrix and \mathbf{y}_t is the $P \times T_N$ response matrix of the training matrix. In the above equation T_N should be more than L ($T_N \geq L$). The most generally used estimation techniques are Least Squares (LS) and Minimum Mean Square Error (MMSE), which are discussed below.

2.5.1 Least Square (LS) estimator

The LS estimator estimates $\hat{\mathbf{H}}$ with an assumption that there is no noise component, that is, $\mathbf{y}_t \approx \hat{\mathbf{H}}\mathbf{x}_t$. The LS estimator minimizes the Euclidean norm of the squared error, that is $\hat{\mathbf{H}}\mathbf{x}_t - \mathbf{y}_t$, which results:

$$\begin{aligned} \|\hat{\mathbf{H}}\mathbf{x}_t - \mathbf{y}_t\|^2 &= (\hat{\mathbf{H}}\mathbf{x}_t - \mathbf{y}_t)^H (\hat{\mathbf{H}}\mathbf{x}_t - \mathbf{y}_t) \\ &= \mathbf{x}_t^H \hat{\mathbf{H}}^H \hat{\mathbf{H}}\mathbf{x}_t - \mathbf{x}_t^H \hat{\mathbf{H}}^H \mathbf{y}_t - \mathbf{y}_t^H \hat{\mathbf{H}}\mathbf{x}_t + \mathbf{y}_t^H \mathbf{y}_t \end{aligned}$$

The minimum of the above equation is found by taking its derivative and equating it to zero, that is:

$$\partial (\mathbf{x}_t^H \hat{\mathbf{H}}^H \hat{\mathbf{H}}\mathbf{x}_t - \mathbf{x}_t^H \hat{\mathbf{H}}^H \mathbf{y}_t - \mathbf{y}_t^H \hat{\mathbf{H}}\mathbf{x}_t + \mathbf{y}_t^H \mathbf{y}_t) / \partial \hat{\mathbf{H}} = 0$$

$$2\mathbf{x}_t^H \mathbf{x}_t \hat{\mathbf{H}} - 2\mathbf{x}_t^H \mathbf{y}_t = 0$$

Therefore, $\hat{\mathbf{H}}_{LS}$ will be given by

$$\hat{\mathbf{H}}_{LS} = (\mathbf{x}_t^H \mathbf{x}_t)^{-1} \mathbf{x}_t^H \mathbf{y}_t \quad (2.11)$$

The term $(\mathbf{x}_t^H \mathbf{x}_t)^{-1} \mathbf{x}_t^H$ is called pseudo-inverse of matrix \mathbf{x}_t , and denoted by \mathbf{x}_t^\dagger .

2.5.2 Minimum Mean Square Error (MMSE) estimator

The MMSE estimator estimates $\hat{\mathbf{H}}$ by minimizing the Mean Square Error (MSE), with a linear combiner. It can be expressed as:

$$\hat{\mathbf{H}}_{MMSE} = \mathbf{A} \mathbf{y}_t \quad (2.12)$$

where \mathbf{A} is obtained so that the $\text{MSE} = E \left[\left| \mathbf{H} - \hat{\mathbf{H}}_{MMSE} \right|^2 \right]$ is minimized.

$$\mathbf{A} = \arg \min_{\mathbf{A}} E \left[\left| \mathbf{H} - \mathbf{A} \mathbf{y}_t \right|^2 \right]$$

The estimation error can be express as:

$$\begin{aligned} \varepsilon &= E \left[(\mathbf{H} - \mathbf{A} \mathbf{y}_t)^H (\mathbf{H} - \mathbf{A} \mathbf{y}_t) \right] \\ &= E \left[\mathbf{H}^H \mathbf{H} - \mathbf{H}^H \mathbf{A} \mathbf{y}_t - \mathbf{y}_t^H \mathbf{A}^H \mathbf{H} + \mathbf{y}_t^H \mathbf{A}^H \mathbf{A} \mathbf{y}_t \right] \\ &= R_H - \mathbf{A} R_{Hy} - \mathbf{A} R_{Hy} + R_y \mathbf{A}^H \mathbf{A} \end{aligned}$$

where R_H is the auto covariance matrix of \mathbf{H} , R_y is the auto covariance matrix of \mathbf{y} and R_{Hy} is the cross covariance matrix between \mathbf{H} and \mathbf{y} . The optimal value of \mathbf{A} can be found from $\partial \varepsilon / \partial \mathbf{A} = 0$.

$$\frac{\partial \varepsilon}{\partial \mathbf{A}} = -2 R_{Hy} + 2 R_y \mathbf{A} = 0$$

$$\mathbf{A} = R_{Hy} R_y^{-1}$$

From eq. (2.12),

$$\mathbf{H}_{MMSE} = R_{Hy} R_y^{-1} \mathbf{y}_t \quad (2.13)$$

$$R_{Hy} = E \left[\mathbf{H} \mathbf{y}^H \right] = E \left[\mathbf{H} (\mathbf{H} \mathbf{x}_t + \mathbf{n}_t)^H \right] = R_H \mathbf{x}_t^H$$

$$\begin{aligned}
 R_y &= E[\mathbf{y}\mathbf{y}^H] = E[(\mathbf{H}\mathbf{x}_t + \mathbf{n}_t)(\mathbf{H}\mathbf{x}_t + \mathbf{n}_t)^H] \\
 &= \mathbf{x}_t R_H \mathbf{x}_t^H + \sigma_n^2 \mathbf{I}_P
 \end{aligned}$$

R_{Hy} and R_y are assumed to be known at the estimator. Then eq. (2.13) will be:

$$\mathbf{H}_{MMSE} = R_H \mathbf{x}_t^H (\mathbf{x}_t R_H \mathbf{x}_t^H + \sigma_n^2 \mathbf{I}_P)^{-1} \mathbf{y}_t \quad (2.14)$$

Figure 2.12 (a) and (b) shows the comparison of frequency response of actual CSI with LS and MMSE estimated channels respectively for a 2×2 SDMA–OFDM system. As shown in this figure, the MMSE estimates more accurate compared to the LS estimator, since it assumes a prior knowledge about the noise and the channel covariance.

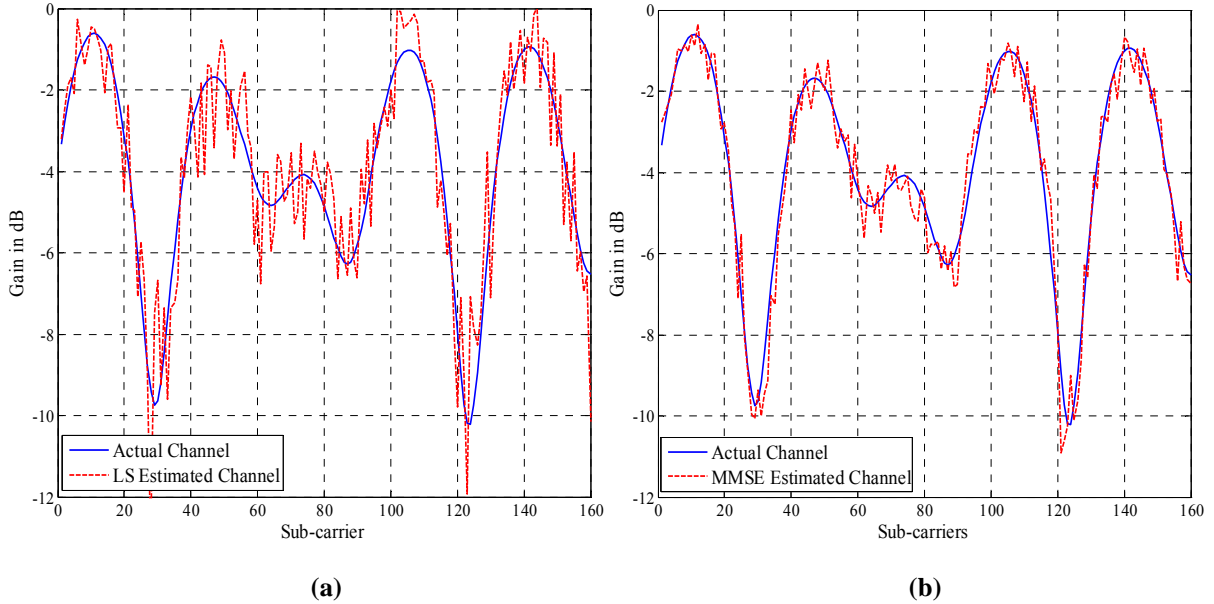


Figure 2.12: Frequency response of the SUI channel link between User-1 and Receiving Antenna-1 using:
 (a) LS estimator (b) MMSE estimator

2.6 Classical Multiuser Detection (MUD) schemes

Multiuser detection is one of the receiver design technology that detects the desired user signal by eliminating noise and interference from neighborhood user's signal. Generally, in SDMA system, the BS receiver often suffers from the multi user interference due to the influence of a strong user signal source on the reception of weak user signal [46]. Several MUD techniques are used to overcome this problem over the last fifteen years [46–72]. Using the multiuser detection process, the estimated signal vector $\hat{\mathbf{x}}$ can be expressed as:

$$\hat{\mathbf{x}} = \mathbf{w}^H \mathbf{y} \quad (2.15)$$

where \mathbf{w} is the $P \times L$ dimension weight matrix. The broad classification of MUD schemes is presented in Figure 2.13.

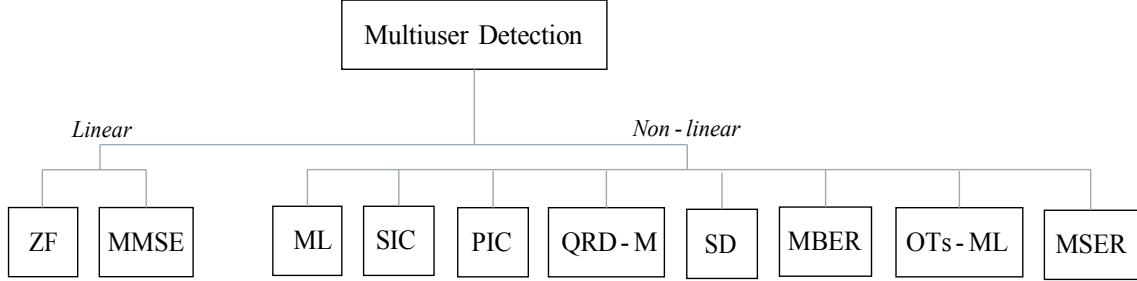


Figure 2.13: Classification of MUD schemes

Descriptions of some of the classical MUDs are given as follows. Among various classical MUD schemes, the linear Zero Forcing (ZF) and Minimum Mean Square Error (MMSE) MUDs exhibit low complexity at the cost of limited performance.

2.6.1 Zero Forcing (ZF) MUD

The ZF MUD scheme involves a linear transformation between the output signal and estimated channel. The transmitted signal is detected from the least square error $\|\mathbf{y} - \mathbf{H}\mathbf{x}\|^2$ as:

$$\begin{aligned} \|\mathbf{y} - \mathbf{H}\mathbf{x}\|^2 &= (\mathbf{y} - \mathbf{H}\mathbf{x})^H (\mathbf{y} - \mathbf{H}\mathbf{x}) \\ &= -2\mathbf{H}^H \mathbf{y} + 2\mathbf{H}^H \mathbf{H}\mathbf{x} \end{aligned}$$

The optimal minima of \mathbf{x} can be obtained from $\partial \|\mathbf{y} - \mathbf{H}\mathbf{x}\|^2 / \partial \mathbf{x} = 0$. Hence,

$$-2\mathbf{H}^H \mathbf{y} + 2\mathbf{H}^H \mathbf{H}\mathbf{x} = 0$$

$$\hat{\mathbf{x}} = (\mathbf{H}^H \mathbf{H})^{-1} \mathbf{H}^H \mathbf{y} \quad (2.16)$$

In the above equation $(\mathbf{H}^H \mathbf{H})^{-1} \mathbf{H}^H = \mathbf{H}^\dagger$, where \mathbf{H}^\dagger is the pseudo inverse of \mathbf{H} .

2.6.2 Minimum Mean Square Error (MMSE) MUD

The linear MMSE MUD scheme assumes a priori knowledge of noise variance and channel covariance. In this MMSE MUD, the weight matrix ' \mathbf{w} ' can be expressed by minimizing the mean square error, i.e. $\text{MSE} = E[|\hat{\mathbf{x}} - \mathbf{x}|^2]$, where $\hat{\mathbf{x}}$ is the estimate of \mathbf{x} . Hence,

$$E\left[|\hat{\mathbf{x}} - \mathbf{x}|^2\right] = E\left[\left(\mathbf{w}^H \mathbf{y} - \mathbf{x}\right)^H \left(\mathbf{w}^H \mathbf{y} - \mathbf{x}\right)\right]$$

The optimal value of \mathbf{w}^H can be obtained from $\partial E\left[|\hat{\mathbf{x}} - \mathbf{x}|^2\right] / \partial \mathbf{w} = 0$. This yield:

$$\mathbf{w}^H = R_{yy}^{-1} R_{yx} \quad (2.17)$$

where $R_{yy} = E\left[\mathbf{y}\mathbf{y}^H\right]$ is the auto covariance of \mathbf{y} and $R_{yx} = E\left[\mathbf{y}\mathbf{x}^H\right]$ is the cross covariance of \mathbf{y} and \mathbf{x} , those are given by [56]:

$$R_{yy} = \left(\mathbf{H}^H \mathbf{H} + \sigma_n^2 \mathbf{I}_P\right) \quad (2.18)$$

$$R_{yx} = \mathbf{H}^H \quad (2.19)$$

Replacing R_{yy} and R_{yx} in eq. (2.17),

$$\begin{aligned} \mathbf{w}^H &= (\mathbf{H}^H \mathbf{H} + 2\sigma_n^2 \mathbf{I}_P)^{-1} \mathbf{H}^H \\ \hat{\mathbf{x}} &= (\mathbf{H}^H \mathbf{H} + 2\sigma_n^2 \mathbf{I}_P)^{-1} \mathbf{H}^H \mathbf{y} \end{aligned} \quad (2.20)$$

where $(.)^H$ indicates Hermitian transpose and \mathbf{I}_P is P -dimensional identity matrix. In the above equation, if SNR is high then σ_n^2 will become negligible. Hence, at higher SNR values the performance of ZF and MMSE MUDs are almost equal.

In general, the received signal contains residual interference which is not Gaussian distributed due to multiuser interference. But these linear detectors assume that the received signal is corrupted by AWGN only. In addition to that, the linear detectors fail to mitigate the nonlinear degradation caused by the wireless radio environment. Hence, the requirement of a non-linear detector is essential to detect users appropriately.

2.6.3 Maximum Likelihood (ML) MUD

The ML detector uses the Maximum a Posteriori (MAP) detection when all the users are equally likely to transmit. The ML detector supporting L simultaneous transmitting users, invokes a total of 2^{mL} metric evaluations in order to detect the possible transmitted symbol vector $\hat{\mathbf{x}}$, where m denotes the number of bits per symbol. This detector calculates the Euclidean distance for all possible transmitted signal vectors and estimates the signals as expressed here [28, 46]:

$$\hat{\mathbf{x}} = \arg \left\{ \min_u \left\| \mathbf{y} - \mathbf{H} \tilde{\mathbf{x}}_u \right\|^2 \right\}, \quad u = 1, 2, \dots, 2^{mL} \quad (2.21)$$

where u is the set of total metric evaluations associated with the specific modulation order and $\tilde{\mathbf{x}}_u = [\tilde{x}_u^1, \dots, \tilde{x}_u^L]^T$, $u = 1, 2, \dots, 2^{mL}$ is a possible transmitted symbol. This optimal detector uses an exhaustive search for finding the most likely transmitted user's signal.

2.6.4 Ordered Successive Interference Cancellation (OSIC) MUD

This algorithm provides improved performance over both the linear ZF and MMSE MUDs at the cost of increased computational complexity [16, 47]. Rather than jointly decoding all users at a time, this nonlinear detection scheme first detects the user with strongest SNR, and cancels its effect from the overall received signal vector. Then, it proceeds to detect the next strongest user. Thus, the iterative detection of the OSIC algorithm is described as follows:

Initialization: Initialize $r = r_1$ at iteration $i=1$

Ordering: The optimal detection order by choosing the row with minimum Euclidian norm (strongest SNR).i.e. most reliable signal is determined.

$$\mathbf{G}_1 = \mathbf{H}^\dagger \quad (\text{For Zero Forcing Receiver})$$

$$\mathbf{G}_1 = (\mathbf{H}^H \mathbf{H} + \sigma_n^2 \mathbf{I}_P)^{-1} \mathbf{H}^H \quad (\text{For MMSE Receiver})$$

$$k_i = \arg \min_l \left\| (\mathbf{G}_i)_l \right\|^2, \quad l = 1, 2, \dots, L$$

Nulling: The strongest transmit signal by nulling out all the weaker transmit signals is estimated.

$$\mathbf{w}_{k_i} = (\mathbf{G}_i)_{k_i}$$

Detection: The transmitted signal identified in the previous step is detected and decision is taken.

$$y_{k_i} = \mathbf{w}_{k_i}^T r_i$$

Slicing: The value of the strongest transmit signal by slicing to the nearest signal constellation value is detected.

$$\hat{a}_{k_i} = Q(y_{k_i})$$

Interference Cancellation: The effect of the detected signal from the received signal vector is cancelled to reduce the detection complexity for the remaining signals, i.e. removing interference from \hat{a}_{k_i} is done.

$$r_{i+1} = r_i - \hat{a}_{k_i} (\mathbf{H})_{k_i}$$

Recursion: $\mathbf{G}_{i+1} = \mathbf{H}_{k_i}^\dagger$ (For Zero Forcing Receiver)

$$\mathbf{G}_{i+1} = (\mathbf{H}_i^H \mathbf{H}_i + \sigma_n^2 \mathbf{I}_L)^{-1} \mathbf{H}_i^H \quad (\text{For MMSE Receiver})$$

$$k_{i+1} = \arg \min_{l \in \{k_1, \dots, k_i\}} \|(\mathbf{G}_{i+1})_l\|^2$$

$$i = i + 1$$

Instead of detecting all users in a sequential manner, the OSIC MUD detects users in an iterative manner. The basic idea of OSIC MUD scheme is based on the principle of removing the effects of the interfering users during each detection stage. Though this detector is a nonlinear one, it has a problem of error propagation, which occurs due to the erroneously detected signals of the previous stages. In order to mitigate the effects of error propagation, design of new nonlinear detector, which detects all users simultaneously rather than detecting iteratively, is suggested.

2.6.5 QR Decomposition –M (QRD–M) MUD

The complexity of ML detection is increases exponentially with the constellation size and the number of users. This drawback can be overcome by decomposing the channel matrix \mathbf{H} in to two separate matrices such that $\mathbf{H} = \mathbf{QR}$, where \mathbf{Q} is a $(P \times P)$ unitary matrix, i.e. $\mathbf{Q}^H \mathbf{Q} = \mathbf{I}$ and \mathbf{R} is $(P \times L)$ upper triangular matrix [51–53]. From eq. (2.4)

$$\mathbf{y} = \mathbf{H}\mathbf{x} + \mathbf{n} = \mathbf{QR}\mathbf{x} + \mathbf{n} \quad (2.22)$$

$$\mathbf{Q}^H \mathbf{y} = \mathbf{R}\mathbf{x} + \mathbf{Q}^H \mathbf{n}$$

$$\tilde{\mathbf{y}} = \mathbf{R}\mathbf{x} + \tilde{\mathbf{n}}$$

$$\begin{bmatrix} \tilde{y}_1 \\ \tilde{y}_2 \\ \vdots \\ \tilde{y}_P \end{bmatrix} = \begin{bmatrix} R_{1,1} & R_{1,2} & \cdots & R_{1,L} \\ 0 & R_{2,2} & \cdots & R_{2,L} \\ \vdots & \vdots & \ddots & \vdots \\ 0 & 0 & \cdots & R_{P,L} \end{bmatrix} \begin{bmatrix} x_1 \\ x_2 \\ \vdots \\ x_L \end{bmatrix} + \begin{bmatrix} \tilde{n}_1 \\ \tilde{n}_2 \\ \vdots \\ \tilde{n}_P \end{bmatrix}$$

where $R_{p,l}$ is the $(p, l)^{\text{th}}$ component of \mathbf{R} . The statistical properties of \mathbf{n} and $\tilde{\mathbf{n}}$ are equal. Therefore, the ML detection problem given in eq. (2.21) can be reformulated as:

$$\begin{aligned}\hat{\mathbf{x}} &= \arg \min_{\mathbf{x}} \{ \|\tilde{\mathbf{y}} - \mathbf{R}\mathbf{x}\| \} \\ &= \arg \min_{\mathbf{x}} \left\{ \sum_{p=1}^L \left| \tilde{y}_p - \sum_{l=p}^L \mathbf{R}_{p,l} \mathbf{x}_l \right|^2 \right\}\end{aligned}$$

In the above expression, $|\cdot|$ denotes the absolute value. Let us assume,

$$d(\hat{\mathbf{x}}) = \sum_{p=1}^L \left| \tilde{y}_p - \sum_{l=p}^L \mathbf{R}_{p,l} \mathbf{x}_l \right|^2 \quad (2.23)$$

Here, d is partial Euclidian distance. When the decision is made on symbols from \mathbf{x}_L to \mathbf{x}_k , $1 \leq k \leq L$, the above expression can be generalized as:

$$d_k(\mathbf{x}) = \sum_{p=k}^L \left| \tilde{y}_p - \sum_{l=p}^L \mathbf{R}_{p,l} \mathbf{x}_l \right|^2 \quad (2.24)$$

where $\mathbf{x} = [\mathbf{x}_k, \mathbf{x}_{k+1}, \dots, \mathbf{x}_L]^T$ of length $L - k + 1$. In order to approach the ML performance, a fairly large ‘ M ’ number of branches are needed to be taken for QRD– M detector. The maximum value of ‘ M ’ can be constellation size of modulation used. For example, in 16–QAM modulated system, M can be taken up to 16. The tree structure using of the QRD– M algorithm for a 4×4 SDMA–OFDM system with 4–QAM is depicted in Figure 2.14. The QRD– M algorithm provides near ML detection performance with comparatively low complexity. It is basically a breadth first tree traversal algorithm. At each detection layer, QRD– M algorithm keeps M reliable nodes instead of deciding the symbol. Detection is done after processing all layers. The concept of QRD– M is basically to apply the tree search in order to detect the symbols in a sequential manner. Starting from the first layer i.e. $i = L$, the algorithm calculates Euclidean distance for all possible values of \hat{y}_i using eq. (2.24). The metrics of these points or nodes are then ordered, and only M nodes with the smallest metrics are retained and the rest of the list is deleted. The same process is applied to the next layer nodes, and this process continues to the last layer i.e. $i = 1$. To achieve near ML detection performance for QRD– M algorithm, M should be large enough for the selected paths to include the correct one. For example in Figure 2.14, the number of stages in the signal tree is

4. The number of survived branches M is equal to 4, and the solid line and solid bold line denotes the searched branch and the survived branch, respectively.

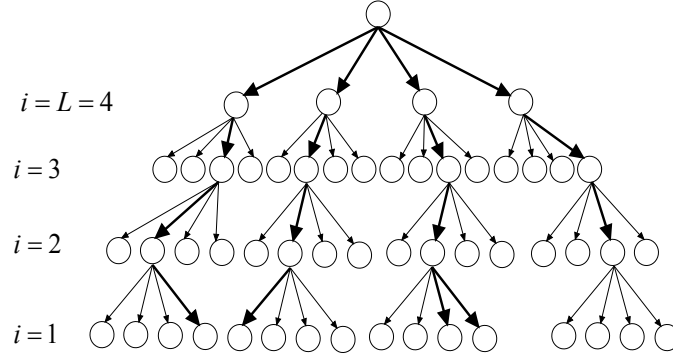


Figure 2.14: Tree structure of QRD- M ($M = 4$) algorithm for 4×4 SDMA–OFDM system with 4-QAM

2.6.6 Minimum Bit Error Rate (MBER) MUD

The MBER technique detects users iteratively by minimizing the probability of error P_E , which is a function of \mathbf{w}_l [63]. Here, \mathbf{w}_l is the weight vector associated with user ' l '. Hence, the user $\hat{\mathbf{x}}_l$ can be determined by:

$$\hat{\mathbf{x}}_l = \mathbf{w}_l^H \mathbf{y} \quad (2.25)$$

The probability of error for BPSK modulation, providing l^{th} users transmitting symbol $b_l \in \{+1, -1\}$, is characterized at the receiver end of the SDMA–OFDM system as:

$$P(\mathbf{w}_l) = \Pr[\text{sgn}(b_l) \Re\{\bar{\mathbf{x}}_l\} < 0]$$

$$\Pr[z_l < 0]$$

where z_l is the decision boundary for BPSK, \Re represents real component and $\bar{\mathbf{x}}_l$ is the estimated symbol of the l^{th} user from the noiseless received symbol $\bar{\mathbf{y}}$, that is,

$$\bar{\mathbf{x}}_l = \mathbf{w}_l^H \bar{\mathbf{y}} \quad (2.26)$$

The Probability Density Function (PDF) of the decision variable z_l for all the possible transmitted symbol vectors, which are Gaussian distributed and equiprobable, is

$$p_{z_l}(z_l; \mathbf{w}_l) = \frac{1}{N_b \sigma_n \sqrt{2\pi} \sqrt{\mathbf{w}_l^H \mathbf{w}_l}} \sum_{k=1}^{N_b} \exp\left(-\frac{z_l - \text{sgn}(b_l^k) \Re(\bar{\mathbf{x}}_l^k)}{2\sigma_n^2 \mathbf{w}_l^H \mathbf{w}_l}\right) \quad (2.27)$$

Here N_b is the number of equiprobable trail vectors. i.e. $N_b=2^L$. The erroneous decision occurs under the area of the PDF in the interval $(-\infty, 0)$ for a real valued transmitted symbol, which is quantified as:

$$P_E(\mathbf{w}_l) = \int_{-\infty}^0 p_{z_l}(z_l; \mathbf{w}_l) dz_l$$

$$\text{Assuming, } t_k = \frac{z_l - \text{sgn}(b_l^k) \Re(\bar{\mathbf{x}}_l^k)}{\sigma_n \sqrt{\mathbf{w}_l^H \mathbf{w}_l}}$$

The probability of error in eq. (2.27) becomes

$$\begin{aligned} P_E(\mathbf{w}_l) &= \frac{1}{N_b \sqrt{2\pi}} \sum_{k=1}^{N_b} \int_{-\infty}^0 \exp\left(-\frac{(t_k)^2}{2}\right) dt_k \\ &= \frac{1}{N_b} \sum_{k=1}^{N_b} Q[c_k(\mathbf{w}_l)] \end{aligned} \quad (2.28)$$

where $c_k(\mathbf{w}_l)$ is given by

$$c_k(\mathbf{w}_l) = \frac{\text{sgn}(b_l^k) \Re(\bar{\mathbf{x}}_l^k)}{\sigma_n \sqrt{\mathbf{w}_l^H \mathbf{w}_l}} = \frac{\text{sgn}(b_l^k) \Re(\mathbf{w}_l^H \bar{\mathbf{y}}_k)}{\sigma_n \sqrt{\mathbf{w}_l^H \mathbf{w}_l}}$$

Finally, The MBER solution from the probability of error is defined as:

$$\mathbf{w}_{l(MBER)} = \arg \min_{\mathbf{w}_l} P_E(\mathbf{w}_l) \quad (2.29)$$

In general, an iterative strategy based on the steepest descent gradient method may be used for finding the MBER solution. According to this method, the linear SDMA MUD's weight vector \mathbf{w}_l is iteratively updated until the specific SDMA MUD weight vector that exhibits the lowest BER is arrived. The MMSE weights may be taken as initial weights. In each step, the weight vector is updated according to a specific step size μ in the direction opposite to the gradient of the BER cost function. The BER is independent of the magnitude of the MUD's weight vector, and hence the knowledge of the orientation of the detector's weight vector is sufficient for defining the decision boundary of the linear MBER detector [63]. The gradient of the cost function is derived as:

$$\nabla_{\mathbf{w}_l} P_E(\mathbf{w}_l) = \frac{1}{N_b \sqrt{2\pi} \sigma_n} \left(\frac{\mathbf{w}_l \mathbf{w}_l^H - \mathbf{w}_l^H \mathbf{w}_l I}{(\mathbf{w}_l^H \mathbf{w}_l)^{3/2}} \right) \sum_{k=1}^{N_b} \exp \left(-\frac{(\Re(\bar{\mathbf{x}}_l^k))^2}{2\sigma_n^2 \mathbf{w}_l^H \mathbf{w}_l} \right) \text{sgn}(b_l^{(k)}) \bar{\mathbf{y}}_k \quad (2.30)$$

The CG algorithm [61] is used for updating the weights, which is summarized as:

Initialization: Choose step size $\eta > 0$ and termination scalar $\beta > 0$. Set iteration $i = 1$.

$$\mathbf{w}_l(i) = (\mathbf{H}\mathbf{H}^H + 2\sigma_n^2 \mathbf{I}_P)^{-1} \mathbf{H}_l \quad (\text{MMSE Weight})$$

$$\mathbf{d}(i) = -\nabla P_E(\mathbf{w}_l(i))$$

Loop: If, $\|\nabla P_E(\mathbf{w}_l(i))\| = \sqrt{(\nabla P_E(\mathbf{w}_l(i)))^T \nabla P_E(\mathbf{w}_l(i))} < \beta$: go to stop else,

$$\mathbf{w}_l(i+1) = \mathbf{w}_l(i) + \eta \mathbf{d}(i) = \frac{\mathbf{w}_l(i+1)}{\|\mathbf{w}_l(i+1)\|}$$

$$\phi_l = \frac{\|\nabla P_E(\mathbf{w}_l(i+1))\|^2}{\|\nabla P_E(\mathbf{w}_l(i))\|^2}$$

$$\mathbf{d}(i+1) = \phi_l \mathbf{d}(i) - \nabla P_E(\mathbf{w}_l(i+1))$$

$i = i+1$, go to *Loop*.

2.6.7 Minimum Symbol Error Rate (MSER) MUD

The MBER MUD mentioned in previous section is basically designed for BPSK modulation scheme, whereas the MSER MUD is developed for detection of square type QAM signals [71, 72]. Let, the symbols of M -QAM are assumed as:

$$S \cong \left\{ s_{m,n} \mid s_{m,n} = z_m + jz_n, 1 \leq m, n \leq \sqrt{M} \right\} \quad (2.31)$$

where $\Re\{s_{m,n}\} = z_m = 2m - \sqrt{M} - 1$ and $\Im\{s_{m,n}\} = z_n = 2n - \sqrt{M} - 1$. Let, \mathbf{x} is a $(L \times N_{sb})$ - dimensional trail vector symbols, where $N_{sb} = 2^{m(L-1)}$, user l of \mathbf{x} is transmitting $z_m + jz_n$ always and rest of the users are transmitting all possible symbols from set ‘ S ’. The PDF of the real-part $\tilde{\mathbf{x}}_{l,R}$, conditioned both on \mathbf{w}_l is a Gaussian mixture and $\mathbf{x}_{l,R} = z_m$ is:

$$f(\tilde{\mathbf{x}}_{l,R} \mid \bar{\mathbf{x}}_{l,R} | \mathbf{x}_l = z_m, \mathbf{w}_l) = \frac{1}{\sqrt{M}} \sum_{n=1}^{\sqrt{M}} f(\tilde{\mathbf{x}}_{l,R} \mid \bar{\mathbf{x}}_{l,R} | \mathbf{x}_l = z_m, \mathbf{w}_l)$$

Here, \bar{x}_l is the estimated symbol of the l^{th} user from the noiseless received symbol \bar{y} . Let, if $z_1 + jz_1$ is transmitted from user l , then the probability of error for the real part of $\tilde{x}_{l,R}$ is characterized by $\tilde{x}_{l,R} < z_1 + 1$, i.e.,

$$P_{E,R}(\mathbf{w}_l)_{|x_{l,R}=z_1} = \int_{z_1+1}^{\infty} f(\tilde{x}_{l,R} | \bar{x}_{l,R}|_{x_{l,R}=z_1}, \mathbf{w}_l) d\tilde{x}_{l,R} \quad (2.32)$$

$$= \frac{1}{2N_{sb}} \sum_{i=1}^{N_{sb}} \text{erfc}[C_{R,i}(\mathbf{w}_l)]$$

where $\text{erfc}(\cdot)$ denotes the complementary error function, and $C_{R,i}(\mathbf{w}_l)$ is defined as:

$$C_{R,i}(\mathbf{w}_l) = \frac{(z_1 + 1) - \bar{x}_{l,R,i}|_{x_{l,R}=z_1}}{\sigma_n \sqrt{\mathbf{w}_l^H \mathbf{w}_l}} \quad (2.33)$$

Due to the symmetry of the symbol set given in eq. (2.31), the probability of error is identical for $\mathbf{x}_{l,R} = z_1$ and $\mathbf{x}_{l,R} = z_{\sqrt{M}}$, and the probability of error for $\mathbf{x}_{l,R} = z_m$, $m = 2, 3, \dots, \sqrt{M} - 1$ is twice that of $\mathbf{x}_{l,R} = z_1$. Since all symbols of M -QAM are equally likely transmitted, the total error probability of the real-part of $\tilde{x}_{l,R}$ is given as:

$$P_{E,R}(\mathbf{w}_l) = \frac{\sqrt{M} - 1}{\sqrt{M} N_{sb}} \sum_{i=1}^{N_{sb}} \text{erfc}[C_{R,i}(\mathbf{w}_l)]$$

In the square type M -QAM modulation, the real and imaginary parts are symmetric each other, hence the total error probability is given by:

$$P_E(\mathbf{w}_l) = 2P_{E,R}(\mathbf{w}_l) - P_{E,R}^2(\mathbf{w}_l) \quad (2.34)$$

Subsequently, the MSER solution $\hat{\mathbf{w}}_{l,MSER}$ is defined as the weight vector that minimizes the SER using $P_E(\mathbf{w}_l)$, which is given by:

$$\hat{\mathbf{w}}_{l,MSER} = \arg \min_{\mathbf{w}_l} P_E(\mathbf{w}_l) \quad (2.35)$$

Similarly, the weight vector for all rest of the users can be evaluated iteratively. After finding weights of all users the transmitted signals can be determined using eq. (2.15).

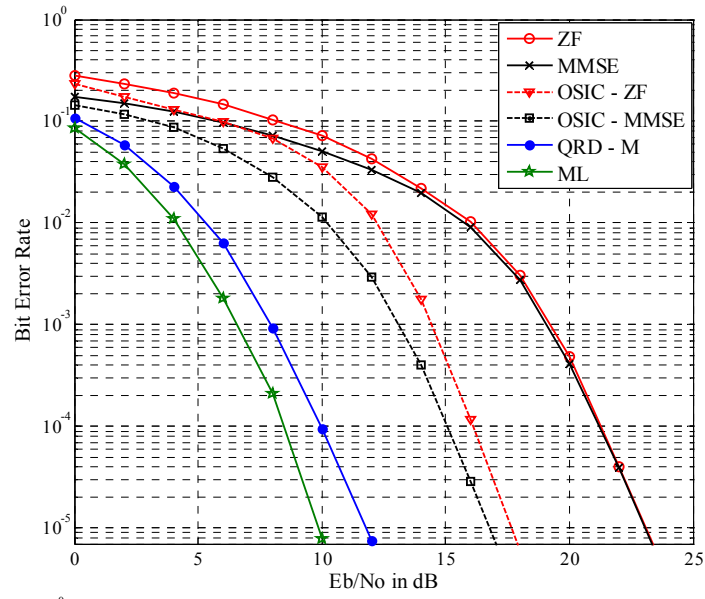
2.7 Simulation study and performance analysis

This section presents simulation study and results by comparing the performances of classical linear and nonlinear MUD techniques in the SDMA–OFDM system. All the classical MUD schemes have been investigated when all the users are transmitting 4–QAM signals. Further, as the MBER MUD is basically designed for BPSK modulation, performance of this detector is investigated when all the users are transmitting BPSK signals. The parameters of the standard wireless channels used in simulation analysis are presented in Appendix A. The performances of these detectors are evaluated with an assumption that the receiver has a perfect knowledge about the statistics of the wireless channel. The rest of the simulation parameters are provided in Table 2.1.

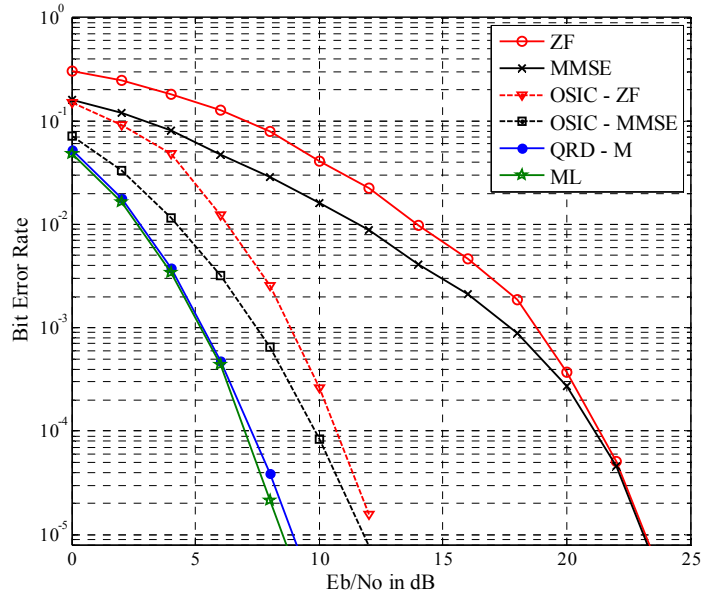
Table 2.1: Basic simulation parameters of the SDMA–OFDM with classical MUDs

Parameters	Value
Number of Sub-carrier	128
Length of Guard Band	32
Number of OFDM Frames	1000
Number of Receiving Antennas (P)	4
Number of Users (L)	4
Conjugate Gradient algorithm	
Learning Rate (η)	0.08
Error Precision (β)	0.0001
Initial condition	MMSE solution
FEC Code	
FEC Scheme	Convolutional code
Code rate	1/2
polynomial	(133, 171)

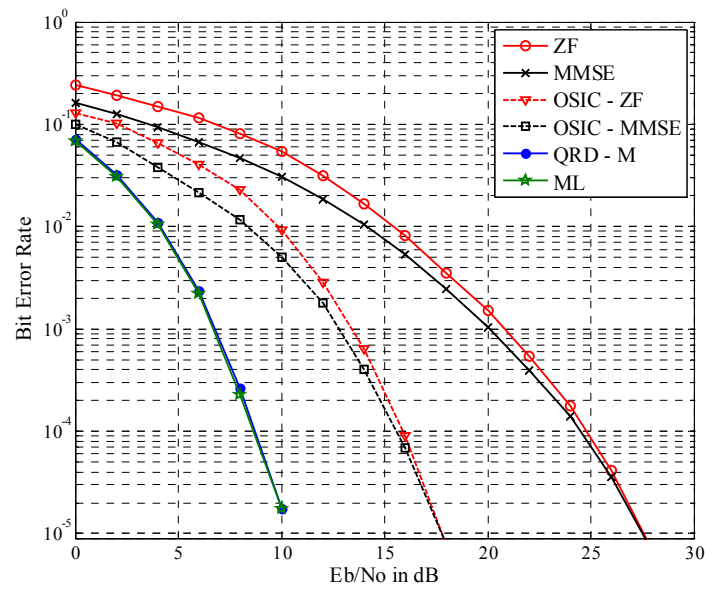
Figure 2.15 shows the average BER performance of all users using various MUD techniques under different channel conditions. It is observed that, the responses of all detectors are varying according to the different channel conditions and their parameters. Here, the maximum delay spread (τ_{\max}) normalized with sampling frequency with respect to MIMO Rayleigh fading, SUI and SWATM channels are 1, 4 and 11.12 respectively. As the resulting ISI is proportional to the τ_{\max} , the channel with high τ_{\max} is subjected to more interference. Hence, the detection in SWATM channel environment as shown in Figure 2.14 (c) while compared to the other two channels is poor.



(a)



(b)



(c)

Figure 2.15: Average BER performance of all users using various classical MUDs under different channel conditions (a) MIMO Rayleigh fading (b) SUI (c) SWATM

It is inferred from the Figure 2.15 that being linear detectors, the ZF and MMSE MUDs cannot mitigate multiuser interference adequately, hence these result in poor BER performance. It is also observed that the performance of ZF and MMSE detectors are almost same at higher SNR values because the noise variance is negligible at higher SNR values. On the other hand, the performance of the ML MUD is optimal as it uses an exhaustive search for finding the most likely transmitted signals. The nonlinear successive ZF and MMSE detectors may outperform the linear ZF and MMSE detectors, but the performance is still sub optimal when compared with ML detector. By incorporating the tree search algorithm based non linear detector such as QRD– M scheme, a significant improvement in performance is noticed and also it is achieving a near optimal performance. The number of survival branches considered in this tree search is four.

The improvement in average BER of all four users while varying number of survived branches of QRD– M detector is shown in Figure 2.16, where the number of survival branches (M) of the QRD– M algorithm is varied from 2 to 4. As the number of reliable nodes increases, the possibility of reaching the optimal solution also increases. Specifically, to maintain BER level of 10^{-4} , the QRD– M with $M = 4$ has around 4.5 dB and 8 dB E_b/N_o gain over the QRD– M with $M = 3$ and 2 respectively, and the QRD– M with $M = 4$ has a performance close to the optimal ML detector.

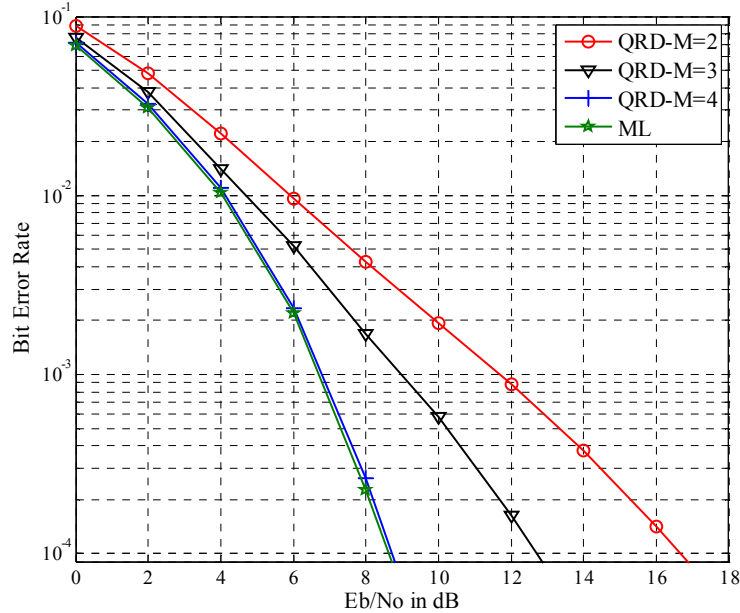


Figure 2.16: Average BER performance of all users using QRD– M detector communicating over the SWATM channel for different number of branches (M)

Though the ML detector is optimal one, the complexity is very intensive as shown in Table 2.2. This table compares the complexity of the optimal ML with near optimal QRD– M

detector on the basis of multiplications, addition and compares operations. This analysis is done considering 1000 OFDM symbols each having 128 subcarriers. From Figure 2.16 and Table 2.2, it is found that the complexity of the QRD– M detector ($M = 4$) is much less and the performance is closed compared to ML detector. Thus, the value of M is to be chosen maintaining a tradeoff between complexity and BER performance.

Table 2.2: Complexity comparison between ML and QRD– M detectors

	ML	QRD- $M=4$	QRD- $M=3$	QRD- $M=2$
Multiplications	4096	164	128	92
Aditions / Subtractions	1004	196	148	100
Compare operations	256	52	40	28

In Figure 2.17, the BER performance of all different users using CG MBER MUD is compared with classical MMSE and ML detectors in the SDMA–OFDM system equipped with four users and four receiving antennas. Parameters of the CG algorithm are given in Table 2.1 [64]. In this figure, it is found that the BER performance of CG MBER MUD is consistently outperforming the MMSE detector as the CG MBER directly minimizes the probability of error. By contrast, as the MMSE MUD minimizes MSE rather than probability of error, it may not give assure minimization of the probability of error. It is observed that, at a 10^{-4} BER level, the CG MBER detector has around 4.5 dB E_b/N_o gain over MMSE one.

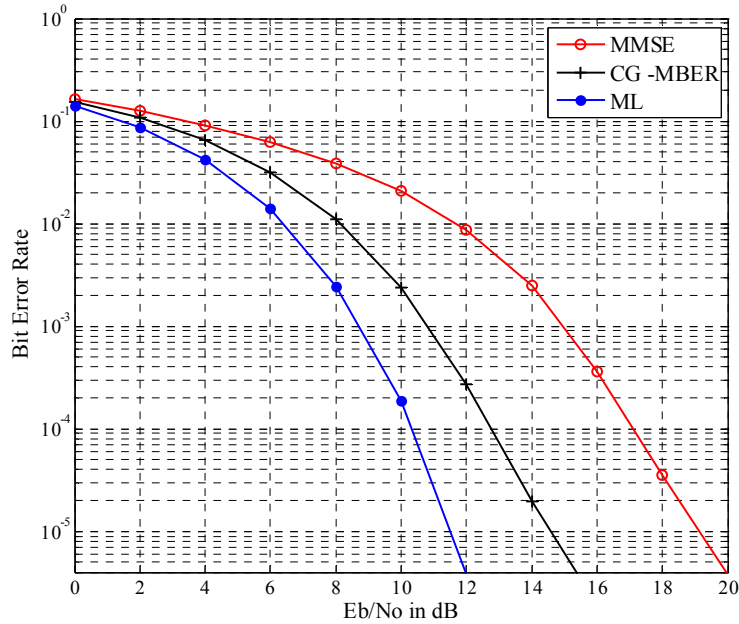
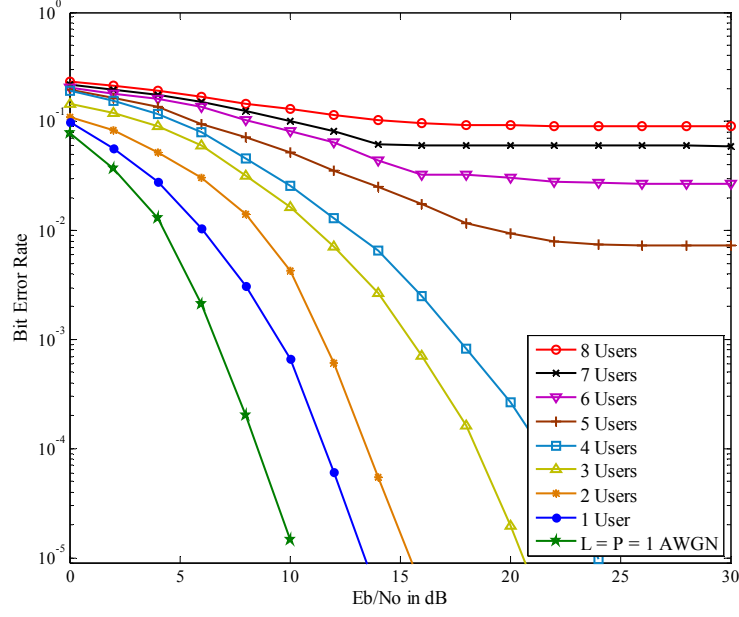
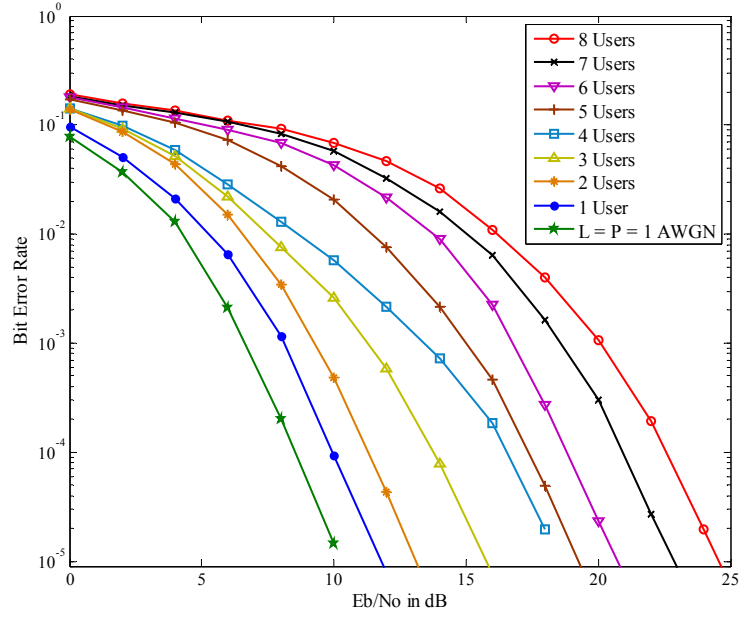


Figure 2.17: Comparison of the average BER performance of all users using MBER MUD with respect to MMSE and ML detectors under MIMO fading channel model



(a)



(b)

Figure 2.18: Average BER performance of all users using the MMSE and CG MBER MUDs in the SDMA–OFDM system equipped with $L = 4$ while varying the numbers of users under the SUI channel condition (a) MMSE MUD (b) CG MBER MUD

As it is required to observe the detector's performance for increasing load condition, the average BER performances of all users using MMSE and CG MBER MUDs are shown in Figure 2.18 (a) and Figure 2.18 (b) respectively. Here, when the SDMA–OFDM system is supporting a different number of users keeping number of receiving antennas fixed at four, the BER performance degrades while the number of users increases due to the additional imposition of the multiuser interference. In the absence of multiuser interference, when only

one user is communicating with four receiving antennas, the performances of MMSE and CG MBER are almost similar and close to the performance of single user–single receiving antenna system communicating over the AWGN channel. However, under multiuser interference environment, the MMSE MUD as shown in Figure 2.18 (a) can only support a maximum number of users that is equal to the number of receiving antennas, which is four in this case. Once the number of users exceeds the number of receiver antennas, the MMSE MUD becomes incapable of differentiating the users, which results in the high residual BER as seen in this figure. By contrast, the MBER MUD performs significantly better since it directly minimizes the probability of error. Hence, it is capable of supporting more users than the number of BS receiver antennas as seen in Figure 2.18 (b).

2.8 Summary:

In this chapter, the basic background of this research work including MIMO system, OFDM scheme and SDMA–OFDM system model is presented. Detection schemes may be invoked for the sake of separating different users at the BS in an uplink SDMA system. Different classical multiuser detection techniques have been introduced. The performance evaluation of all MUD techniques based on simulation study has been carried out over three typical wireless channel environments in order to shown their adaptability and robustness. The advantages and drawbacks of the linear detection techniques like ZF and MMSE along with some nonlinear detection techniques like ML, OSIC, and QRD–M MUD schemes have been explained. It is observed that, the performance the ML detector is optimal at the cost of additional complexity, especially in the context of a high number of users and for higher order modulation schemes. Also, the ZF and MMSE detectors exhibit low complexity at a cost of performance. The nonlinear successive detection technique outperforms the liner techniques, but still its performance is sub-optimal due to error propagation problem. Further, the tree search based QRD–M is achieving near optimal performance with low complexity compared with the optimal ML one. However, all these MUD schemes fail to differentiate users in the critical overload scenario, when the number of users exceed number of BS receiving antenna. Keeping BER minimization rather than MSE as the prime objective, receiver design incorporating MBER MUD has been preferred as this can sustain in overload scenario. The gradient descent algorithm such as CG can be used for updating receiver weights in the MBER MUD scheme. However, as the CG algorithm requires derivative information and the initial solutions of weights. So a new direction of research for optimizing the receiver weights has been proposed in the next chapter.

Chapter 3

Proposed Metaheuristic Optimization Techniques Aided Minimum Error Rate MUD Schemes

As discussed in Chapter–2, the Minimum Error Rate (MER) MUDs such as Minimum Bit Error Rate (MBER) and Minimum Symbol Error Rate (MSER) directly minimize the probability of error rather than MSE. The MER MUDs uses the probability of error function as cost function, which is defined by the receiver weight vector. The weight vector can be adaptively updated using the gradient descent algorithms as discussed in the previous chapter such that the gradient of the probability of error is minimized. The traditional gradient descent methods work on a strategy that generates variations of the design parameters using derivative information. The new parameter is accepted only if it reduces the cost value [62]. This method is sometimes named as the greedy search. The greedy search converges fast but can be trapped by local minima. Besides that, these techniques also require proper selection of initial condition of the weight vectors along with differentiable and continuous cost functions. Another parameter that affects the performance of these techniques is the step size, which is used for updating the receiver weights in the direction opposite to the BER gradient. The choice of this step size must be appropriate. If the step-size is too high it may not allow convergence to the minimum BER level, else if the step size is too low it will require large number of iterations for attaining minimum BER level. These problems can be eliminated by running several vectors simultaneously. This is the principle idea for the family of metaheuristic Optimization Techniques (OTs). A metaheuristic is as an iterative generation process which guides a subordinate heuristic by combining intelligently different concepts for exploring the search space. The OTs does not require derivatives of the cost function and thus can deal with discontinuous cost functions. These techniques update weight vectors from random positions and converge the cost function directly to global minima. Hence, the OTs has been recognized as an effective alternative to gradient search algorithms [63–72]. This chapter suggests the development of new OTs aided MER MUD schemes for SDMA–OFDM system using popular intelligent search algorithms like Adaptive Genetic Algorithm (AGA), Adaptive Differential Evolution Algorithm (ADEA) and Invasive Weed Optimization (IWO).

In order to establish the context and motivation for this research work undertaken clearly, the details of OTs for MBER/MSER MUD schemes are discussed in the following sections. Hence, Section 3.1, Section 3.2 and Section 3.3 elaborate the proposed adaptive GA, adaptive DEA and IWO assisted MBER/MSER MUDs respectively. Section 3.4 presents the details of the simulation study and performance comparison of proposed OTs aided MER detectors with conventional MMSE and ML ones. Finally, this chapter concludes with Section 3.5.

3.1 Adaptive Genetic Algorithm (AGA) aided MER MUD

GA is an optimization algorithm inspired by the well-known biological processes of genetics and evolution. The basic concept of GAs is deliberated according to the principles first laid down by Charles Darwin of survival of the fittest. The idea of evolutionary computing was introduced by Rechenberg in 1960 in his research work “*Evolutionary strategies*”.

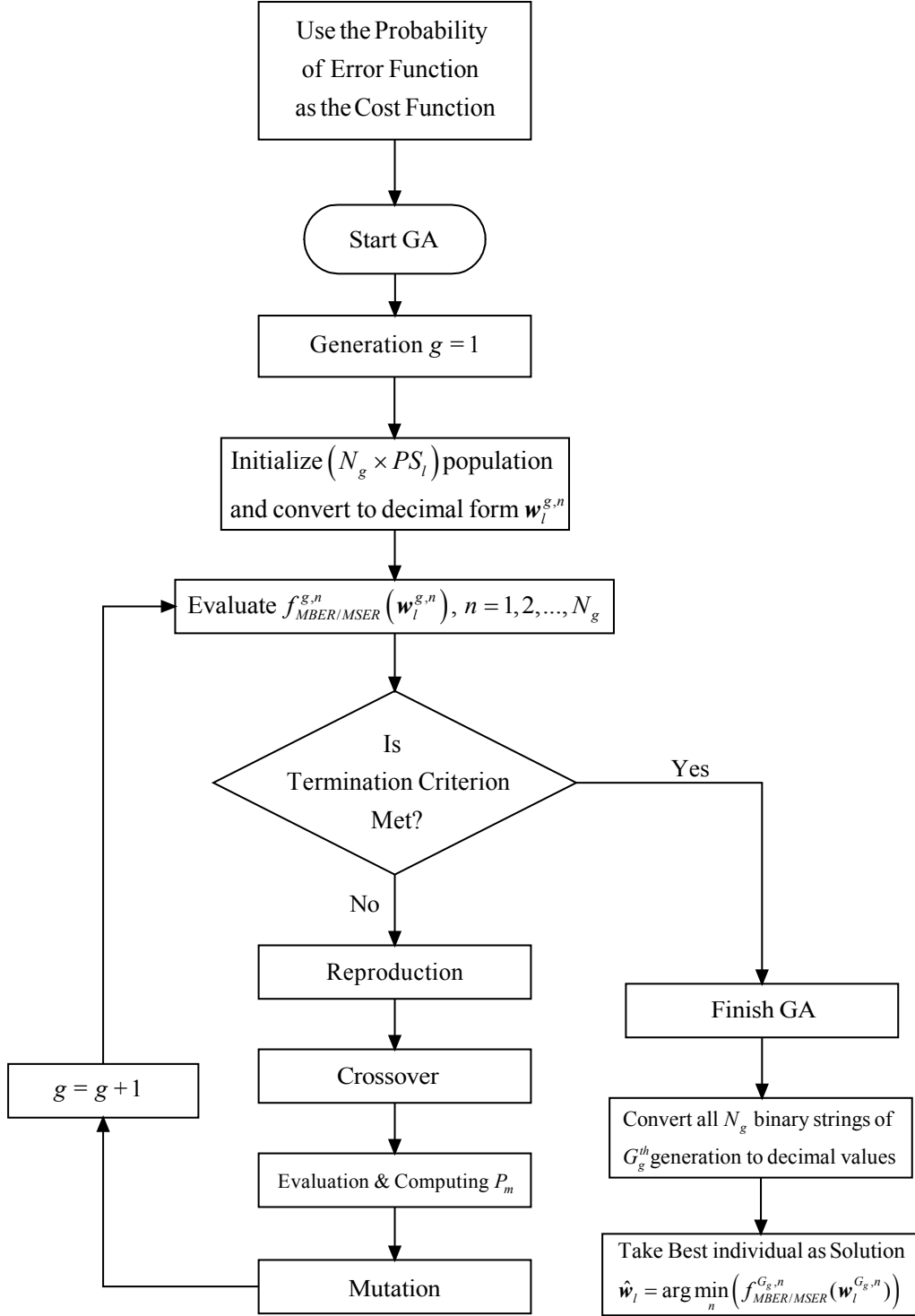


Figure 3.1: Flowchart of the working principle for an adaptive genetic algorithm

Later, Prof. J. Holland introduced the concept of GA in the mid-sixties and published an achievement “Adaptation in Natural and Artificial System” in 1975 [113]. GAs have been widely studied, experimented and applied in many engineering problems such as the area of networking and communication [114–119]. Further, in order to maintain diversity in the population and sustaining the convergence of the GA, some Adaptive GAs (AGAs) are proposed [120–124]. AGA uses three basic operators similar to natural genetic operators such as selection, crossover and mutation. Figure 3.1 shows the flow chart of the AGA employed for the MBER/MSER MUD’s weights optimization. The procedure adopted here for the MBER/MSER MUD’s weights optimization is summarized below.

i. Initialization: The GA algorithm starts with initializing a population containing N_g number of individual chromosomes randomly, where each individual consists of P number of variables or genes. The value of P is selected according to number of receiving antennas equipped in the SDMA–OFDM system. The variable in each population is represented by the fixed length two dimensional binary arrays, which store the real and imaginary part of the receiver’s weight values. Each individual population represents a legitimate solution to the given optimization problem. The solution of MMSE MUD can be included in the initial population for the sake of expediting the search as well as for reducing the complexity of the search. The total population of N_g chromosome, each consisting of P number of variables, can be represented as:

$$Population = \begin{bmatrix} Cr_1 \\ Cr_2 \\ \vdots \\ Cr_{N_g} \end{bmatrix} = \begin{bmatrix} g_{11} & g_{12} & \cdots & g_{1P} \\ g_{21} & g_{22} & \cdots & g_{2P} \\ \vdots & \vdots & \ddots & \vdots \\ g_{N_g 1} & g_{N_g 2} & \cdots & g_{N_g P} \end{bmatrix} \quad (3.1)$$

The p^{th} problem variable or gene is coded in a binary substring of length S_l . The string length of each chromosome is $P \times S_l$. The lower bound and upper bound of the variable g_{np} , $n = 1, 2, \dots, N_g$, $p = 1, 2, \dots, P$ is represented as $g_{min} = (0, 0, \dots, 0)$ and $g_{max} = (1, 1, \dots, 1)$ respectively each of length S_l . Accordingly, the string g_{np} decodes to a solution $w_l^{n,p}$, which denotes p^{th} element of the receiver weight vector for the l^{th} user, as follows:

$$w_l^{n,p} = g_{min} + \frac{g_{max} - g_{min}}{2^{S_l} - 1} \times \text{decoded value of string } g_{np} \quad (3.2)$$

Thus, the decoded n^{th} individual is expressed as $w_l^{g,n} = [w_l^{g,n,1}, w_l^{g,n,2}, \dots, w_l^{g,n,P}]^T$, $n = 1, 2, \dots, N_g$.

ii. *Fitness Evaluation*: Each chromosome is fed to an objective function as the input. The cost or fitness associated with each chromosome is calculated by the objective function one at a time. The cost determines the fitness of an individual in the population. In a cost function minimization problem such as MBER or MSER, a low cost implies a high fitness. The fitness of the n^{th} individual in the g^{th} generation has been evaluated respectively for the MBER and MSER MUDs as follows:

$$f_{\text{MBER}}^{g,n}(\mathbf{w}_l^{g,n}) = \frac{1}{N_b} \sum_{k=1}^{N_b} \mathcal{Q} \left[\frac{\text{sgn}(b_l^k) \Re \left((\mathbf{w}_l^{g,n})^H \bar{\mathbf{y}}_k \right)}{\sigma_n \sqrt{(\mathbf{w}_l^{g,n})^H \mathbf{w}_l^{g,n}}} \right] \quad (3.3)$$

$$f_{\text{MSER}}^{g,n}(\mathbf{w}_l^{g,n}) = 2P_{E,R}(\mathbf{w}_l^{g,n}) - P_{E,R}^2(\mathbf{w}_l^{g,n}),$$

$$\text{where } P_{E,R}(\mathbf{w}_l^{g,n}) = \frac{\sqrt{M}-1}{\sqrt{M}N_{sb}} \sum_{i=1}^{N_{sb}} \text{erfc} \left[\frac{(z_1+1) - \bar{\mathbf{x}}_{l,R,i} |x_{l,R}=z_1|}{\sigma_n \sqrt{(\mathbf{w}_l^{g,n})^H \mathbf{w}_l^{g,n}}} \right] \quad (3.4)$$

Here, all the notations are according to eq. (2.29) and (2.34) as discussed in Chapter 2.

iii. *Natural Selection*: In this step, only the healthiest members of the population are allowed to survive and proceed to the next generation while discarding the rest. In this approach, the cost values are sorted in order to determine the relative fitness of the chromosomes.

iv. *Mate Selection*: This operation usually selects the healthy strings in a population and forms a mating pool. The commonly used reproduction operator is the fitness proportionate selection operator, where a chromosome in the current population is selected with probability proportional to the chromosome's cost value. Thus, the n^{th} chromosome in the current population is selected with a probability proportional to p_n . In a simple GA, the population size is usually kept fixed, hence the cumulative probability for all chromosome in the population must be one. Therefore, the probability for selecting n^{th} chromosome in the MBER/MSER problem is:

$$p_{\text{MBER/MSER}}^{g,n} = \frac{1/f_{\text{MBER/MSER}}^{g,n}}{\sum_{n=1}^{N_g} f_{\text{MBER/MSER}}^{g,n}} \quad (3.5)$$

The Roulette Wheel selection criterion is the most commonly used algorithm for mate selection [64]. The Roulette Wheel assigns a probability for each chromosome on the basis of

its cost. The chromosomes with low costs have a higher chance of being selected than the higher cost ones. The selected chromosomes are considered as parents for reproduction.

v. *Adaptive Cross-over and Mutation*: Crossover is applied to the mating pool with an expectation that the possibility of good solutions can generated by the better individual. The main aim of the crossover operation is to exploit the search space. This operation is performed by swapping some parts of two parent chromosomes with a fixed crossover probability P_c and produce offsprings. In a single-point crossover operator, both parental chromosomes are split at a randomly determined crossover point and a new offspring is created by appending the second part of the second parent to the first part of the first parent. The role of mutation in GAs has been that of restoring lost or unexplored genetic material into the population to prevent the premature convergence. A binary mutation changes a one to a zero or a zero to a one with a small fixed mutation probability P_m . For example, 00000 \rightarrow 00010. In this example, fourth gene has changed its value, thereby creating a new solution. The need for mutation is to maintain diversity in population.

The classical GA uses fixed values of P_c and P_m . If these values are low, then the GA search strategy requires large number of generations otherwise if these values are high it may cause the disruption of the near optimal solutions when a population is at the verge of approaching a globally optimal solution. In contrast, the adaptive GA chooses lower values of P_c and P_m for low fitness solutions and higher values of P_c and P_m for high fitness solutions automatically [120]. The high fitness solutions help in faster convergence of the GA while the low fitness solutions prevent the GA from getting stuck at a local optimum. As the MER MUDs are the cost function minimization problems, the convergence of the population to the optimum solution can be obtained through the minimization of $f^{g,avg} - f^{g,min}$, where $f^{g,avg}$ and $f^{g,min}$ denote the best and average fitness values of the current generation respectively. Thus, the adaptive crossover and mutation rates are described below:

$$P_c = \begin{cases} k_1 (f^{g,best} - f^{g,min}) / (f^{g,avg} - f^{g,min}) & \text{if } f^{g,best} \leq f^{g,avg}, \\ k_2 & \text{otherwise,} \end{cases} \quad (3.6)$$

$$P_m = \begin{cases} k_3 (f^{g,n} - f^{g,min}) / (f^{g,avg} - f^{g,min}) & \text{if } f^{g,n} \leq f^{g,avg}, \\ k_4 & \text{otherwise,} \end{cases} \quad (3.7)$$

Here, $f^{g,best}$ is the lower fitness value of the parent ones to be crossed in the g^{th} generation. The constants k_1 , k_2 , k_3 and k_4 are chosen as 0.5, 0.5, 0.05 and 0.05 respectively [119].

vi. *Elitism*: After creating new population by crossover and mutation operations, we have a chance to lose the best chromosome from the present population. Elitism is an operator that copies the best chromosome (or a few best chromosomes) in the present population to the new one.

This evolution process will be repeated from selection phase until the termination criterion is met. The termination criterion may be either attainment maximum number of generations (G_g) or obtaining minimum acceptable fitness value.

vii. *Optimal Solution*: After meeting termination criterion, the best individual having minimum fitness value is taken as the optimized weight vector of user l . From this optimal solution, the user symbol is estimated as:

$$\hat{\mathbf{w}}_l = \arg \min_n \left(\int_{MBER/MSER}^{G_g, n} (\mathbf{w}_l^{G_g, n}) \right), \quad n = 1, 2, \dots, N_g \quad (3.8)$$

$$\hat{\mathbf{x}}_l = \hat{\mathbf{w}}_l^H \mathbf{y} \quad (3.9)$$

Similarly, the entire optimization process is repeated for remaining $(L - 1)$ users.

3.2 Adaptive Differential Evolution Algorithm (ADEA) aided MER MUD

The Differential Evaluation Algorithm (DEA) algorithm is another popular population based algorithm like GA that uses the similar operators such as crossover, mutation, selection, and reproduction to locate global optima. The DEA has a computational flexibility compared to GA as it defines individual variables in a decimal format rather than in a binary form. The main difference in finding optimal solutions is that GAs depends on crossover operation while DEA depends on mutation operation. This algorithm mainly has three advantages such as finding the true global optima regardless of the initial parameter values, fast convergence and using a few control parameters. The DEA is first proposed by Storn [125]. It has been applied to several Antenna design problems [126–129]. Further, the DEA is modified to Adaptive DEA (ADEA) by incorporating a self-adaptive mechanism to adjust the control parameters during the evolutionary process [130–134]. Figure 3.2 shows the flow chart of the ADEA employed for the MBER/MSER MUD's weight optimization. The procedure adopted here for the MBER/MSER MUD's weights optimization is summarized below.

Initialization: DEA begins its search from a randomly initialized population containing N_d individuals each consisting P number of variables. The n^{th} individual of the population in the g^{th} generation is expressed as:

$$\mathbf{w}_l^{g,n} = [\mathbf{w}_l^{g,n,1}, \mathbf{w}_l^{g,n,2}, \dots, \mathbf{w}_l^{g,n,P}]^T, \quad n = 1, 2, \dots, N_d, \quad g = 1, 2, \dots, G_d \quad (3.10)$$

where, the index l refers to user and P is the number of receiving antennas. The first individual has been taken from the solution of MMSE MUD. i.e. $\mathbf{w}_l^{1,1} = \hat{\mathbf{w}}_l^{MMSE}$.

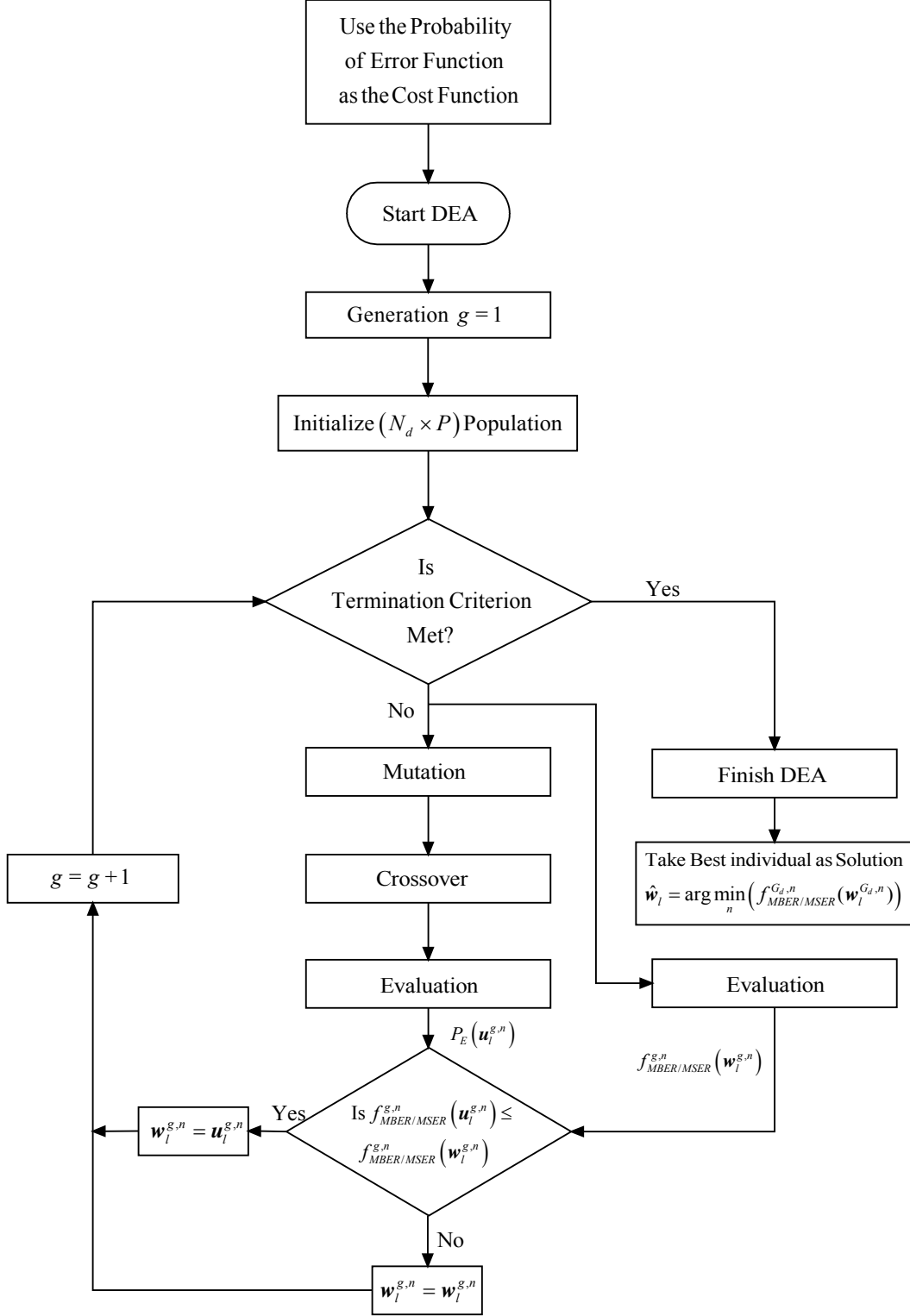


Figure 3.2: Flowchart of working principle for an adaptive differential evolution algorithm

i. Adaptive Mutation and crossover: The DEA uses mutation operation as a search mechanism to increase the search space with the aid of a fixed mutation factor F . This algorithm depends on the population in perturbing the candidate solutions by adding an appropriately scaled and randomly selected difference vector to the actual population vector. This can be expressed by combining three different randomly chosen vectors to produce a mutant vector using the adaptive mutation factor, which is according to:

$$\mathbf{v}_l^{g,n} = \mathbf{w}_l^{g,r_1} + F(\mathbf{w}_l^{g,r_2} - \mathbf{w}_l^{g,r_3}) \quad (3.11)$$

where the random indexes are integers, mutually different and $r_1, r_2, r_3 \in \{1, 2, \dots, N_d\}$. The randomly chosen integers r_1, r_2 and r_3 are also taken to be different from the running index n . The mutation factor $F \in (0, 1]$ is a positive real-valued number and its controls the amplification of the differential variation $(\mathbf{w}_l^{g,r_2} - \mathbf{w}_l^{g,r_3})$.

In order to increase the diversity of the perturbed parameter vectors, crossover is introduced. The crossover operator generates a trial vector by restoring certain parameters of the target vector with the resultant parameters of a randomly selected donor vector. This algorithm also uses a non-uniform crossover that can take child vector variables from one parent more often than it does from others. The crossover operator efficiently shuffles information with a fixed crossover probability $C_p \in (0, 1]$ about successful combinations to enable the search for a better solution space. The p^{th} variable of the n^{th} individual in the population at the g^{th} generation is given by:

$$\mathbf{u}_l^{g,n,p} = \begin{cases} \mathbf{v}_l^{g,n,p} & \text{rand}_p(0, 1) \leq C_p \text{ or } p = p_{rand}, \\ \mathbf{w}_l^{g,n,p} & \text{otherwise.} \end{cases} \quad (3.12)$$

where $\text{rand}_p \in [0, 1]$ is the p^{th} evaluation of an uniform random number and p_{rand} is a randomly chosen index $\in 1, 2, \dots, P$ which ensures that $\mathbf{u}_l^{g,n,p}$ gets at least one parameter from $\mathbf{v}_l^{g,n,p}$.

The adaptive DEAs uses a self-adaptive control mechanism, which changes the mutation factor F and crossover probability C_p during each evolution or generation in order to achieve best performance with high convergence speed [130]. The self-adaptive control parameters F^{g+1} and C_p^{g+1} are calculated at generation $g + 1$ as follows:

$$F^{g+1} = \begin{cases} F_1 + rand_1 F_2 & \text{if } rand_2 < \tau_1, \\ F^g & \text{otherwise,} \end{cases} \quad (3.13)$$

$$C_p^{g+1} = \begin{cases} rand_3 & \text{if } rand_4 < \tau_2, \\ C_p^g & \text{otherwise,} \end{cases} \quad (3.14)$$

where $rand_j, j \in \{1, 2, 3, 4\}$, are uniform pseudo-random values $\in [0, 1]$, τ_1 and τ_2 are constants that represent the probabilities to adjust F and C_p respectively. τ_1, τ_2, F_1 and F_2 are assigned with fixed values of 0.1, 0.1, 0.1 and 0.9, respectively according to [130]. The new F takes value from $[0.1, 1.0]$ and the new C_p from $[0, 1]$ randomly. The control parameter values F^{g+1} and C_p^{g+1} are obtained before the mutation operation is performed as they influence the mutation, crossover, and selection operations of the new population vector.

ii. *Fitness Evaluation*: Each individual of the both population sets $\mathbf{w}_l^{g,n}$ and $\mathbf{u}_l^{g,n}$ is fed to an objective function as input. The fitness value determines the fitness of those individuals in the population. The fitness of the n^{th} individual in the g^{th} generation of $\mathbf{w}_l^{g,n}$ and $\mathbf{u}_l^{g,n}$ for the MBER MUD has been evaluated as:

$$f_{\mathbf{w}_{MBER}^{g,n}} = \frac{1}{N_b} \sum_{k=1}^{N_b} \mathcal{Q} \left[\frac{\text{sgn}(b_l^k) \Re \left((\mathbf{w}_l^{g,n})^H \bar{\mathbf{y}}_k \right)}{\sigma_n \sqrt{(\mathbf{w}_l^{g,n})^H \mathbf{w}_l^{g,n}}} \right] \quad (3.15)$$

$$f_{\mathbf{u}_{MBER}^{g,n}} = \frac{1}{N_b} \sum_{k=1}^{N_b} \mathcal{Q} \left[\frac{\text{sgn}(b_l^k) \Re \left((\mathbf{u}_l^{g,n})^H \bar{\mathbf{y}}_k \right)}{\sigma_n \sqrt{(\mathbf{u}_l^{g,n})^H \mathbf{u}_l^{g,n}}} \right] \quad (3.16)$$

Similarly, the fitness of the n^{th} individual in the g^{th} generation of $\mathbf{w}_l^{g,n}$ and $\mathbf{u}_l^{g,n}$ for the MSER MUD has been evaluated as:

$$f_{\mathbf{w}_{MSER}^{g,n}} = 2P_{E,R}(\mathbf{w}_l^{g,n}) - P_{E,R}^2(\mathbf{w}_l^{g,n}), \text{ where } P_{E,R}(\mathbf{w}_l^{g,n}) = \frac{\sqrt{M}-1}{\sqrt{M}N_{sb}} \sum_{i=1}^{N_{sb}} \text{erfc} \left[\frac{(z_1+1) - \bar{\mathbf{x}}_{l,R,i} |x_{l,R}=z_1|}{\sigma_n \sqrt{(\mathbf{w}_l^{g,n})^H \mathbf{w}_l^{g,n}}} \right] \quad (3.17)$$

$$f_{\mathbf{u}_{MSER}^{g,n}} = 2P_{E,R}(\mathbf{u}_l^{g,n}) - P_{E,R}^2(\mathbf{u}_l^{g,n}), \text{ where } P_{E,R}(\mathbf{u}_l^{g,n}) = \frac{\sqrt{M}-1}{\sqrt{M}N_{sb}} \sum_{i=1}^{N_{sb}} \text{erfc} \left[\frac{(z_1+1) - \bar{\mathbf{x}}_{l,R,i} |x_{l,R}=z_1|}{\sigma_n \sqrt{(\mathbf{u}_l^{g,n})^H \mathbf{u}_l^{g,n}}} \right] \quad (3.18)$$

Here, all the notations are according to eq. (2.29) and (2.34) as discussed in Chapter 2.

iii. *Selection*: In order to keep the fixed population throughout all generations, the selection operator compares the cost function performance of the target vector $\mathbf{w}_l^{g,n}$ with the trial vector $\mathbf{u}_l^{g,n}$ and better one is carried to the next generation. If the target vector is still better, it is retained in the population. More specifically, the selection procedure may be described as:

$$\mathbf{w}_l^{g+1,n} = \begin{cases} \mathbf{u}_l^{g,n} & f\mathbf{u}_{MBER/MSER}^{g,n} \leq f\mathbf{w}_{MBER/MSER}^{g,n} \\ \mathbf{w}_l^{g,n} & \text{otherwise.} \end{cases} \quad (3.19)$$

The entire process will be repeated from mutation phase until the termination criterion is met. The termination criterion may be either attainment maximum number of generations (G_d) or obtaining minimum acceptable fitness value.

iv. *Optimal Solution*: After meeting termination criterion, the best individual having minimum fitness value is taken as the optimized weight vector of user l . From this optimal solution, the user symbol is estimated as:

$$\hat{\mathbf{w}}_l = \arg \min_n \left(P_E(\mathbf{w}_l^{G_d,n}) \right), \quad n = 1, 2, \dots, N_d \quad (3.20)$$

$$\hat{\mathbf{x}}_l = \hat{\mathbf{w}}_l^H \mathbf{y} \quad (3.21)$$

Similarly, the entire optimization process is repeated for finding the optimal weight vectors of the remaining $(L - 1)$ users.

3.3 Invasive Weed Optimization (IWO) aided MER MUD¹

In recent times, the research of developing optimization algorithms is carrying out by inspiring from ecological phenomena. The IWO algorithm is also such an algorithm proposed by Mehrabian et al. [135]. The IWO algorithm has become good alternative to the other optimization algorithms due to its fast convergence and its affordable complexity in a number of different application domains. This algorithm is already applied efficiently in several antenna design problems [136–139]. This algorithm is basically motivated from a common phenomenon in agriculture that the colonization of invasive weeds. The term weed refers to a robust wild plant that grows in gardens or fields of crops and prevents the growth of actual plant. The basic steps involved to model and simulate IWO algorithm are initialization, reproduction, spatial distribution and competitive exclusion.

¹This part of research is included in the paper published by *International Journal of Communication Systems, Wiley*, entitled as “Minimum Symbol Error Rate Multiuser Detection Using an Effective Invasive Weed Optimization for MIMO/SDMA–OFDM System”

The IWO allows all of the individuals to participate in the reproduction process. Sometimes, it is also possible that some of the individuals with the lower fitness carry more useful information than the fitter ones. This algorithm, gives a chance to the less fit plants to reproduce and if the seeds produced by them have good fitnesses in the colony, they can survive. Fitter individuals produce more seeds than less fit individuals, which tends to improve the convergence of the algorithm. Hence, the IWO algorithm can be efficiently used for determining optimal solution in MER MUD scheme [140]. Figure 3.3 shows the flow chart of the IWO employed for the MBER/MSER MUD's weights optimization. The process of this optimization technique for determining weight vector of User- l is summarized below.

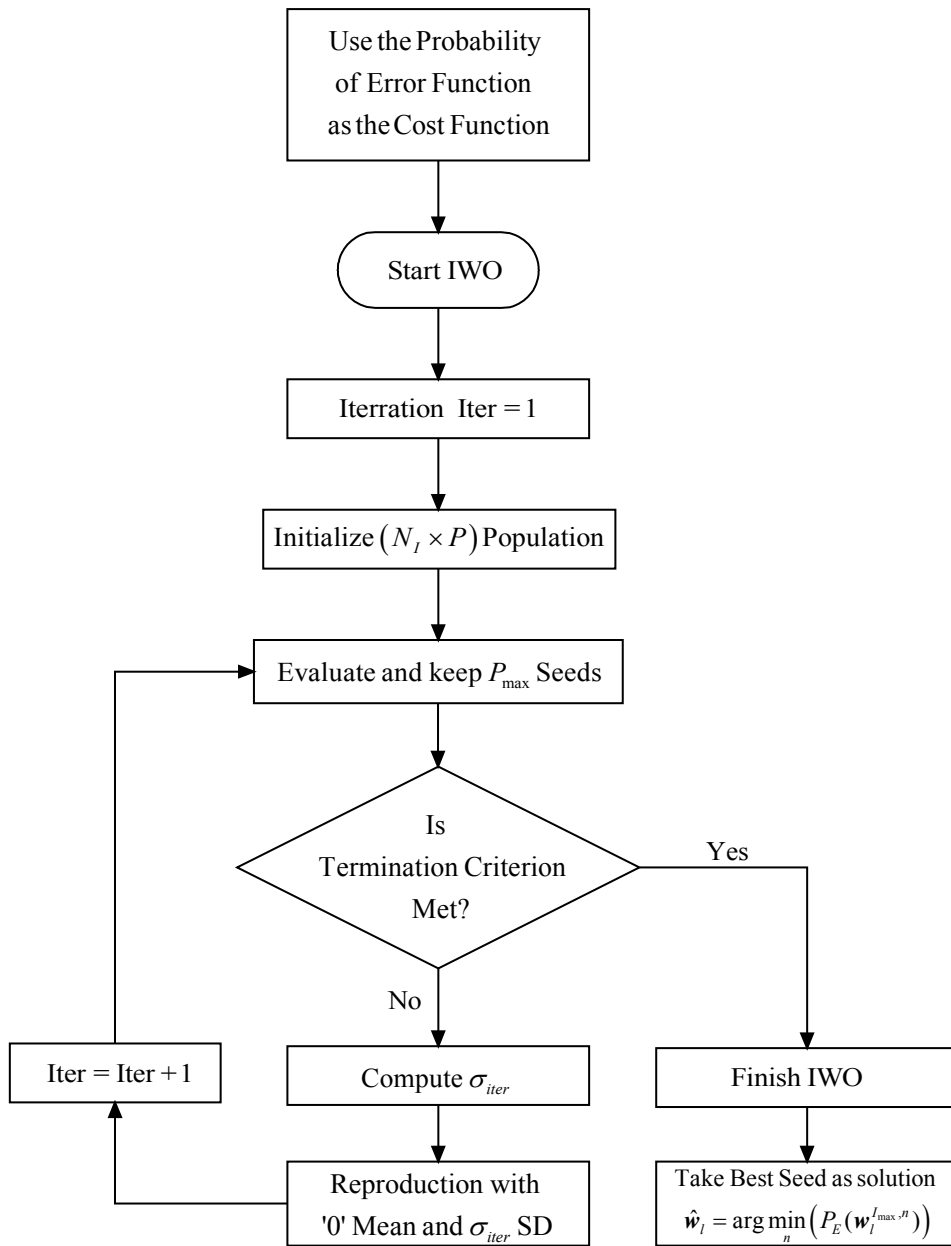


Figure 3.3: Flowchart of working principle for an invasive weed optimization algorithm

i. *Initialization*: The initial population containing N_I individuals each consisting P number of variables is generated randomly. The n^{th} individual in the population of i^{th} iteration is represented as $\hat{\mathbf{w}}_l^{i,n} = [\hat{\mathbf{w}}_l^{i,n,1}, \hat{\mathbf{w}}_l^{i,n,2}, \dots, \hat{\mathbf{w}}_l^{i,n,P}]^T$, where P is the number of receiving antennas in the SDMA–OFDM system. Each individual in the population is a complex decimal array rather than a binary array as used in GA. In the initial population, the solution of the MMSE MUD is included for the sake of prompt search. i.e. $\mathbf{w}_l^{1,1} = \hat{\mathbf{w}}_l^{MMSE}$.

ii. *Fitness Evaluation*: Each individual will be assigned with its corresponding fitness value, which is obtained from the fitness function, and become a plant. The fitness of the n^{th} individual in the i^{th} iteration has been evaluated respectively for the MBER and MSER MUDs as:

$$f_{MBER}^{i,n} = \frac{1}{N_b} \sum_{k=1}^{N_b} \mathcal{Q} \left[\frac{\text{sgn}(b_l^k) \Re \left((\mathbf{w}_l^{i,n})^H \bar{\mathbf{y}}_k \right)}{\sigma_n \sqrt{(\mathbf{w}_l^{i,n})^H \mathbf{w}_l^{i,n}}} \right] \quad (3.22)$$

$$f_{MSER}^{i,n} = 2P_{E,R}(\mathbf{w}_l^{i,n}) - P_{E,R}^2(\mathbf{w}_l^{i,n}), \text{ where } P_{E,R}(\mathbf{w}_l^{i,n}) = \frac{\sqrt{M}-1}{\sqrt{M}N_{sb}} \sum_{i=1}^{N_{sb}} \text{erfc} \left[\frac{(z_1+1) - \bar{\mathbf{x}}_{l,R,i} | \mathbf{x}_{l,R} = z_1}{\sigma_n \sqrt{(\mathbf{w}_l^{i,n})^H \mathbf{w}_l^{i,n}}} \right] \quad (3.23)$$

Here, all the notations are according to eq. (2.29) and (2.34) as discussed in Chapter 2.

Reproduction and spatial dispersal: Each of these plants produces seeds and these numbers of seeds are proportional to its fitness value. All plants in the colony are arranged in an ascending order using their fitness values and each is assigned with an individual rank. The plant with minimum fitness value is assigned with 1st rank and it will produce maximum number of seeds (S_{max}). Similarly, the n^{th} plant in the colony will produce S_n number of seeds, which lies in between S_{max} and S_{min} as shown in Figure 3.4.

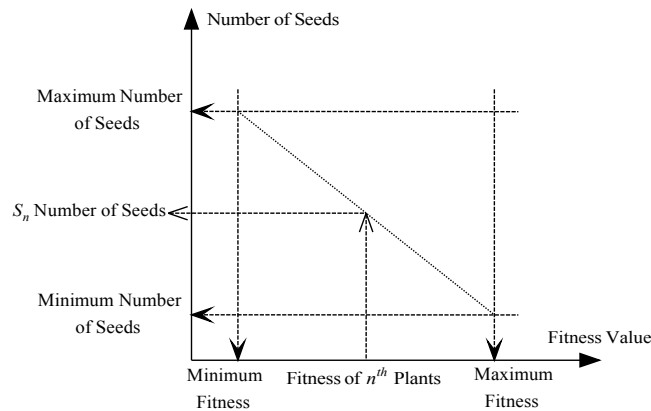


Fig. 3.4: Seed reproduction in a weed colony

Following the fitness evaluation process, in the reproduction stage, the n^{th} plant will generate S_n number of seeds with zero mean and σ_{iter} standard deviation. These new seeds will be distributed over the entire search space. The Standard Deviation (SD) will start from σ_i at initial iteration and it will become σ_f while iteration reaches to maximum number of iterations ' I_{max} '. Thus, the standard deviation at each iteration can be expressed as [135]:

$$\sigma_{iter} = \left(\frac{I_{max} - iter}{I_{max}} \right)^r (\sigma_i - \sigma_f) + \sigma_f \quad (3.24)$$

where r is the nonlinear modulation index, which decides the convergence speed.

iii. Competitive exclusion: The fitness of each seed in the new colony ' $\hat{\mathbf{w}}_s^l$, $s = 1, 2, \dots, N_s$ ', where $N_s > N_l$ is again evaluated and among them the best N_l number of seeds will be retained in the colony by discarding remaining $(N_s - N_l)$ seeds.

This process will be repeated from fitness evaluation phase until the termination criterion is met. The termination criterion may be either attainment maximum number of iterations (I_{max}) or obtaining minimum acceptable fitness value.

iv. Optimal Solution: After meeting termination criterion, the best individual having minimum fitness value is taken as the optimized weight vector of user l . From this optimal solution, the user symbol is estimated as:

$$\hat{\mathbf{w}}_l = \arg \min_n (P_E(\mathbf{w}_l^{I_{max}, n})), \quad n = 1, 2, \dots, N_l \quad (3.25)$$

$$\hat{\mathbf{x}}_l = \hat{\mathbf{w}}_l^H \mathbf{y} \quad (3.26)$$

Similarly, the entire optimization process is repeated for finding the optimal weight vectors of the remaining $(L - 1)$ users.

3.4 Simulation study and performance analysis

An extensive simulation study has been undertaken for comparing the performances of the proposed AGA, ADEA and IWO assisted MER detection techniques with the classical MUD techniques. The signal mapper used for the MBER MUD is BPSK and the signal mapper used for the MSER MUD is 4-QAM/16-QAM. In the SDMA-OFDM systems uplink module, each user's data is protected with their individual half rate Convolutional encoders

consisting polynomials (133, 171) in octal notation. The simulations for MBER MUDs and MSER MUDs are averaged over 1000 and 100 OFDM frames respectively, where each OFDM frame consisting 128 subcarriers along with a cyclic prefix of length 32. The simulation model of SDMA–OFDM system for MUD is shown in Figure 3.5. The performance evaluation is in general carried out for the SDMA–OFDM system with four users and four receiving antennas and the BER is averaged over all users. The performance of the MER detection techniques are also discussed for three system conditions, namely under load, full load and over load assuming that the channel transfer functions are perfectly known at the receiver's end. The number of receiving antennas (P) is fixed at four and the number of users (L) considered are three, four and six according to under load, full load and over load scenarios respectively. The standard MIMO wireless used in these investigations are as described in Appendix A. The efficacy of the proposed MUD techniques is evaluated through the BER performance, convergence speed and complexity analysis. The BER for each user is calculated by varying the E_b/N_o value, the convergence speed is evaluated through the rate of minimizing the cost value over number of iterations and the complexity of each detector is estimated through number of Cost Function (CF) evaluations and computational operations. The details of the simulation study have been separately addressed for MBER and MSER MUD techniques in the subsequent subsection.

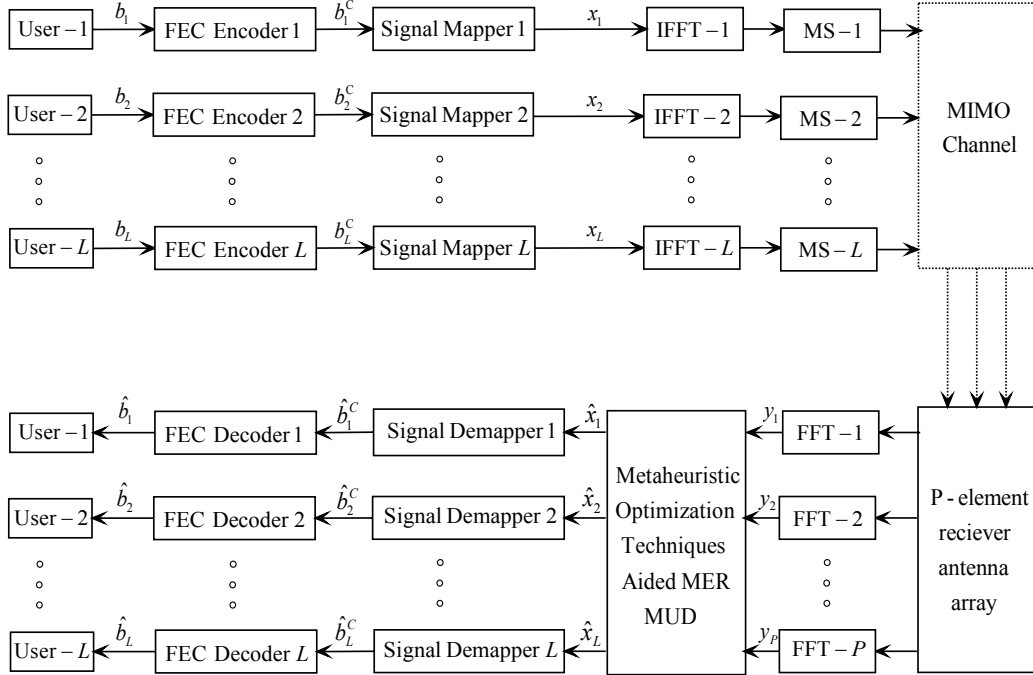


Figure 3.5: Simulation model of the SDMA–OFDM system for multiuser detection using proposed OTs aided MER schemes

3.4.1 Results and discussion for OTs aided MBER MUD

3.4.1.1 Selection of control parameters

It is observed that the various control parameters of the OTs affect significantly the MUD performance and hence these are chosen according to the performance of the SDMA–OFDM system model, rather than selecting them arbitrarily. The following subsections describe the modality for selection of those.

A. AGA control parameters: The performance of the AGA is mainly influenced by the basic parameters such as crossover probability (P_c), mutation probability (P_m), number of generations (G_g) and population count (N_g). So, the effect of those four parameters on the performance is studied in detailed and their selection is done accordingly.

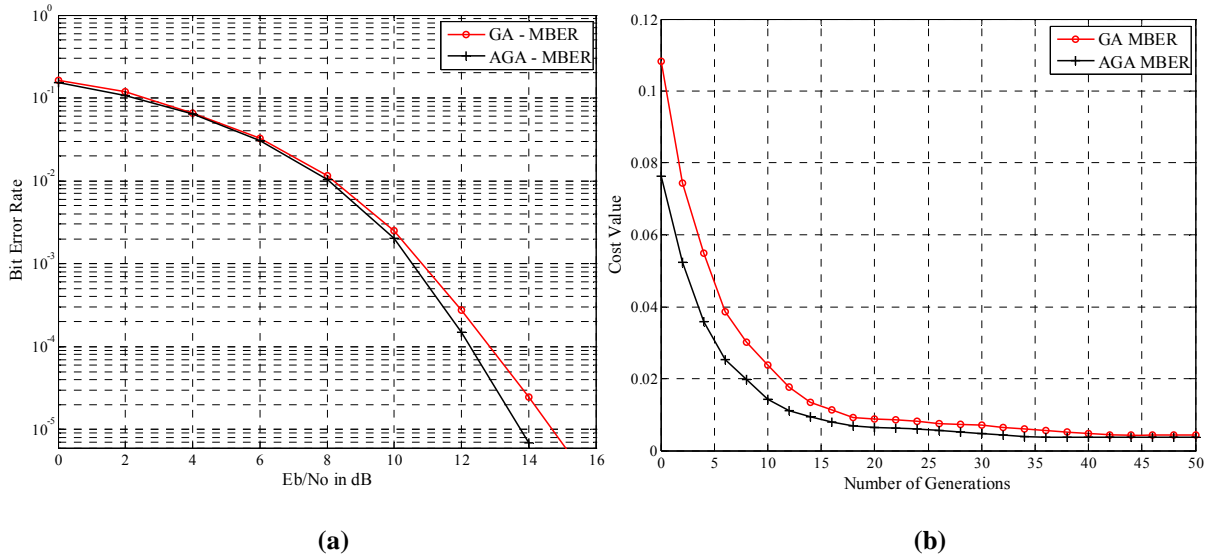


Figure 3.6: Performance comparison between GA and AGA aided MBER MUDs (a) BER performance (b) Convergence speed

In general, the GA adopts a moderately large value of P_c ($0.5 < P_c < 1.0$), and small value of P_m ($0.001 < P_m < 0.05$) for finding the optimal solution. The moderately large values of P_c promote an extensive recombination of individuals, while small value of P_m is necessary to prevent the disruption of the solutions. Following these considerations, $P_c = 0.7$ and $P_m = 0.01$ are chosen for GA MBER MUD while comparing with the AGA MBER MUD, which adopts P_c and P_m according to the equations eq. (3.6) and eq. (3.7). Figure 3.6 shows the average BER and convergence speed comparisons between GA and AGA aided MBER MUDs keeping both G_g and N_g fixed at 50. The average BER of all users is evaluated using SUI channel model given in Appendix A. As observed, the AGA MBER MUD provides a higher convergence speed and improved BER performance compared to classical

GA. Specifically, the AGA MBER detector has around 1 dB E_b/N_o gain over the classical GA MBER detector at 10^{-5} BER level as shown in Figure 3. 6 (a).

The effect of GA's generation index (G_g) and population count (N_g) on the BER performance of the AGA MBER MUD is illustrated in Figure 3.7 by varying G_g and N_g at a fixed E_b/N_o value of 15 dB. Here, while increasing both G_g and N_g , the BER gets reduced and it reaches a minimum BER that around 10^{-4} level at $G_g = 50$ and $N_g = 50$. This is due to the fact that the possibility of finding global solution improves with a large solution space. Increasing the solution space further there is no added improvement in BER, moreover it imposes additional complexity. Hence, these parameters are chosen with the value of 50. The control parameters required for the AGA MBER detector are summarized in Table 3.1.

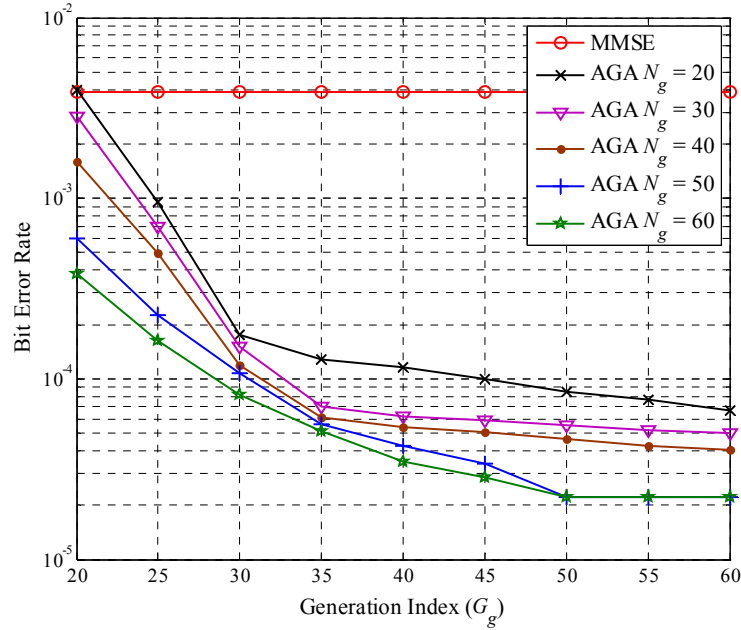


Figure 3.7: BER performance comparison of AGA MBER MUD while varying N_g and G_g at 15 dB E_b/N_o

Table 3.1: Simulation parameters of AGA MBER MUD

Parameter	Value
Number of Generations (G_g)	50
Population Size (N_g)	50
Crossover type	Adaptive Crossover
Mutation type	Adaptive Mutation
Initial P_c for adaptive crossover	0.7
Initial P_m for adaptive mutation	0.01
Selection Type	Roulette wheel
Selection Method	Fitness Proportionate
Elite Count	2
Termination Criteria	Maximum Number of Generations

B. *ADEA control parameters*: Differential evolution algorithm has the important control parameters like the mutation factor (F), crossover probability (C_p), population size (N_d) and number of generations (G_d), which influence the performance of MBER MUD. So, the effect of those parameters on the performance is studied in detaile and their selection is done.

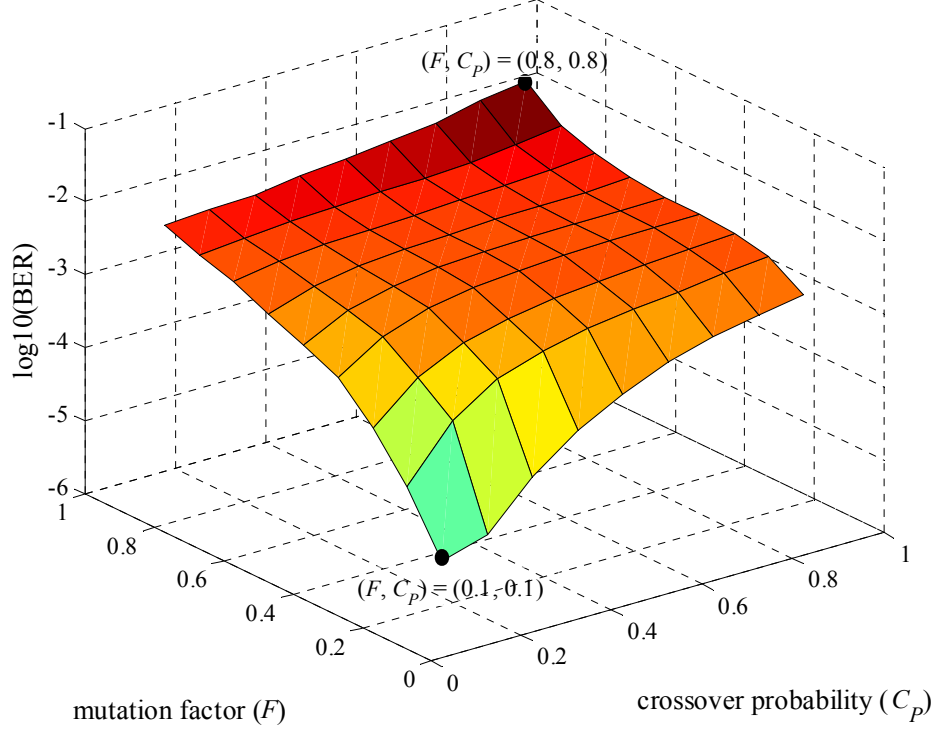


Figure 3.8: BER performance comparison of the ADEA MBER MUD while varying C_p and F at 15 dB E_b/N_o

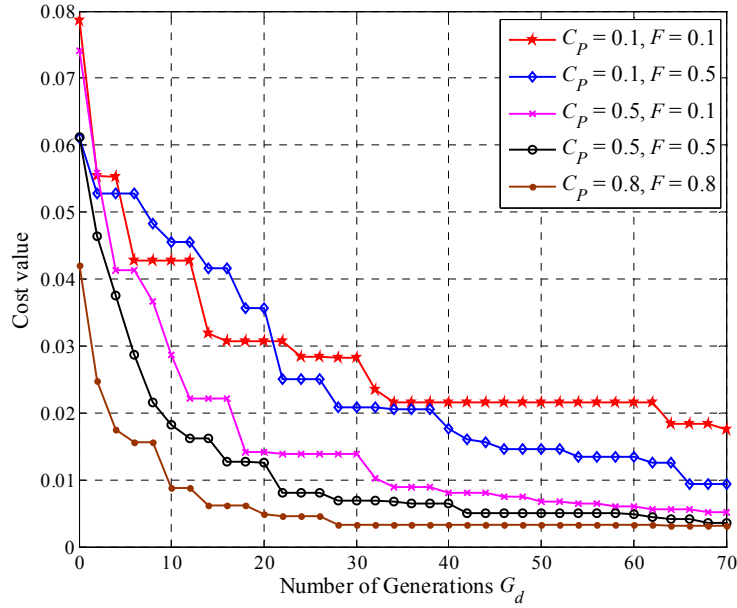


Figure 3.9: Convergence speed comparison of ADEA MBER MUD while varying C_p and F at 15 dB E_b/N_o

The effect of the mutation factor (F) and the crossover probability (C_P) on the performance of ADE assisted MBER MUD is discussed in Figure 3.8 and Figure 3.9. The average BER performance of the DEA aided MBER MUD is studied for $0.1 \leq F \leq 0.8$ and $0.1 \leq C_P \leq 0.8$ at a fixed E_b/N_o value of 15 dB using SUI channel model is shown in Figure 3.8. The BER performance of the system is very poor at the operating point $(C_P, F) = (0.8, 0.8)$, because the algorithm converges to a local minimum rather than global one without thoroughly exploring the entire solution space. It is further observed in figure 3.9, though the BER performance is optimal at the operating point $(C_P, F) = (0.1, 0.1)$, its convergence speed will be very slow. The cost value of User-1 is evaluated for different combinations of C_P and F by varying number of generations keeping N_d is fixed at 50. Here, the number of generations required for achieving the minimum cost value is monotonically decreased upon increasing both the C_P and F . The operating point $(C_P, F) = (0.8, 0.8)$ results faster convergence of the algorithm and it reaches the minimum cost level with less number of generations ($G_d \approx 28$). At the lower operating point $(C_P, F) = (0.1, 0.1)$, the convergence speed of the algorithm is much slow, it takes more number of generations ($G_d > 50$) to converge. So a tradeoff between complexity and system performance is thought of and an operating point (C_P, F) of (0.5, 0.5) value is considered as initial C_P and F for ADEA based MBER MUD technique.

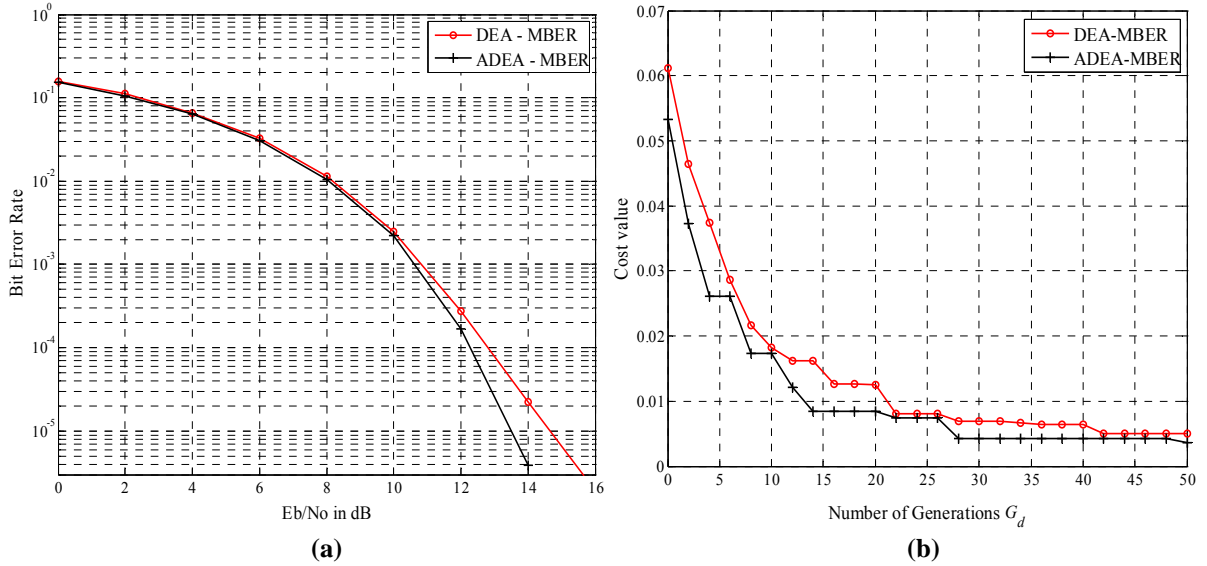


Figure 3.10: Performance comparison between DEA and ADEA MBER MUDs (a) BER performance (b) Convergence speed

In Figure 3.10, we have compared the performance and convergence speed of the proposed adaptive DEA MBER MUD technique with classical DEA aided MBER MUD, where both F and C_P are adapted according to eq. (3.13) and (3.14) respectively. The average

BER of all users is calculated over the same SUI channel model keeping both G_d and N_d are fixed at 50. The ADEA outperforms the classical DEA in terms of both BER performance and convergence speed. Specifically, the ADEA MBER detector has around 1.5 dB E_b/N_o gain over the classical one at 10^{-5} BER floor.

Further, Figure 3.11 shows the BER performance of User-1 using ADEA MBER MUD for different values of population size and number of generations at a fixed E_b/N_o value of 15 dB. In is observer that, while increasing G_d and N_d , the BER level is reduced and attended a minimum level at $G_d = 45$ and $N_d = 50$. Since there is no further improvement in BER value beyond this complexity level, the G_d and N_d values are fixed at (45, 50). Thus, all the control parameters for the ADEA MBER detector are summarized in Table 3.2.

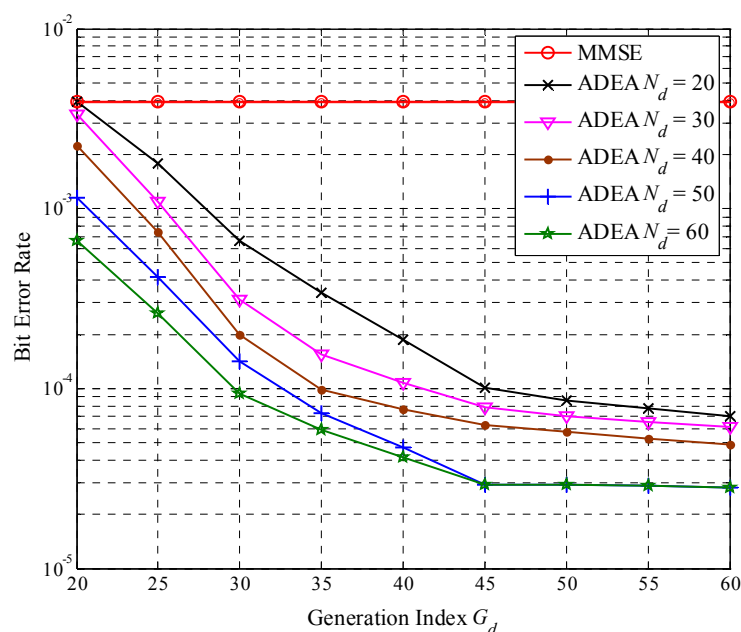


Figure 3.11: BER performance comparison of ADEA MBER MUD while varying N_d and G_d at 15 dB E_b/N_o

Table 3.2: Simulation parameters of ADEA MBER MUD

Parameter	Value
Number of Generations (G_d)	45
Population Size (N_d)	50
Crossover type	Adaptive Crossover
Mutation type	Adaptive Mutation
Initial C_p for adaptive crossover	0.5
Initial F for adaptive mutation	0.5
Initialization of the Population	Randomly Generated
Termination Criteria	Maximum Number of Generations

C. *IWO algorithm control parameters*: The influencing control parameters of the IWO based MBER MUD are the maximum number of seeds generated by a plant (S_{max}), initial standard deviation (σ_i), Final standard deviation (σ_f), nonlinear modulation index (r), population size (N_l) and maximum number of iterations (I_{max}). These parameter values should be chosen carefully in order to achieve proper value of the SD, so that the algorithm results faster converge to the optimal solution.

Table 3.3 shows the complexity and performance variation of the IWO MBER MUD varying S_{max} from 2 to 8. Here, the complexity refers to the number of seed per iteration and the performance refers to the cost value of User-1 keeping E_b/N_o value fixed at 15 dB. It is observed that while increasing the value of S_{max} beyond 5, there is no further improvement in performance despite of introducing an extra complexity. Hence, S_{max} is chosen to be 5.

Table 3.3: Effect of S_{max} on complexity and performance of the IWO MBER MUD at 15 dB E_b/N_o

S_{max}	Seed per iteration	Cost Value
2	58	0.0097
3	64	0.0045
4	76	0.0038
5	85	0.0031
6	102	0.0031
7	120	0.0031
8	137	0.0031

The selection of initial standard deviation (σ_i) and final standard deviation (σ_f), which affects the convergence as shown in Figure 3.12. So, both of these parameters should be chosen carefully to locate the optimal solution. The IWO algorithm requires a high initial standard deviation to explore the entire search area, aggressively. The final SD should be much smaller than the variable precision value of the solution, such that the change in SD doesn't affect the final error value. Hence, when $\sigma_i = 10\%$ of the dynamic range of entire search space (i.e. 0.1) and $\sigma_f = 0.001\%$ of the dynamic range of entire search space (i.e. 0.00001), the search strategy starts with large σ_i , then decreases SD in a nonlinear fashion while increasing iterations and it finally terminates with a small σ_f . Among different combinations of σ_i and σ_f investigated here, the combination with $(\sigma_i, \sigma_f) = (0.1, 0.00001)$ provides the best performance with high convergence speed, because this combination ensures a high possibility of locating optimal solution.

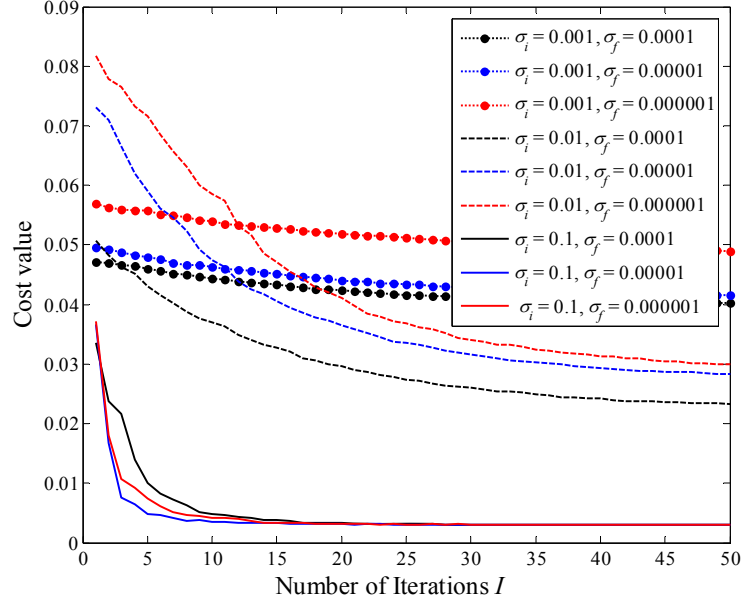


Figure 3.12: Convergence speed comparisons of IWO MBER MUD for different combinations of initial and final standard deviations

The effect of the maximum number of iterations (I_{max}) and seed count N_I on the performance of the IWO MBER MUD with respect to BER level is illustrated in Figure 3.13 at a fixed E_b/N_o value of 15 dB. In this figure the BER of User–1 is plotted while varying I_{max} and N_I . It is observed that the BER is reduced by increasing I_{max} and N_I and it is reaching a minimum BER level with $I_{max} = 40$ and $N_I = 50$ as possibility of finding a global solution increases with the larger solution space. Increasing both the I_{max} and N_I beyond this values results no further improvement in performance and moreover that it adds to the complexity.

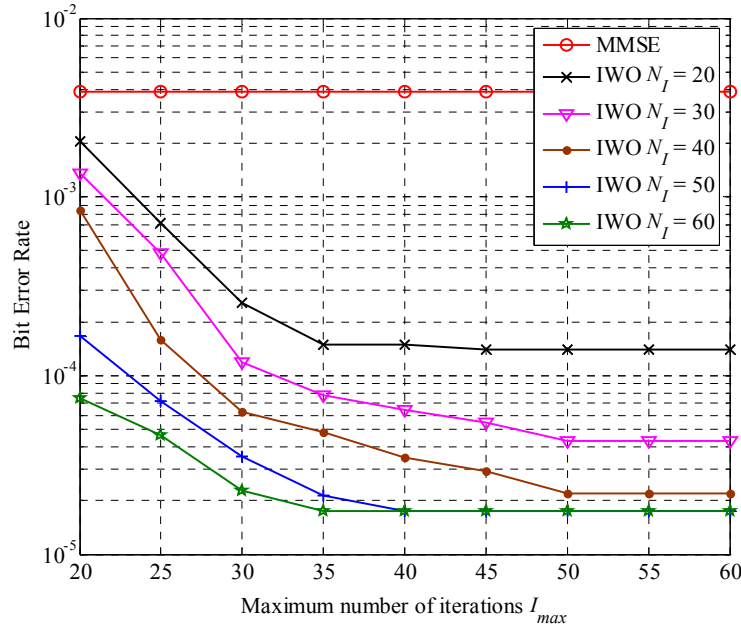


Figure 3.13: BER performance comparison of IWO MBER MUD while varying N_I and I_{max} at 15 dB

Figure 3.14(a) shows the variation of Standard Deviation (SD) while changing the nonlinear modulation index following eq. (3.24). In this figure, the SD is reduced from the initial SD to the final SD with different velocities. The rate of change of SD is more by increasing the r . At the initial iteration, this algorithm will search solution in the whole search space with high initial SD. As the number of iterations is increased, the SD value will fall gradually to reach the global optimal solution. Accordingly, the cost value also follows the change with increasing r as shown in Figure 3.14(b). Considering these two observations, the modulation index ($r = 3$) is chosen to achieve fast convergence. The simulation parameters selected for IWO aided MBER detector is summarized in Table 3.4.

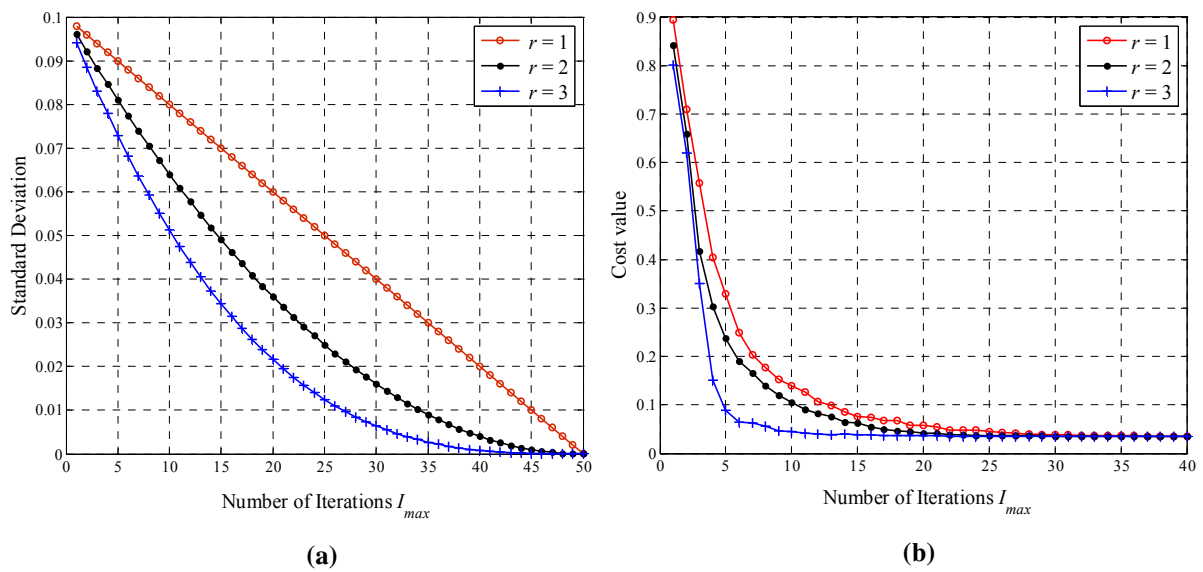


Figure 3.14: Rate of change in (a) Standard deviation (b) Cost value, for different valued of nonlinear modulation index ‘ r ’ while varying number of iterations

Table 3.4: Simulation parameters of IWO MBER MUD

Parameter	Value
Number of iterations (I_{max})	40
Population size (N_I)	50
Number of seeds (N_S)	85
Search range	[0,1]
Maximum number of seeds (S_{max})	5
Minimum number of seeds (S_{min})	1
Nonlinear modulation index (r)	3
Initial standard deviation (σ_i)	10% of entire search rage (0.1)
Final standard deviation (σ_f)	0.001% of entire search rage (0.00001)
Seed selection	Rank based
Termination criteria	Maximum number of generations

3.4.1.2 Performance analysis

In this section, the average BER performance of all users using the proposed OTs assisted MBER techniques are compared with the conventional MMSE and ML detectors through simulation study as shown in Figure 3.15 under various channel conditions in order to verify their robustness. As we discussed in Chapter 2, the SWATM channel imposes more degradation compared to other two channels. Hence, the performances of all detectors in such a channel environment are poor as shown in Figure 3.15 (c). It is also inferred from Figure 3.15 is that a linear detector like MMSE results in poor BER performance since it cannot mitigate multiuser interference adequately. On the other hand, the ML MUD one can deliver optimal performance with an exhaustive search mechanism. Further, unlike the linear detector, the nonlinear OTs aided MBER MUDs are able to mitigate the nonlinear degradation caused by wireless radio environment. Hence, these detectors consistently outperform the linear MMSE detector in such case. Specifically, at a BER level of 10^{-4} , the OTs aided MBER can give 5 dB, 5 dB and 7 dB E_b/N_o gain approximately over MMSE under MIMO Rayleigh fading, SUI and SWATM channel conditions respectively.

The average BER performance of all the users in under load, full load and over load scenarios considering the MIMO Rayleigh fading channel model is shown in Figure 3.16(a), Figure 3.16(b) and Figure 3.16(c) respectively. As the number of users (L) is increased from 3 to 6 keeping the number of receiving antennas (P) fixed at 4, the discrepancy between the performances of MMSE and ML MUDs is also increases. Because, in overloaded scenarios, the weight matrix calculated by the MMSE algorithm becomes a singular matrix, which will lead to a theoretically un-resolvable detection problem. As a result the linear MMSE MUD gives high residual BER as seen in Figure 3.16 (c). By contrast, the proposed OTs aided MBER MUDs can minimize the residual error by directly minimizing probability of error. Hence, it can detect users even in such a over load scenario. Further, amongst the various OTs used to find weight solution of MBER MUD, the IWO is performing slightly better than other algorithms especially in over load condition. It may be due to the fact that the IWO algorithm allows all of the individual plants to participate in the reproduction process, because sometimes it is also possible that some of the plants with the lower fitness carry more useful information compared to the fitter plants. This algorithm also gives a chance to the less fit plants to reproduce and if the seeds produced by them have good fitnesses in the colony, they can survive. In this way fitter plants produce more seeds than less fit plants, which tend to improve the convergence speed of the algorithm.

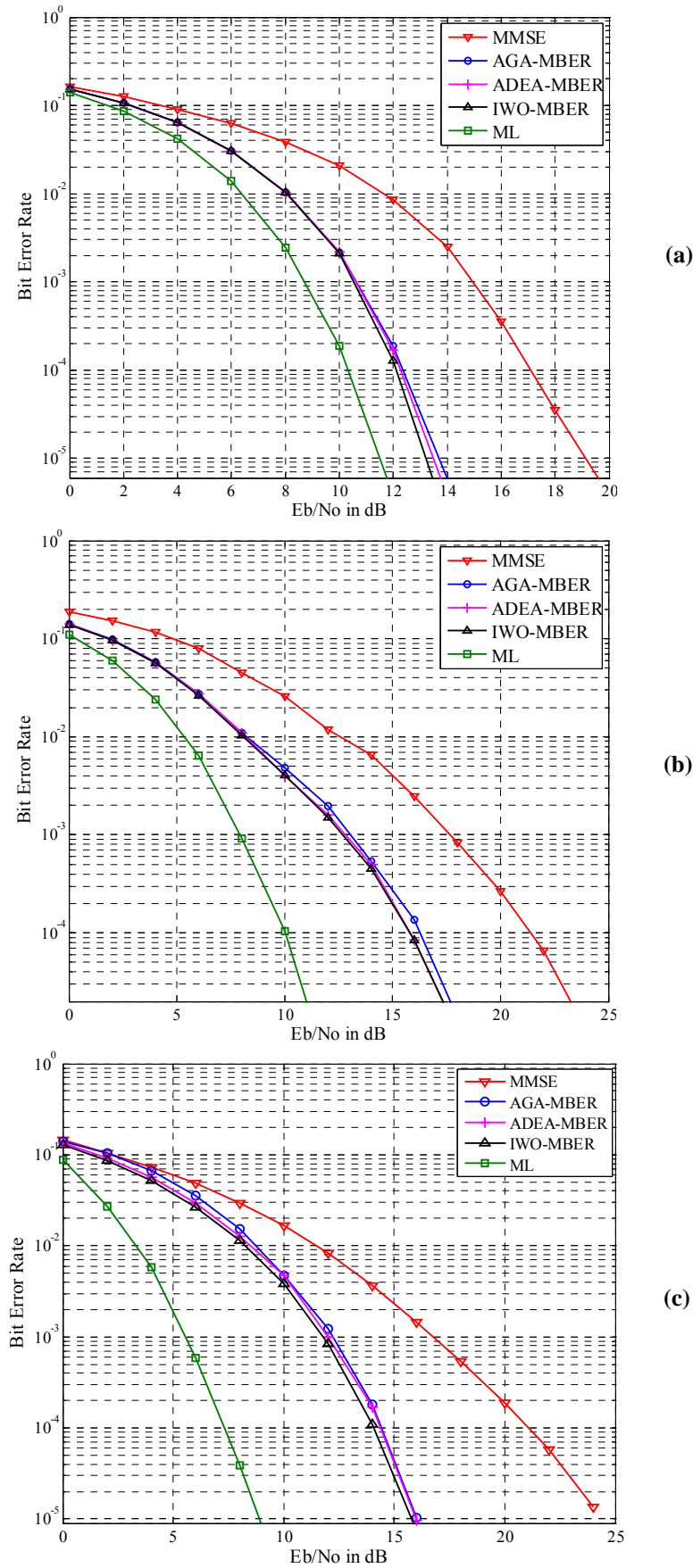


Figure 3.15: Average BER performance of all users using MMSE, OTs aided MBER and ML MUDs under different channel conditions (a) MIMO Rayleigh fading (b) SUI (c) SWATM

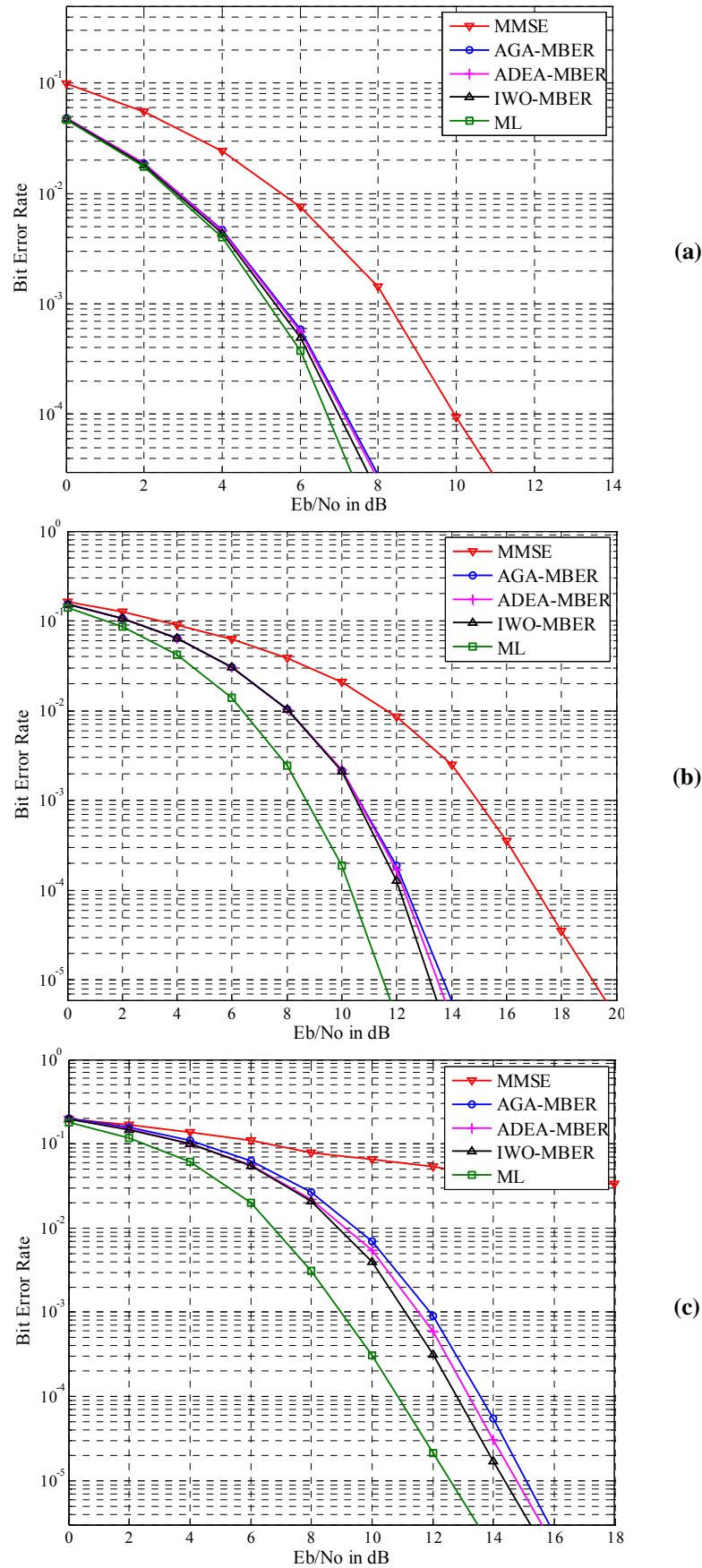


Figure 3.16: Average BER performance of all users using MMSE, OTs aided MBER and ML MUDs under load conditions (a) Under Load ($L = 3, P = 4$) (b) Full Load ($L = P = 4$) (c) Over Load ($L = 6, P = 4$)

The performances of the MMSE and OTs aided MBER MUDs in the over load scenario is more explicitly interpreted by means of scatter plots, which displays symbols in a two dimensional complex plane. Figure 3.17 shows the detected symbols of the User-1 from the noiseless received symbols (i.e. $\mathbf{y} = \mathbf{H}\mathbf{x}$), when it is always transmitting ‘+1’ over one complete OFDM frame considering MIMO Rayleigh fading channel in the SDMA-OFDM system with $L = 6$ and $P = 4$. It is observed that, some of the detected symbols using the MMSE MUD technique are closer to the BPSK decision boundary and even some of them cross the decision boundary entering in the wrong half plane. Hence, the MMSE detector fails to detect users in overload scenario. By contrast, the detected symbols using the proposed AGA, ADEA, and IWO aided MBER MUDs lie far away from the decision boundary and close to the transmitted symbol location in the constellation diagram shown in Figure 3.17 (b), (c) and (d), which result better user classification at the BS receiver.

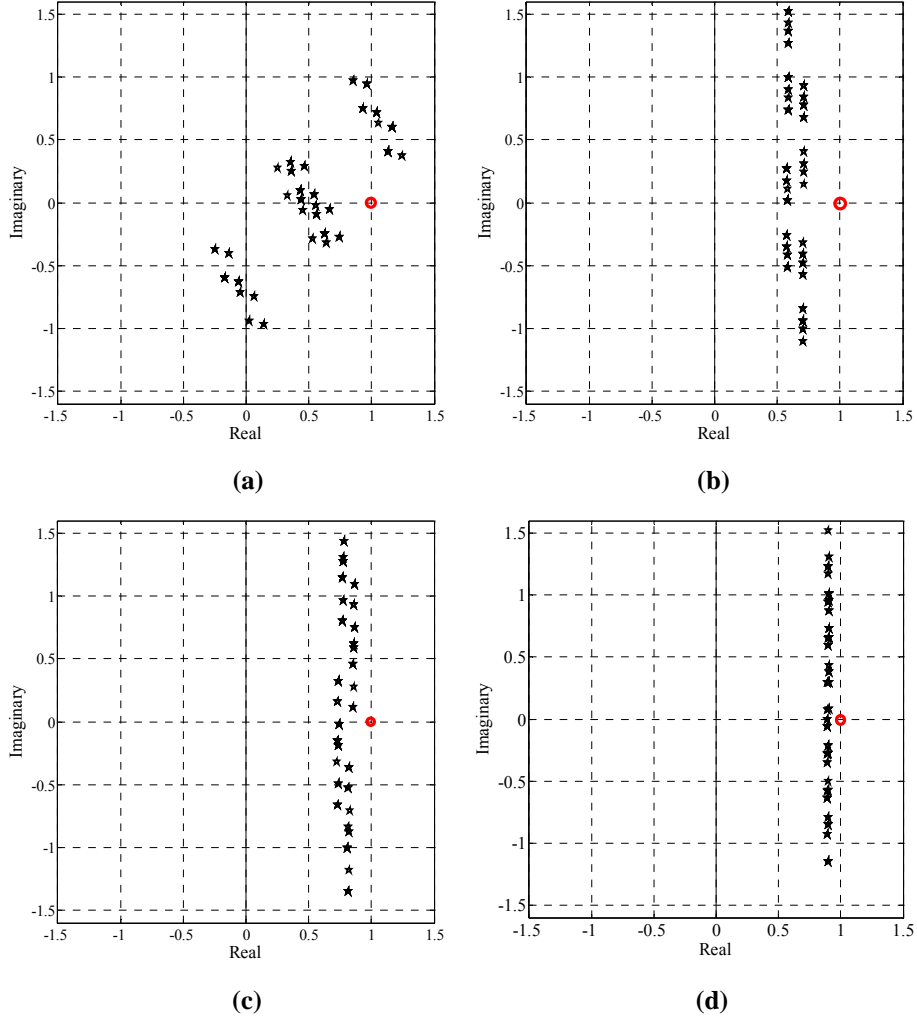


Figure 3.17: Estimated symbol distribution of User-1 from noise less received symbols using various MUD schemes for the case of $L = 6$ and $P = 4$ when User-1 is always transmitting +1 (a) MMSE (b) AGA MBER (c) ADEA MBER (d) IWO MBER

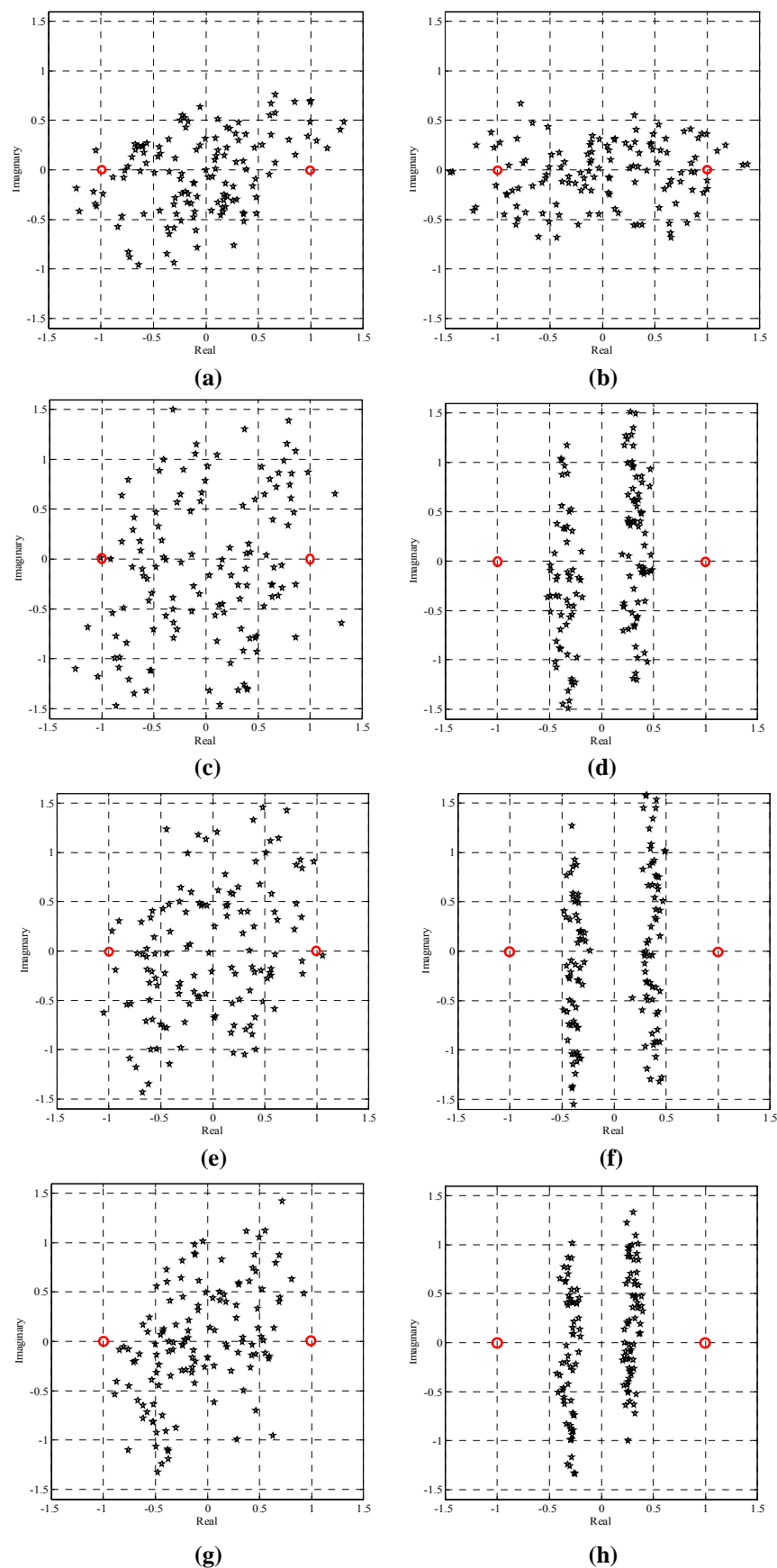


Figure 3.18: Estimated symbol distribution of User-1 using various MUD schemes for the case of $L = 6$ and $P = 4$ (a, b) MMSE at $E_b/N_o = 5, 20$ dB (c, d) AGA MBER at $E_b/N_o = 5, 20$ dB (e, f) ADEA MBER at $E_b/N_o = 5, 20$ dB (g, h) IWO MBER at $E_b/N_o = 5, 20$ dB

Further, among these three detectors, it is found that the concentration of detected symbols using IWO MBER detector is much close to the transmitted symbol. This indicates the robustness of the proposed IWO algorithm in finding the optimal solution for MBER MUD to give the better BER performance.

In Figure 3.18, the detected symbol constellations of the User-1 for noisy channel condition at different E_b/N_o values using MMSE and OTs aided MBER MUDs is shown for one complete transmission of OFDM frame with 128 symbols in the SDMA-OFDM system with $L = 6$ and $P = 4$ considering MIMO Rayleigh fading channel model. It is noticed that the MMSE and the proposed OTs aided MBER MUDs fail to classify the received symbols in high noise condition (5 dB E_b/N_o) as the received symbols are intermingled. But in practical scenario (20 dB E_b/N_o), the classification using the proposed OTs aided MBER MUD schemes has improved over the MMSE one as the detected symbols lie in the correct decision plane.

3.4.1.3 Convergence speed

The improved convergence speed of the IWO MBER MUD over AGA and ADEA MBER MUD is observed by plotting the rate of change in cost value verses number of iterations/generations in Figure 3.19 under SWATM channel condition. Here, in order to compare all OTs, 50 generations/iterations each consisting of 50 individuals is chosen.

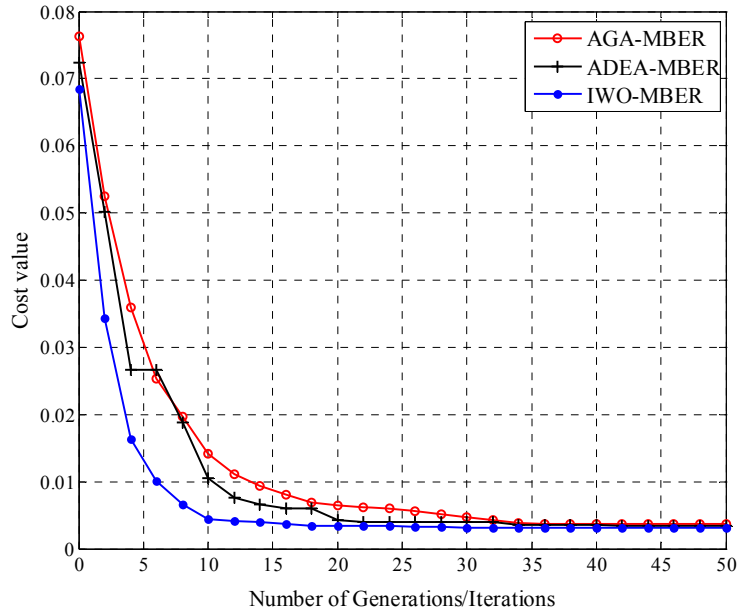


Figure 3.19: Convergence speed comparison of proposed OTs aided MBER MUDs at 15 dB E_b/N_o

From Figure 3.19, it is observed that the AGA and IWO algorithms are converging smoothly, whereas the ADEA algorithm is converging in an uneven fashion since it is not a fitness proportionate algorithm. Among all these OTs, the IWO algorithm has a faster convergence by reaching the minimum cost value with less number of iterations compared to the AGA and ADEA techniques to reach a minimum cost value level.

3.4.1.4 Complexity

The over-all complexity of the ML detector is very high especially under the block fading channel environment and overload scenarios. In this section, the complexity of the proposed OTs aided MBER MUDs is compared with the ML detector based on both Cost Function (CF) evaluations and computational operations (multiplication and addition) performed as shown in Table 3.5 and 3.6 respectively. The AGA evaluates the cost function given in eq. (3.3) before and after crossover operation. Hence, the Complexity of AGA MBER MUD is proportional to $2 \times G_g \times N_g$. Similarly, the ADEA evaluates the cost function twice for computing both $\hat{\mathbf{v}}_{g,n,p}^l$ and $\hat{\mathbf{w}}_{g,n,p}^l$ as given in eq. (3.15) and eq. (3.16). Thus, the complexity of the ADEA MBER MUD is proportional to $2 \times G_d \times N_d$. The IWO algorithm evaluates number of seeds (N_S) times cost function as given in eq. (3.22) and hence the complexity of the IWO MBER is proportional to $N_S \times I_{max}$. All these comparisons of various MUDs are considered for a block fading channel condition and in an overload scenarios, where the L users simultaneously transmit their BPSK data to the P antenna receiver over N_C subcarriers along with N_{CP} cyclic prefix ($N_{CP} = 128$, $N_{CP} = 32$). The channel is assumed to be time-invariant over $N_F = 1000$ consecutive OFDM frames. The FEC employed is the half rate Convolutional code. Further, the complexities of the MMSE and OTs aided MBER MUDs are compared with the ML detectors while increasing L and presented in Table 3.7.

Table 3.5: Complexity comparison of OTs aided MBER and ML MUD schemes with respect to CF evaluations when $L = 6$ and $P = 4$

MUD Technique	Cost Function Evaluations	Total	% of ML
AGA MBER	$2 \times G_g \times 2N_g \times (N_C + N_{CP}) \times L$	9.600×10^6	46.9
ADEA MBER	$2 \times G_d \times 2N_d \times (N_C + N_{CP}) \times L$	8.640×10^6	42.2
IWO MBER	$2 \times I_{max} \times N_S \times (N_C + N_{CP}) \times L$	6.528×10^6	31.9
ML Detector	$2 \times 2^{mL} \times (N_C + N_{CP}) \times N_F$	2.048×10^7	100

Table 3.6: Complexity comparison of MMSE, OTs aided MBER and ML MUD schemes with respect to number of computational operations when $L = 6$ and $P = 4$

MUD	Operation	Computational Complexity	Total	% of ML
MMSE	Multiplications	$2(N_c + N_{CP})\{2PL + P^2 + P(P-1)(4P+1)/6\}$	2.384×10^4	6.5×10^{-5}
	Additions	$2(N_c + N_{CP})\{2P(L-1) + P(P-1) + P(P-1)(4P+1)/6\}$	2.752×10^4	5.1×10^{-4}
AGA MBER	Multiplications	$2(N_c + N_{CP})(G_g \times 2N_g)(2P-1)(2^{mL} + 1)L$	4.368×10^9	23.83
	Additions	$2(N_c + N_{CP})(G_g \times 2N_g)(2^{mL}P + P-1)L$	2.486×10^9	7.02
	Q functions	$2(N_c + N_{CP})(G_g \times 2N_g)(2^{mL})L$	6.144×10^8	–
ADEA MBER	Multiplications	$2(N_c + N_{CP})(G_d \times 2N_d)(2P-1)(2^{mL} + 1)L$	7.862×10^9	21.42
	Additions	$2(N_c + N_{CP})(G_d \times 2N_d)(2^{mL}P + P-1)L$	2.238×10^9	6.32
	Q functions	$2(N_c + N_{CP})(G_d \times 2N_d)(2^{mL})L$	5.529×10^8	–
IWO MBER	Multiplications	$2(N_c + N_{CP})(G_I \times N_S)(2P-1)(2^{mL} + 1)L$	6.989×10^9	19.04
	Additions	$2(N_c + N_{CP})(G_I \times N_S)(2^{mL}P + P-1)L$	1.691×10^9	4.79
	Q functions	$2(N_c + N_{CP})(G_I \times N_S)(2^{mL})L$	4.178×10^8	–
ML Detector	Multiplications	$2(N_c + N_{CP})N_F(PL + P)2^{mL}$	3.670×10^{10}	100
	Additions	$2(N_c + N_{CP})N_F(PL + P-1)2^{mL}$	3.539×10^{10}	100

Table 3.7: Complexity comparison of OTs aided MBER and ML MUD schemes with respect to CF evaluations while varying L keeping P fixed at four

L	AGA	ADEA	IWO	ML
4	6.4×10^6	5.76×10^6	5.2×10^6	5.12×10^6
5	8×10^6	7.2×10^6	6.04×10^6	1.024×10^7
6	9.6×10^6	8.64×10^6	7.68×10^6	2.048×10^7
7	1.12×10^7	1.008×10^7	8.96×10^6	4.096×10^7
8	1.28×10^7	1.152×10^7	1.024×10^7	8.192×10^7

It is noticed from Table 3.5 and Table 3.6 that all the proposed AGA, ADEA and IWO MBER MUDs are computationally economical compared to the intensive ML detector in terms of both number of CF evaluations and computational operations. Further it is also observed from Table 3.7 that as the number of users increase, the complexity of the ML detector increases exponentially, whereas the complexity of the proposed OTs aided MUDs increases at a lesser rate. Among the discussed OTs, the IWO has considerable complexity gain compared to AGA and ADEA MBER MUDs. Finally, the advantage of using IWO aided MBER MUD in terms of both complexity and BER performance is summarized in Table 3.8. The simulation study carried out for complexity analysis is done on a PC with 3.2 GHz i5 processor and 4 GB RAM using Matlab R2009a.

Table 3.8: Performance and complexity comparisons of OTs aided MBER MUDs at E_b/N_o values 15 dB

Algorithm	CF Evaluations per Generation	CPU Time per Symbol	Bit Error Rate		
			MIMO Rayleigh fading	SUI	SWATM
AGA	100	3.1937 sec	0.000189	0.001975	7.30E-05
ADEA	100	2.5804 sec	0.000168	0.001598	6.25E-05
IWO	85	1.4711 sec	0.000129	0.001521	7.23E-05

3.4.2 Results and discussion for OTs aided MSER MUD

In this section, the simulation results for OTs aided MSER MUD are presented for detecting both the 4-QAM and 16-QAM signals. Compared to the MBER MUD, the number of equiprobable trail vectors required in the MSER MUD for computing fitness of the cost function is increased from 2^L to $2^{m(L-1)}$, where m represents the number of bits per symbol in M -QAM. Proportional to that the search space in terms of number of generation/iterations also has to be increased in all the OTs to reach a global solution. Because a larger number of generation/iterations imply that, a more diverse set of individuals may be evaluated, thus extending the search space is also increases the chance of finding a lower-BER solution. Using similar kind of analysis for selection of control parameter given in Section 3.4.1.1, the (G_g, N_g) of AGA are chosen as (100, 100), the (G_d, N_d) of ADEA are chosen as (90, 100) and the (I_{max}, N_I) of IWO are chosen as (80, 100). Similarly, for MSER with 16-QAM signals, the (G_g, N_g) of AGA are chosen as (200, 200), the (G_d, N_d) of ADEA are chosen as (180, 200) and the (I_{max}, N_I) of IWO are chosen as (160, 200). Number of seeds (N_s) per generation in the IWO MSER detector is 168 and 332 corresponding to 4-QAM and 16-QAM respectively. The rest of the simulation parameters are according to Table 3.1, 3.2 and 3.4 corresponding to AGA, ADEA and IWO aided MSER MUDs respectively.

3.4.2.1 Performance analysis

In this context, the efficacy of the OTs is further compared while locating optimal solution for MSER MUD. Figure 3.20 shows the BER performance comparison of OTs aided MSER MUD with the conventional MMSE and ML detector in all under load, full load and over load scenarios. The signal mapper used is here is 4-QAM and the wireless channel model considered is the MIMO Rayleigh fading channel. The High-order constellations form clusters closer together. This assures more transmitted bits per symbol but is more susceptible to noise and other channel degradations. As a result the BER performance of all users during the detection of 4-QAM signals is poor as shown in Figure 3.20 and delivers less reliable data compared to the detection of BPSK signals as shown in Figure 3.16.

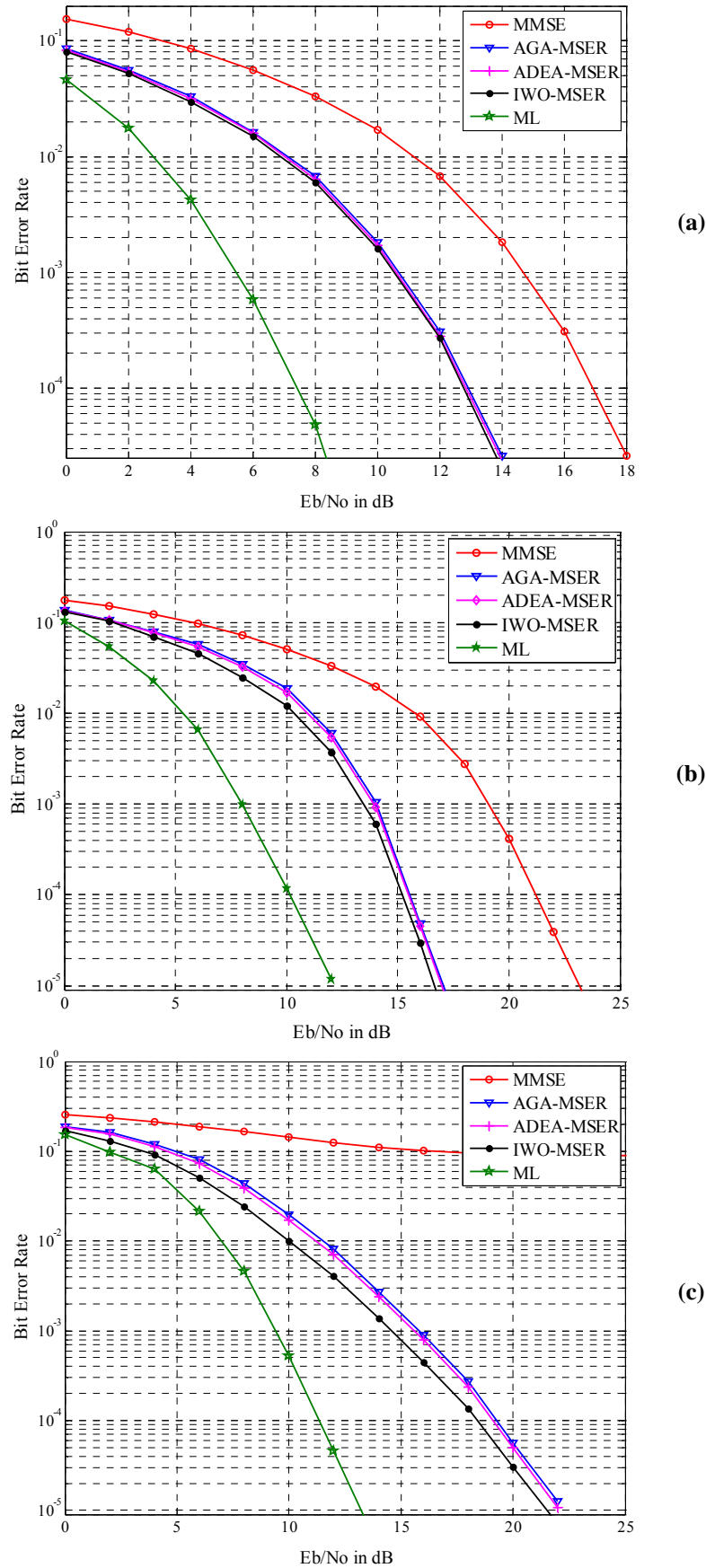


Figure 3.20: Average BER performance of all users using MMSE, OTs aided MSER and ML MUDs under load conditions (a) Under Load ($L=3, P=4$) (b) Full Load ($L=P=4$) (c) Over Load ($L=6, P=4$)

From Figure 3.20, it is observed that the OTs are well capable of finding optimal solution for MSER similar to MBER MUD. Especially, the OTs aided MSER MUDs consistently outperforming the MMSE MUD in overload scenario as seen in Figure 3.20(c). Further, the BER performance of the MSER can be improved with the aid of the IWO compared to AGA and ADEA algorithms. Specifically, at 10^{-4} target BER level, the IWO MSER MUD produces around 1.5 dB E_b/N_o gain approximately over both the AGA and ADEA aided MSER MUDs in over load case considering $L = 6$ and $P = 4$.

Figure 3.21 shows the performance comparison of various MUDs used to detect 16-QAM signals. The average BER performance of four different users using various MUDs in the SDMA-OFDM system with $L = P = 4$ is shown in Figure 3.21. As the 16-QAM symbols are more close to each other than 4-QAM, the BER performances of all MUDs while detection 16-QAM signals are further degraded as shown in Figure 3.21 than the BER performances of all MUDs while detection 4-QAM signals as shown in Figure 3.20 (b). Specifically, at 10^{-4} target BER level, the IWO MSER MUD using 4-QAM as shown in Figure 3.20 (b) has around 4 dB E_b/N_o gain over the IWO MSER MUD using 16-QAM as shown in Figure 3.21.

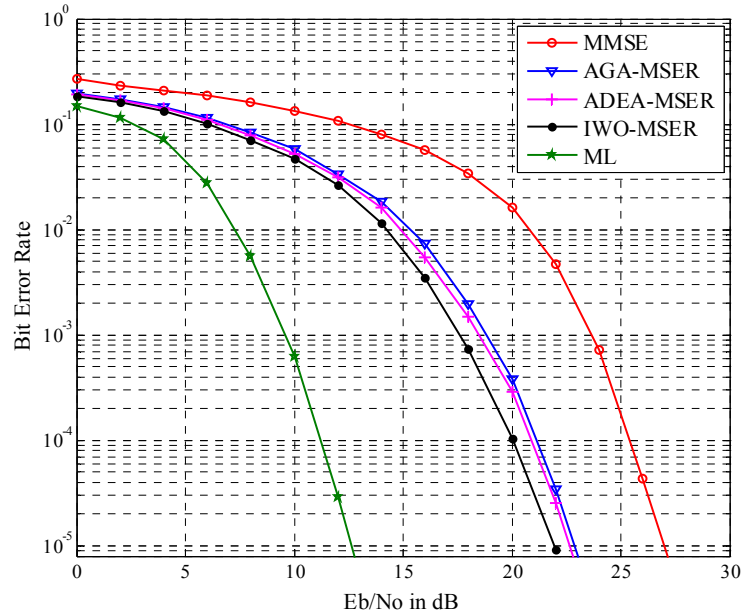


Figure 3.21: Average BER performance of all users using MMSE, OTs aided MSER and ML MUDs in the SDMA-OFDM system transmitting 16-QAM signals

Further, the performance study in over load scenario is more explicitly illustrated with the aid of symbol constellation plots as shown in Figure 3.22 and Figure 3.23. Figure 3.22 depicts the estimated symbol distribution of the User-1 from the noiseless received symbols (i.e. $\mathbf{y} = \mathbf{H}\mathbf{x}$) using MMSE and OTs aided MSER MUDs. The signal mapper used here is 4-

QAM and User-1 is always transmitting ‘1+j’ over one complete OFDM frame under the MIMO Rayleigh fading channel condition. It is noticed from Figure 3.22 is that some of the detected symbols of the MMSE MUD lie on the wrong side of the decision boundary resulting poor performance while the detected symbols using the OTs aided MSER MUDs lies in the correct plane. Further, the IWO MSER detector are closely located around the actual transmitted symbol ‘1+j’.

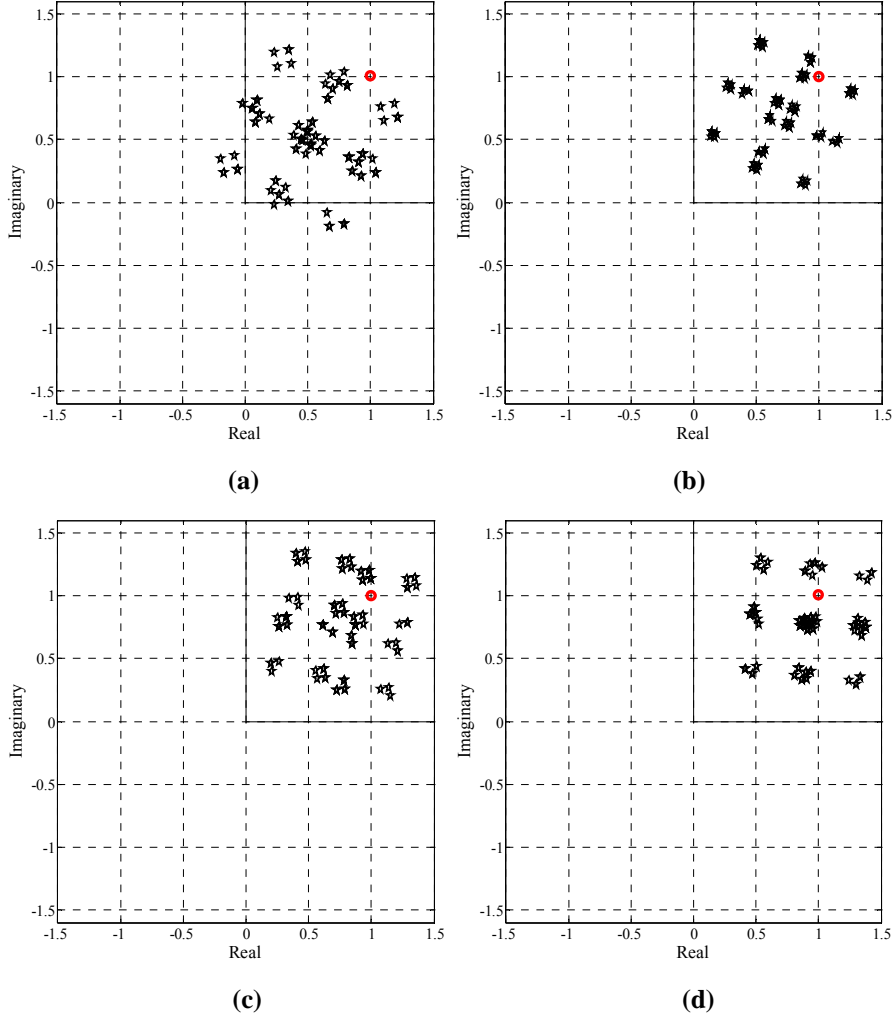


Figure 3.22: Estimated symbol distribution of User-1 from noise less received symbols using MMSE and OTs aided MSER MUDs for the case of $L = 6$ and $P = 4$ when User-1 is always transmitting 1+j (a) MMSE (b) AGA MSER (c) ADEA MSER (d) IWO MSER

Effect of noise on the received symbol constellation and performance of various MUDs is studied in Figure 3.23. Here, the linear MMSE detector fails to form clusters around the transmitted symbols even the value of E_b/N_o increased from 5 to 20 dB as it cannot mitigate MUI in overload scenario. However, the proposed OTs aided MSER MUDs fails to perform the detection under higher noise condition at $E_b/N_o = 5$ dB, but the detection gets better at higher E_b/N_o case (20 dB).

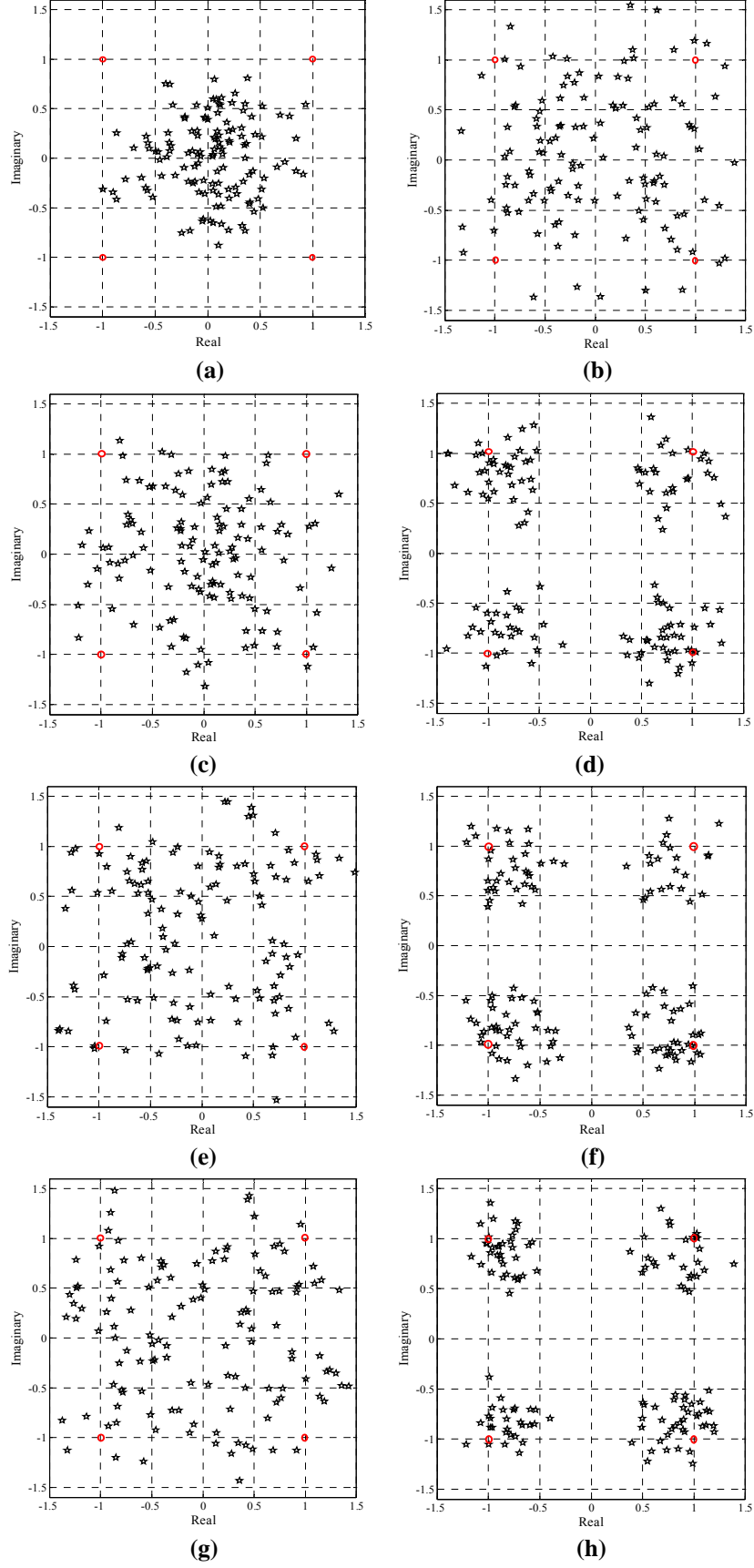


Figure 3.23: Estimated symbol distribution of User-1 using MMSE and OTs aided MSER MUDs for the case of $L = 6$ and $P = 4$ (a, b) MMSE at $E_b/N_o = 5, 20$ dB (c, d) AGA MSER at $E_b/N_o = 5, 20$ dB (e, f) ADEA MSER at $E_b/N_o = 5, 20$ dB (g, h) IWO MSER at $E_b/N_o = 5, 20$ dB

The efficacy of MSER MUD while detecting higher order signals such as 16-QAM of User-1 is evaluated as illustrated in Figure 3.24. These signals are communicated over the MIMO Rayleigh fading channel in the SDMA-OFDM system with $L = 4$ and $P = 4$ at 20 dB E_b/N_o value. In this figure, the radius of the clusters is squeezed more using the IWO based MSER MUD compared to other ones. Hence, IWO algorithm gets prominence for finding solution for MSER MUD.

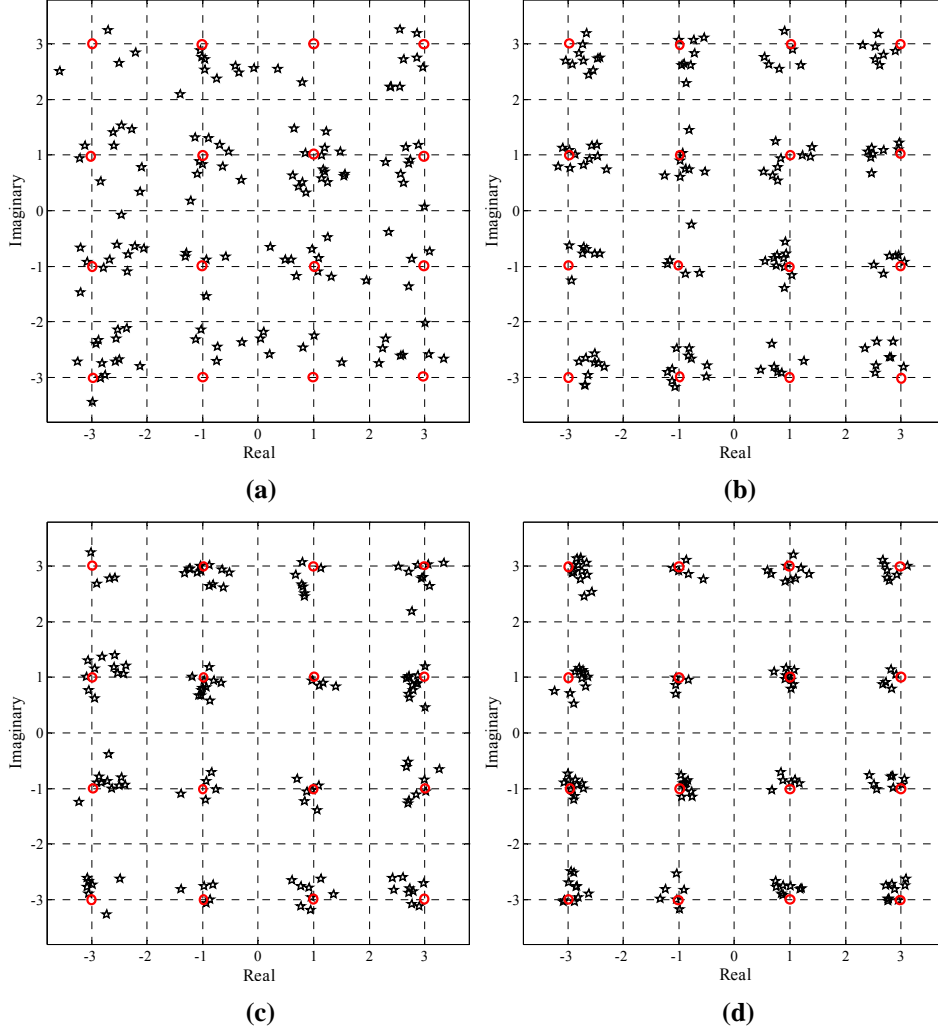


Figure 3.24: Estimated symbol distribution of User-1 using MMSE and OTs aided MSER MUDs for the case of $L = P = 4$ in the SDMA-OFDM system transmitting 16-QAM signals at 20 dB E_b/N_o (a) MMSE (b) AGA MSER (c) ADEA MSER (d) IWO MSER

3.4.2.2 Convergence speed

The convergence speed of the proposed OTs aided MSER MUDs are compared with respect to the rate of change in cost value of User-1 while increasing the number of generations/iterations as shown in Figure 3.25. The signal mapper used is 4-QAM and the wireless

channel considered is the SWATM channel. Here, in order to compare all OTs, 100 generations/iterations each consisting of 100 individuals is chosen. Among various OTs, the cost value of the IWO algorithm fall to a minimum at a faster rate compared to both the AGA and ADEA algorithms while finding optimal solution for the MSER MUD.

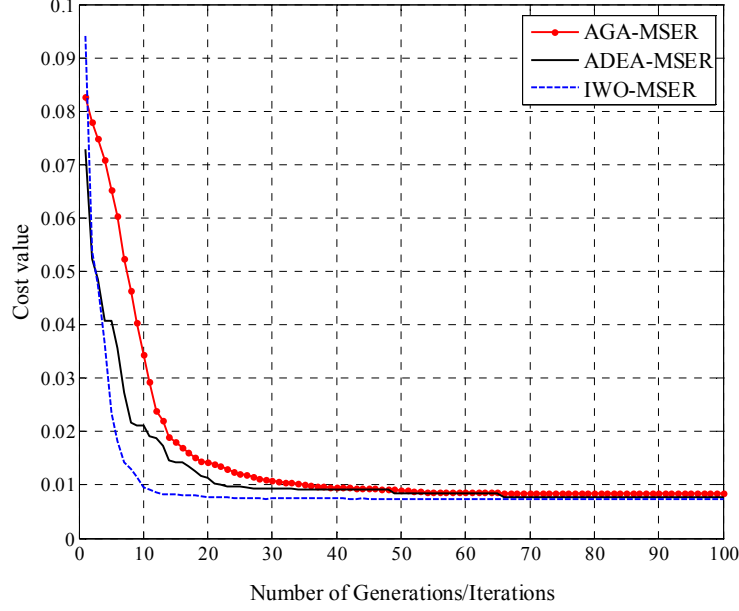


Figure 3.25: Convergence speed comparison of proposed OTs aided MSER MUDs at 15 dB E_b/N_o

3.4.2.3 Complexity

The complexity of the MSER MUD can be compared with the ML Detector on the basis of number of the CF evaluations and computational operations as presented in Table 3.9 and 3.10 respectively. The CF evaluations presented in Table 3.9 are derived from equations given in Table 3.6. All these comparisons for various MUD schemes are considered in a block-fading scenario, where the L users simultaneously transmit either 4-QAM or 16-QAM signals to a P -element antenna BS receiver over N_C subcarriers along with N_G cyclic prefix samples ($N_C = 128$, $N_{CP} = 32$). The channel is assumed to be time-invariant over $N_F = 100$ consecutive OFDM symbols. The FEC used here is the half rate Convolution coding. Further, the complexity of the MMSE and OTs aided MBER MUDs is compared with that of the ML detectors while increasing number of users and is presented in Table 3.11. Finally, the summarized performance comparisons of all proposed OTs while finding the solution for MSER problem in the SDMA-OFDM system with $L = 4$ and $P = 4$ and employing 4-QAM are given in Table 3.12.

Table 3.9: Complexity comparison of OTs aided MSER and ML MUD schemes with respect to CF evaluations when $L = 6$ and $P = 4$

MUD Technique	4-QAM		16-QAM	
	Complexity	% of ML	Complexity	% of ML
AGA MSER ($2 \times G_g \times 2N_g \times (N_C + N_{CP}) \times L$)	3.84×10^7	29.31	1.54×10^8	0.0287
ADEA MSER ($2 \times G_d \times 2N_d \times (N_C + N_{CP}) \times L$)	3.46×10^7	26.41	1.38×10^8	0.0257
IWO MSER ($2 \times I_{max} \times N_S \times (N_C + N_{CP}) \times L$)	2.58×10^7	19.69	1.02×10^8	0.0189
ML Detector ($2 \times 2^{mL} \times (N_C + N_{CP}) \times N_F$)	1.31×10^8	100	5.37×10^{11}	100

Table 3.10: Complexity comparison of MMSE, OTs aided MSER and ML MUD schemes with respect to number of computational operations when $L = 6$ and $P = 4$

MUD	Operator	Computational Complexity	4-QAM		16-QAM	
			Total	% of ML	Total	% of ML
MMSE	\times	$2P(N_C + N_{CP}) \left\{ \frac{2L + P + LN_F + (P-1)(4P+1)/6}{(P-1) + L(P-1)(4P+1)/6} \right\}$	7.99×10^5	1.8×10^{-2}	7.99×10^5	4.8×10^{-6}
	$+$	$2(N_C + N_{CP}) \left\{ \frac{2L(L-1) + (P-1)LN_F + (P-1) + L(P-1)(4P+1)/6}{(P-1) + L(P-1)(4P+1)/6} \right\}$	6.12×10^5	1.7×10^{-2}	6.12×10^5	4.2×10^{-6}
AGA MSER	\times	$2L(N_C + N_{CP}) \left[\frac{(2G_g N_g)(P+7) + P2^{m(L-1)} + PN_F}{P2^{m(L-1)} + PN_F} \right]$	4.31×10^8	9.19	9.74×10^9	0.0532
	$+$	$2L(N_C + N_{CP}) \left[\frac{(2G_g N_g)(LP+2) + P2^{mL} + (P-1)N_F}{P2^{mL} + (P-1)N_F} \right]$	1.03×10^9	29.10	1.33×10^{11}	0.917
ADEA MSER	\times	$2L(N_C + N_{CP}) \left[\frac{(2G_d N_d)(P+7) + P2^{m(L-1)} + PN_F}{P2^{m(L-1)} + PN_F} \right]$	3.89×10^8	8.72	9.57×10^9	0.0523
	$+$	$2L(N_C + N_{CP}) \left[\frac{(2G_d N_d)(LP+2) + P2^{mL} + (P-1)N_F}{P2^{mL} + (P-1)N_F} \right]$	9.31×10^8	26.30	1.32×10^{11}	0.910
IWO MSER	\times	$2L(N_C + N_{CP}) \left[\frac{(I_{max} N_S)(P+7) + P2^{m(L-1)} + PN_F}{P2^{m(L-1)} + PN_F} \right]$	2.92×10^8	6.55	9.17×10^9	0.0501
	$+$	$2L(N_C + N_{CP}) \left[\frac{(I_{max} N_S)(LP+2) + P2^{mL} + (P-1)N_F}{P2^{mL} + (P-1)N_F} \right]$	7.03×10^8	19.86	1.31×10^{11}	0.903
ML Detector	\times	$2(N_C + N_{CP})N_F(PL+2P+2)2^{mL}$	4.46×10^9	100	1.83×10^{13}	100
	$+$	$2(N_C + N_{CP})N_F(PL+P-1)2^{mL}$	3.54×10^9	100	1.45×10^{13}	100

From Table 3.9 and 3.10, it is clear that the proposed OTs especially the IWO aided MSER MUD are computationally economical compared to the ML one in terms of both CF evaluations and computational operations.

Table 3.11: Complexity comparison of OTs aided MSER and ML MUD schemes with respect to CF evaluations while varying L keeping P fixed at four

Number of Users (L)	AGA–MSER	ADEA–MSER	IWO–MSER	ML
4	2.56×10^7	2.304×10^7	2.048×10^7	8.192×10^6
5	3.2×10^7	2.88×10^7	2.56×10^7	3.2768×10^7
6	3.84×10^7	3.456×10^7	3.072×10^7	1.3107×10^8
7	4.48×10^7	4.032×10^7	3.584×10^7	5.2929×10^8
8	5.12×10^7	4.608×10^7	4.096×10^7	2.0972×10^9

Further, it is observed from Table 3.11 that as the number of users is increasing, the complexity of the ML detector increases exponentially, whereas the complexity of the OTs aided MUDs increases at a lesser rate.

Table 3.12: Performance and complexity comparisons of OTs aided MSER MUDs at E_b/N_o values 15 dB

Algorithm	CF Evaluations per Generation	CPU Time per Symbol	Bit Error Rate		
			MIMO Rayleigh fading	SUI	Gaussian
AGA	200	25.895 sec	4.83E-5	0.00011	7.23E-05
ADEA	200	20.030 sec	4.50E-5	5.86E-5	6.32E-05
IWO	168	12.821 sec	2.98E-5	4.94E-5	4.36E-05

3.5 Summary

This chapter investigates various OTs based on popular heuristic search algorithms such as AGA, ADEA and IWO to locate the optimal solution for MER MUD schemes (both MBER and MSER). Extensive simulation study is done to establish the proposed schemes. The CG algorithm requires proper initial selection of the weights while finding the optimal weight vectors of the MBER cost function as discussed in Chapter–2. This lacuna can be overcome by using the OTs for MER MUD schemes, which rely on an intelligent search of a large but finite solution space using statistical methods starting from random locations and they do not require taking cost function derivatives. Among various OTs discussed in this chapter, the IWO algorithm comes out to be a clear winner in various simulation results. The IWO algorithm is a powerful optimization algorithm mimicking the properties of the invasive weeds. Implementation of the IWO is much simpler than the GA, because it uses decimal individuals rather than binary ones and also it doesn't use complex operations such as mutation and cross over. It is also observed that the control parameters of the OTs highly

influence the performance of the MER MUDs. The performance the AGA is controlled by proper selection of G_g and N_g while the ADEA is influenced by G_d and N_d . Similarly, the IWO MER MUDs is highly influenced by parameters such as N_I , I_{max} , S_{max} , σ_{max} , σ_{min} and r . Hence, selection of right combination of these control parameters yields a better performance. The simulation study also shows that proposed OTs aided MER detectors consistently outperform the linear MMSE MUD. Amongst the discussed MUD schemes, the IWO aided MER has a little edge over the AGA and ADEA aide MER MUD schemes in full load and over load conditions, whereas all of these exhibit almost the same performance in under load case. Further, the IWO algorithm outperforms the AGA and ADEA in terms of the convergence rate and computational complexity. The proposed OTs aided MBER/MSER MUDs also provide remarkable complexity gain over the exhaustive classical ML detector as observed in a typical block fading channel environment. Finally, the IWO algorithm emerges to be a good alternative for MER MUDs weight optimization in the investigated SDMA–OFDM system in spite of having more control parameters. It is observed that, in the overload SDMA–OFDM system, the channel's output phasor constellation often becomes nonlinearly separable. So this research in motivated to utilize better nonlinear classifiers for detection of multiuser signals in the SDMA–OFDM system.

Chapter 4

Proposed Neural Network Based Adaptive MUD Schemes

In previous chapters, the fundamentals of classical MUD schemes and details of proposed OTs aided MER MUD schemes are discussed. However, most of these MUDs assume that the channel dynamics are perfectly known at the receiver's end, whereas in the practical systems estimation of the channel response is a must, which imposes additional complexity. In such a condition, employing the highly nonlinear Neural Networks (NNs) [75] can become a good alternative as these models approximate channel parameters in training phase and detect signals in testing phase. During past decade, it has been already established that the NN models can be efficiently utilized for MUD in CDMA system [76–80], but they have not been applied for the SDMA–OFDM system [30]. The ongoing chapter aims to explore the possibility of using NN based MUDs for such a system so that these can achieve better performance with reduced complexity. Among various NN models, the Multilayer Perceptron (MLP) and Radial Basis Function (RBF) are considered to be powerful tools in the area of pattern classification. The MLP models can perform complex mapping between its input and output space and are capable of forming decision regions separated by nonlinear boundaries, whereas the RBF network models form clusters such as hyper spheres around the similar group of input signals. Both these widely used models have their own merits and limitations. Generally, the RBF and MLP models form mapping between real valued input and output signal. However, with the growth of multimedia applications, there is an increased demand for high bandwidth applications. Hence, most of the communication systems need to process complex higher order signals, as these signals are known for their bandwidth efficiency. In such a case, the real valued NN models may fail to transfer the complete input information to the output layer. Therefore, complex valued NNs such as Complex MLP (CMLP) [81–83] and Complex RBF (CRBF) [84–88] are developed to detect higher order signals. Thus, the major contribution of this chapter comprises of designing structures and suitable training algorithms for NN based adaptive MUDs. NN based MUDs are adaptive in nature as they adapt to unknown time varying channel conditions through training.

Section 4.1 introduces the possibility of NN models as multiuser detectors for the SDMA–OFDM system. Section 4.2 and 4.3 describe the real valued MLP and RBF model based MUDs respectively. Section 4.4 presents the necessity of complex valued NNs for MUD. Subsequently, Section 4.5 and 4.6 discuss the CMLP and CRBF NN MUD schemes respectively. Simulation study of the proposed adaptive NN MUDs and comparison with previously discussed classical MMSE, ML and the proposed IWO MER MUDs are presented in Section 4.7. Finally, summary of this chapter is provided in Section 4.8.

4.1 Neural network as multiuser detector for the SDMA–OFDM system

Artificial Neural Network (ANN) or simply Neural Network (NN) is a massively parallel distributed processing system inspired from the biological neural system made up of highly interconnected neural computing elements such as neurons that have the ability to learn and thereby acquire knowledge and make it available for use [75].

Since the evolution of NNs, these models are vastly utilizing in several applications like machine vision, pattern detection, signal filtering, data segmentation, data compression, optimization, classification, complex mapping etc. These models are already well established for signal detection and channel equalization in several communication systems [141, 142], since these are also pattern classification problems. Generally, in multiuser systems, the multiple user's signals gets corrupted with noise and these noisy signals need to be classified at the receiver appropriately. When signal classification in a communication system requires a nonlinear solution, NN can provide better solution. NNs also exhibit high parallelism and adaptability to system parameters. Hence, these models have become an attractive alternative to the classical MUDs. Thus, in recent past, the NN models are extensively utilized for MUD for CDMA system. Especially, the NN models like MLP and RBF based MUDs are drawing considerable research attention [76–80]. However, in the present research, the NN based MUD schemes are applied for another famous multiuser system such as the SDMA–OFDM [143, 144]. Both these MLP and RBF networks have their own mechanisms for nonlinear classification. The classification mechanism in a simple two-dimension case is shown in Figure 4.1. The MLP network classifies the input pattern with arbitrarily shaped nonlinear decision boundaries as shown in Figure 4.1 (a), whereas the RBF networks classifies the input pattern with clusters in form of hyper surfaces or ellipse as shown in Figure 4.1 (b).

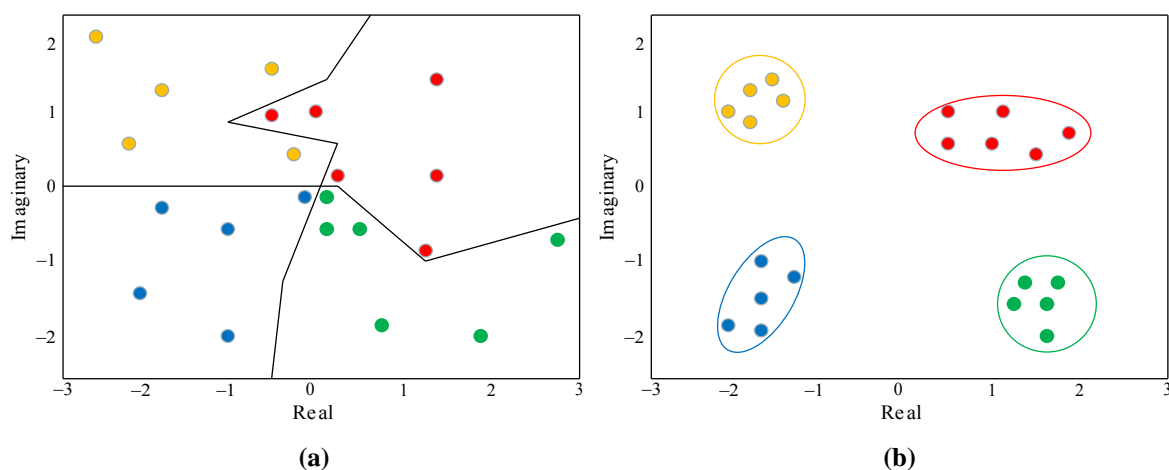


Figure 4.1: Classification mechanisms in two dimension space: (a) MLP network (b) RBF network

As described in Chapter–2, the received signal in the SDMA–OFDM system from eq. (2.4) is expressed as:

$$\mathbf{y} = \mathbf{H}\mathbf{x} + \mathbf{n}$$

The linear detector estimates signal using a linear function such as:

$$\hat{x}_l = \mathbf{w}_l^H \mathbf{y}$$

However, incorporating such a linear detector may allow residual interference and it will fail to mitigate the nonlinear degradation caused by the error prone radio environment. Therefore, incorporating a nonlinear detector is essential to improve detector classification ability. As the NNs models are massively parallel and highly nonlinear, these can become a possible alternative to detect signals of multiple users appropriately. In order to derive the MUD task in terms of NNs, it is essential to define an appropriate Lyapunov energy function corresponding to a specific optimality criterion. This optimality has to be minimized iteratively so that the lowest energy state will yield the desired estimate. The derivation of the Lyapunov function converts the minimization problem into a set of ordinary differential equations [145]. Based on this derivative information, appropriate synaptic weights and input excitations are chosen for the design of NN models. The Lyapunov energy function for MUD of the SDMA–OFDM system can be defined as:

$$E = \frac{1}{2} \sum_{l=1}^L \|e_l\|^2, \text{ where } e_l = \hat{x}_l - x_l \quad (4.1)$$

Here, \hat{x}_l represents estimated signal of l^{th} user. The commonly used nonlinear activation functions in the NN models are *tanh* and *Gaussian* functions, which are given as follows:

$$\rho(y_l) = \tanh y_l = \frac{1 - \exp(-2y_l)}{1 + \exp(-2y_l)} \quad (4.2)$$

$$\rho(y_l) = \exp\left(\frac{-y_l^2}{\sigma^2}\right), \text{ with } \sigma > 0 \quad (4.3)$$

During MUD process, training symbols are periodically sent to the network and detection is accomplished by minimizing the Lyapunov function as given in eq. (4.1). The performance of the NN MUDs is mainly depends on the tracking ability of the training algorithm employed.

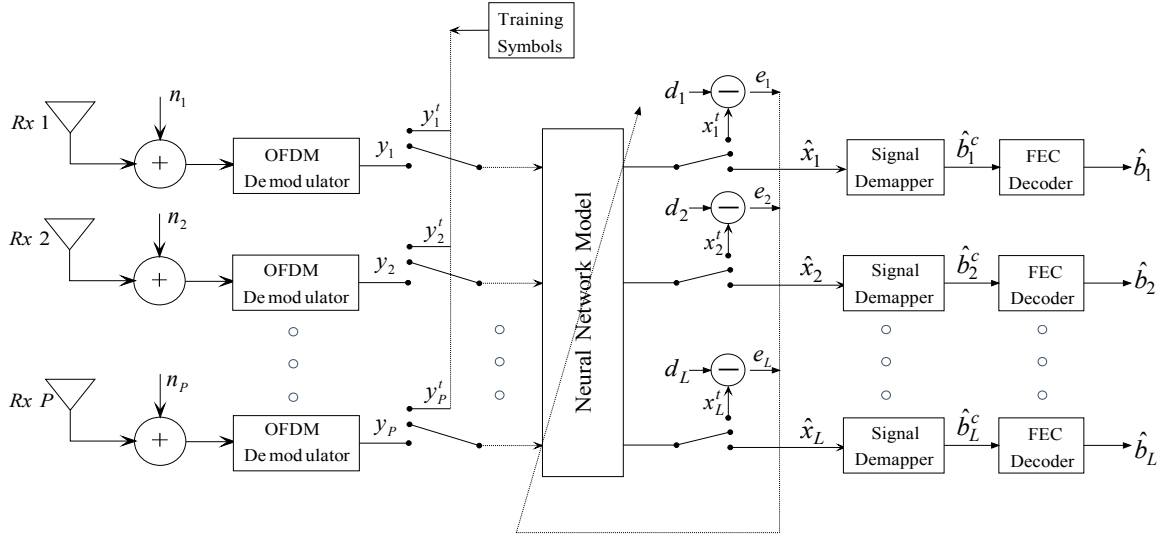


Figure 4.2: NN based multiuser detector for the SDMA-OFDM system with L number of users and P number of receiving antennas

The configuration of an NN based multiuser detector is shown in Figure 4.2. In the NN based MUD process, the model is designed according to the SDMA structure and then the corresponding model is trained using training symbols. After the training, the well trained NN model is switched to the testing mode and it can be used as a multiuser detector. The process of training a NN involves the adjustment of the weights between each pair of the individual neurons and corresponding biases until a close approximation of the desired output is achieved. During network training, an adaptive algorithm has to be applied recursively to update the free parameters of the network based on the error obtained. In this figure, a known sequence \mathbf{y}^t is given as an input to the NN model and its response is available at the output layer. By comparing this with desired response \mathbf{d} , the error signal is computed.

4.2 Multilayer Perceptron (MLP) based MUD scheme²

Among various NN models, the feed forward MLP model is considered as a very general model for the nonlinear processing of real valued signals [73]. It consists of at least three layers of neurons such as an input layer, one or more hidden layers and an output layer. The hidden and output layers may have a non-linear activation function. The MLP network can be trained with the conventional Back Propagation (BP) algorithm, which is a supervised learning algorithm that uses two passes through the network to calculate the change in network weights. In the forward pass, the weights are fixed and the input vector is propagated through the network to produce an output.

²This part of research is included in the paper published by *Neural computing and Applications, Springer*, entitled as “Neural network-based adaptive multiuser detection schemes in SDMA-OFDM system for wireless application”

An output error is calculated from the difference between actual output and the desired output. This error is then propagated backwards through the network, making changes to the weights as required. The details of this algorithm are presented in Appendix B. The architecture of MLP model used for MUD in the SDMA–OFDM system is shown in Figure 4.3, which consists of an input layer of $2P$ units, one hidden layer of H_N neurons and an output layer of L neurons. Here, P and L are equal to number of receiving antenna and number of users in the SDMA–OFDM system respectively. These layers have feed forward connections between neurons. Each neuron in the hidden has a summer along with a non-linear activation. Hence, the resultant output at h^{th} node in the hidden layer is expressed as:

$$z_h = \phi \left(\sum_{k=1}^{2P} U_{hk} y_k' + b_h \right), \quad h = 1, 2, \dots, H_N \quad (4.4)$$

In the above equation y_k' , $k = 1, 2, \dots, 2P$ consist of real and imaginary components of y_p , $p = 1, 2, \dots, P$, that is:

$$y_{2p-1}' = \Re(y_p), \quad p = 1, 2, \dots, P$$

$$y_{2p}' = \Im(y_p), \quad p = 1, 2, \dots, P$$

Here, \Re and \Im represent real and imaginary components respectively. The output layer has a simple summation operator. Hence, the resultant output at l^{th} node in the output layer is expressed as:

$$\hat{x}_l = \sum_{h=1}^{H_N} V_{lh} z_h + b_l, \quad l = 1, 2, \dots, L \quad (4.5)$$

where U_{hk} denotes a weight associated between the hidden node h and input node k ,

V_{lh} denotes a weight associated between the output node l and hidden node h ,

b_h denotes bias of the h^{th} hidden node,

b_l denotes bias of the l^{th} output node,

$\phi(t)$ denotes a nonlinear function such as bi-polar sigmoid, that is $\phi(t) = \tanh(t)$

$\phi'(t)$ denote derivative of $\phi(t)$, if $\phi(t)$ is $\tanh(t)$, then,

$$\phi'(t) = (1 - \tanh^2(t)) \quad (4.6)$$

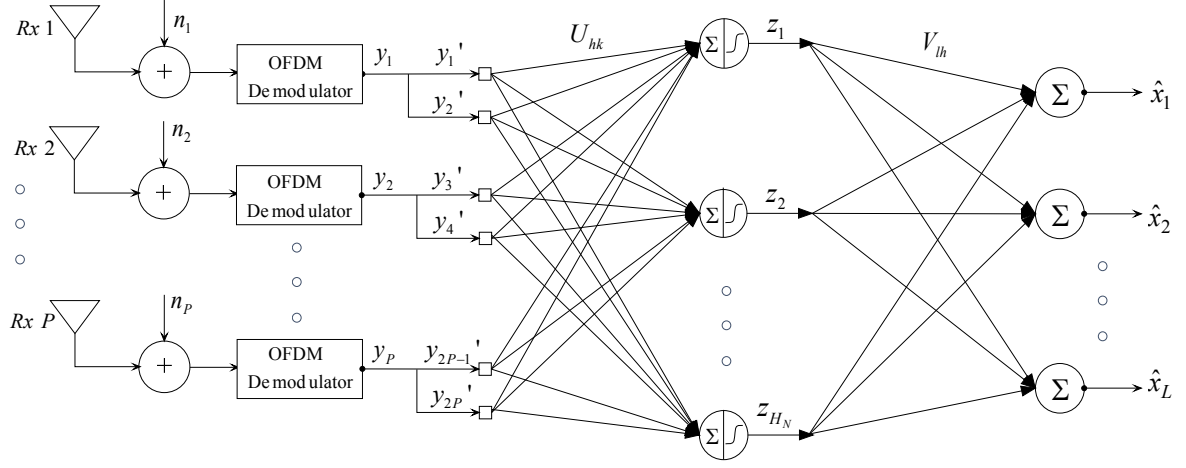


Figure 4.3: Schematic diagram of proposed MLP based MUD scheme for the SDMA-OFDM system

4.2.1 Network training procedure for MLP MUD

In the MLP network training process, an iterative algorithm like the conventional BP algorithm that minimizes an empirical error function can be used efficiently to update connection weights and biases [73]. The procedure is summarized below.

- Initialize randomly all connection weights and thresholds such as $U_{hk}(i)$, $V_{lh}(i)$, $b_h(i)$ and $b_l(i)$ at iteration i ($=1$).
- Compute the hidden vector $z_h(i)$ and output vector $x_l^t(i)$ from eq. (4.4) and eq. (4.5) respectively using training vector $y_k^t(i)$.
- Compute the error term $e_l(i)$ of each output node as:

$$e_l(i) = d_l(i) - x_l^t(i), \quad l = 1, 2, \dots, L$$

- However, the back propagation algorithm requires the calculation error gradient δ at each layer. Thus, the error gradient at l^{th} node of output layer and h^{th} node of hidden layer are given respectively:

$$\delta_l = e_l \phi'(x_l^t), \quad l = 1, 2, \dots, L$$

$$\delta_h = \sum_l V_{lh}^T \delta_l \phi'(z_h), \quad h = 1, 2, \dots, H_N$$

Here, $(.)^T$ represents Transpose.

- Update the network weights of hidden and output nodes according to eq. (B.3) and (B.4):

$$U_{hk}(i+1) = U_{hk}(i) + \mu \delta_h(i) y_k^t(i)$$

$$b_h(i+1) = b_h(i) + \mu \delta_h(i)$$

$$V_{lh}(i+1) = V_{lh}(i) + \mu \delta_l(i) z_h(i)$$

$$b_l(i+1) = b_l(i) + \mu \delta_l(i)$$

where μ is the learning rate parameter, which should be chosen in between zero and one.

- f.* Compute the total error $\|d(i) - x^t(i)\|^2$ and proceed for the computation to the next iteration $(i + 1)$ from Step *b* until this error is less than a defined value or specific convergence criteria is met.

4.3 Radial Basis Function (RBF) based MUD scheme³

RBF networks are popular in several classification problems for their close relation with Bayesian estimators due to the Gaussian activation function. This activation depends on the distance between the input vector and the centre. By properly selecting the number of hidden neurons, approximately 2^L , where L is the number of users in the SDMA–OFDM system, and by training all free parameters accurately, the RBF is able to detect users appropriately. Due to their ability to form complex nonlinear mapping, the RBF network is considered for MUD in CDMA system. Generally, the RBF model uses Gradient Descent (GD) algorithm for network training to update all network parameters at a time [85]. The details of this algorithm are presented in Appendix D.

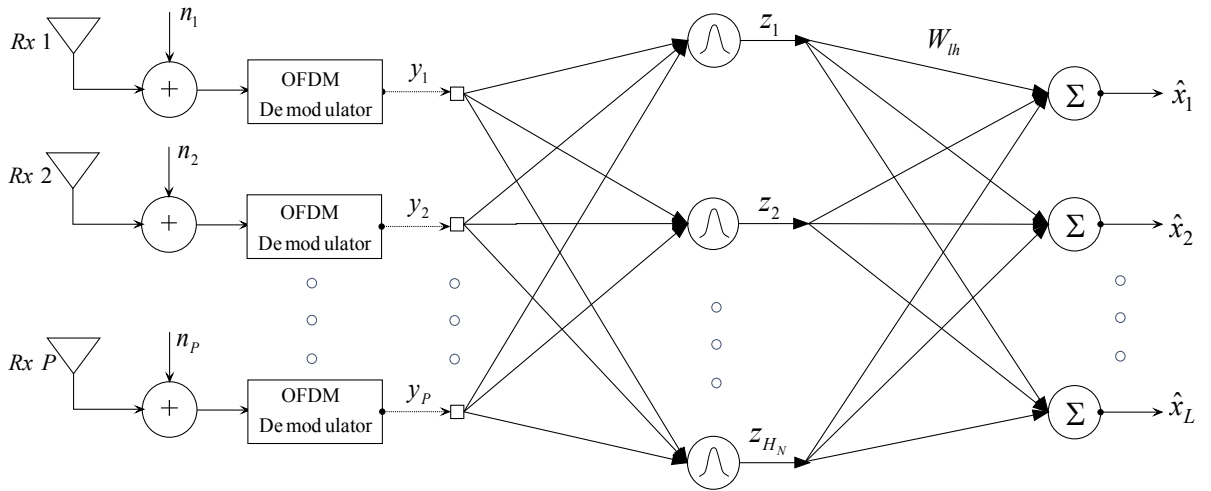


Figure 4.4: Schematic diagram of proposed RBF based MUD scheme for the SDMA–OFDM system

³This part of research is included in the paper published by *International Journal of Electronics, Taylor and Francis*, entitled as “Neural Network–based multiuser detection for SDMA–OFDM system over IEEE 802.11n indoor wireless local area network channel models”

The architecture of RBF model is a three layer feed forward network, which consists of an input layer of P number of input units, an output layer of L number of neurons and the hidden layer with H_N number of neurons existing between input and output layers as shown in Figure 4.4. The values of P and L are corresponding to number of receiving antennas and number of users in the SDMA–OFDM system respectively. The inter connection between input layer and hidden layer forms hypothetical connection and between the hidden and output layer forms weighted connections. In general, the RBF network incorporate Gaussian activation functions, hence the output of each neuron in the hidden layer is expressed as:

$$z_h = \exp\left(-\frac{\|\mathbf{y} - \mathbf{C}_h\|^2}{2\sigma_h^2}\right), \quad h = 1, 2, \dots, H_N \quad (4.7)$$

where \mathbf{C}_h is the $(P \times 1)$ dimensional complex-valued center and σ_h is the spread parameter of the h^{th} hidden neuron. The neurons in the output layer are simple summing elements. Hence, the output of each neuron of output layer is calculated as:

$$\hat{\mathbf{x}}_l = \sum_{h=1}^{H_N} W_{lh} z_h, \quad l = 1, 2, \dots, L \quad (4.8)$$

4.3.1 Network training procedure for RBF MUD

In the RBF network training process, an iterative algorithm like Gradient Descent (GD) that minimizes an empirical error function can be used to update free parameters of the network [85]. The procedure of this algorithm is summarized below.

- a. Initialize randomly all the network free parameters such as $W_{lh}(i)$, $C_h(i)$ and $\sigma_h(i)$ at iteration i ($=1$). The network centers can be initialized using k-means clustering algorithm, which is presented in Appendix D.
- b. Compute the hidden vector $z_h(i)$ and output vector $x_l^t(i)$ from eq. (4.7) and eq. (4.8) respectively using training vector $y_p^t(i)$.
- c. Compute the error term $e_l(i)$ of each output node as:

$$e_l(i) = d_l(i) - x_l^t(i), \quad l = 1, 2, \dots, L$$

- d. Update the weights, centers and spreads according to eq. (D.2), (D.4) and (D.6):

$$W_{lh}(i+1) = W_{lh}(i) + \mu_w z_h e_l$$

$$C_h(i+1) = C_h(i) + \mu_c e \frac{W_{lh} z_h}{\sigma_h^2} \left(\sum_{p=1}^P (y_p^t - C_h)^R + j \sum_{p=1}^P (y_p^t - C_h)^I \right)$$

$$\sigma_h(n+1) = \sigma_h(n) + \mu_s e W_{lh} z_h \frac{\|y^t - C_h\|^2}{\sigma_h^3}$$

where μ_w , μ_c and μ_s are the weight, center and spread learning parameters respectively.

- e. Compute the total error $\|d(i) - x'(i)\|^2$ and proceed for the computation to the next iteration $(i+1)$ from Step *b* until this error is less than a defined value or specific convergence criteria is met.

4.4 Necessity of complex valued neural networks

In recent past, several researches have proved that the real valued NNs can be effectively incorporated in several equalization and MUD problems when the signals are lower ordered ones. However, the SDMA–OFDM system with higher order signal mapper has to process complex valued desired signals. In addition to that, to exploit effectiveness of digital radio links, the high-power amplifiers of the transmitter introduces nonlinearities, which cause degradation of the received signal. This degradation may affect both amplitude and phase of the signal. It is well known that the signals like M–QAM are very sensitive to nonlinear distortion which causes spectral spreading, Inter Symbol Interference (ISI), constellation warping and IQ imbalance [146]. Therefore, the classical real valued NNs cannot be applied directly because these models cannot mitigate the impairment of phase distortion. In order to extend the real valued NN models to complex valued NN models, the neurons should be modeled with complex activation function and processing has to be done in a complex multidimensional space. This basic approach motivated the development of several algorithms for equalization of communication using complex-valued NNs [81–88].

While extending the nonlinear real valued activation function to nonlinear complex valued activation function through a standard procedure of analytic continuation, the obtained complex function may become unbounded in the complex plane. To solve this problem, the classical real valued activation function $\phi(t)$ can be written in the complex form as:

$$F(t) = \phi(\Re(t)) + j\phi(\Im(t)) \quad (4.9)$$

The complex function $F(t)$ is always bounded for all t and behaves in a similar manner to its real valued counterpart. The magnitude plots of the real and complex valued activation function for both *tanh* and *Gaussian* approximations are plotted in Figure 4.5. However, as $F(t)$ is complex in nature, the standard BP and GD algorithms cannot be used directly. For NNs with above complex activation function and complex inputs, a suitable training algorithm are developed in the proceeding sections such that the NN based MUDs are well suited to deal with the complex-valued signals.

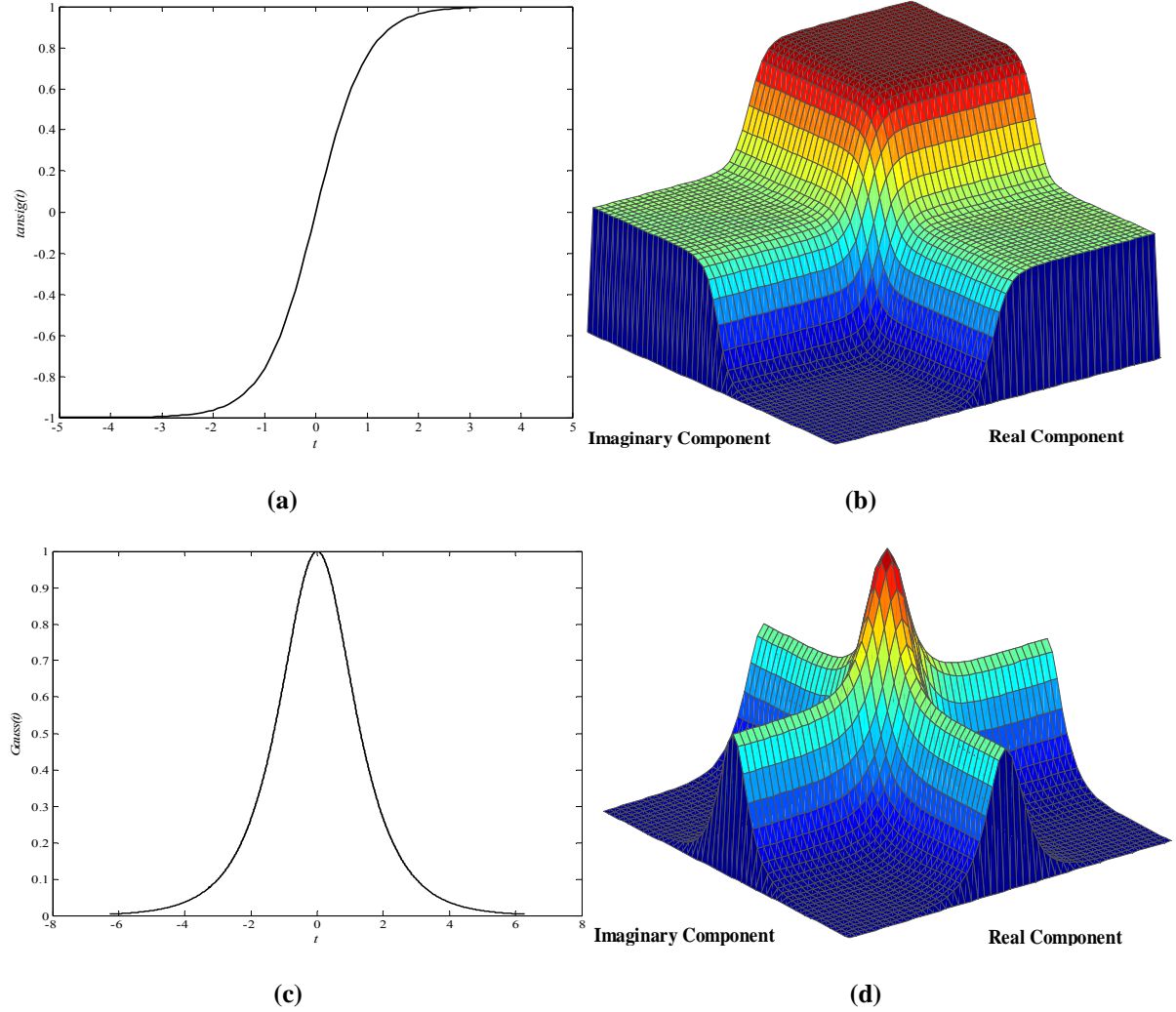


Figure 4.5. Magnitude plot of activation functions used in different NN models (a) Real valued MLP (b) Complex valued MLP (c) Real valued RBF (d) Complex valued RBF

4.5 Complex MLP (CMLP) based MUD scheme

The classical MLP network requires both input and desired response to be real valued. However, if the signals of the SDMA–OFDM system are in complex form, it fails to transfer the complete input information to the output layer. In such cases, as the response of the neurons in the CMLP model is complex and hence it can be efficiently used as a multiuser

detector. During the network training process, the CMLP MUD with complex signals and weights employs complex BP algorithm for selecting the network parameters [147, 148].

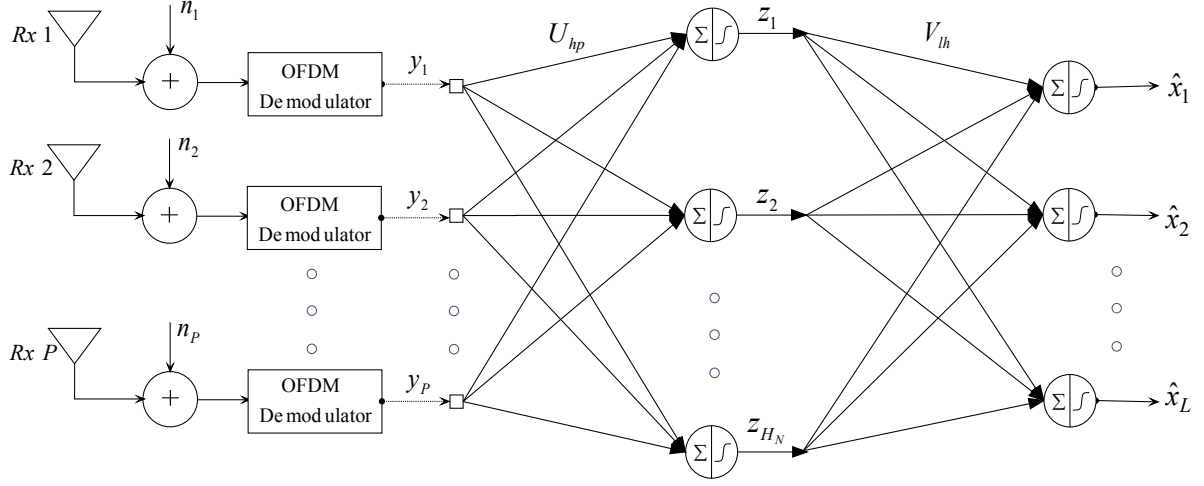


Figure 4.6: Schematic diagram of proposed CMLP based MUD scheme for the SDMA-OFDM system

The architecture of MLP shown in Figure 4.6 consists of an input layer of P units, one hidden layer of H_N neurons and an output layer of L neurons. In the CMLP, the classical real-valued sigmoid function is extended to the complex plane such that it is bounded everywhere. The resultant complex activation function can be expressed as:

$$\text{TANH}(t) = \varphi(\Re(t)) + j\varphi(\Im(t)) \quad (4.10)$$

The nonlinear activation function $\varphi(t)$ is $\tanh(t)$. The behavior of this activation function in the complex plane is plotted in Figure 4.5(b). Each neuron in the hidden and output layer has a nonlinear activation and a summation operator. Hence, the resultant output at h^{th} node in the hidden layer can be expressed as:

$$z_h = \varphi\left(\Re\left(\sum_{p=1}^P U_{hp} y_p + b_h\right)\right) + j\varphi\left(\Im\left(\sum_{p=1}^P U_{hp} y_p + b_h\right)\right), \quad h = 1, 2, \dots, H_N \quad (4.11)$$

The resultant output at l^{th} node in the output layer is expressed as:

$$\hat{x}_l = \varphi\left(\Re\left(\sum_{h=1}^{H_N} V_{lh} z_h + b_l\right)\right) + j\varphi\left(\Im\left(\sum_{h=1}^{H_N} V_{lh} z_h + b_l\right)\right), \quad l = 1, 2, \dots, L \quad (4.12)$$

where U_{hp} denotes a weight associated between the hidden node h and input node p ,

V_{lh} denotes a weight associated between the output node l and hidden node h ,

b_h denotes bias of the h^{th} hidden node,

b_l denotes bias of the l^{th} output node,

4.5.1 Development of the complex BP algorithm for CMLP network training

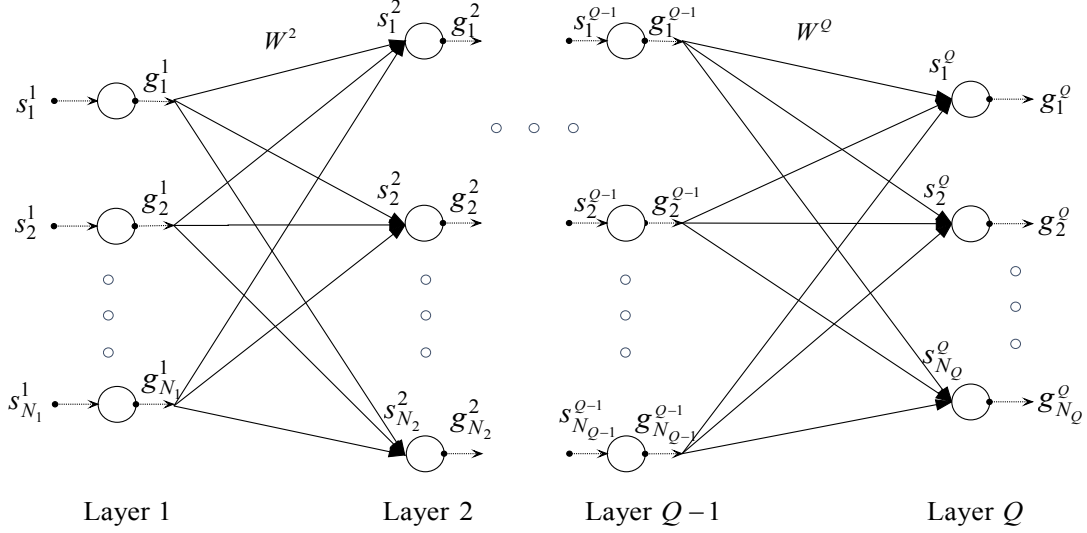


Figure 4.7: Training model of CMLP network

During the proposed CMLP network training, the conventional BP algorithm cannot be applied directly as all connection weights and biases are complex in form. For BP algorithm to be applied for CMLP network training, it is required to compute the gradient of the instantaneous error with respect to real and imaginary components of all network weights and biases. Thus, the modifications incorporated in this algorithm are derived as follows.

Figure 4.7 represents a typical training model of CMLP model with Q number of layers each consisting n neurons. Let, g_n^q is the activation output of the n^{th} neuron in the q^{th} layer, then the net activation value of the n^{th} neuron in the q^{th} layer is given by:

$$s_n^q = \sum_{m=0}^{N_{q-1}} W_{nm}^q g_m^{q-1}, \quad n=1,2,\dots,N_q, \quad q=1,2,\dots,Q$$

where $g_n^q = \text{TANH}(s_n^q)$, and $n=0$ refers to the bias input: i.e. $g_0^q = 1$. Also, when $q=0$, then g_n^0 , $n=1,2,\dots,N_0$ refers the input signal. Assuming $g_n^q = u_n^q + jv_n^q$,

$$s_n^q = \sum_{m=0}^{N_{q-1}} (W_{nm}^{qR} + jW_{nm}^{qI})(u_m^{q-1} + jv_m^{q-1})$$

$$= \sum_{m=0}^{N_{q-1}} (W_{nm}^{qR} u_m^{q-1} - W_{nm}^{qI} v_m^{q-1}) + j (W_{nm}^{qR} v_m^{q-1} + W_{nm}^{qI} u_m^{q-1})$$

The superscripts R and I corresponds to real and imaginary values respectively. In the complex BP algorithm, the network weights are adjusted such that the error in the output layer is minimized. Hence, the sum squared global instantaneous error at the output layer ‘ Q ’ is expressed as:

$$E = \frac{1}{2} \sum_{n=1}^{N_Q} \|e_n\|^2$$

where $e_n = d_n - g_n^Q$, $n=1,2,...,N_Q$ and d_n is the desired response. The gradient of E with respect to g_n^q is:

$$\nabla_{g_n^q} E = \frac{\partial E}{\partial g_n^q} = \frac{\partial E}{\partial g_n^{qR}} + j \frac{\partial E}{\partial g_n^{qI}} \quad (4.13)$$

Similarly, the gradient of E with respect to s_n^q is:

$$\nabla_{s_n^q} E = \frac{\partial E}{\partial s_n^q} = \frac{\partial E}{\partial s_n^{qR}} + j \frac{\partial E}{\partial s_n^{qI}} \quad (4.14)$$

From eq. (4.13) and eq. (4.14), the error gradient of n^{th} neuron in the q^{th} layer is derived as:

$$\delta_n^q = \frac{\partial E}{\partial g_n^{qR}} \frac{\partial g_n^{qR}}{\partial s_n^{qR}} + j \frac{\partial E}{\partial g_n^{qI}} \frac{\partial g_n^{qI}}{\partial s_n^{qI}}$$

$$\delta_n^{qR} + j \delta_n^{qI} = e_n^{qR} \varphi'(s_n^{qR}) + j e_n^{qI} \varphi'(s_n^{qI})$$

Since the weight vector in complex valued, the gradient of instantaneous error can be obtained by calculating the gradient of the error with respect to both the real and imaginary components of the W_{nm}^q , which is according to:

$$\nabla_{W_{nm}^q} E = \frac{\partial E}{\partial W_{nm}^q} = \frac{\partial E}{\partial W_{nm}^{qR}} + j \frac{\partial E}{\partial W_{nm}^{qI}}$$

Using the chain rule,

$$\frac{\partial E}{\partial W_{nm}^{qR}} = \frac{\partial E}{\partial s_n^{qR}} \frac{\partial s_n^{qR}}{\partial W_{nm}^{qR}} + \frac{\partial E}{\partial s_n^{qI}} \frac{\partial s_n^{qI}}{\partial W_{nm}^{qR}}$$

$$\frac{\partial E}{\partial W_{nm}^{qI}} = \frac{\partial E}{\partial s_n^{qR}} \frac{\partial s_n^{qR}}{\partial W_{nm}^{qI}} + \frac{\partial E}{\partial s_n^{qI}} \frac{\partial s_n^{qI}}{\partial W_{nm}^{qI}}$$

In the above equations

$$\frac{\partial s_n^{qR}}{\partial W_{nm}^{qR}} = u_m^{q-1}, \frac{\partial s_n^{qI}}{\partial W_{nm}^{qR}} = -v_m^{q-1}, \frac{\partial s_n^{qR}}{\partial W_{nm}^{qI}} = v_m^{q-1}, \frac{\partial s_n^{qI}}{\partial W_{nm}^{qI}} = u_m^{q-1}$$

$$\frac{\partial E}{\partial W_{nm}^{qR}} = -\delta_n^{qR} u_m^{q-1} - \delta_n^{qI} v_m^{q-1}$$

$$\frac{\partial E}{\partial W_{nm}^{qI}} = -\delta_n^{qR} (-v_m^{q-1}) - \delta_n^{qI} u_m^{q-1}$$

From above equations $\nabla_{W_{nm}^q} E$ can be obtained as:

$$\begin{aligned} \nabla_{W_{nm}^q} E &= \left(-\delta_n^{qR} u_m^{q-1} - \delta_n^{qI} v_m^{q-1} \right) + j \left(\delta_n^{qR} v_m^{q-1} - \delta_n^{qI} u_m^{q-1} \right) \\ &= - \left(\delta_n^{qR} + j \delta_n^{qI} \right) \left(g_m^{q-1} \right)^* \\ &= - \left(g_m^{q-1} \right)^* \delta_n^q \end{aligned}$$

where $(.)^*$ denote the complex conjugate. The correction ΔW_{nm}^q applied to W_{nm}^q is defined by delta rule as:

$$\Delta W_{nm}^q = -\mu \nabla_{W_{nm}^q} E \quad (4.15)$$

where μ is the learning parameter.

The generalized error gradient for $q = Q, Q-1, \dots, 1$ and $n = 1, 2, \dots, N_q$ as:

$$e_n^q = \begin{cases} e_n, & \text{for } q = Q \\ \sum_{r=l}^{N_{q+1}} W_{rn}^{*(q+1)} \delta_r^{q+1}, & \text{for } q = Q-1, \dots, 1 \end{cases} \quad (4.16)$$

$$\delta_n^q = e_n^{qR} \phi'(s_n^{qR}) + j e_n^{qI} \phi'(s_n^{qI}) \quad (4.17)$$

4.5.2 Network training procedure for CMLP MUD

In the CMLP network training process, an iterative algorithm like the complex BP algorithm that minimizes an empirical error function can be used efficiently to update connection weights and biases [147, 148]. The procedure is summarized below.

- a. Initialize randomly all connection weights and thresholds such as $U_{hp}(i), V_{lh}(i), b_h(i)$ and $b_l(i)$ at iteration i ($=1$).
- b. Compute the hidden vector $z_h(i)$ and output vector $x_l^t(i)$ from eq. (4.11) and eq. (4.12) respectively from the training symbol $y_k^t(i)$.
- c. Compute the error term $e_l(i)$ of each output node as:

$$e_l(i) = d_l(i) - x_l^t(i), \quad l = 1, 2, \dots, L$$

- d. However, the BP algorithm requires the error gradient δ at each layer. Thus, the error gradient at l^{th} node of output layer and h^{th} node of hidden layer are given respectively:

$$\delta_l = \Re(e_l) \phi'(\Re(x_l^t)) + j \Im(e_l) \phi'(\Im(x_l^t))$$

$$\delta_h = \Re\left(\sum_l V_{lh}^H \delta_l\right) \phi'(\Re(z_h)) + j \Im\left(\sum_l V_{lh}^H \delta_l\right) \phi'(\Im(z_h))$$

Here, $(.)^H$ represents Hermitian transpose.

- e. Update the weights and biases of hidden nodes and output nodes are from:

$$U_{hp}(i+1) = U_{hp}(i) + \mu \delta_h(i) y_p^H(i)$$

$$b_h(i+1) = b_h(i) + \mu \delta_h(i)$$

$$V_{lh}(i+1) = V_{lh}(i) + \mu \delta_l(i) z_h^H(i)$$

$$b_l(i+1) = b_l(i) + \mu \delta_l(i)$$

where μ is the learning rate parameter, which should be in between zero and one.

- f. Compute the total error $\|d(i) - x^t(i)\|^2$ and proceed for the computation to next iteration ($i+1$) from Step b until this error is less than a defined value or specific convergence criteria is met.

4.6 Complex RBF (CRBF) based MUD scheme⁴

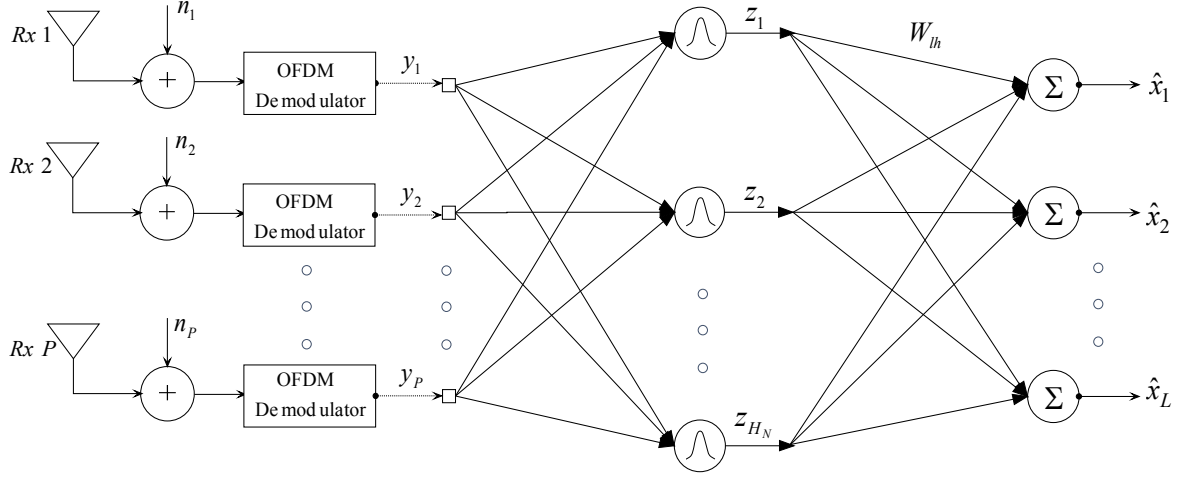


Figure 4.8: Schematic diagram of proposed CRBF based MUD scheme for the SDMA-OFDM system

In general, the RBF network uses Gaussian activation function, which produces always a real valued response. If the available and desired signals are in complex form, then this network fails to transfer the complete complex input information to the output layer. Hence, R. Savitha et al. proposed a Complex RBF (CRBF) model with *sech* activation function to solve various adaptive signal processing problems [149–151]. The behavior of the *sech* function is same as Gaussian approximation and it also able to generate complex response. Further, in this research, this activation function is expanded by splitting it in to two independent components to respond individually for real and imaginary inputs in order to make it computationally economical while evaluating error gradient. The architecture of CRBF model is as same as real valued RBF with three layer feed forward network, which consists an input layer of P number of input units, an output layer of L number of neurons and a hidden layer of H_N number of neurons as shown in Figure 4.8. The inter connection between input layer and hidden layer forms hypothetical connection and between hidden and output layer forms weighted connections. The CRBF network processes complex valued signals and produces outputs in a bounded complex plane. The resultant activation function is defined as:

$$\text{SECH}(t) = \phi(\Re(t)) + j\phi(\Im(t)) \quad (4.18)$$

Here, the nonlinear activation function $\phi(t)$ is the $\text{sech}(t)$ function and the behavior of the this function is plotted in Figure 4.5(d). In the CRBF network, each neuron in the hidden has a complex nonlinear activation function as given in eq. (4.18).

⁴This part of research is included in the paper accepted by *IET Communications*, entitled as “An Efficient Complex Radial Basis Function Model for Multiuser Detection in an SDMA/MIMO – OFDM System”

Hence, the resultant output at h^{th} node in the hidden layer can be expressed as:

$$z_h = \phi\left((V_h^R)^T(y - C_h)^R\right) + j\phi\left((V_h^I)^T(y - C_h)^I\right), \quad h = 1, 2, \dots, H_N \quad (4.19)$$

where V_h and C_h are the $(P \times 1)$ dimensional complex-valued scaling factor and centers of the h^{th} hidden neuron respectively. The neurons in the output layer are simple summing elements. Hence, the output of each neuron in the output layer is:

$$\hat{x}_l = \sum_{h=1}^{H_N} W_{lh} z_h, \quad l = 1, 2, \dots, L \quad (4.20)$$

4.6.1 Development of the complex GD algorithm for CRBF network training

During the proposed CRBF network training, the classical GD algorithm cannot be applied directly, since all network free parameters are in complex form. For GD algorithm to be applied for CRBF network training, it is required to compute the gradient of the instantaneous error with respect to real and imaginary components of all network free parameters. The complex GD algorithm computes the instantaneous gradient of the squared error $\|e_l\|^2$ and updates the network free parameters in the opposite direction of their respective gradients. Let q be the network parameter (it might be W , C or V) at iteration i then the updated parameter at iteration $i + 1$ be according to:

$$q_{i+1} = q_i - \mu_i \frac{\partial E}{\partial q_i} = q_i + \Delta q_i \quad (4.21)$$

where μ_i is the momentum parameter and. The sum squared error is defined as:

$$E = \frac{1}{2} \sum_{l=1}^L \|e_l\|^2, \quad \text{where } e_l = d_l - x_l^t$$

Assuming $z_h = u_h + jv_h$, the response vector x_l^t corresponding to the training vector y_p^t , $p = 1, 2, \dots, P$, is expressed as:

$$\begin{aligned} x_l^t &= \sum_{h=1}^{H_N} W_{lh} z_h = \sum_{h=1}^{H_N} (W_{lh}^R + jW_{lh}^I)(u_h + jv_h) \\ &= \sum_{h=1}^{H_N} (W_{lh}^R u_h - W_{lh}^I v_h) + j(W_{lh}^R v_h + W_{lh}^I u_h) \end{aligned}$$

Since the weight vector is complex valued, the gradient of the instantaneous error can be obtained by calculating the gradient of the error with respect to both the real and imaginary components of the W_{lh} , which is according to:

$$\frac{\partial E}{\partial W_{lh}} = \nabla_{W_{lh}} E = \frac{\partial E}{\partial W_{lh}^R} + j \frac{\partial E}{\partial W_{lh}^I}$$

Using the chain rule,

$$\frac{\partial E}{\partial W_{lh}^R} = \frac{\partial E}{\partial x_l^{tR}} \frac{\partial x_l^{tR}}{\partial W_{lh}^R} + \frac{\partial E}{\partial x_l^{tI}} \frac{\partial x_l^{tI}}{\partial W_{lh}^R}; \quad \frac{\partial E}{\partial W_{lh}^I} = \frac{\partial E}{\partial x_l^{tR}} \frac{\partial x_l^{tR}}{\partial W_{lh}^I} + \frac{\partial E}{\partial x_l^{tI}} \frac{\partial x_l^{tI}}{\partial W_{lh}^I}$$

In the above equations

$$\frac{\partial E}{\partial x_l^{tR}} = -e^R; \quad \frac{\partial E}{\partial x_l^{tI}} = -e^I$$

$$\frac{\partial x_l^{tR}}{\partial W_{lh}^R} = u_h; \quad \frac{\partial x_l^{tI}}{\partial W_{lh}^R} = -v_h; \quad \frac{\partial x_l^{tR}}{\partial W_{lh}^I} = v_h; \quad \frac{\partial x_l^{tI}}{\partial W_{lh}^I} = u_h$$

$$\frac{\partial E}{\partial W_{lh}^R} = -e^R u_h - e^I v_h; \quad \frac{\partial E}{\partial W_{lh}^I} = -e^R (-v_h) - e^I u_h$$

Using above solutions $\nabla_{W_{lh}} E$ can obtain that:

$$\nabla_{W_{lh}} E = -e_l z_h^* \quad (4.22)$$

From eq. (4.21) and (4.22) the update of weight is defined as:

$$\Delta W_{lh} = -\mu_w \nabla_{W_{lh}} E$$

$$\Delta W_{lh} = \mu_w e_l z_h^* \quad (4.23)$$

where $(.)^*$ denotes the complex conjugate and μ_w is the learning parameter of weight. Similarly, the update of V_h requires calculation of gradient of error with respect to real and imaginary components of V_h .

$$\frac{\partial E}{\partial V_h} = \nabla_{V_h} E = \frac{\partial E}{\partial V_h^R} + j \frac{\partial E}{\partial V_h^I} \quad (4.24)$$

Using the chain rule,

$$\frac{\partial E}{\partial V_h^R} = \frac{\partial E}{\partial x_l^{tR}} \left[\frac{\partial x_l^{tR}}{\partial u_h} \frac{\partial u_h}{\partial V_h^R} + \frac{\partial x_l^{tR}}{\partial v_h} \frac{\partial v_h}{\partial V_h^R} \right] + \frac{\partial E}{\partial x_l^{tI}} \left[\frac{\partial x_l^{tI}}{\partial u_h} \frac{\partial u_h}{\partial V_h^R} + \frac{\partial x_l^{tI}}{\partial v_h} \frac{\partial v_h}{\partial V_h^R} \right]$$

$$\frac{\partial E}{\partial V_h^R} = -\phi' \left((V_h^R)^T (y^t - C_h)^R \right) (y^t - C_h)^R \left[e^R W_{lh}^R + e^I W_{lh}^I \right] \quad (4.25)$$

$$\frac{\partial E}{\partial V_h^I} = \frac{\partial E}{\partial x_l^{tR}} \left[\frac{\partial x_l^{tR}}{\partial u_h} \frac{\partial u_h}{\partial V_h^I} + \frac{\partial x_l^{tR}}{\partial v_h} \frac{\partial v_h}{\partial V_h^I} \right] + \frac{\partial E}{\partial x_l^{tI}} \left[\frac{\partial x_l^{tI}}{\partial u_h} \frac{\partial u_h}{\partial V_h^I} + \frac{\partial x_l^{tI}}{\partial v_h} \frac{\partial v_h}{\partial V_h^I} \right]$$

$$\frac{\partial E}{\partial V_h^I} = -\phi' \left((V_h^I)^T (y^t - C_h)^I \right) (y^t - C_h)^I \left[e^I W_{lh}^R - e^R W_{lh}^I \right] \quad (4.26)$$

From eq. (2.24)–eq. (2.26) above solutions, the update of scaling factor is determined as:

$$\Delta V_h = -\mu_v \nabla_{V_h} E$$

$$\Delta V_h = \mu_v \left[\phi' \left((V_h^R)^T (y^t - C_h)^R \right) (y^t - C_h)^R \left(e^R W_{lh}^R + e^I W_{lh}^I \right) + \right. \\ \left. \phi' \left((V_h^I)^T (y^t - C_h)^I \right) (y^t - C_h)^I \left(e^I W_{lh}^R - e^R W_{lh}^I \right) \right] \quad (4.27)$$

Here, μ_v is the learning parameter of scaling factor. If $\phi(t) = \text{sech}(t)$ then the derivative is $\phi'(t) = -\tanh(t)\text{sech}(t)$. Further, the update of C_h requires gradient of error with respect to real and imaginary components of C_h .

$$\frac{\partial E}{\partial C_h} = \nabla_{C_h} E = \frac{\partial E}{\partial C_h^R} + j \frac{\partial E}{\partial C_h^I} \quad (4.28)$$

Using chain rule,

$$\frac{\partial E}{\partial C_h^R} = \frac{\partial E}{\partial x_l^{tR}} \left[\frac{\partial x_l^{tR}}{\partial u_h} \frac{\partial u_h}{\partial C_h^R} + \frac{\partial x_l^{tR}}{\partial v_h} \frac{\partial v_h}{\partial C_h^R} \right] + \frac{\partial E}{\partial x_l^{tI}} \left[\frac{\partial x_l^{tI}}{\partial u_h} \frac{\partial u_h}{\partial C_h^R} + \frac{\partial x_l^{tI}}{\partial v_h} \frac{\partial v_h}{\partial C_h^R} \right]$$

$$\frac{\partial E}{\partial C_h^R} = \phi' \left((V_h^R)^T (y^t - C_h)^R \right) V^R \left[e^R W_{lh}^R + e^I W_{lh}^I \right] \quad (4.29)$$

$$\frac{\partial E}{\partial C_h^I} = \frac{\partial E}{\partial x_l^{tR}} \left[\frac{\partial x_l^{tR}}{\partial u_h} \frac{\partial u_h}{\partial C_h^I} + \frac{\partial x_l^{tR}}{\partial v_h} \frac{\partial v_h}{\partial C_h^I} \right] + \frac{\partial E}{\partial x_l^{tI}} \left[\frac{\partial x_l^{tI}}{\partial u_h} \frac{\partial u_h}{\partial C_h^I} + \frac{\partial x_l^{tI}}{\partial v_h} \frac{\partial v_h}{\partial C_h^I} \right]$$

$$\frac{\partial E}{\partial C_h^I} = \phi' \left((V_h^I)^T (y^t - C_h)^I \right) V^I \left[e^I W_{lh}^R - e^R W_{lh}^I \right] \quad (4.30)$$

From eq. (4.28)–eq. (4.30) the update of center is defined as:

$$\begin{aligned} \Delta C_h &= -\mu_c \nabla_{C_h} E \\ \Delta C_h &= -\mu_c \left[\phi' \left((V_h^R)^T (y^t - C_h)^R \right) V^R \left(e^R W_{lh}^R + e^I W_{lh}^I \right) + \right. \\ &\quad \left. \phi' \left((V_h^I)^T (y^t - C_h)^I \right) V^I \left(e^I W_{lh}^R - e^R W_{lh}^I \right) \right] \end{aligned} \quad (4.31)$$

where μ_c learning parameter of center.

4.6.2 Network training procedure for CRBF MUD

In the complex CRBF training process, an iterative algorithm such as complex GD that minimizing an empirical error function is used efficiently to update network free parameters, which is summarized as given below:

- a. Initialize randomly all connection weights and thresholds such as $W_{lh}(i)$, $C_h(i)$ and $V_h(i)$ at iteration $I (=1)$.
- b. Compute $z_h(i)$ and $x_l^t(i)$ from eq. (4.19) and eq. (4.20) respectively from the training symbol $y_k^t(i)$.
- c. Compute the error term $e_l(i)$ of each output node as:

$$e_l(i) = d_l(i) - x_l^t(i), \quad l = 1, 2, \dots, L$$

- d. Update the weights, centers and scaling factors according to:

$$W_{lh}(i+1) = W_{lh}(i) + \Delta W_{lh}(i)$$

$$C_h(i+1) = C_h(i) + \Delta C_h(i)$$

$$V_h(i+1) = V_h(i) + \Delta V_h(i)$$

- e. Compute the total error $\|d(i) - x^t(i)\|^2$ and proceed for the computation to next iteration $(i+1)$ from Step b until this error is less than a defined value or specific convergence criteria is met.

4.7 Simulation study and performance analysis

In this section, the proposed NN model based adaptive MUD schemes have been examined under different channel conditions as presented in Appendix A. Simulation results obtained by using MLP and RBF MUDs are compared to that of the conventional MMSE, ML and the proposed IWO aided MBER MUDs. Similarly, simulation results obtained by using CMLP and CRBF MUDs are compared to that of the conventional MMSE, ML and the proposed IWO aided MSER MUDs. All these simulations are considered for the SDMA–OFDM system and simulation parameters of the system are according to the parameters given in Section 2.7 of Chapter 2.

4.7.1 Results and discussion for real valued NN based MUDs

The simulation parameters of NN models are selected based on the SDMA–OFDM system parameters. The number of input and output neurons of the NN models are considered according to number of receiving antennas (P) and number of users (L) in the SDMA–OFDM system respectively. As the input and output dimension are kept constant, the only factor that influences the performance NN based MUDs for SDMA–OFDM system is the selection of the number of hidden nodes (H_N). Figure 4.9 shows the BER performance of MLP and RBF aided MUDs in the SDMA–OFDM system while varying number of hidden neurons. In this figure, it is observed that, as the number of hidden neurons increases from 4 to 24, the performance of MLP detector does not improve much, whereas the performance of RBF MUD is significantly enhanced. This is due to the fact that the MLP network outputs are decided by all the neurons and the RBF network outputs are determined by specified hidden units in certain local receptive fields. Also, the MLP forms arbitrarily shaped decision boundaries while the RBF forms decision in form of hyper spheres around the clusters. Hence, the RBF network cannot perform well unless sufficient number of hidden neurons is taken. It is illustrated that with 16 hidden neurons, both the networks performing at their best. From this, it is empirically shown that H_N can be based on number of users in the SDMA–OFDM system, i.e. $H_N = 2^L$, to maintain a good performance level. Similarly, during network training, the learning rate parameters are to be chosen carefully. If the values of the learning rate parameters are too high it may not allow convergence to the minimum MSE level, else if the learning rate parameters are too low it will require a high number of iterations for attaining minimum MSE level. Therefore, they must be selected through exhaustive trial and error studies. Thus, the simulation parameters selected for NN based detectors are summarized in Table 4.1.

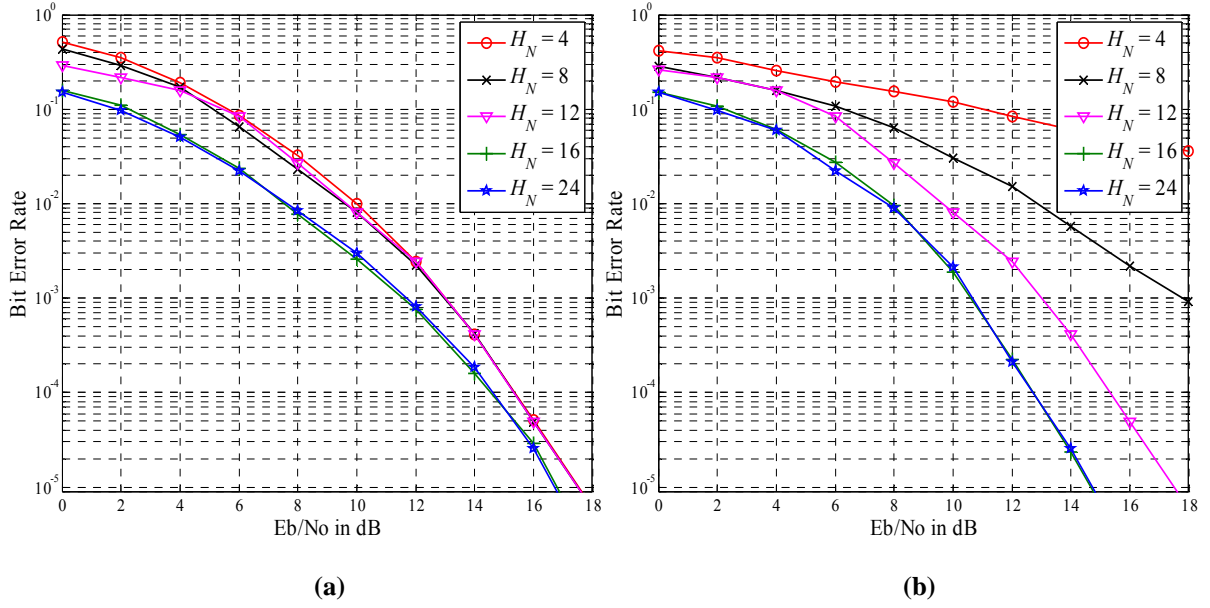


Figure 4.9: Average BER performance of NN model based MUDs for the case of $L = P = 4$ with a variable number of hidden neurons (a) MLP detector (b) RBF detector

Table 4.1: Simulation parameters of NN based MUD schemes

Parameter	Value
Number of input nodes	4 (size of P)
Number of output nodes	4 (size of L)
Number of hidden nodes	16 (size of 2^L)
MLP learning algorithm	Back propagation
Average number of training symbols taken for MLP (N_M)	5000
RBF learning algorithm	Gradient descent
Average number of training symbols taken for RBF (N_{RB})	3000
MLP weight learning rate (η)	0.1
RBF weight learning rate (μ_w)	0.08
RBF center learning rate (μ_c)	0.03
RBF spread learning rate (μ_s)	0.05
RBF initial center selection algorithm	k -means clustering

4.7.1.1 Performance analysis

Figure 4.10 illustrates the average Bit Error Rate (BER) performance of four different users communicating over different channel conditions in the SDMA–OFDM system employing four receiving antennas while varying E_b/N_o . It is inferred from this figure that, the NN model based MUD schemes are consistently outperforming both the classical MMSE and the proposed IWO MBER MUD schemes.

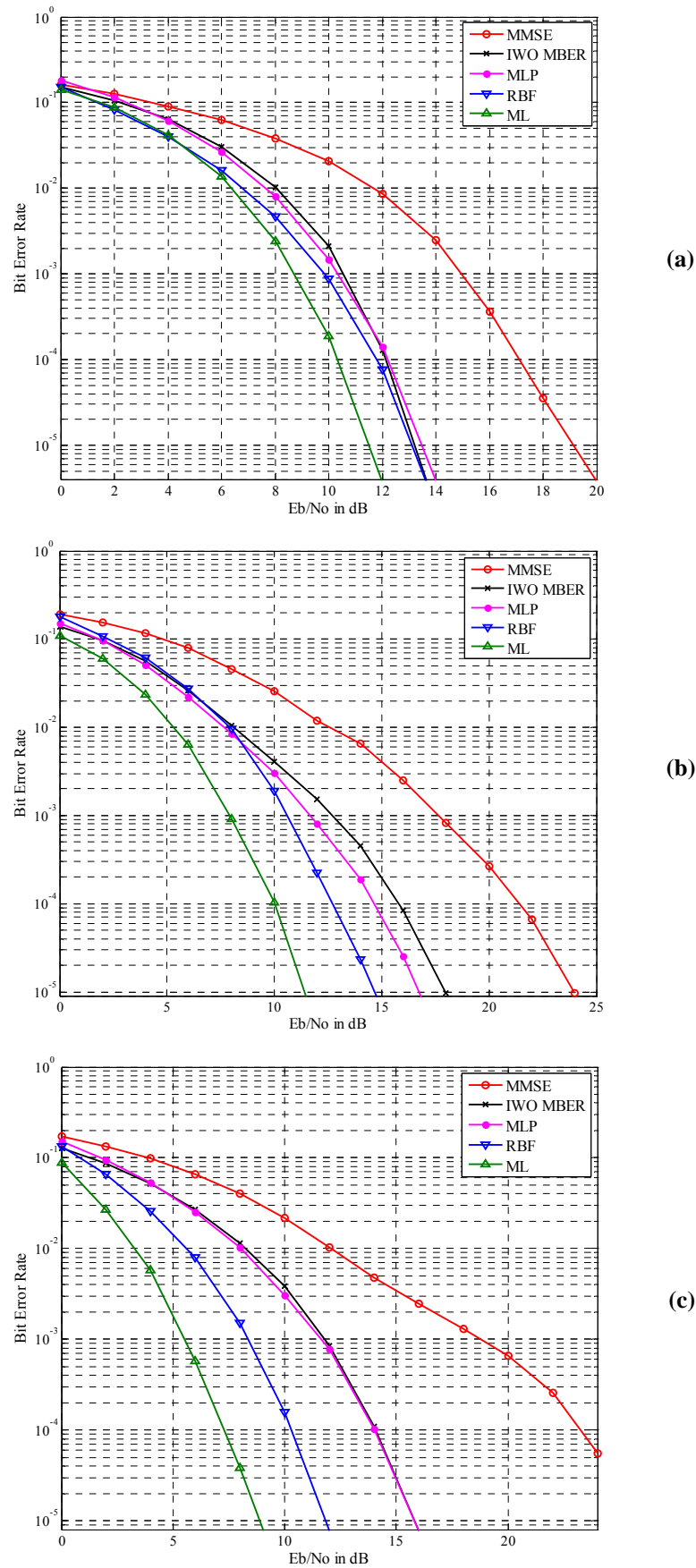


Figure 4.10: Average BER performance of all users using MMSE, IWO aided MBER, NN model based and ML MUDs under different channel conditions (a) MIMO Rayleigh fading (b) SUI (c) SWATM

Further, comparing the MLP, the RBF MUD with sufficient number of hidden units is effective and it has significant improvement in performance for all three different channel conditions. This improvement is achieved since the Gaussian activation can better approximate the Gaussian noise distribution and the spread parameter can better approximate the noise variance. However, as the MLP is a simple nonlinear input-output mapper, its performance does not match the performance of the RBF. Specifically, at 10^{-4} BER level the RBF detector has about 0.5, 2 and 4 dB E_b/N_o gains compared to MLP MUD with respect to MIMO Rayleigh fading, SUI and SWATM channels respectively. Similarly, the RBF detector has about 0.5, 3 and 4 dB E_b/N_o gains compared to MBER detector while users have communicated over MIMO Rayleigh fading, SUI and SWATM channels respectively maintaining the same BER level.

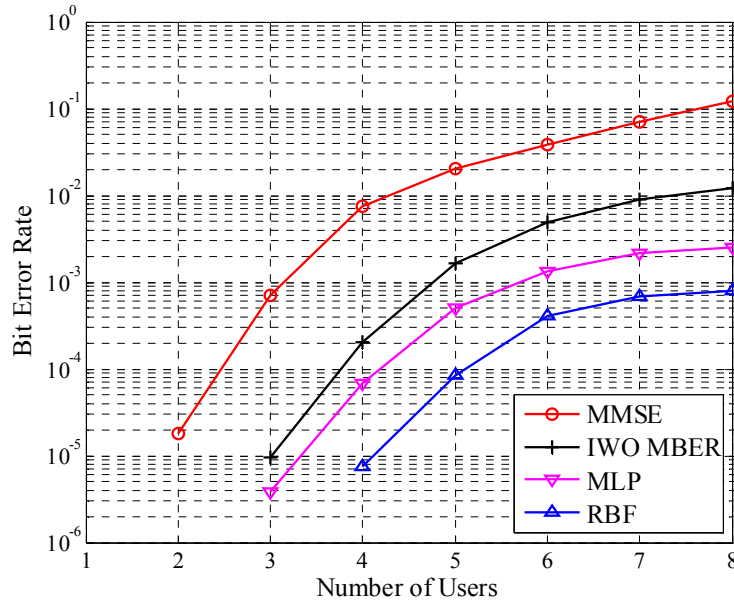


Figure 4.11: Average BER performance of all users using MMSE, IWO MBER and NNs MUD schemes in the SDMA-OFDM system with $P = 4$ and increasing L at 15 dB E_b/N_o

Robustness of proposed NN MUD schemes is further illustrated through simulation of the SDMA-OFDM system with different load conditions. Figure 4.11 shows the average BER of all users using various detectors at a fixed E_b/N_o of value 15 dB, when the system is supporting different number of users keeping number of receiving antennas fixed at four under SUI channel condition. Here, as the number of users increases, the resultant BER becomes worse due to the impairment of added MUI. Especially, when the number of users exceeds the number of receiving antennas as in the case of overload scenario, the BER performance is severely affected because in this case the receiver will lose its degree of freedom to detect the users. As a result, the performance of the linear MMSE detector fails totally and the nonlinear MBER detector performs well compared to MMSE MUD. Further,

even in such a high load conditions, the NN model based MUDs especially the RBF MUD has considerable performance gain. More specifically, the MBER, MLP and RBF MUDs are able to detect users when $L = 8$ at the cost of 0.0124, 0.003742 and 0.0008189 BERs respectively.

The performance of the SDMA–OFDM system in overload scenario can be more explicitly investigated through constellation diagrams as shown in Figure 4.12 and 4.13. Figure 4.12 depicts the detected symbol distribution of the User–1 from the noiseless received symbols using various MUDs while it is always transmitting ‘+1’ over one complete OFDM frame under MIMO Rayleigh fading channel. It is observed from this figure is that, though the detected symbols using the IWO aided MBER MUD lie close to the actual transmitted symbol they spread over the imaginary plane, because this detector cannot correct the arbitrary phase shift of the output symbols automatically. However, due to adaptability, the NN based MUDs use phase correction mechanism during the network training and hence these can continually correct the arbitrary phase shift of output symbols. Thus, the detected symbols form close clusters around the actual transmitted symbol. Further, as the RBF has better approximation capabilities, the detected symbols are exactly overlapped on the actual symbol. Similarly, the analysis of constellation plots is further elaborated in presence of noise (i.e. $E_b/N_o = 20$ dB) as shown in Figure 4.13. This figure shows detected symbol distribution of User–1, when it is transmitting all possible symbols of the BPSK scheme. This figure again provides evidence of better approximation capability of RBF detector over IWO MBER MUD, as it forms close clusters around the actual transmitted symbols while the detected symbols of the IWO MBER MUD are found to be widely distributed.

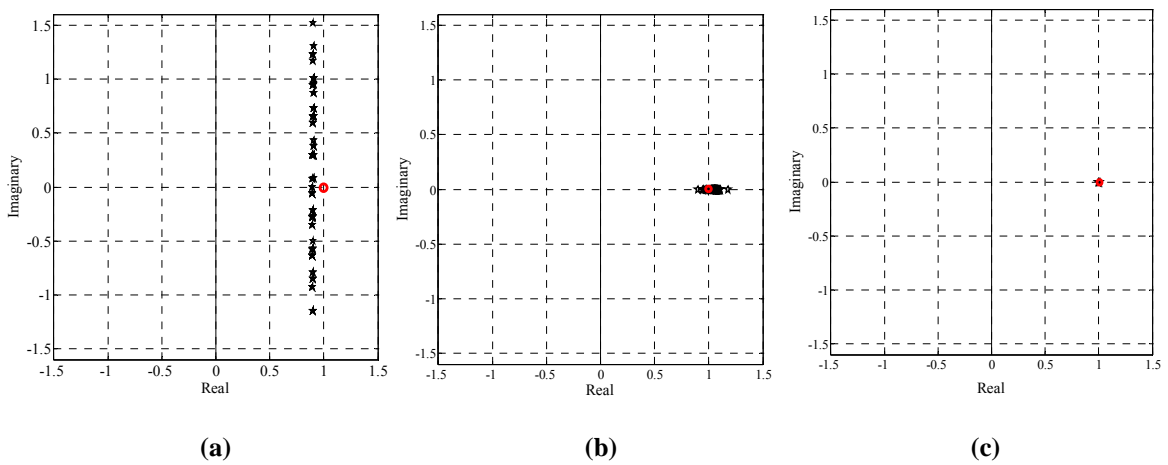


Figure 4.12: Estimated symbol distribution of User-1 from noise less received symbols using various MUD schemes for the case of $L = 6$ and $P = 4$ when User–1 is always transmitting +1 (a) IWO MBER (b) MLP (c) RBF

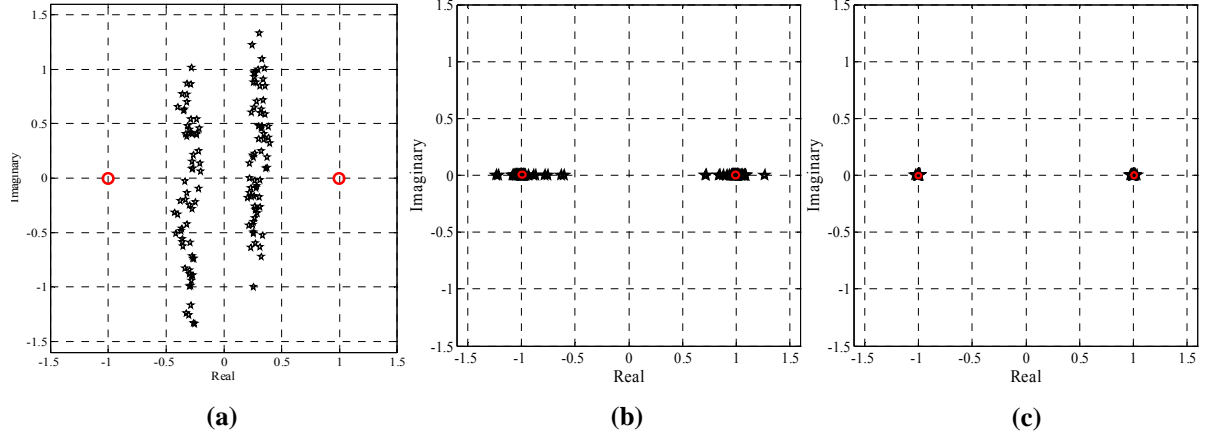


Figure 4.13: Estimated symbol distribution of User-1 using various MUD schemes for the case of $L = 6$ and $P = 4$ at 15 dB E_b/N_o (a) IWO MBER (b) MLP (c) RBF

4.7.1.2 Convergence speed

In the training phase, the NN learns the forward relation between input and output. The forward learning error in terms of MSE is shown in Figure 4.14 to analyze convergence speed of the neural network models. In this figure, the MSE plots of MLP and RBF based MUDs at 15 dB E_b/N_o are presented considering the SWATM channel as given in Appendix A. It is shown that, the RBF MUD is faster than that of MLP MUD in tracking the network free parameters since the RBF has good tracking ability compared to MLP. Due to this faster tracking, the RBF reaches the minimum MSE level with less number of training symbols compared to that of MLP network. It is confirmed that the RBF network is trained much rapidly and the network parameters are updated accordingly.

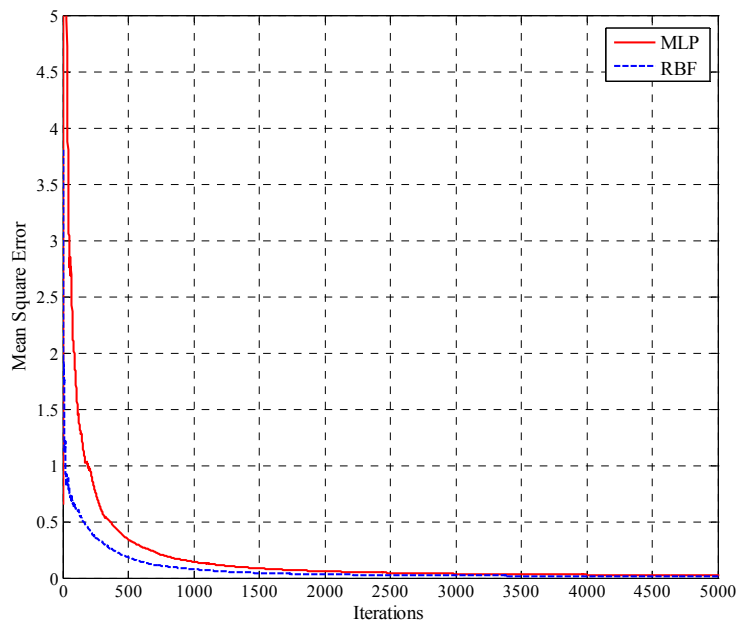


Figure 4.14: Convergence speed comparison of NN based MUDs at 15 dB E_b/N_o

4.7.1.3 Complexity

Similar to Section 3.4.1.4, the over-all complexity of the proposed NN MUDs is compared with the ML detector based on both computational operations (multiplication and addition) and Cost Function (CF) evaluations as given in Table 4.2 and 4.3 respectively. The complexity of NNs mainly depends on the number of training samples fed to the network model to reach the minimum MSE level. Hence, the complexities of MLP and RBF MUDs are proportional to $N_M \times (N_C + N_{CP})$ and $N_{RB} \times (N_C + N_{CP})$ respectively, where N_M and N_{RB} are number of training symbols for MLP and RBF models respectively. All these comparisons of various MUD schemes are considered for a block-fading channel condition and in an overload scenarios, where the L users simultaneously transmit their BPSK data to the P antenna receiver over N_C subcarriers along with N_{CP} cyclic prefix ($N_C = 128$, $N_{CP} = 32$). The channel is assumed to be time-invariant over $N_F = 1000$ consecutive OFDM symbols. The FEC scheme employed here is the $\frac{1}{2}$ rate Convolutional coding. The number of training symbols N_M and N_{RB} are taken as 5000 and 3000 respectively as mentioned in Table 4.1.

Table 4.2: Complexity comparison of MMSE, IWO MBER, NN and ML MUD schemes with respect to number of computational operations when $L = 6$ and $P = 4$

MUD	Operation	Computational Complexity	Total	% of ML
MMSE	Multiplications	$2(N_C + N_{CP})\{2PL + P^2 + P(P-1)(4P+1)/6\}$	2.384×10^4	6.5×10^{-5}
	Additions	$2(N_C + N_{CP})\left\{2P(L-1) + \frac{P(P-1) + P(P-1)(4P+1)}{6}\right\}$	2.752×10^4	5.1×10^{-4}
IWO MBER	Multiplications	$2(N_C + N_{CP})(G_I \times N_S)(2P-1)(2^{mL} + 1)L$	6.989×10^9	19.04
	Additions	$2(N_C + N_{CP})(G_I \times N_S)(2^{mL}P + P-1)L$	1.691×10^9	4.79
	Q functions	$2(N_C + N_{CP})(G_I \times N_S)(2^{mL})L$	4.178×10^8	—
MLP	Multiplications	$2(N_C + N_{CP})\left[N_M\{H_N(6P+4L+2)+2L\} + N_F H_N(2P+L)\right]$	7.862×10^9	21.42
	Additions	$2(N_C + N_{CP})\left[N_M\{H_N(4P+2L+3)+L\} + N_F H_N(2P+L)\right]$	2.238×10^9	6.32
	Tansig	$2(N_C + N_{CP})H_N(N_M + N_F)$	3.072×10^7	—
RBF	Multiplications	$2(N_C + N_{CP})H_N[N_{RB}(2P+3L+9) + N_F(P+L+1)]$	5.939×10^9	16.18
	Additions	$2(N_C + N_{CP})\left[N_{RB}\{2H_N(3P+L)+L\} + N_F\{H_N(2P+L+1)-L\}\right]$	6.336×10^8	1.79
	Exponentials	$2(N_C + N_{CP})H_N(N_{RB} + N_F)$	2.048×10^7	—
ML	Multiplications	$2(N_C + N_{CP})N_F(PL+2P+2)2^{mL}$	3.670×10^{10}	100
	Additions	$2(N_C + N_{CP})N_F(PL+P-1)2^{mL}$	3.539×10^{10}	100

Table 4.3: Complexity comparison of IWO MBER, NN and ML MUD schemes with respect to CF evaluations when $L = 6$ and $P = 4$

MUD Technique	C F Evaluations	Total	% of ML
IWO MBER	$2 \times I_{max} \times N_S \times (N_C + N_{CP}) \times L$	6.528×10^6	31.9
MLP	$2 \times N_M \times (N_C + N_{CP})$	1.6×10^6	7.8125
RBF	$2 \times N_R \times (N_C + N_{CP})$	9.6×10^5	4.6875
ML	$2 \times 2^{mL} \times (N_C + N_{CP}) \times N_F$	2.048×10^7	100

From Table 4.2 and Table 4.3, it is noticed that the complexities of the proposed NN based MUD schemes are a small fraction of the complexity imposed by the optimal ML MUD.

4.7.2 Results and discussion for complex valued NN based MUDs

In this section, the simulation results using complex valued NNs based MUDs are presented for detecting higher order signals (4-QAM and 16-QAM). In the higher order constellations, as the number of bits per symbols is more, the number of equiprobable transmitting vectors is more compared to BPSK constellations. Hence, the complex NN models may require comparatively more training symbols than real valued NNs in order to reach minimum MSE level. The rest of the simulation parameters of complex valued NNs are chosen according to the parameters of the SDMA-OFDM system and are summarized in Table 4.4.

Table 4.4: Simulation parameters of complex valued NN based MUD schemes

Parameter	Value
Number of Input nodes	4 (size of P)
Number of Output nodes	4 (size of L)
Number of Hidden nodes	16 (size of 2^L)
CMLP learning algorithm	Complex BP
Average number of training symbols taken for CMLP using 4-QAM (N_{CM})	12000
Average number of training symbols taken for CMLP using 16-QAM (N_{CM})	30000
CRBF learning algorithm	Complex GD
Average number of training symbols taken for CRBF using 4-QAM (N_{CR})	10000
Average number of training symbols taken for CMLP using 16-QAM (N_{CR})	20000
CMLP Weight Learning Rate (η)	0.15
CRBF Weight Learning Rate (μ_w)	0.1
CRBF Center Learning Rate (μ_c)	0.02
CRBF Scaling factor's Learning Rate (μ_v)	0.08
CRBF initial center selection algorithm	k -means clustering

4.7.2.1 Performance analysis

Figure 4.15 presents the BER comparison of complex valued NN model based MUDs with MMSE, ML and IWO MSER detectors in the SDMA–OFDM system while transmitting the 4–QAM signals. Here, as the real valued NNs cannot correct the arbitrary phase degradation and hence these detector exhibits a high error floor. On the other hand, the complex valued NN based MUDs achieve improved BER performance because these models can correct both amplitude and phase degradations simultaneously. In addition to that, as the complex NN models are also highly nonlinear classifiers, these are able to achieve significant performance gain over the MMSE and IWO MSER MUDs. Especially, the performance gain of the CRBF MUD is quite remarkable compared to the MMSE, MSER and CMLP MUDs and exhibits a performance close to the optimal ML detector. Specifically, at a target BER level of 10^{-4} , the CRBF has around 3 dB E_b/N_o gain approximately over both the MSER and CMLP MUDs. Similar observations are made when simulations are performed for detection of 16–QAM signals as shown in Figure 4.16. The robustness of proposed complex valued NN MUD schemes is further analyzed through simulation of the SDMA–OFDM system under different load conditions as shown in Figure 4.17. This figure shows the average BER of various detectors, when the system is supporting different number of users under SUI channel condition keeping number of receiving antennas fixed at four. It is observed that, irrespective to any load conditions (i.e. $L > P$ or $L = P$ or $L < P$), the CRBF detector provides a better performance compared to MMSE, CMLP and IWO MSER MUDs.

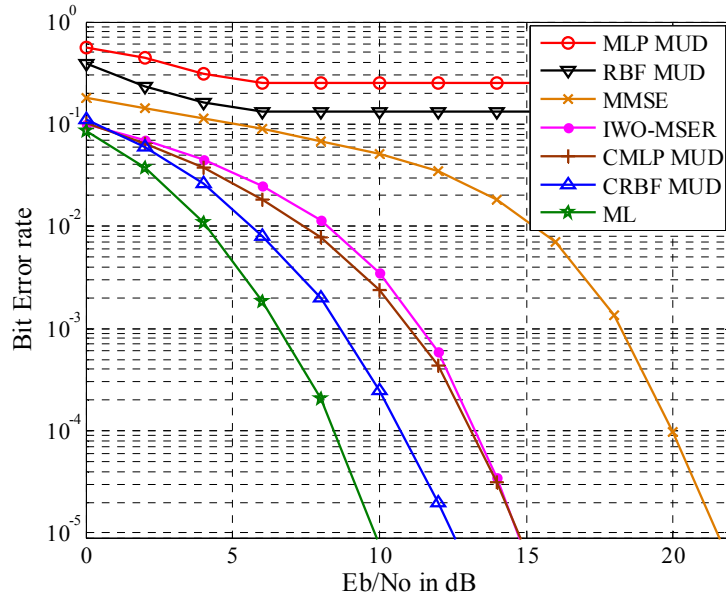


Figure 4.15: Average BER performance of all users using various MUDs, when the SDMA–OFDM with $L = P = 4$ is transmitting 4-QAM signals

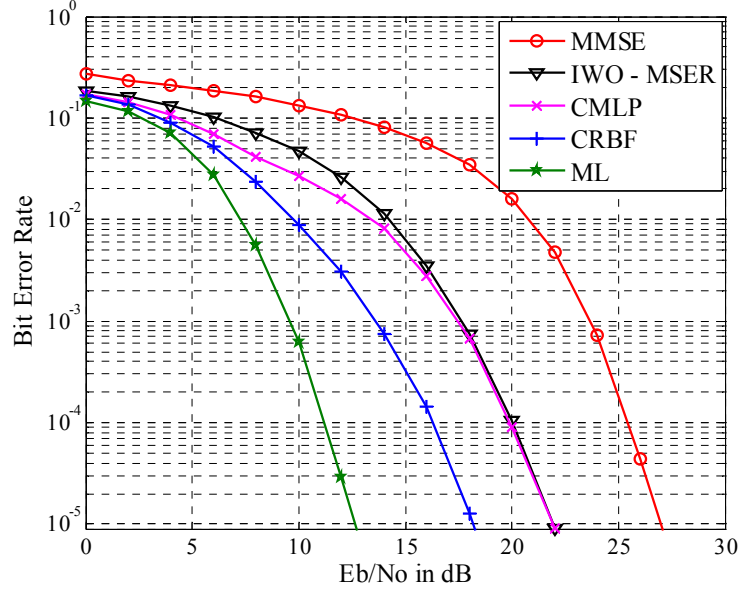


Figure 4.16: Average BER performance of all users using various MUDs, when the SDMA-OFDM with $L = P = 4$ is transmitting 16-QAM signals

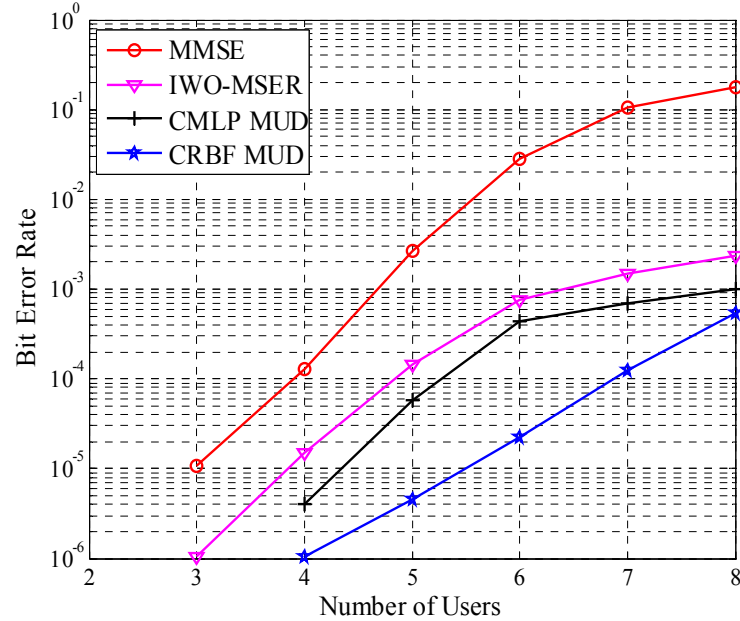


Figure 4.17: Average BER performance of all users using MMSE, IWO MSER and complex NN MUD schemes in the SDMA-OFDM system with $P = 4$ and increasing L at 15 dB E_b/N_o

The performance of SDMA-OFDM system in overload scenario ($L = 6, P = 4$) can be further illustrated through constellation diagrams as shown in Figure 4.18 and 4.19. Figure 4.18 depicts the detected symbol distribution of the User-1 from the noiseless received symbols using various MUDs while it is always transmitting ‘1+j’ over one complete OFDM frame under MIMO Rayleigh fading channel. It is observed from this figure is that the complex valued NNs are able to correct automatically the distortion in both real and

imaginary components of the 4-QAM symbol distributions. Further, comparing MLP, the CRBF one better approximates the real and imaginary parts of the detector output to the desired values.

The constellation plots are further elaborated in presence of noise (i.e. $E_b/N_o = 15$ dB) as presented in Figure 4.19 considering the practical scenario, where the User-1 is transmitting all possible 4-QAM symbols. This figure provides evidence of satisfactory approximation capability of CRBF detector. Similar observations are made in Figure 4.20 when detecting 16-QAM symbols, which are transmitted through User-1 of the SDMA-OFDM system with $L = P = 4$.

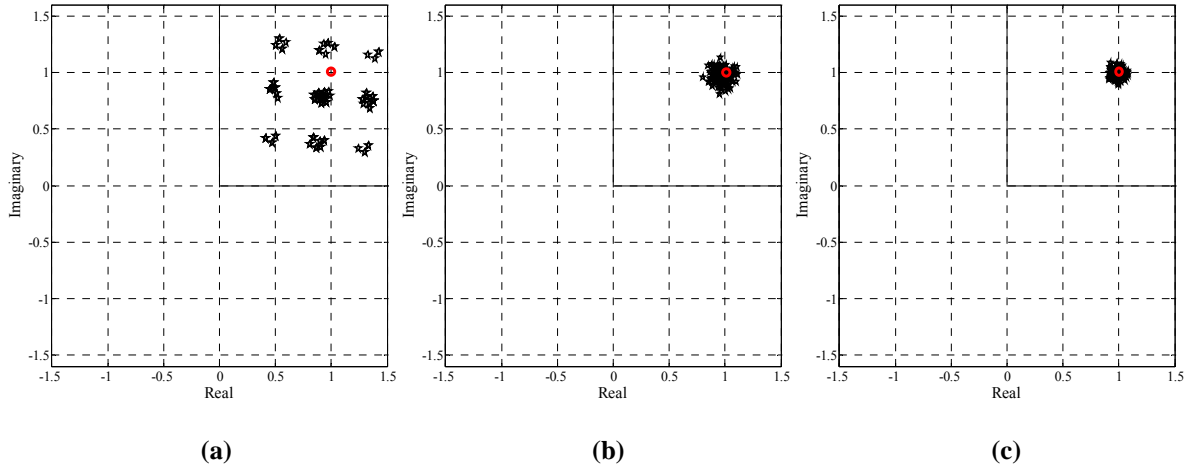


Figure 4.18: Estimated symbol distribution of User-1 from noise less received symbols using various MUD schemes for the case of $L = 6$ and $P = 4$ when User-1 is always transmitting $1+j$ (a) IWO MSER (b) CMLP (c) CRBF

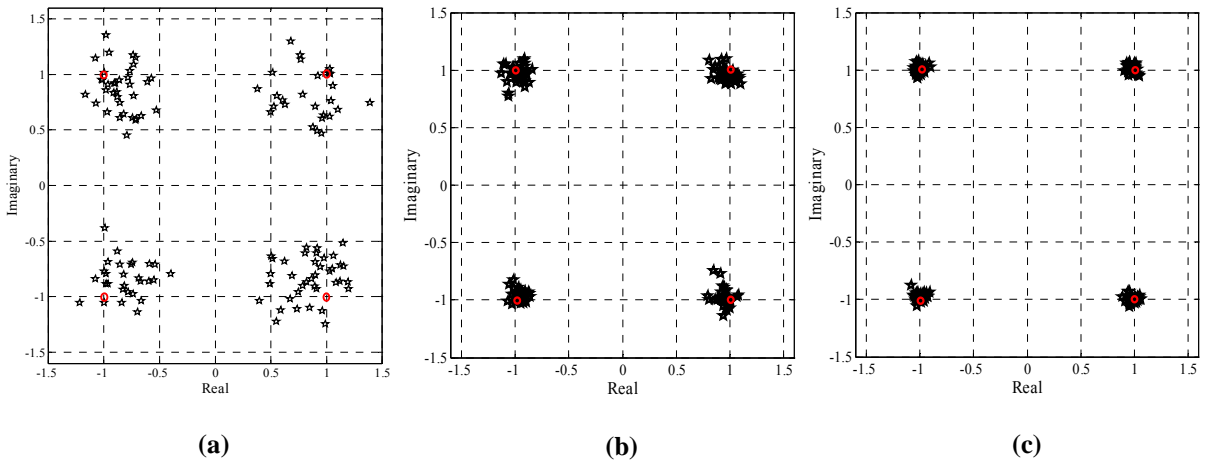


Figure 4.19: Estimated symbol distribution of User-1 using various MUDs for the case of $L = 6$ and $P = 4$ when User-1 is transmitting 4-QAM signals at 15 dB E_b/N_o (a) IWO MSER (b) CMLP (c) CRBF

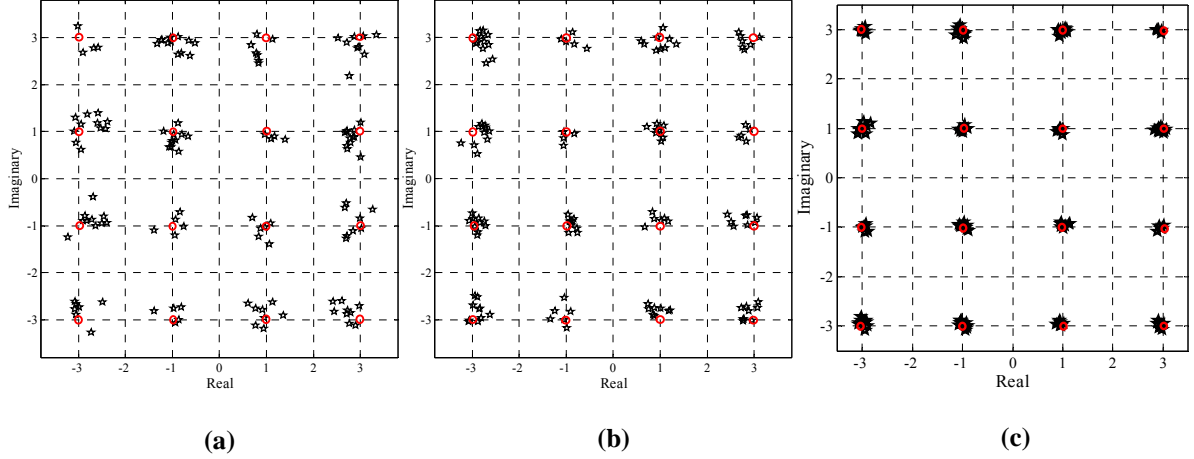


Figure 4.20: Estimated symbol distribution of User-1 using various MUDs for the case of $L = 4$ and $P = 4$ when User-1 is transmitting 16-QAM signals at 15 dB E_b/N_o (a) IWO MSER (b) CMLP (c) CRBF

4.7.2.2 Convergence speed

The MSE plots of various NN models in training phase are shown in Figure 4.21 when all users are transmitting 4-QAM signals over SWATM channel at 15 dB E_b/N_o . In this figure, as the real valued NN models cannot mitigate distortion in imaginary component, these curved are not converging to minimum MSE level, whereas the input-output relation can be learned sufficiently in case of complex NN models. As a result, the convergence of MSE using CMLP and CRBF are stable and faster while reaching a minimum level. These results imply that the complex NN parameters are properly learned. Among all these NN MUDs, the proposed CRBF MUD works well in all benchmark testing by reaching a minimum level of MSE with less number of training symbols.

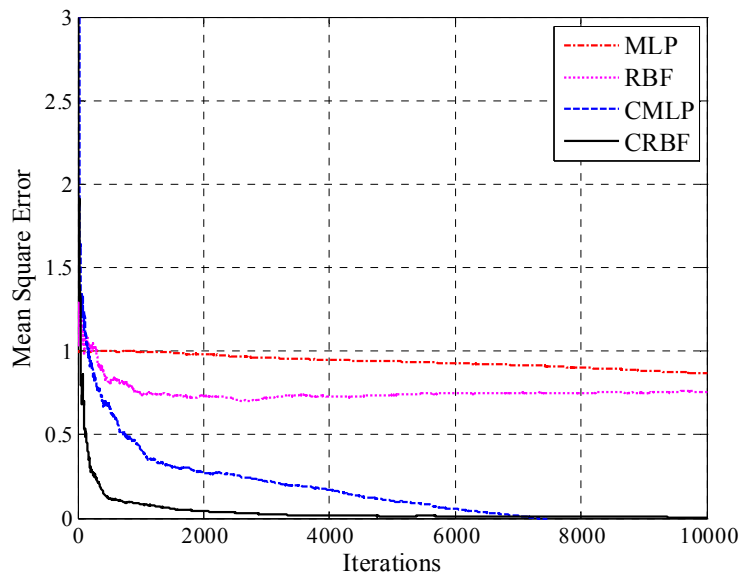


Figure 4.21: Convergence speed comparison of real and complex valued NN based MUDs at 15 dB E_b/N_o

4.7.2.3 Complexity

Similar to the comparisons given in Table 4.2 and Table 4.3, the complexity of the complex valued NN based MUDs is compared with the ML detector on the basis of number of computational operations and the CF evaluations and presented in Table 4.5 and 4.6 respectively. All these comparisons for various MUD schemes are considered in a block-fading scenario, where the L users simultaneously transmit their 4-QAM/16-QAM data to a P antenna receiver over N_C subcarriers along with N_{CP} cyclic prefix ($N_C = 128$, $N_{CP} = 32$). The channel is assumed to be time-invariant over $N_F = 100$ consecutive OFDM symbols. The FEC used here is the $\frac{1}{2}$ rate convolution coding. The number of training symbols N_{CM} and N_{CR} are taken as 12000 and 10000 respectively for 4-QAM signals. Similarly, the number of training symbols N_{CM} and N_{CR} are taken as 30000 and 20000 respectively for 16-QAM signal.

Table 4.5: Complexity comparison of MMSE, IWO MSER, complex valued NN and ML MUD schemes with respect to number of computational operations when $L = 6$ and $P = 4$

MUD	Operation	Computational Complexity	4-QAM		16-QAM	
			Total	% of ML	Total	% of ML
MMSE	\times	$2P(N_C + N_{CP}) \left\{ \frac{2L + P + LN_F + (P-1)(4P+1)/6}{(P-1) + L(P-1)(4P+1)/6} \right\}$	7.99×10^5	1.8×10^{-2}	7.99×10^5	4.8×10^{-6}
	$+$	$2(N_C + N_{CP}) \left\{ \frac{2L(L-1) + (P-1)LN_F + (P-1) + L(P-1)(4P+1)/6}{(P-1) + L(P-1)(4P+1)/6} \right\}$	6.12×10^5	1.7×10^{-2}	6.12×10^5	4.2×10^{-6}
IWO MSER	\times	$2L(N_C + N_{CP}) \left[\frac{(I_{\max} N_S)(P+7) + P2^{m(L-1)} + PN_F}{P2^{mL} + (P-1)N_F} \right]$	2.92×10^8	6.55	9.17×10^9	0.0501
	$+$	$2L(N_C + N_{CP}) \left[\frac{(I_{\max} N_S)(LP+2) + P2^{mL} + (P-1)N_F}{P2^{mL} + (P-1)N_F} \right]$	7.03×10^8	19.86	1.31×10^{11}	0.903
CMLP	\times	$2(N_C + N_{CP}) \left[\frac{N_{CM} \{H_N(4P+5L+5) + 5L\}}{+N_F \{2H_N(P+L)\}} \right]$	3.89×10^8	8.72	9.57×10^9	0.0523
	$+$	$2(N_C + N_{CP}) \left[\frac{N_{CM} \{H_N(3P+4L+4) + 6L\}}{+N_F \{2H_N(P+L)\}} \right]$	9.31×10^8	26.30	1.32×10^{11}	0.910
	TANH	$4(N_C + N_{CP})(H_N + L)(N_{CM} + N_F)$	1.71×10^8	—	9.01×10^8	—
CRBF	\times	$2(N_C + N_{CP})H_N \left[\frac{N_{CR}(14P+7L+2) + N_F(2P+L)}{N_F(2P+L)} \right]$	2.92×10^8	6.55	9.17×10^9	0.0501
	$+$	$2(N_C + N_{CP}) \left[\frac{N_{CR} \{H_N(6P+8L-1) + 2L\}}{+N_F \{H_N(2P+L-1) - L\}} \right]$	7.03×10^8	19.86	1.31×10^{11}	0.903
	SECH	$4(N_C + N_{CP})H_N(3N_{CR} + N_F)$	3.08×10^8	—	2.46×10^9	—
ML	\times	$2(N_C + N_{CP})N_F(PL + 2P + 2)2^{mL}$	4.46×10^9	100	1.83×10^{13}	100
	$+$	$2(N_C + N_{CP})N_F(PL + P - 1)2^{mL}$	3.54×10^9	100	1.45×10^{13}	100

Table 4.6: Complexity comparison of IWO MSER, complex valued NN and ML MUD schemes with respect to CF evaluations when $L = 6$ and $P = 4$

MUD Technique	4-QAM		16-QAM	
	Complexity	% of ML	Complexity	% of ML
IWO MSER ($2 \times I_{max} \times N_s \times (N_c + N_{CP}) \times L$)	2.58×10^7	19.69	1.02×10^8	0.0189
CMLP ($2 \times N_{CM} \times (N_c + N_{CP})$)	3.84×10^6	2.93	9.6×10^6	1.79×10^{-3}
CRBF ($2 \times N_{CR} \times (N_c + N_{CP})$)	3.2×10^6	2.44	6.4×10^6	1.19×10^{-3}
ML Detector ($2 \times 2^{mL} \times (N_c + N_{CP}) \times N_F$)	1.31×10^8	100	5.37×10^{11}	100

From Table 4.5 and Table 4.6, it is noticed that the complexities of the proposed complex valued NN based MUD schemes are a small fraction of the complexity imposed by the optimal ML MUD. Thus, these detectors have a clear edge over the computationally exhaustive ML one.

4.8 Summary

This chapter has contributed to the development of adaptive MUD schemes using both real and complex valued NN models for the SDMA–OFDM wireless communication system. The efficacy of these detectors and the appropriate training algorithms are also discussed in detail. The performances of these detectors are compared with the linear MMSE, optimal ML and proposed sub optimal IWO assisted MER MUD schemes in terms of the BER performance, convergence speed and complexity analysis. Among various NN models, the two well known nonlinear classifiers such as MLP and RBF are considered for classification of real valued signals. It is observed that, the RBF networks and MLP networks have distinct behaviors. The initial states of the RBF network can be determined a prior to network training, but the MLP network always use randomly generated parameters initially. With the selection of sufficient number of hidden neurons, the RBF network can work efficiently for signal classification at BS receiver. From extensive simulation study, it is observed that the real valued NN models are not suitable for higher ordered signal as these models cannot mitigate phase distortion caused by the channel environment. In such case, the complex valued NNs such as the proposed CMLP and CRBF can be good alternatives as these models can simultaneously correct the amplitude and phase distortions of the transmitted signals. Activation functions of the neurons have been selected for nonlinear mapping of complex input and output in both the CMLP and CRBF structures. Suitable modifications for the BP and GD algorithm have been incorporated to train the CMLP and CRBF models respectively.

These make the weight vectors to converge to the optimal solutions with minimum number of training symbols. It is observed that, the CRBF MUD is found to be more effective since its activation function better approximates the Gaussian noise distribution and it does better non-linear mapping of input and output. The NN based adaptive MUD techniques are preferred due to their great complexity gain over the exhaustive ML one. Thus, the proposed CRBF comes out to be clear winner as it gives a BER performance close to the optimal ML for MUD in the SDMA–OFDM systems, especially for channels with nonlinear distortion and in the critical overload scenarios. However, while the number of users in the system increases, the number of hidden nodes in the neural structure H_N has to be increased accordingly to maintain a near optimal performance of the detector.

Chapter 5

Progressive Image Transmission and Detection Using Proposed MUD Schemes

In previous two chapters, new MUD schemes using OTs aided MER and NN based adaptive models are proposed for the SDMA–OFDM wireless communication system. In this chapter, all the proposed MUD schemes are validated by reconstructing images efficiently at the receiving end of the SDMA–OFDM system, when all users in the system simultaneously transmitting individual images through wireless fading channels. Recently, progressive image transmission over noisy channel using Set Partitioning Hierarchical Tree (SPIHT) [90] coding has become an active field of research. The SPIHT coding will convert a two dimensional image into compressed binary bit streams. This algorithm uses Discrete Wavelet Transform (DWT) for de-correlation to remove special redundancy. As wireless communication channels often suffer from multipath fading, shadowing and ISI, the transmission of such a compressed image is a major concern due to the error prone propagation environment. Transmission errors may degrade the received image quality a lot. By incorporating an efficient MUD at the receiving end, these degraded images can be recovered. This kind of image transmission and detection analysis is extensively studied for space time coded MIMO–OFDM system in the literatures [91, 92]. Unlike SDM/MIMO, the SDMA is basically designed for improving capacity gain but not for achieving transmit diversity. Hence, image transmission and detection in SDMA–OFDM system is quite challenging compare to SDM/MIMO system. However, this research work attempts to investigate the image transmission and recovery using both the proposed OTs aided MER and NN based MUD techniques for SDMA–OFDM system and proposed suitable image detection schemes.

This chapter describes the image compression technique such as Set Partitioning in Hierarchical Trees (SPIHT) algorithm with its advantages over another classical image compression technique such as Embedded Zero tree Wavelet (EZW) algorithm in Section 5.1. In the SPIHT algorithm, the coefficient ordering for progressive image transmission, the basic objectives of set partitioning used in SPIHT and set partitioning rules are also discussed. Application of this algorithm for the typical SDMA–OFDM system model used in image transmission is presented in Section 5.2. Further, Section 5.3 introduces various statistical parameters for image quality analysis such as Bias, Standard Deviation Difference (SDD), Root Mean Square Error (RMSE), Peak Signal to Noise Ratio (PSNR) and Correlation Coefficient (CC). Image reconstruction using proposed MUD schemes is analyzed through simulation study and described in Section 5.4. Finally, summary of the chapter is presented in Section 5.5.

5.1 SPIHT image coding for progressive image transmission

With the recent development of the multimedia applications, the total amount of image data accessed and exchanged by users has grown enormously. Hence, the research for compression of still image has grown extremely. Compression algorithms are to be reversible or lossless, which means that the images reconstructed from the coded bit stream are identical to the originals. The classical image compression scheme consists of a decorrelator, followed by a quantizer and an entropy coding stage. The purpose of the decorrelator is to remove the spatial redundancy. Hence, it must be tailored to the specific characteristics of the data to be compressed. The commonly used decorrelators are Discrete Cosine Transforms (DCTs) and Discrete Wavelet Transforms (DWTs). Compared to DCT, the DWT decorrelators are advantageous since it was noticed that a full-frame DWT allows long-range correlation to be effectively removed, whereas in DCTs, the full-frame processing leads to a spread of energy in the transformed plane due to the fact that these are not suitable for the analysis of non-stationary signals. Once a signal has been decorrelated, it is necessary to find a compact representation of its coefficients, which may be in form of sparse data. Eventually, an entropy coding algorithm is used to map such coefficients into code words in a way that the average codeword length is minimized. One of such classical coding technique which uses DWT decorrelators is the EZW introduced by Shapiro [89]. This technique has become popular as it offers good performance, is extremely fast in both producing the embedded bit stream and fast in execution. With this embedded bit stream, the image can be decompressed and reconstructed if the reception of code bits is stopped at any point of transmission. Therefore, such an image transmission is called as progressive image transmission.

Later, Said and Pearlman proposed a modified form of the EZW algorithm, that is, the Set Partitioning in Hierarchical Trees (SPIHT) [90]. SPIHT algorithm carries the significant strengths of EZW and orders transmitted coefficients across similar sub bands. This algorithm also identifies every significant coefficient and partitions the set of coefficients into subsets of insignificant coefficients. This algorithm achieves improved performance over EZW algorithm, because of its ability to distinguish the insignificant coefficient groups.

5.1.1 Coefficient ordering for progressive image transmission

Initially, the image is defined by a set of pixel values i_{p_1, p_2} , where (p_1, p_2) is the pixel coordinate. The transformation of hierarchical sub bands (Ex. Wavelet) for the pixel i is expressed in a general form as:

$$k = \Omega(i) \quad (5.1)$$

where i , k and Ω are the original image array, transformed coefficient array and unitary hierarchical sub band transformations respectively. Both the coefficient array and the original image array have the same dimensions. The encoder transmits the coefficients and the decoder updates itself according to the received bit stream. It is possible to reconstruct an approximated form of image \hat{i} from the approximated coefficient array \hat{k} , by the inverse transformation as given by:

$$\hat{i} = \Omega^{-1}(\hat{k}) \quad (5.2)$$

At the decoder, the mean squared reconstruction error of the image is given by:

$$E_m(i - \hat{i}) = \frac{\|i - \hat{i}\|^2}{N} = \frac{1}{N} \sum_{p_1} \sum_{p_2} (i_{p_1, p_2} - \hat{i}_{p_1, p_2})^2 \quad (5.3)$$

where N is total number of pixels and i_{p_1, p_2} is the pixel intensity at the location (p_1, p_2) . The sub band transformation is considered as lossless, and hence the mean square error is transformation invariant, that is:

$$E_m(i - \hat{i}) = E_m(k - \hat{k}) = \frac{1}{N} \sum_{p_1} \sum_{p_2} (k_{p_1, p_2} - \hat{k}_{p_1, p_2})^2 \quad (5.4)$$

where k_{p_1, p_2} is the transform coefficient at the location (p_1, p_2) . Initially, the decoder sets $\hat{k}_{p_1, p_2} = 0$ for all coefficients, and if exact value of the coefficient k_{p_1, p_2} is sent to the decoder, then the mean-square error given in (5.4) reduces by $(\hat{k}_{p_1, p_2})^2 / N$. This implies in an embedded bit stream, the large valued coefficients should be transmitted initially as they provide better reconstruction quality by decreasing the mean square error at a greater extent. Hence, the transform coefficients should be ordered according to the magnitude in an embedded bit stream generation. The concept of coefficient ordering can be further extended to bit-planes if the coefficients are ranked according to their binary representations and the most significant bits are transmitted first. If the coefficients are ranked in decreasing order of the minimum number of bits required for its magnitude representation, then the ordering is done according to:

$$\left\lceil \log_2 |k_\eta(c)| \right\rceil \geq \left\lceil \log_2 |k_\eta(c+1)| \right\rceil, \quad c = 1, 2, \dots, N \quad (5.5)$$

where the coefficients in the ordered space are represented by $k_\eta(c)$.

5.1.2 Features of set partitioning

In set partitioning approach, the ordered information need not be explicitly transmitted. As an alternative, the encoder and the decoder follow the same execution path and if the decoder receives the results of magnitude comparisons from the encoder, then it can recover the ordered information from the execution path. In set partitioning, no explicit sorting of coefficients is also done. Instead, for a given value of n , the coefficients are examined only if they fall within $2^n \leq |c_{p_1, p_2}| < 2^{n+1}$. Given the generic set T_m , the significance of T_m with respect to the n^{th} bit plane is defined as:

$$\max_{p_1, p_2 \in T_m} |c_{p_1, p_2}| \geq 2^n \quad (5.6)$$

If this condition is not satisfied, then the subset T_m is insignificant and if the condition is satisfied, then the subset T_m is further partitioned to determine insignificant and significant subsets. The significant subsets are repetitively partitioned till single significant coefficients are identified. The set partitioning algorithm relies on the tree structure, often referred as spatial orientation tree, which includes the hierarchy, as shown in Figure 5.1. Based on the spatial orientation tree, the set partitioning algorithm defines some particular sets of wavelet coefficients, which are used for sorting the coefficients according to their significance. The spatial orientation tree establishes the sub band spatial relationship in the form of a recursive four-band split composed by a pyramid. Each node of the tree corresponds to a pixel and is identified by its pixel coordinate. Each of these nodes has four offspring at the same position in the same orientation pyramid in the next finer level, as clearly shown by arrows in the figure. The only exceptional case is the LL sub band existing at the highest level of pyramid. Pixels in this sub band form the root and groups of adjacent 2×2 pixels are composed. Other than one of the pixel, all the remaining three pixels have their four offspring in the HL, LH and HH sub bands of the same scale. For determining the descendant one out of the four is obviously left out since only three sub bands are exist. The hierarchical tree structure is used to examine the zero trees and the zero tree roots in EZW algorithm has similarity with the spatial orientation tree discussed as above. Every LL sub band pixel at the highest level has three offspring at the HL, LH and HH sub bands in the hierarchical tree of EZW.

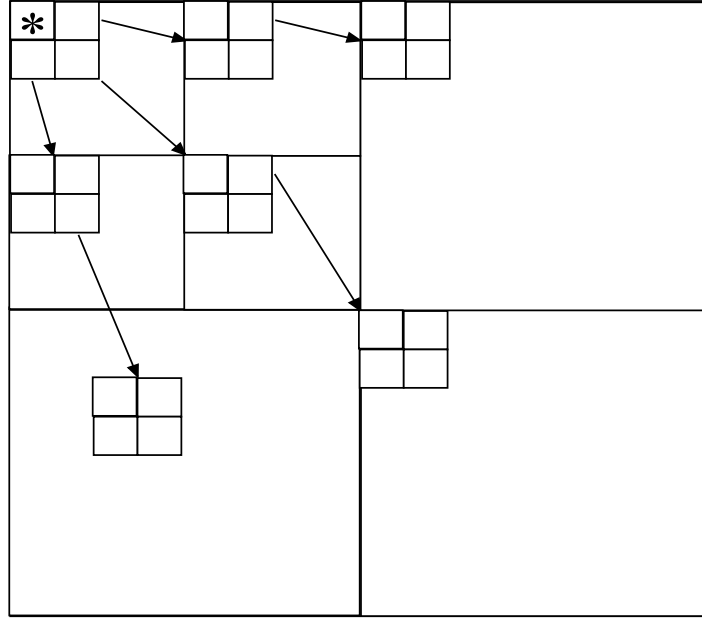


Figure 5.1: Example of descendant trees in a three-level wavelet decomposition

5.1.3 Set partitioning rules

The main feature of SPIHT algorithm is a set partitioning rule that is used to divide the set of wavelet coefficients into significant and insignificant subsets. The rule is based on the well-known self similarity properties of the wavelet decomposition and aims for obtaining the insignificant subsets with a large number of elements, so that they can be coded easily. The set partitioning rule is designed to work in the subband hierarchy. The objective of the set partitioning algorithm should be such that the subsets expected to be insignificant contain larger number of elements and the subsets expected to be significant contain only one element. Given wavelet decomposition, the set of four coefficients at the coarsest resolution is used to initialize the algorithm. Then, with respect to a generic coefficient denoted by the index (p_1, p_2) , the following sets are defined:

$O(p_1, p_2)$: This represents off spring set and these are the offspring of the node (p_1, p_2) . It consists of all the pixel coordinates.

$D(p_1, p_2)$: This represents descendants set and these are descendants of the node (p_1, p_2) . It consists of all the pixel coordinates.

$L(p_1, p_2)$: This is the difference set of $D(p_1, p_2)$ and $O(p_1, p_2)$. It consists of the node (p_1, p_2) descendants, other than the offspring.

$H(p_1, p_2)$: It contains all spatial orientation tree roots coordinates. It belongs to the pyramid highest level, that is the LL sub band.

Based on these definitions, the set partitioning rules are given below:

Rule – 1: The initial partition contains $D(p_1, p_2)$ for each $(p_1, p_2) \in H$.

Rule – 2: If $D(p_1, p_2)$ is found significant, then it is partitioned into $L(p_1, p_2)$ and four single element sets with $(i, j) \in O(p_1, p_2)$.

Rule – 3: If $L(p_1, p_2)$ is found significant, then it is partition into four sets of $D(i, j)$, where $(i, j) \in O(p_1, p_2)$.

5.1.4 SPIHT encoding and decoding

Initially, the set partitioning rules are on the sub band coefficients. The spatial orientation tree is identical for both encoder and decoder and hence there is no explicit transmission of ordering information, as needed in other progressive transmission schemes. So this makes the algorithm more coding efficient compared to the previous techniques. In this algorithm, the order of the splitting pass is stored by means of three ordered lists, namely

- List of Insignificant Pixels (LIP)
- List of Significant Pixels (LSP)
- List of Insignificant Sets (LIS)

In all these lists, each entry is identified by a coordinate (p_1, p_2) . In LIP and LSP, the entry represents individual pixels, whereas in LIS, the entry represents either the set $D(p_1, p_2)$ or the set $L(p_1, p_2)$. As an initialization step, the number of magnitude refinement passes (n) is determined from the maximum magnitude of the coefficients. Initially, all pixels are treated as insignificant. The initialization is followed by three major passes—the sorting pass, the magnitude refinement pass and the quantization step update pass, which are iteratively repeated in this order till the least significant refinement bits are transmitted. During the sorting pass, the pixels in the LIP, which were insignificant till the previous pass, are tested and those that become significant are moved to the LSP. Similarly, the sets in LIS are examined in order for significance and those which are found to be significant are removed from the list and partitioned. The new subsets with more than one element are added to the LIS and the single pixels are added to LIP or the LSP by depending upon their significance. During the magnitude refinement pass, the pixels in the LSP are encoded for n^{th} most significant bit. The encoding algorithm used in the SPIHT can be summarized in the following steps:

Step – 1: Initialization:

Output $n = \left\lfloor \log_2 \left(\max_{p_1, p_2} \{c(p_1, p_2)\} \right) \right\rfloor$;

Set the LSP as an empty list, that is, $LSP = \{\emptyset\}$, add all $(p_1, p_2) \in H$ to the LIP and only the three with descendants also to the LIS = $\{D(p_1, p_2)\}$.

Step – 2: Sorting pass:

Step–2.1: For each entry in the LIP, the significance is tested (“1” if significant, “0” if not significant). If it found as significant, remove it from the LIP and add to the LSP.

Step–2.2: For each entry in the LIS, the significance is tested. If it found significant, output is its sign. Perform the set partitioning using the *Rule–2* or *Rule–3*, depending upon whether it is the $D(p_1, p_2)$ set or the $L(p_1, p_2)$ set. According to the significance, update the LIS, LIP and LSP.

Step – 3: Refinement pass:

For each (p_1, p_2) in the LSP, except those included in the last sorting pass, output the n^{th} bit of $c(p_1, p_2)$.

Step – 4: Quantization step update:

In this pass, n is reduced by 1 and the Steps 2, 3 and 4 are repeated until $n = 0$.

The decoder steps are exactly identical. Only the output from the encoder will be replaced by the input to the decoder.

5.2 Proposed SDMA–OFDM system model for image transmission

Figure 5.2 demonstrates the proposed SDMA–OFDM system uplink model for progressive image transmission. In this figure, each of the four simultaneous users (Mobile Stations (MS)) is equipped with a single transmitting antenna and the base station receiver is equipped with a four element antenna array. In this system, each of the four users transmits a unique gray scale image. The image from each user is first fed to the embedded SPIHT image coder to produce a sequence of bit stream. The data bit stream \mathbf{b}_l ($l = 1, 2, \dots, 4$) of the four mobile users are then encoded by the four independent FEC encoders. The resultant coded bit streams \mathbf{b}_l^c is then mapped to higher order \mathbf{x}_l , which are modulated by the IFFT based OFDM modulators and transmitted over the MIMO channel. At the base station receiver, the received symbol vector \mathbf{y}_p ($p = 1, 2, \dots, 4$) is forwarded to the MUD block. Then the detected

soft bits \hat{b}_l^c are generated, which are forwarded to the four independent FEC decoders to produce detected bit streams \hat{b}_l . Further, the received data stream of each user is fed to their individual SPIHT decoder to recover the transmitted image. The mathematical representation of the transmitted symbols, received symbols and the MIMO channel models are according to the representation given in Section 2.3.

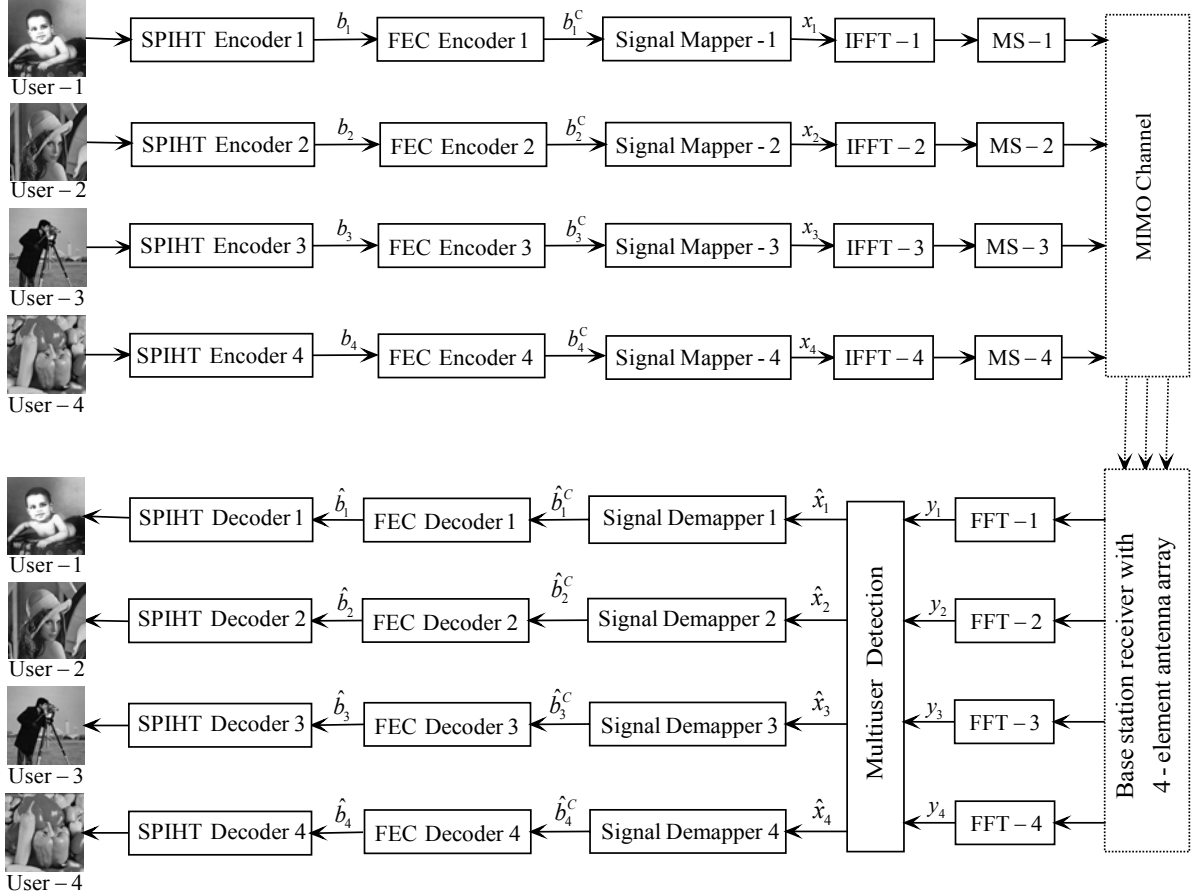


Figure 5.2: Block diagram of the SDMA-OFDM system used for image transmission with $L = P = 4$

In the SDMA-OFDM system, if the transmitted images are RGB images instead of gray scale images, then RGB image encoders and decoders are incorporated as shown in Figure 5.3. The RGB image encoders and decoders use three separated SPIHT algorithms for three color frames. Generally, a color image (RGB image) is characterized by a correlation between the neighboring pixels of each color channel. The correlation can be reduced by transforming RGB plane into a de-correlated color space such as luminance and chrominance plane ($Y C_R C_B$). The three de-correlated planes will feed into independent SPIHT image coders to produce sequence of bit streams. Now the three independent data streams are converted into a single data stream as: $b_l = [b_{Y,1}, b_{C_R,1}, b_{C_B,1}, \dots, b_{Y,N_e}, b_{C_R,N_e}, b_{C_B,N_e}]$, where N_e is

the size of encoded data stream from each SPIHT coder. Then, similar to gray scale image transmission, the transmitted data bit stream b_l ($l = 1, 2, \dots, 4$) of the four mobile users is encoded and transmitted through MIMO channel. The received symbol vector y_p ($p = 1, 2, \dots, 4$) is then forwarded to the MUD block and recovered. The FEC decoded data stream \hat{b}_l of each user is split for $Y C_R C_B$ planes and forwarded through independent SPIHT decoders. Further, the colored image can be obtained by converting this $Y C_R C_B$ plane to RGB plane.

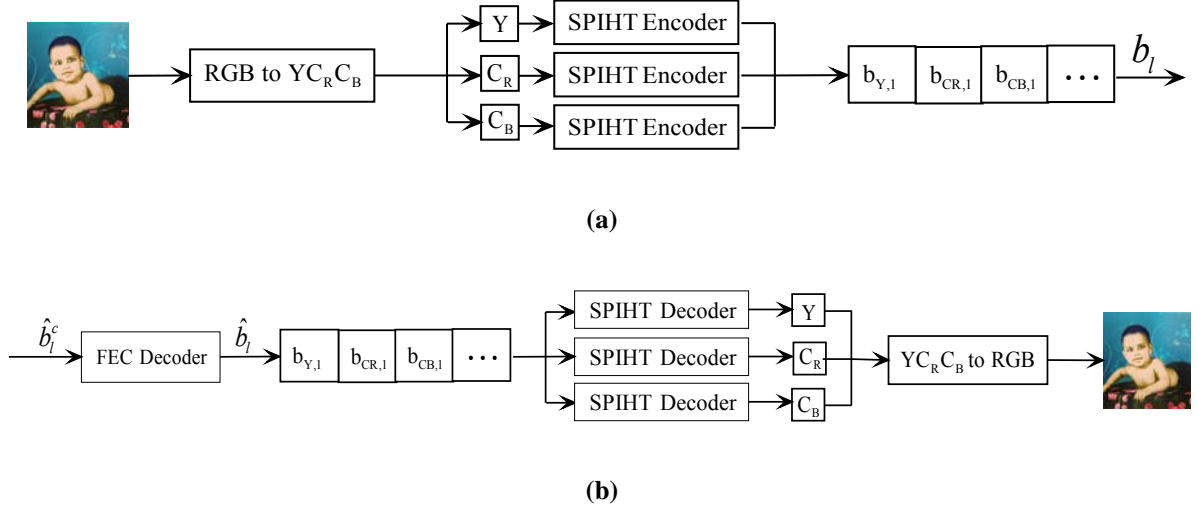


Figure 5.3: (a) RGB Image encoder (b) RGB Image decoder

5.3 Statistical parameters for image quality analysis

Image transmission over wireless media requires some sort of image compression as well as channel coding. Even though, the compressed image is more sensitive towards channel fading and noisy environment, which can be overcome by using various proposed MUDs discussed in the previous chapters. The quality of the reconstructed image can be evaluated through some statistical parameters like Bias, Standard Deviation Difference (SDD), Root Mean Square Error (RMSE), Correlation Coefficient (CC), Peak Signal to Noise Ratio (PSNR) etc. The mathematical description about these parameters is given below. Let A and B are transmitted and reconstructed images respectively of size $m \times n$ then:

Bias: The bias refers to the difference in radiance between the means of the original and reconstructed images and the value of the difference relative to the mean of the original image. The smaller *Bias* represents better image quality.

$$Bias(A, B) = \frac{1}{m \times n} \left(\sum_{m,n} A - \sum_{m,n} B \right) \quad (5.7)$$

Standard Deviation Difference (SDD): The standard deviation of the difference image is relative to the mean of the original image, which indicates the level of the error at any pixel. The smaller *SDD* represents better image quality. Let C is the difference image between A and B then:

$$SDD(C) = \left(\frac{1}{m \times n} \sum_{m,n} (C - \bar{C})^2 \right)^{1/2}, \text{ where } \bar{C} = \frac{1}{m \times n} \sum_{m,n} C \quad (5.8)$$

Root Mean Square Error (RMSE): The RMSR is a frequently used measure of the difference between the reconstructed image B and the actual image A . These individual differences are also called residuals, and the RMSE serves to aggregate them into a single measure of predictive power. The RMSE of a model prediction with respect to the estimated variable B is defined as the square root of the mean squared error:

$$RMSE = \sqrt{\frac{\sum_{m,n} (B - A)^2}{m \times n}} \quad (5.9)$$

Correlation Coefficient (CC): The CC represents how similar is the features of the reconstructed image with the original image. The CC is defined as:

$$CC(A, B) = \frac{\sum_{m,n} (A_{m,n} - \bar{A})(B_{m,n} - \bar{B})}{\sqrt{\left(\sum_{m,n} (A_{m,n} - \bar{A})^2 \right) \left(\sum_{m,n} (B_{m,n} - \bar{B})^2 \right)}} \quad (5.10)$$

where \bar{A} and \bar{B} stand for the mean values of the corresponding images. The CC is calculated globally for the entire image. The result of this equation shows similarity in the small structures between the original and reconstructed images.

PSNR: The PSNR is the ratio between peak power of an image and the power of noisy image that due to reliability of its representation. The PSNR is the most commonly used quality measure for reconstructed compressed images. The higher *PSNR* represents better image quality. The PSNR is most simply defined using the mean squared error (MSE) as given below:

$$PSNR(dB) = \log_{10} \left(\frac{255^2}{MSE} \right) dB \quad (5.11)$$

5.4 Simulation study and performance analysis

In this section, simulation results are provided to show the efficacy of the proposed MUD schemes in the four user four receiving antenna 4×4 SDMA–OFDM system while all of its four users are transmitting separate images. The performance evaluations are basically considered for two cases, namely, when the system is transmitting gray scale images and when the system is transmitting color images.

5.4.1 Results and discussion for gray scale image transmission

In this case, 256×256 pixel size standard Kid, Lena, Cameraman and Peppers images as shown in Figure 5.4 are considered to be transmitted through User–1, User–2, User–3 and User–4 of the SDMA–OFDM system respectively.

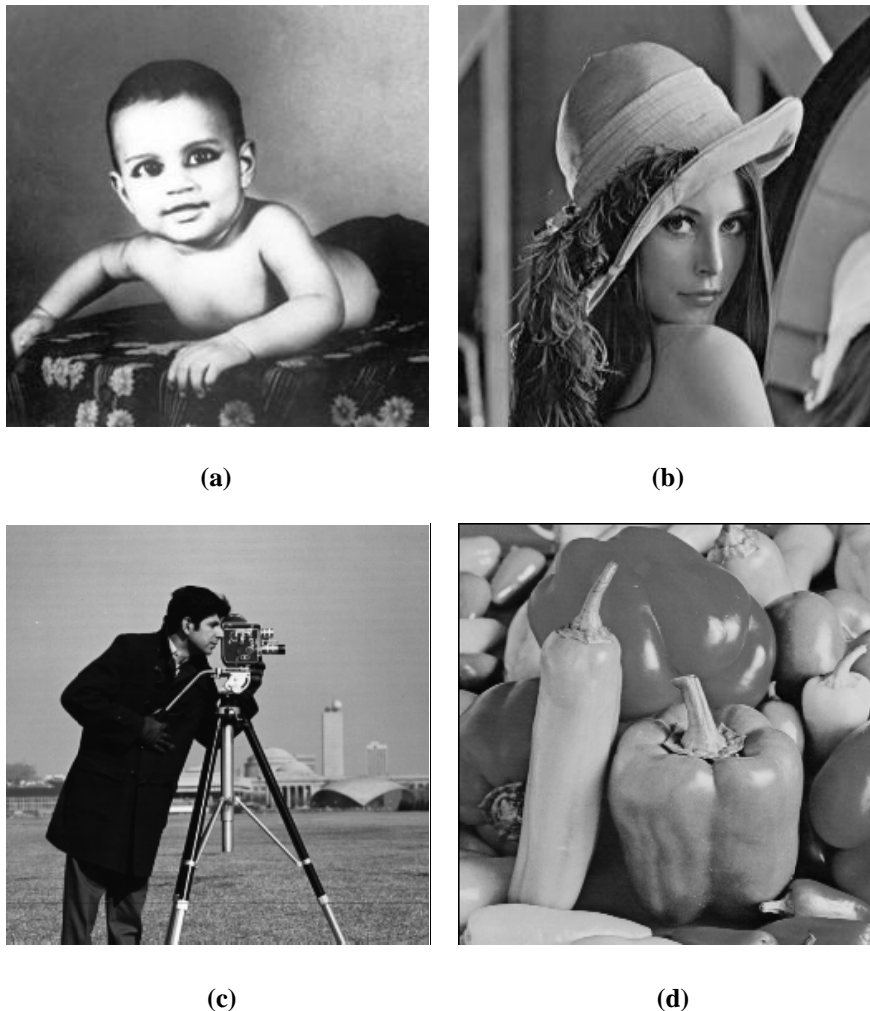


Figure 5.4: 256×256 pixel size gray scale test images transmitted through four different users in the SDMA–OFDM system (a) Kid (b) Lena (c) Cameraman (d) Peppers

Each of the test images is compressed using the efficient SPIHT coder with a bit rate of 2 bpp (bits per pixel). In the SPIHT technique, “bior 4.4” is used to get the wavelet coefficients and then the coefficients are processed as per the SPIHT algorithm to generate an embedded bit stream. The stream length of image is $N_e = 131072$. The entire user’s data is protected with their individual half rate Convolutional Encoders consisting polynomials (133, 171) in octal notation. Thus, after FEC the stream length is 262144. The symbol mapper chosen for all these simulations is a BPSK modulator. Hence, a total of 2048 OFDM frames each of 128 sub carrier length along with a guard interval of length 32 symbols are employed for transmitting a single image. The wireless MIMO channel considered here is the SUI channel mode as presented in Appendix A. This channel is assumed to be OFDM symbol-invariant, which means the channel multipath delays are assumed to be constant over the transmission of one OFDM symbol.

In the beginning of the simulation study, the reconstructed image of the MMSE detector while varying E_b/N_o is shown in Figure 5.5. The features of the original images may not be restored in the reconstructed image at $E_b/N_o = 10$ dB due to the influence of the noise in the channel. By increasing the signal power ($E_b/N_o = 20$ dB) the quality of the reconstructed image gets improved.

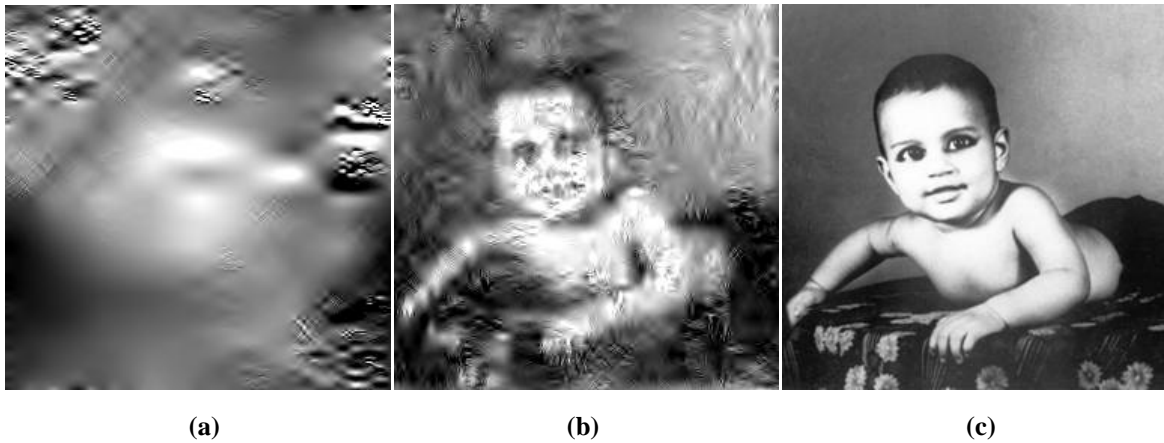


Figure 5.5: Reconstructed Kid image using MMSE MUD at different values of E_b/N_o (a) $E_b/N_o = 10$ dB (b) $E_b/N_o = 15$ dB (c) $E_b/N_o = 20$ dB

Figure 5.6 depicts the rate distortion plot with respect to PSNR value while increasing bpp. The reconstructed images at three different bpp values are shown pictorially in Figure 5.7. The images are reconstructed at 15 dB E_b/N_o using MMSE detectors. It is observed that, at lower bpp values the reconstruction performance is very poor since compression is more and these compressed images are more prone to channel noise. On the other hand, as the bpp

value increases, the total number of bits require to represent an image also increases, which requires high bandwidth though the reconstruction is good. Explicitly, the total number of bits require to represent a gray scale image of size 256×256 are 32768, 131072 and 524288 at $\text{bpp} = 0.5, 2, 8$ respectively. Hence, bpp value is chosen as 2 in rest of simulations considering the tradeoff between the performance and band width.

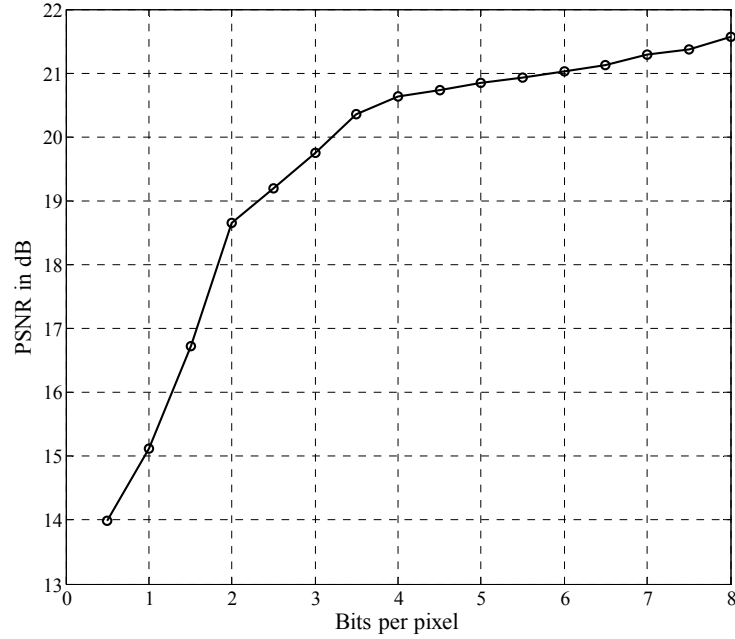


Figure 5.6: PSNR of Kid image while varying bits per pixels at 15 dB E_b/N_o

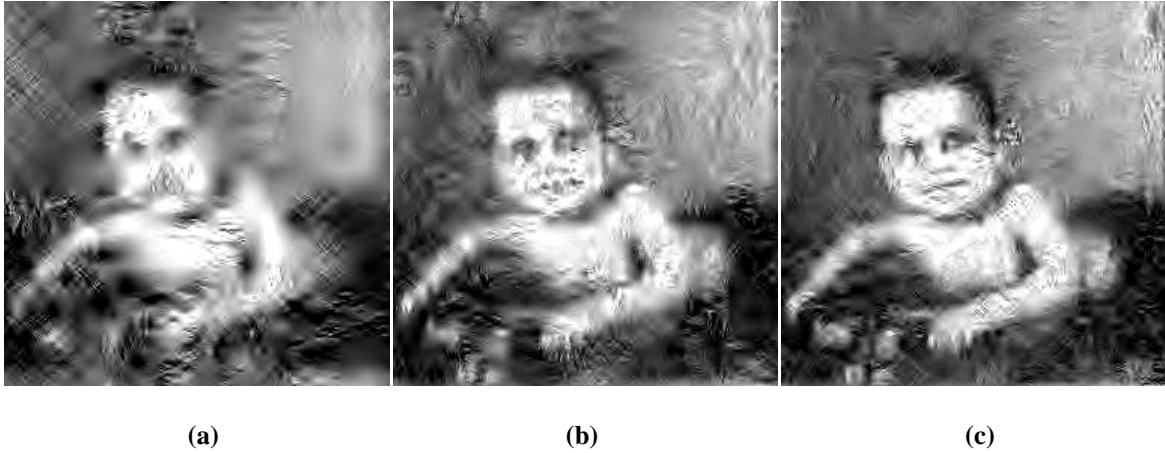


Figure 5.7: Reconstructed Kid image using MMSE MUD at different compression rates (a) $\text{bpp} = 0.5$ (b) $\text{bpp} = 2$ (c) $\text{bpp} = 8$

Figure 5.8 to Figure 5.11 depict the reconstructed image of User-1 to User-4 respectively, using classical MMSE, ML, proposed OTs aided MBER and proposed NN based MUD schemes under multiuser environment. All of these images are transmitted through the SUI channel as given in Appendix A at 15 dB E_b/N_o .

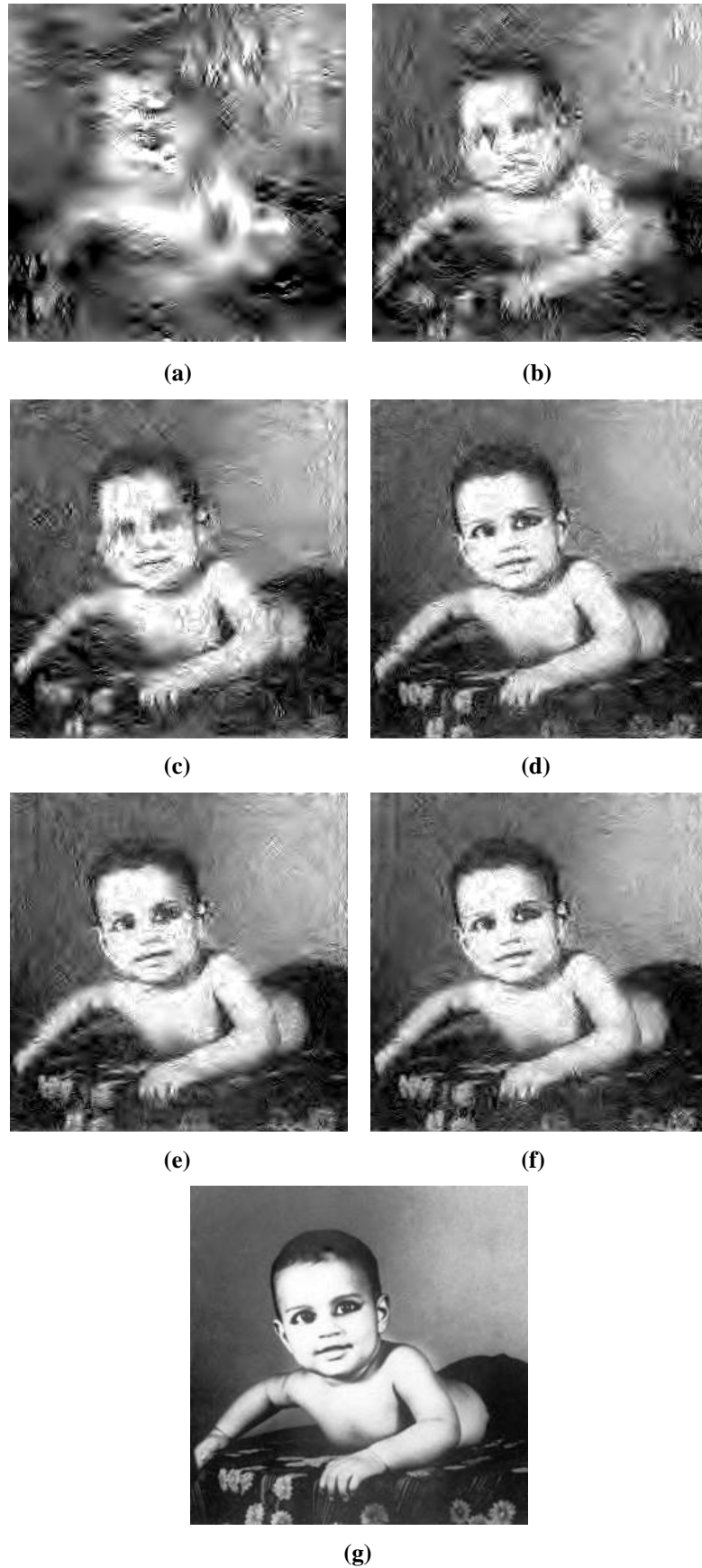


Figure 5.8: Reconstructed Kid image using various MUDs (a) MMSE (b) AGA MBER (c) ADEA MBER (d) IWO MBER (e) MLP (f) RBF (g) ML



Figure 5.9: Reconstructed Lena image using various MUDs (a) MMSE (b) AGA MBER (c) ADEA MBER (d) IWO MBER (e) MLP (f) RBF (g) ML

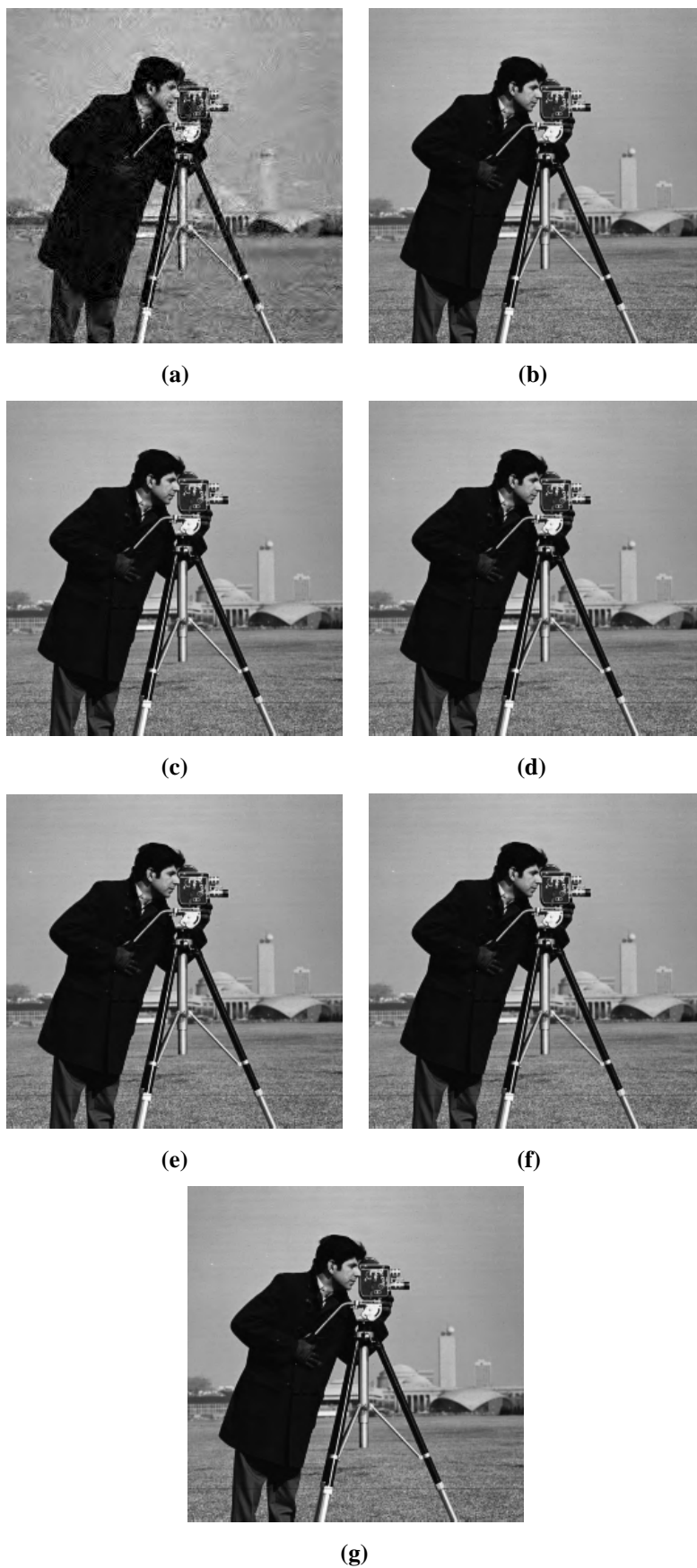


Figure 5.10: Reconstructed Cameraman image using various MUDs (a) MMSE (b) AGA MBER (c) ADEA MBER (d) IWO MBER (e) MLP (f) RBF (g) ML

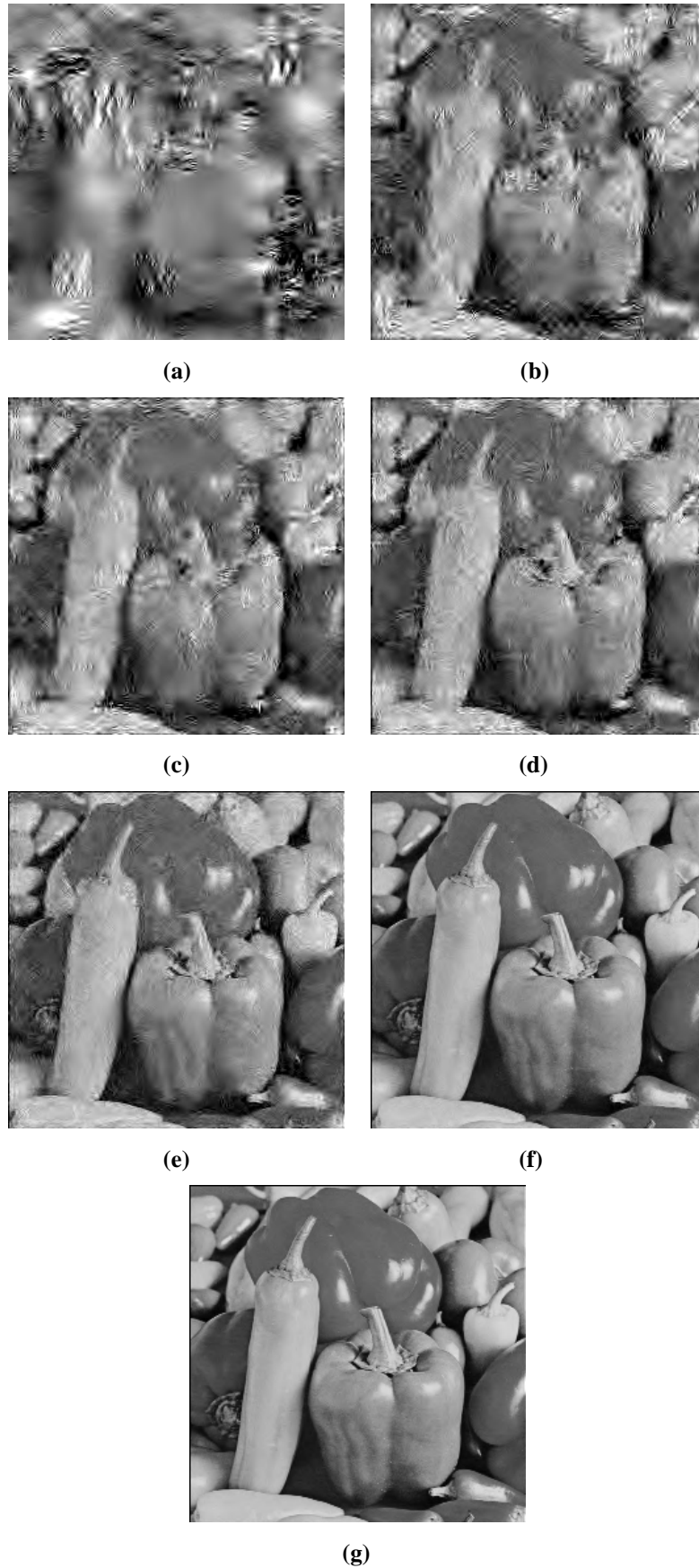


Figure 5.11: Reconstructed Peppers image using various MUDs (a) MMSE (b) AGA MBER (c) ADEA MBER (d) IWO MBER (e) MLP (f) RBF (g) ML

From Figure 5.8 to 5.11, it is noticed that, the spectral quality gets improved from MMSE to optimal ML detectors. The MMSE detector produced blurred pictures due to poor detection ability while the ML detector is preserving more spectral details. Although the reconstruction performance of the restored images using OTs aided MBER MUDs are better compared to the MMSE one, the severe impulsive-like noise still exists in these image. However, the reconstructed images using NN based MUDs especially RBF MUD are more correlated with the image reconstructed by the optimal ML detector as these model is a better nonlinear classifier.

In Figure 5.8–Figure 5.11, the visual comparisons of the reconstructed images using various MUD techniques are illustrated for the SDMA–OFDM system. Further, in Table 5.1–Table 5.4, the comparison between actual and reconstructed images using various MUD schemes by means of some statistical parameters for image quality analysis are provided for all four user in the SDMA–OFDM system at 15 dB E_b/N_o value.

Table 5.1: Performance comparison of MMSE, OTs aided MBER, NN and ML MUD schemes based on statistical parameters while reconstructing Kid image

MUD	Bias	SDD	RMSE	CC	PSNR in dB
MMSE	2.2871	46.157	2132.098	0.772	11.079
AGA MBER	1.3907	41.083	1693.036	0.826	17.024
ADEA MBER	0.2754	27.275	744.0275	0.921	20.666
IWO MBER	0.1954	19.353	374.5447	0.961	22.326
MLP	0.0938	14.313	280.6799	0.971	31.177
RBF	0.0937	1.6753	204.8943	0.976	34.971
ML	0.0039	1.0427	1.087147	0.999	47.768

Table 5.2: Performance comparison of MMSE, OTs aided MBER, NN and ML MUD schemes based on statistical parameters while reconstructing Lena image

MUD	Bias	SDD	RMSE	CC	PSNR in dB
MMSE	0.1286	22.708	515.6853	0.903	21.470
AGA MBER	0.0466	7.0464	49.65385	0.938	27.877
ADEA MBER	0.0016	5.2078	27.12151	0.964	31.767
IWO MBER	0.0009	1.4312	3.310033	0.991	33.521
MLP	0.0003	1.4292	2.048375	0.995	39.029
RBF	0.0003	0.1819	2.042692	0.999	41.029
ML	0.0002	0.1387	1.924197	0.999	45.029

Table 5.3: Performance comparison of MMSE, OTs aided MBER, NN and ML MUD schemes based on statistical parameters while reconstructing Cameraman image

MUD	Bias	SDD	RMSE	CC	PSNR in dB
MMSE	0.0917	7.2761	52.9497	0.980	33.80837
AGA MBER	0.0312	4.1148	16.9320	0.993	40.56111
ADEA MBER	0.0177	3.2164	6.35622	0.998	42.81202
IWO MBER	0.0136	2.1239	4.51119	0.999	42.81202
MLP	0.0027	1.8519	3.42946	0.999	42.81202
RBF	0.0021	1.8448	3.40318	0.999	42.81202
ML	0.0003	0.1239	1.53628	0.999	42.81202

Table 5.4: Performance comparison of MMSE, OTs aided MBER, NN and ML MUD schemes based on statistical parameters while reconstructing Peppers image

MUD	Bias	SDD	RMSE	CC	PSNR in dB
MMSE	2.328	51.187	2625.57	0.593	9.458214
AGA MBER	0.259	29.159	850.299	0.844	12.66148
ADEA MBER	0.100	25.846	668.072	0.878	14.00151
IWO MBER	0.094	20.973	439.882	0.921	14.81834
MLP	0.065	13.369	178.749	0.968	22.82056
RBF	0.034	4.3146	18.6165	0.997	26.18914
ML	0.005	2.0428	4.17309	0.999	41.92629

From Table 5.1–Table 5.4, it is observed that the recovered image using MMSE MUD suffers from highly spectral distortion by providing low correlation with actual transmitted image. It is also noticed that the *Bias*, *SDD*, *RMSE*, *CC* and *PSNR* of the proposed NN based detector are better than the classical MMSE and proposed OTs aided MBER detectors and close to the optimal ML detector.

Figure 5.12 describes the performance evaluation through PSNR curves while varying E_b/N_o values for all four users in the SDMA–OFDM system. It is observed that, the peak PSNR values of the four users are different, as each of these individual users undergoes through individual channel fading. At any E_b/N_o value, the PSNR values of the proposed NN based MUDs always have substantial improvement over the MMSE and OTs aided MBER detectors. Hence, the NN based MUDs have better image restoring capability and reconstruct images which are more correlated with the images reconstructed by the optimal ML detectors.

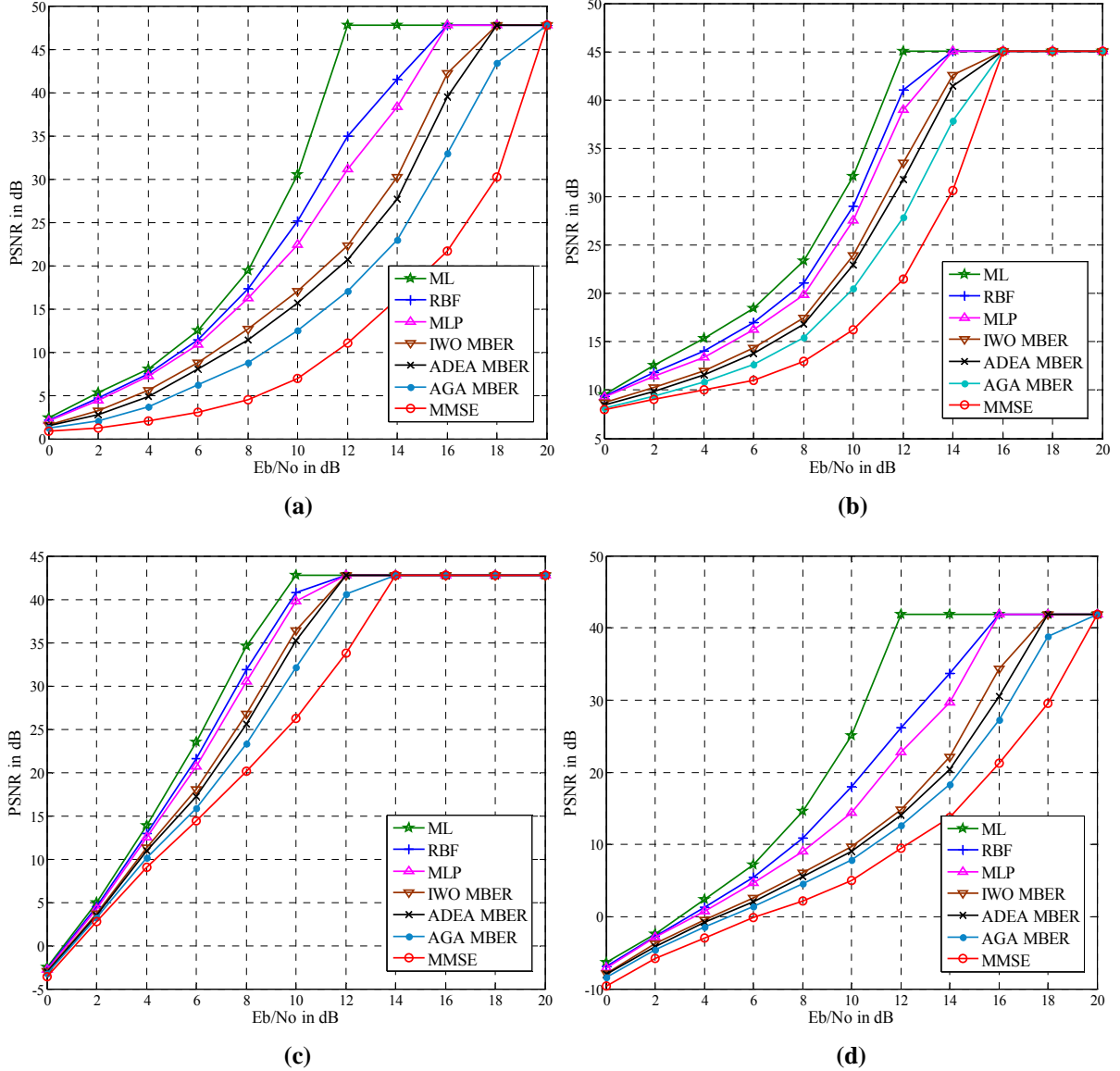


Figure 5.12: PSNR of reconstructed images using various MUDs for all four different users (a) Kid (b) Lena (c) Cameraman (d) Peppers

5.4.2 Results and discussion for color image transmission

In this section, the MMSE, ML, proposed OTs aided MSER and complex valued NN based MUDs are utilized for reconstructing color images. In this case, 256×256 pixel size standard RGB Kid, RGB Lena, RGB Cameraman and RGB Peppers images as shown in Figure 5.13 are considered to be transmitted through User-1, User-2, User-3 and User-4 of the SDMA-OFDM system respectively. All of these images are transmitted through the MIMO Rayleigh fading channel as given in Appendix A at 15 dB E_b/N_0 . The color images have three planes namely Red (R), Green (G) and Blue (B) planes. Hence, each of the test images is first compressed using three separate SPIHT coders with a bit rate of 2 bpp for those. In the SPIHT technique, “bior 4.4” is used to get the wavelet coefficients and then the coefficients

are processed as per the SPIHT algorithm to get an embedded bit stream. Initially, the R, G and B planes are converted to Y , C_R and C_B planes. The stream length of each bit stream among Y , C_R and C_B planes is $N_e=131072$. Total stream length of all three planes is 393216. This entire data is protected with their individual half rate Convolutional Encoders consisting polynomials (133, 171) in octal notation. Thus, after FEC the stream length is 786432. The symbol mapper chosen for all these simulations is a 4-QAM modulator. Hence, 3072 OFDM frames each of 128 sub carrier length along with a cyclic prefix of length 32 symbols are employed. The channel is also assumed to be OFDM symbol-invariant, which means the channel multi path delays are constant over the transmission of one OFDM symbol.

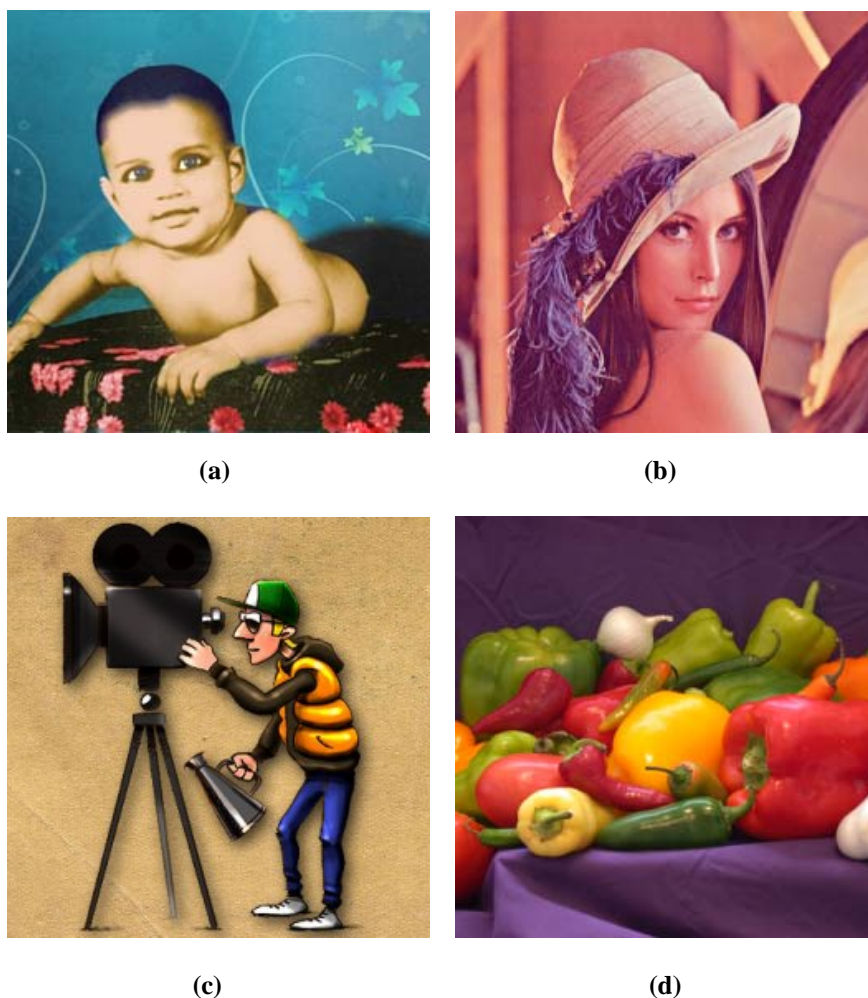


Figure 5.13: 256×256 pixel size RGB test images transmitted through four different users in the SDMA–OFDM system (a) RGB Kid (b) RGB Lena (c) RGB Cameraman (d) RGB Peppers

Figure 5.14 to Figure 5.17 depict the reconstructed images of User–1 to User–4 respectively, using classical MMSE, ML, proposed OTs aided MSER and proposed complex valued NN based MUD schemes under multiuser environment.

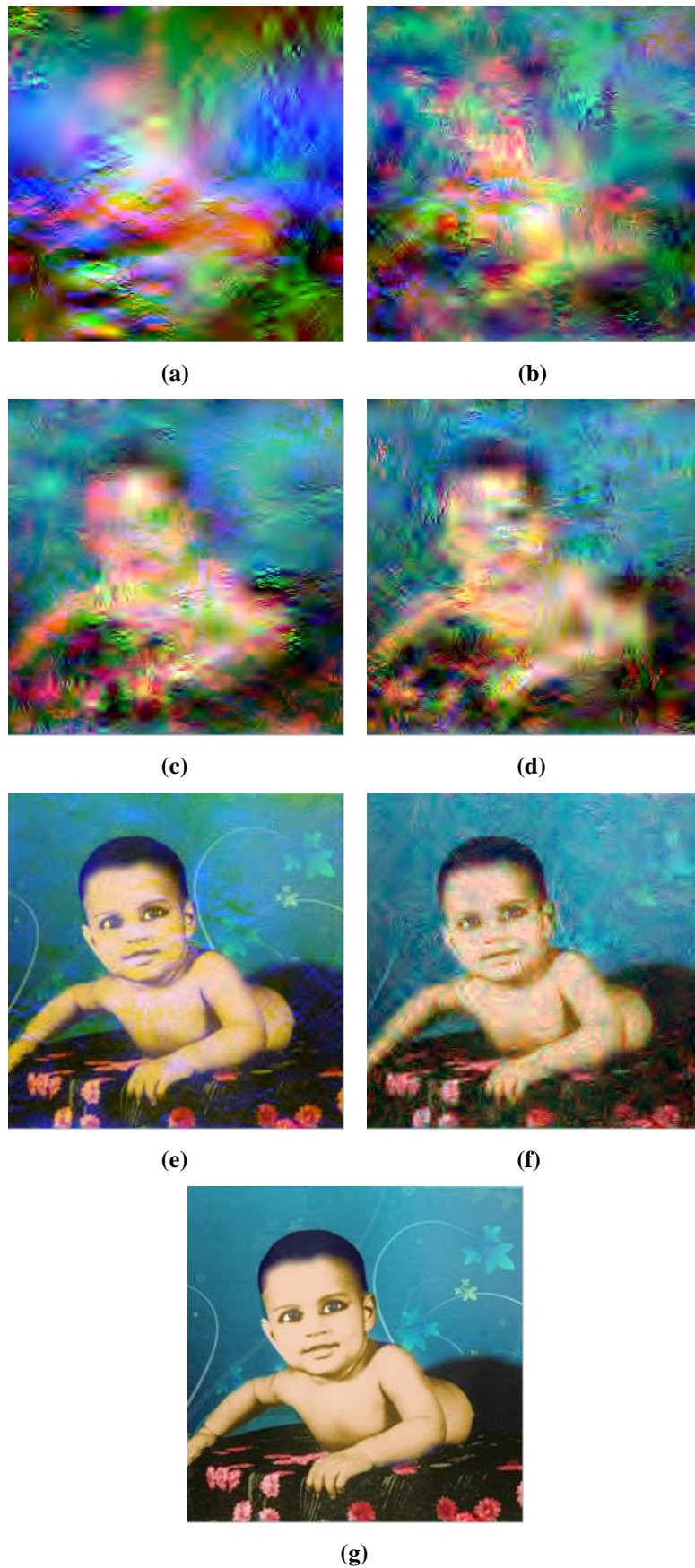


Figure 5.14: Reconstructed RGB Kid image using various MUDs (a) MMSE (b) AGA MSER (c) ADEA MSER (d) IWO MSER (e) CMLP (f) CRBF (g) ML



Figure 5.15: Reconstructed RGB Lena image using various MUDs (a) MMSE (b) AGA MSER (c) ADEA MSER (d) IWO MSER (e) CMLP (f) CRBF (g) ML

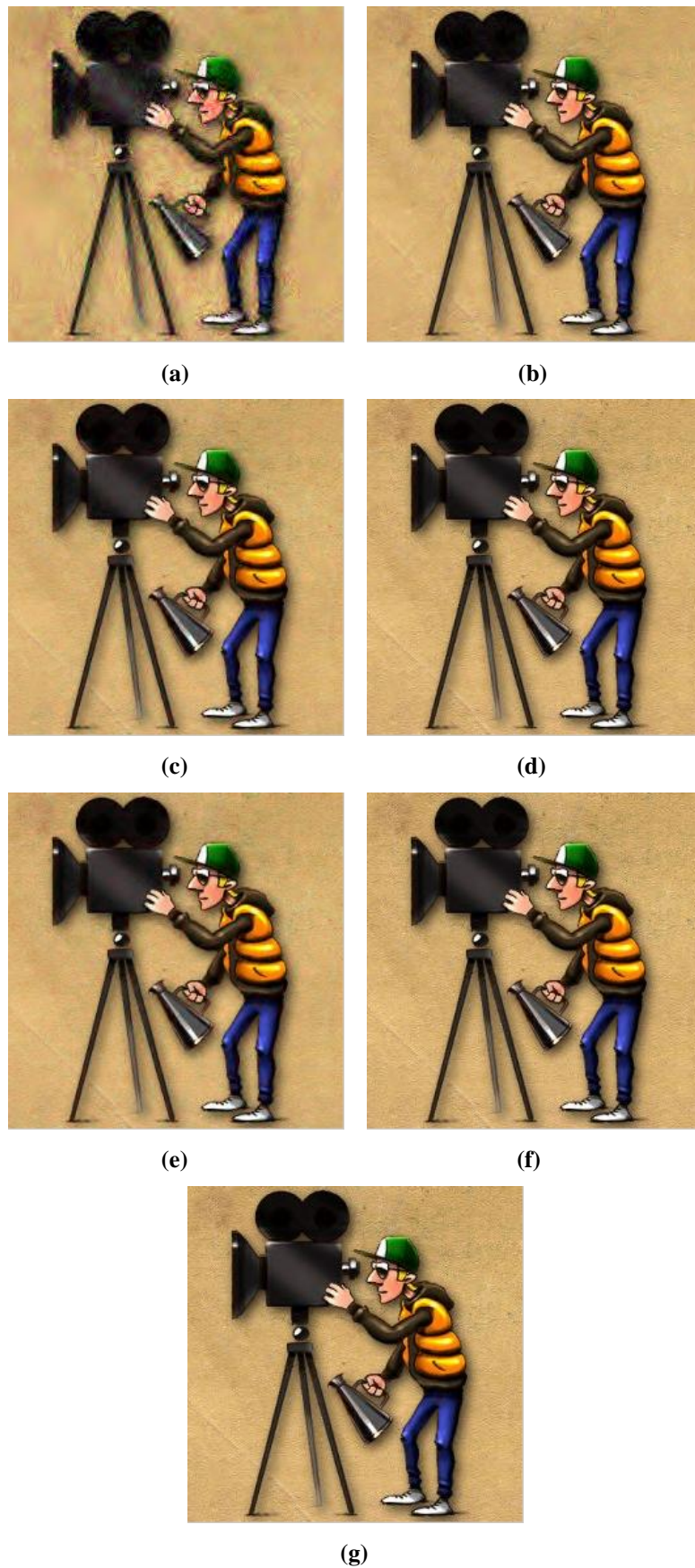


Figure 5.16: The reconstructed RGB Cameraman image using various MUDs (a) MMSE (b) AGA MSER (c) ADEA MSER (d) IWO MSER (e) CMLP (f) CRBF (g) ML

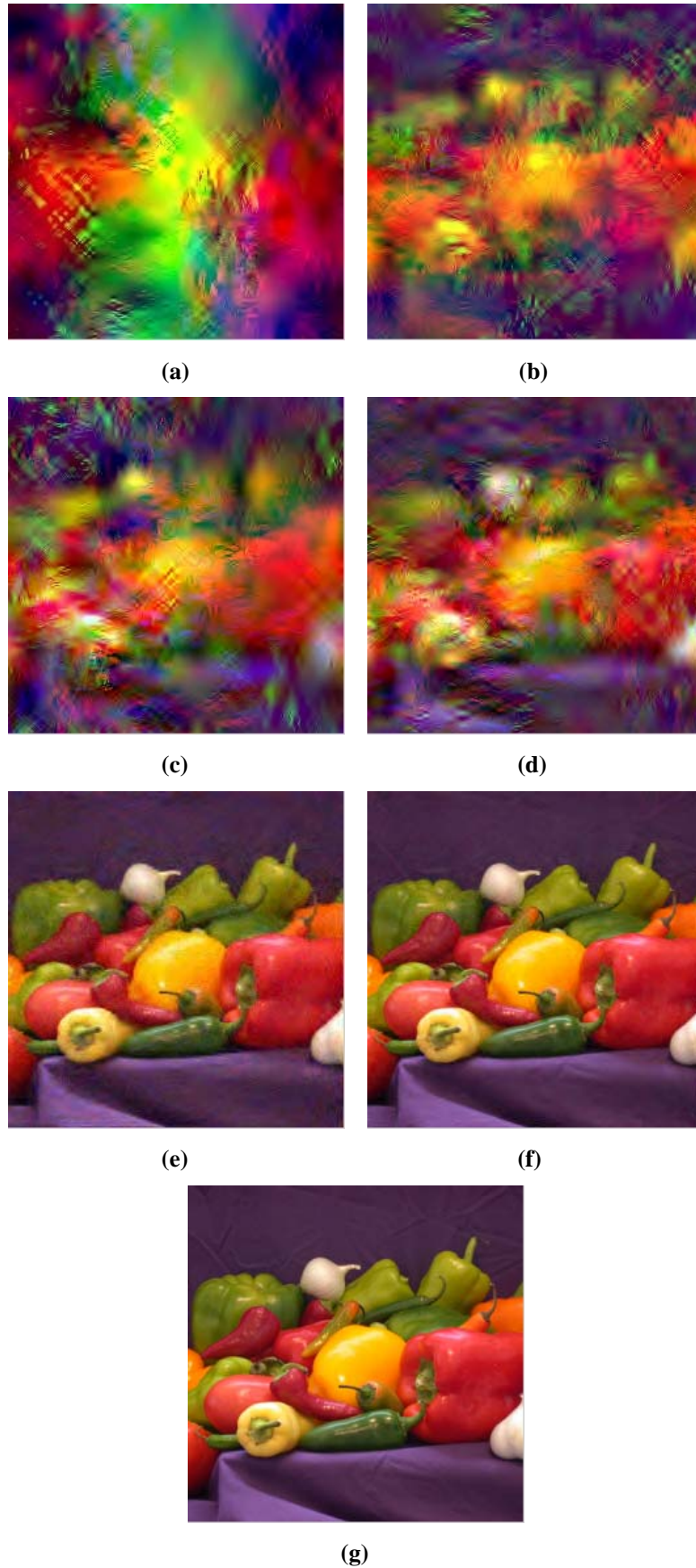


Figure 5.17: Reconstructed RGB Peppers image using various MUDs (a) MMSE (b) AGA MSER (c) ADEA MSER (d) IWO MSER (e) CMLP (f) CRBF (g) ML

Figure 5.14–Figure 5.17 show the visual comparison among the reconstructed images using various MUD schemes at 15 dB E_b/N_o . The enhancement in the spectral quality is observed clearly from MMSE detector to ML detector. Here, the inability of the MMSE detector is once again evident through a noisy reconstructed image. On the other hand, the proposed complex valued NN based MUDs especially the CRBF, restore images accurately and preserving more spatial details compared to the MMSE and OTs aided MSER MUDs. However, under low fading environment, the visual comparisons may not be distinguishable, for example like the reconstructed image of User-3 as shown in Figure 5.16. Therefore, comparisons based on statistical parameters like *Bias*, *SD*, *RMSE*, *CC* and *PSNR* may be more accurate. The comparisons of all MUDs with respect to these statistical parameters are presented in Table 5.5–Table 5.8 at 15 dB E_b/N_o value. From these tables, it is found that the ML has the best performance, while the MMSE performs the worst. It is also observed that, the average values of these parameters for all three planes using the proposed CRBF detector are better than the MMSE and OTs aided MSER detectors and close to optimal ML detector.

Table 5.5: Performance comparison of MMSE, OTs aided MSER, complex valued NN and ML MUD schemes based on statistical parameters while reconstructing RGB Kid image

MUD	Bias	SDD	RMSE	CC	PSNR in dB
MMSE	78.5105	62.923	21535.85	0.455	2.574
AGA MSER	1.53611	55.787	3170.079	0.609	9.102
ADEA MSER	1.41948	40.238	1672.297	0.789	10.11
IWO MSER	0.17168	19.451	625.3441	0.814	10.81
CMLP	0.00328	1.3179	3.472037	0.921	20.59
CRBF	0.00283	0.1601	1.737453	0.966	28.98
ML	0.00075	0.0411	1.692936	0.999	45.73

Table 5.6: Performance comparison of MMSE, OTs aided MSER, complex valued NN and ML MUD schemes based on statistical parameters while reconstructing RGB Lena image

MUD	Bias	SDD	RMSE	CC	PSNR in dB
MMSE	1.174	48.669	2492.739	0.631	10.2412
AGA MSER	0.136	23.035	474.8325	0.851	13.3366
ADEA MSER	0.131	19.717	472.4277	0.883	14.8022
IWO MSER	0.038	19.493	309.2142	0.888	16.1038
CMLP	0.011	17.561	164.7168	0.915	24.8608
CRBF	0.004	12.277	5.582896	0.943	31.0146
ML	0.001	1.7582	3.152403	0.999	43.3221

Table 5.7: Performance comparison of MMSE, OTs aided MSER, complex valued NN and ML MUD schemes based on statistical parameters while reconstructing RGB Cameraman image

MUD	Bias	SDD	RMSE	CC	PSNR in dB
MMSE	0.0012	9.044	209.59	0.963	31.4732
AGA MSER	0.0828	7.470	83.379	0.984	38.2432
ADEA MSER	0.0338	6.125	67.407	0.991	38.2432
IWO MSER	0.0203	3.963	55.737	0.994	38.2432
CMLP	0.0177	3.129	17.166	0.998	38.2432
CRBF	0.0107	3.122	9.7905	0.998	38.2432
ML	0.0107	0.144	9.7459	0.999	38.2432

Table 5.8: Performance comparison of MMSE, OTs aided MSER, complex valued NN and ML MUD schemes based on statistical parameters while reconstructing RGB Peppers image

MUD	Bias	SDD	RMSE	CC	PSNR in dB
MMSE	4.359	71.963	5698.83	0.361	3.4292
AGA MSER	2.292	39.279	1547.76	0.629	12.695
ADEA MSER	1.164	35.147	1290.75	0.662	13.748
IWO MSER	1.057	28.654	828.225	0.831	14.381
CMLP	0.076	10.276	111.344	0.974	23.682
CRBF	0.028	3.6485	17.1873	0.997	30.449
ML	0.002	1.0854	1.19081	0.999	43.983

Similar to the Figure 5.12, Figure 5.18 shows the PSNR of all reconstructed images while varying E_b/N_o value in the 4×4 SDMA–OFDM system. Here, the PSNR value of each image is averaged for all three planes (R, G and B). It is observed that, the peak PSNR values of the four images are different as each individual user undergoes separate channel fading. Precisely, the peak PSNR values of the RGB Kid, RGB Lena, RGB Cameraman and RGB Peppers images using the MMSE MUD are obtained at 22, 20, 12, 20 dB E_b/N_o values respectively. Among various MUDs, the PSNR loss is more in case of MMSE MUD and less in case of ML MUD. Further, it can also be seen that, the proposed NN based adaptive MUDs provide better PSNR gain over the MMSE and OTs aided MSER detectors for all users at the same E_b/N_o value. As a result the complex NN based MUDs have better image restoring capability. Particularly, the CRBF MUD provides a reconstructed image which is more correlated to the images reconstructed by the optimal ML detector.

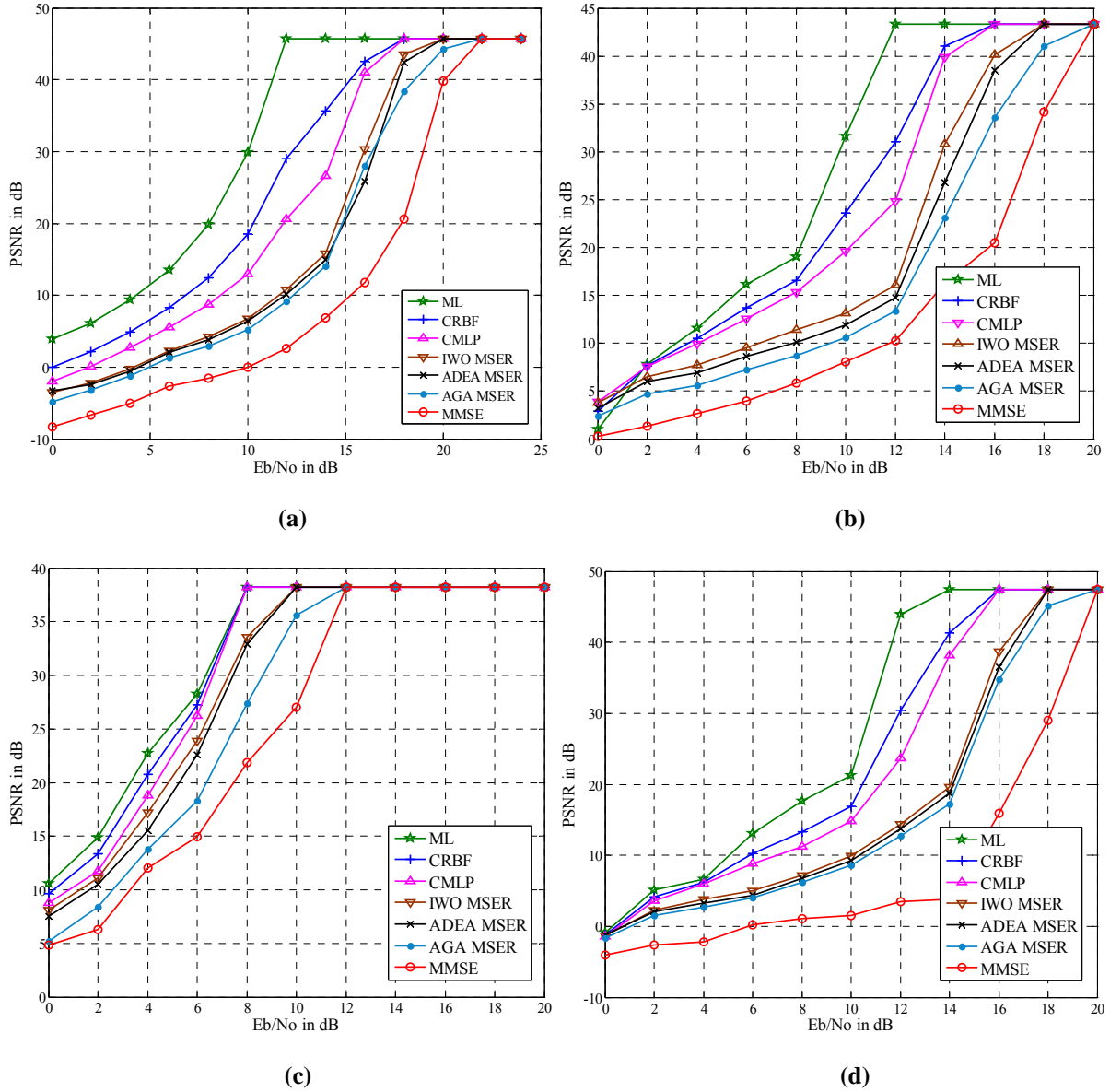


Figure 5.18: PSNR of reconstructed images using various MUDs for all four different users (a) RGB Kid (b) RGB Lena (c) RGB Cameraman (d) RGB Peppers

5.5 Summary

This chapter gives insights into the suitability of the proposed OTs aided MER and NN based MUD schemes through reconstruction of both gray scale and colored images transmitted by multiple users simultaneously through wireless channels. A progressive image transmission over noisy channel environment using SPIHT coding is addressed in the beginning of the chapter. It is observed that, in the SPIHT algorithm, by increasing the number of bits per pixel, the reconstruction performance gets better and at the same time it requires high bandwidth. So, a compromise between bandwidth and performance has been thought over. This study has also pointed out the potentialities of multi resolution analysis for lossy

compression of still images at different rates. In order to show the efficacy of various detectors in a multiuser environment, a SDMA–OFDM system with four users is considered, where all four users are transmitting separate images. In the simulation study, image reconstruction is studied using various MUDs like MMSE, ML, proposed OTs aided MER and NN models considering a practical scenario by choosing fixed E_b/N_o value of 15 dB. From simulation results, it is found that the ML detector has the best reconstructed image, while the MMSE performs the worst. Further, the reconstructed images of the OTs aided MER MUDs are usable images but still require improvement of image quality. On the other hand, the visual and the statistical parameter comparisons of the reconstructed images using NN based MUDs especially RBF and CRBF are found to be qualitatively better than the MMSE and OTs aided MER detectors by preserving more spectral details. The parameters of statistical comparison metrics considered here are the *Bias*, *SDD*, *RMSE*, *CC* and *PSNR*. Though, the performance of ML detector is optimal, as it imposes quite exhaustive complexity, the RBF and CRBF MUDs offer best receiving solution for fixed wireless SDMA–OFDM systems. The suggested nonlinear MUDs can be suitably implemented for real time image traffic over a radio link in future communication systems.

Chapter 6

Conclusions and Future

Scope of Research

Evolution of WiMAX and 4G networks along with the exponential growth in the number of users has required a system with high spectral efficiency. A promising solution for the same can be achieved by the combination of OFDM with SDMA. In the uplink of SDMA–OFDM system, multiple users communicate with a multiple antenna base station simultaneously on the same frequency band using their own spatial signature. However, there is a chance of correlation among different users due to the channel multipath distortion at the receiver, which is known as Multiple Access Interference (MAI). MAI degrades the performance of the system and hence design of multiuser detector under such situation has become an ever challenging issue. The research undertaken in this thesis is primarily concerned with the development of efficient MUD schemes for SDMA–OFDM wireless communication system. The performance evaluation has been carried out over the standard MIMO Rayleigh fading, SUI and SWATM channel models in order to investigate almost realistic performance utilizing proposed MUD schemes.

Achievements of the undertaken research are highlighted 6.1. Section 6.2 discusses some of the limitations of the present work and points out the future scope of research.

6.1 Summary of the thesis

The work presented in this thesis starts with comparison of performances of some classical linear and nonlinear MUDs applied to SDMA–OFDM system. Further, the proposed OTs aided MER and NN based MUDs are tested for their suitability under various user loads. Comparison with optimal ML and linear MMSE detectors in terms of system performance and complexity analysis has been a major attempt to prove the efficacy of the proposed MUD schemes. Detailed achievements of the research are presented chapter wise as below.

Chapter–2 of the thesis provides details of the SDMA–OFDM system model a brief comparison between all classical MUD schemes. The performance the ML detector is found to be optimal at the cost of dramatically increased complexity, especially in context of a high number of users and higher order modulation schemes. By contrast, the linear ZF and MMSE exhibit low complexity while suffering from performance loss. Therefore, several other nonlinear MUDs are studied to make a tradeoff between performance and complexity. However, all these techniques fail to detect users in overload scenario. In such a condition, it is found that the CG aided MBER MUD is a better alternative. But the CG algorithm requires initial weights and differentiable cost functions, hence a new research direction to overcome these limitations is thought.

Chapter–3 is entirely devoted to discuss one of the major contributions of the work undertaken relating to the design of novel MUD schemes, that is the design of OTs aided MER MUD schemes. Metaheuristic OTs like AGA, ADEA and IWO algorithms are considered for MER weight optimization. The extensive simulation study shows that the proposed MUDs are superior in performance over MMSE and require less computational complexity compared to ML detector. Further it is also observed that, the performance of these OTs is greatly influenced by selection of control parameters. The performance AGA is influenced by P_c , P_m , G_g and N_g while ADEA is influenced by C_p , F , G_d and N_d . Similarly, the IWO MER MUDs is subjective to the parameters like N_I , I_{max} , S_{max} , σ_{max} , σ_{min} and m . Selecting right combination of these control parameters yields a better performance. Hence, development of suitable methods for selection of control parameters has been included in this chapter. Among all the discussed OTs, the IWO algorithm is found to be better as it allows all of the individuals to participate in the reproduction process. Sometimes, it may be also possible that the individuals with the lower fitness may carry more useful information compared to the fitter individuals. Hence, this algorithm, gives a chance to the less fit plants to reproduce and if the seeds produced by them have good fitnesses in the colony, they can survive. Fitter individuals produce more seeds than less fit individuals, which improves the convergence and performance over the AGA and ADEA algorithms.

Chapter–4 of the thesis provides another major contribution of this work through the design of NN based MUD schemes. As the NN models are highly nonlinear classifiers, these are well suited for detection of the multiuser signals, which are corrupted by nonlinear channel distortion. In the NN family, the real valued MLP and RBF models are used for multiuser signal detection when all the users are transmitting BPSK signals. However, in several communication systems, the available signals are in complex form when the system is communicating higher order signals like M-QAM. In this case, the classical real valued NN models cannot be applied directly because it requires real valued inputs and activation functions. In order to extend the real valued NN models to complex signals, the activation function and training algorithms should be redefined. In the CMLP model, the sigmoid function is divided in to two components for responding to the real and imaginary portions of the input signals individually. For CRBF model, the ‘*sech*’ activation function is preferred over Gaussian function, because the Gaussian function always results real valued response. The conventional BP and GD algorithms used for updating the real valued NNs cannot be directly applied for complex valued NN models. Hence, suitable modifications have been

incorporated to these algorithms. The extensive simulation study shows that the proposed OTs aided MER and NN based MUDs are superior in performance compared to MMSE and OTs aided MER MUDs. The performance improvement of these MUDs over the MMSE in full load ($L = P = 4$) condition at 10^{-4} BER is given in Table 6.1.

Table 6.1: Performance comparisons of OTs aided MER and NN MUDs in terms of E_b/N_o gain (in dBs)

Channel	AGA		ADEA		IWO		Real Valued NNs		Complex Valued NNs	
	MBER	MSER	MBER	MSER	MBER	MSER	MLP	RBF	CMLP	CRBF
MIMO Rayleigh	4.5	5.1	4.55	5.1	4.6	5.3	4.6	5.1	6.7	9
SUI	4.1	4.2	4.2	4.25	4.2	4.1	7.1	9.05	4.7	6.8
SWATM	6.8	7.6	6.8	7.5	6.9	7.7	9.8	13.5	8.3	11.6

In the complexity analysis, the percentage of complexity require for OTs aided MER MUDs in terms of computational operations is compared with the computationally exhaustive ML detector and presented in Table 6.2 when $L = 6$ and $P = 4$.

Table 6.2: Complexity comparisons of OTs aided MER and NN MUDs in terms of computational operations

MUD Technique		Percentage of complexity
AGA	MBER	15.43
	MSER	19.145
ADEA	MBER	13.87
	MSER	17.51
IWO	MBER	12.95
	MSER	13.205
Real Valued NNS	MLP	13.87
	RBF	8.985
Complex Valued NNS	MLP	17.51
	RBF	16.49

Chapter–5 illustrates the ability of the proposed MUDs while reconstructing both gray scale and colored images, which are transmitted by multiple users simultaneously through wireless channels. A comparative analysis among all proposed and the classical MUD schemes based on some statistical parameters like *Bias*, *SDD*, *RMSE*, *CC* and *PSNR*. The SPIHT algorithm is considered for image compression and coding as it performs better than

the classical EZW technique. From simulation results, it is observed that the ML detector produces the best restored image, while the MMSE performs the worst. The reconstructed images of the OTs aided MER MUDs are usable images but still require improvement. Finally, both the visual and the statistical parameter comparisons of the NN MUDs are found to be qualitatively better than the MMSE and OTs aided MER detectors.

Finally, the general inference derived from the extensive simulation study is that the proposed NN based MUDs, especially the RBF and CRBF detectors, are efficient in terms of BER performance, faster convergence and computational complexity. Besides that, the NN base detectors has additional complexity gain over classical MMSE, ML and proposed OTs aided MER detectors, because these detectors do channel approximation and signal detection simultaneously. As the ML detector is a highly complex one, the RBF and CRBF MUDs are found to be the suitable alternative for MUD in the SDMA–OFDM system.

6.2 Limitations and future scope of research

- The NN based adaptive MUDs, proposed in the thesis are training based. Sometimes, depending on the channel severity, the use of long training sequences and/or frequent repetition of training for estimation of channel parameters may significantly reduce the information transmission rate resulting in the loss of bandwidth efficiency. So blind NN based adaptive MUD techniques for SDMA–OFDM may be tried to solve this issue.
- In this research, the classical BP and GD algorithms are used for training the NN parameters, whereas these algorithms require differentiable activation functions. Hence, selection of appropriate nonlinear activation function of neuron node to suit the requirements in detection of high order modulated signals is a challenging task. So the free parameters of the NN updating with metaheuristic OT based algorithms may be attempted and a new class of hybrid MUDs for SDMA–OFDM system can be developed.
- Investigation of robust video transmission scheme for SDMA–OFDM system with the proposed soft computing based MUDs may be tried in view of future streaming multimedia requirements with improved video quality.
- In the SDMA based system, when the users are in close proximity, there is a chance of experiencing Co-channel Interference (CCI). So CCI cancellation schemes may be incorporated with the detectors at the BS receiver to improve the system performance further.

Dissemination of Work:

International Journals:

1. Kala Praveen Bagadi and Susmita Das, "Multiuser Detection in SDMA-OFDM Wireless Communication System Using Complex Multilayer Perceptron Neural Network," *Wireless Personal Communications, Springer Publication*, DOI: 10.1007/s11277-013-1492-2.
2. Kala Praveen Bagadi and Susmita Das, "An efficient complex radial basis function model for multiuser detection in an SDMA/MIMO-OFDM system", *IET Communications*, vol.7, no. 13, pp. 1394-1404, 2013.
3. Kala Praveen Bagadi and Susmita Das, "Minimum symbol error rate multiuser detection using an effective invasive weed optimization for MIMO/SDMA-OFDM system", *International Journal of Communication Systems, Wiley*, doi: 10.1002/dac.2579, 2013.
4. Kala Praveen Bagadi and Susmita Das, "Comparative analysis of multiuser detection techniques in SDMA-OFDM system over the correlated MIMO channel model for IEEE 802.16n," *International Journal of Information Engineering, American V-king Scientific Publishing LTD*, vol. 3, no. 1, pp.18-24, 2013.
5. Kala Praveen Bagadi and Susmita Das, "Neural network-based multiuser detection for SDMA-OFDM system over IEEE 802.11n indoor wireless local area network channel models" *International Journal of Electronics, Taylor & Francis*, vol. 100, no. 10, pp. 1332-1347, 2013.
6. Kala Praveen Bagadi and Susmita Das, "Neural network-based adaptive multiuser detection schemes in SDMA-OFDM system for wireless application," *Neural Computing and Application, Springer*, vol. 23, no. 3-4, pp. 1071-1082, 2013.
7. Bagadi K Praveen, Susmita Das and Sridhar K, "Image transmission over space time coded MIMO-OFDM system with punctured turbo codes", *International Journal of Computer Applications, Foundation of Computer Science*, vol. 51, no. 15, pp. 1-6, 2012.
8. Kala Praveen Bagadi and Susmita Das, "MIMO-OFDM channel estimation using pilot carriers", *International Journal of Computer Applications, Foundation of Computer Science*, vol. 2, pp. 81-86, 2010.

Conferences Proceedings:

1. Kala Praveen Bagadi, Susmita das and Sathyam Bonala, "RBF Network Based Receiver Design for Multiuser Detection in SDMA-OFDM System", *Proceedings of Annual IEEE India Conference*, Kochi, India, December 7th-9th, pp. 01-04, 2012. doi: 10.1109/INDCON.2012.6420794.
2. Kala Praveen Bagadi and Susmita Das, "Complex Multi Layered Perceptron Model Based Receiver Design for Multiuser Detection in SDMA-OFDM System", *AIP Proceedings of the Sixth Global Conference on Power Control and Optimization*, Las Vegas, USA, August 6th-8th, pp. 227-233, 2012. doi: <http://dx.doi.org/10.1063/1.4768992>.
3. Kala Praveen Bagadi and Susmita Das, "Comparison of Neural based Multiuser Detection Techniques for SDMA based Wireless Communication System," *Proceedings of IEEE Students Conference Engineering and Systems*, Allahabad, India, March 16th-18th, pp. 01-05, 2012. doi: 10.1109/SCES.2012.6199033.

4. Kala Praveen Bagadi and Susmita Das, "Neural network based multiuser detection techniques in SDMA-OFDM system," *Proceedings of Annual IEEE India Conference*, Hyderabad, India, December 16th–18th, pp. 01–04, 2011. doi: 10.1109/INDCON.2011.6139436
5. Susmita das, and Kala Praveen Bagadi, "Comparative Analysis of Various Multiuser Detection Techniques in SDMA-OFDM System over the Correlated MIMO Channel Model for IEEE 802.16n," *Proceedings of World Academy of Science, Engineering and Technology*, Issue 77, pp. 663-667, June 2011, Paris, France.
6. Kala Praveen Bagadi and Susmita Das, "Low Complexity near Optimal Multiuser Detection Scheme for SDMA-OFDM System," *Proceedings of IEEE International Conference on Devices and Communications*, Ranchi, India, February 24th–25th, pp. 01–05, 2011. doi: 10.1109/ICDECOM.2011.5738463
7. Kala Praveen Bagadi and Susmita Das, "Channel Estimation and Multiuser Detection Techniques in SDMA-OFDM System," *Proceedings of International Conference on Information, Signals and Communications*, Ahmadabad, India, February 5th–6th, 2011.

References

1. R. W. Chang, "Synthesis of band-limited orthogonal signals for multichannel data transmission", *Bell Syst. Tech. J.*, vol. 45, pp. 1775–1796, Dec. 1966.
2. S. B. Weinstein and P. M. Ebert, "Data transmission by frequency-division multiplexing using the discrete Fourier transform", *IEEE Trans. on Commun.*, vol. 19, pp. 628–634, Oct. 1971.
3. B. Hirosaki, "An orthogonally multiplexed QAM system using the discrete Fourier transform," *IEEE Trans. on Commun.*, vol. 29, pp. 982–989, Jul. 1981.
4. B. Hirosaki, "A 19.2 Kbits Voice and Data Modem Based on Orthogonality Multiplexed QAM Techniques", *Proc. of IEEE ICC'85*, pp. 1–5, 1985.
5. IEEE Standard 802.11: Wireless LAN Medium Access Control (MAC) and Physical Layer (PHY) specifications, Nov. 18, 1997.
6. IEEE Standard 802.11a: Wireless LAN Medium Access Control (MAC) and Physical Layer (PHY) specifications: high-speed physical layer in the 5 GHz band, 1999.
7. R. V. Nee and R. Prasad, "OFDM for wireless multimedia communications", *Artech House Inc. Pub.*, London, 2000.
8. L. Hanzo, M. Munster, B. J. Choi, and T. Keller, "OFDM and MC-CDMA for broadband multi-user communications, WLANs and broadcasting", *IEEE Press/Wiley press*, Piscataway, NJ, 2003.
9. R. Prasad, "OFDM for wireless communications systems", *Artech House Inc. Pub.*, London, 2004.
10. J. H. Winters, "Optimum combining in digital mobile radio with co-channel interference", *IEEE J. Sel. Areas in Commun.*, vol. 2, pp. 528–539, Jul. 1984.
11. J. H. Winters, "On the capacity of radio communication systems with diversity in a Rayleigh fading environment", *IEEE J. Sel. Areas in Commun.*, vol. 5, pp. 871–878, Jun. 1987.
12. V. Tarokh, N. Seshadri and A. R. Calderbank, "Space-time codes for high data rate wireless communication: Performance criterion and code construction," *IEEE Tran. Inf. Theory*, vol. 44, pp. 744–765, Mar. 1998.
13. S. M. Alamouti, "A simple transmit diversity technique for wireless communications", *IEEE J. Sel. Areas in Commun.*, vol. 16, pp. 1451–1458, Oct. 1998.
14. G. Foschini, "Layered space-time architecture for wireless communication in a fading environment when using multi-element antennas", *Bell Labs Tech. J.*, pp. 41–59, Autumn 1996.
15. G. D. Golden, C. J. Foschini, R. Valenzuela and P.W. Wolniansky, "Detection algorithm and initial laboratory results using the V-BLAST space-time communication", *IEEE Electron. Lett.*, vol. 35, pp. 14–16, Jan. 1999.
16. G. J. Foschini and M. J. Gans, "On limits of wireless communications in a fading environment when using multiple antennas", *Wireless Personal Commun.*, vol. 6, pp. 311–335, Mar. 1998.
17. G. G. Raleigh and J. M. Cioffi, "Spatio-temporal coding for wireless communication", *IEEE Trans. on Commun.*, vol. 46, pp. 357–366, Mar. 1998.
18. E. Telatar, "Capacity of multi-antenna Gaussian channels," *Europ. Trans. Telecommun.*, vol. 10, pp. 585–595, Nov. 1999.
19. A. J. Paulraj, D. A. Gore, R. U. Nabar and H. Bolcskei, "An overview of MIMO communications: A key to gigabit wireless", *Proc. of IEEE*, vol. 92, pp. 198–218, Feb. 2004.

20. H. Bolcskei, D. Gesbert and A. J. Paulraj, "On the capacity of OFDM based spatial multiplexing system", *IEEE Trans. on Commun.*, vol. 50, pp. 225–234, Feb. 2002.
21. H. Sampath, S. Talwar, J. Tellado, V. Erceg and A. J. Paulraj, "A fourth-generation MIMO–OFDM broadband wireless system: Design, performance, and field trial results", *IEEE Commun. Mag.*, vol. 40, pp. 143–149, Sep. 2002.
22. L. Giangaspero, L. Agarossi, G. Paltenghi, S. Okamura, M. Okada and S. Komaki, "Co-channel interference cancellation based on MIMO OFDM systems", *IEEE wireless Commun.*, vol. 9, pp. 8–17, Dec. 2002.
23. G. L. Stuber, J. R. Barry, S. W. McLaughlin, Y. Li, M. A. Ingram and T. G. Pratt, "Broadband MIMO – OFDM wireless communications", *Proc. of IEEE*, vol. 92, pp. 271–294, Feb. 2004.
24. V. V. Zelst and T.C.W. Schenk, "Implementation of a MIMO OFDM based wireless LAN system", *IEEE Trans. on Signal Process.*, vol. 52, pp. 483–494, Feb. 2004.
25. P. Vandenameele, L. Van der Perre, M.G.E. Engels, B. Gyselinckx and H. J. De Man, "A combined OFDM/SDMA approach", *IEEE J. on Sel. Areas in Commun.*, vol. 18, pp. 2312–2321, Nov. 2000.
26. S. Thoen, L. Van der Perre, M. Engels and H. De Man, "Adaptive loading for OFDM/SDMA based wireless network", *IEEE Trans. on Commun.*, vol. 50, pp. 1798–1810, Nov. 2002.
27. J. S. Blogh and L. Hanzo, "Third generation systems and intelligent wireless networking", *IEEE Press/Wiley*, England, UK, 2002.
28. L. Hanzo, M. Munster, B. J. Choi, T. Keller, "OFDM and MC–CDMA for Broadband Multi-User Communications, WLANs and Broadcasting", *IEEE Press/Wiley*, West Sussex, 2003.
29. M. Jiang and L. Hanzo, "Multiuser MIMO – OFDM using subcarrier hopping", *IEE Proc. Commun.*, vol. 153, pp. 802–809, Dec. 2006.
30. M. Jiang and L. Hanzo, "Multiuser MIMO – OFDM for Next-Generation Wireless Systems", *Proc. of the IEEE*, vol. 95, pp. 1430–1469, Jul. 2007.
31. J. M. F. Xavier, V. A. N. Barroso and J. M. F. Moura, "Closed-form blind channel identification and source separation in SDMA systems through correlative coding", *IEEE J. Sel. Areas in Commun.*, vol. 16, pp. 1506–1517, Oct. 1998.
32. I. Bradaric, A. P. Petropulu and K. I. Diamantaras, "Blind MIMO FIR channel identification based on second-order spectra correlations", *IEEE Trans. on Signal Process.*, vol. 51, pp. 1668–1674, Jun. 2003.
33. S. Yatawatta and A.P. Petropulu, "Blind channel estimation in MIMO OFDM system with multiuser interference", *IEEE Trans. on Signal Process.*, vol. 54, pp. 1054–1068, Mar. 2006.
34. F. Gao and A. Nallanathan, "Blind channel estimation for MIMO OFDM system via non-redundant linear precoding", *IEEE Trans. on Signal Process.*, vol. 55, pp. 784 – 789, Jan. 2007.
35. C. C. Tu and B. Champagne, "Blind recursive subspace-based identification of time-varying wideband MIMO channels", *IEEE Trans. on Veh. Technol.*, vol. 61, pp. 662–674, Feb. 2012.
36. M. Biguesh and A. B. Gerhman, "Training based MIMO channel estimation: A study of estimation tradeoffs and optimal training signals", *IEEE Tran. on Signal Process.*, vol. 54, pp. 884–893, Mar. 2006.
37. X. Dai, "Pilot – aided OFDM/SDMA channel estimation with unknown timing offset", *IEE Proc. Commun.*, vol. 153, pp. 352 – 398, Jun. 2006.

38. M. Jiang, J. Akhtman and L. Hanzo, "Iterative joint channel estimation and multiuser detection for multiple antenna aided OFDM systems", *IEEE Trans. Wireless Commun.*, vol. 6, pp. 2904–2914, Aug. 2007.
39. J. Zhang, L. Hanzo and X. Mu, "Joint decision directed channel and noise variance estimation for MIMO OFDM/SDMA systems based on expectation conditional maximization", *IEEE Tans. on Veh. Technol.*, vol. 60, pp. 2139–2151, Jun. 2011.
40. X. Lu, J. Xu and G. Lin, "Channel estimation techniques based on short preamble and pilot MIMO–OFDM systems", *Inter. J. of Dig. Cont. Technol. and its Appl.*, vol. 6, pp. 449–456, Jul. 2012.
41. G. Kang, Y. Yang, P. Zhang, P. Hasselbach and A. Klein, "Pilot Deign for inter cell interference mitigation in MIMO OFDM system", *IEEE Commun. Lett.*, vol. 11, pp. 237–239, Mar. 2007.
42. K. C. Hung and D. W. Lin, "Theory an deign of near optimal MIMO OFDM transmission system for correlated multipath Rayleigh fading channels", *J. of Commun. and Net.*, vol. 9, pp. 150–158, Jun. 2009.
43. H. Minn and D. Munoz, "Pilot design for channel estimation of MIMO OFDM systems with frequency dependent I/Q imbalances", *IEEE Trans. on Commun.*, vol. 58, pp. 2252–2264, Aug. 2010.
44. J. W. Kang, Y. Whang, H. Y. Lee and K. S. Kim, "Optimal pilot sequence design for multi cell MIMO – OFDM systems", *IEEE Trans. on Wireless Commun.*, vol. 10, pp. 3354–3367, Oct. 2011.
45. Z. Andalibi, H. H. Nguyen and J. E. Salt, "Training design for precoded BICM–MIMO systems in block–fading channels", *EURASIP J. on Wireless Commun. and Net.*, doi:10.1186/1687-1499-2012-80, 2012.
46. S. Verdu, "Multiuser Detection", *Camb. Univ. Press*, Cambridge, U.K, 1998.
47. P.W. Wolniansky, G.J.Foschini, G.D. Golden and R.A. Valenzuela, "V-BLAST: an architecture for realizing very high data rates over the rich-scattering wireless channel," *Inter. Symp. on Sig., Sys., and Electron.*, pp. 295–300, 1998.
48. M. Damen, K. A. Meraim and J. C. Belfiore, "Generalized sphere decoder for asymmetrical space-time communication architecture," *IEEE Electron. Lett.*, vol. 36, pp. 166–167, Jan. 2000.
49. B. Hochwald and S. ten Brink, "Achieving near-capacity on a multiple-antenna channel," *IEEE Trans. on Commun.*, vol. 51, pp. 389–399, Mar. 2003.
50. B. Hassibi and H. Vikalo, "On the sphere decoding algorithm: I expected complexity", *IEEE Trans. on Signal Process.*, vol. 53, pp. 2806–2818, Aug. 2005.
51. K. J. Kim, J. Yue, R. A. Iltis and J. D. Gibson, "A QRD-M/Kalman filter-based detection and channel estimation algorithm for MIMO–OFDM systems," *IEEE Trans. Wireless Commun.*, vol. 4, pp. 710–721, Mar. 2005.
52. M. Arar and A. Yongacoglu, "Efficient detection algorithm for $2N \times 2N$ MIMO systems using alamouti code and QR decomposition", *IEEE Commun. Lett.*, vol. 10, pp. 819–821, Dec. 2006.
53. J. Cha, J. Ha and J. Kang, "Low complexity iterative QRD–M detection algorithm for V–BLAST systems", *IEEE Electron. Lett.*, vol. 43, pp. 1374–1376, Nov. 2007.
54. A. Burg, M. Borgmann, M. Wenk, M. Zellweger, W. Fichtner and H. Bolckei, "VLSI implementation of MIMO detection using the sphere decoding algorithm", *IEEE J. of Solid State Cirt.*, vol. 40, pp. 1566–1577, Jul. 2005.

55. M. El-Khamy, H. Vikalo, B. Hassibi, and R. J. McEliece, "Performance of Sphere Decoding of Block Codes," *IEEE Trans. on Commun.*, vol. 57, pp. 2940–2950, Oct. 2009.
56. J. S. Kim, S. H. Moon, and I. Lee, "A New Reduced Complexity ML Detection Scheme for MIMO Systems," *IEEE Trans. on Commun.*, vol. 58, pp. 1302–1310, Apr. 2010.
57. J. Jalden and P. Elia, "Sphere decoding complexity exponent for decoding full rate codes over the quasi static MIMO channel", *IEEE Trans. on Inf. Theory*, vol. 58, pp. 5785–5803, Sep. 2012.
58. H. Jian, X. Yao and Y. Shi, "A simplified QRD-M signal detection algorithm for MIMO–OFDM systems", *J. of Electron.*, vol. 27, pp. 88–93, Jan. 2010.
59. K. J. Kim, M. O. Pun and R. A. Iltis, "QRD based precoded MIMO–OFDM system with reduced feedback", *IEEE Trans. on Commun.*, vol. 58, pp. 394–398, Feb. 2010.
60. X. Wu, and J. S. Thompson, "A simplified unbiased MMSE metric based QRDM decoder for MIMO systems", *6th Inter. Conf. on Wirel. Commun., Netw. And Mobi. Compu.*, pp. 1–4, 2010.
61. S. Chen, A. K. Samangan, B. Malgrew and L. Hanzo, "Adaptive minimum BER linear multiuser detection for DC–CDMA signals in multipath channels", *IEEE Trans. on Signal Process.*, vol. 49, pp. 1240–1247, Jun. 2001.
62. B. Widrow and S. D. Stearns, "Adaptive Signal Processing", *Pears. Edu. Pub.*, New Delhi, India, 2009.
63. M. Y. Alias, A. K. Samangan, S. Chen and L. Hanzo, "Multiple Antenna Aided OFDM Employing Minimum Bit Error Rate Multiuser Detection," *IEEE Electron. Lett.*, vol. 39, pp. 1769–1770, Nov. 2003.
64. M. Y. Alias, S. Chen and L. Hanzo, "Multiple–Antenna–Aided OFDM Employing Genetic-Algorithm-Assisted Minimum Bit Error Rate Multiuser Detection," *IEEE Trans. on Veh. Technol.*, vol. 54, pp. 1713–1721, Sep. 2005.
65. S. Chen, A. Livingstone and L. Hanzo, "Minimum Bit–Error Rate Design for Space–Time Equalization-Based Multiuser Detection", *IEEE Trans. on Commun.*, vol. 54, pp. 824–832, May 2006.
66. H. Rehman, I. Zaka, M. Naeem, S. I. Shah and Jamil Ahmad, "Minimum Bit Error Rate Multiuser Detection for OFDM–SDMA Using Particle Swarm Optimization", *Springer Lect. Notes in Comp. Sci.*, vol. 4681, pp. 1247–1256, 2007.
67. J. I. Ababneh, T. F. Aldalgamouni, A. A. Alqudah, "Minimum Bit Error Rate Multiuser Detection of SDMA-OFDM System Using Differential Evolutionary Algorithm", *Proc. of IEEE 6th Inter. Conf. on Wireless and Mob. Comp., Net. and Commun.*, pp. 273–279, 2010.
68. M. Jiang, and L. Hanzo, "Genetically enhanced TTCM assisted MMSE multi-user detection for SDMA–OFDM," *Proc. of the IEEE 60th Veh. Technol. Conf.*, vol. 3, pp. 1954–1958, 2004.
69. P. A. Haris, E. Gopinathan, and C. K. Ali, "Performance of Some Metaheuristic Algorithms for Multiuser Detection in TTCM–Assisted Rank–Deficient SDMA–OFDM System," *EURASIP J. on Wireless Commun and Net.*, doi:10.1155/2010/473435, 2010.
70. P. A. Haris, E. Gopinathan, and C. K. Ali, "Artificial Bee Colony and Tabu Search Enhanced TTCM Assisted MMSE Multi–User Detectors for Rank Deficient SDMA-OFDM System," *Wireless Personal Commun.*, doi: 10.1007/s11277-011-0264-0, 2011.

71. J. Zhang, S. Chen, X. Mu, and L. Hanzo, "Turbo Multi-User Detection for OFDM/SDMA Systems Relying on Differential Evolution Aided Iterative Channel Estimation," *IEEE Trans. on Commun.*, vol. 60, pp. 1621–1633, Jun. 2012.
72. J. Zhang, S. Chen, X. Mu and L. Hanzo, "Differential Evolution Algorithm Aided Minimum Symbol Error Rate Multi-user Detection for Multi-user OFDM/SDMA System," *Proc. of IEEE Vehi. Technol. Conf.*, pp. 1–5, 2012.
73. Kurt Hornik, "Multilayer feedforward networks are universal approximators", *Neural Networks*, vol. 2, no. 5, pp. 359–366, 1989.
74. Kurt Hornik, "Approximation capabilities of multilayer feedforward networks", *Neural Networks*, vol. 4, no. 2, pp. 251–257, 1991.
75. S. Haykin, "Neural networks", *Pears. Edu. Pub.*, Singapore 1999.
76. U. Mitra and V. Poor, "Neural network techniques for adaptive multiuser detection", *IEEE J. Sel. Areas Commun.*, vol. 12, pp. 1460–1470, Dec. 1994.
77. K. B. Ko, S. Choi, C. Kang and Daesik Hong, "RBF Multiuser Detector with Channel Estimation Capability in a Synchronous MC-CDMA System," *IEEE Trans. Neural Networks*, vol. 12, pp. 1536–1539, Nov. 2001.
78. T. C. Chuah, B. S. Sharif and O. R. Hinton, "Robust CDMA Multiuser Detection Using a Neural-Network Approach," *IEEE Trans. Neural Networks*, vol. 13, pp. 1532–1539, Nov. 2002.
79. M.G. Shayesteh and H. Amindavar, "Performance analysis of neural network detection in DS/CDMA systems", *AEU Inter. J. of Elect. and Commun.*, vol. 57, pp. 220–236, 2003.
80. C. Sacchi, G. Gera, C. Regazzoni, "Neural Network-Based Techniques for Efficient Detection of Variable-Bit-Rate Signals in MC-CDMA Systems Working over LEO Satellite Networks", *Signal Process.*, vol. 85, pp. 505–522, Mar. 2005.
81. T. Kim and T. Adali, "Fully complex valued mult-layer perceptron for nonlinear signal processing", *J. of VLSI Signal Process. Sys. for. Sig., Image and Technol.*, vol. 32, pp. 29–43, Aug. 2002.
82. T. Kim and T. Adali, "Approximation by fully complex multilayer perceptron", *Neural Computing*, vol. 15, pp. 1641–1666, Jul. 2003.
83. R. Pandey, "Fast blind equalization using complex valued MLP", *Neural Process. Lett.*, vol. 21, pp. 215–225, Jun. 2005.
84. I. Cha and S. A. Kassam, "Channel equalization using adaptive complex radial basis function networks", *IEEE J. of Sel. Areas in Commun.*, vol. 13, pp. 122–131, Jan. 1995.
85. Q. Gan, P. Saratchandran, N. Sundararajan, and K. R. Subramanian, "A Complex Valued Radial Basis Function Network for Equalization of Fast Time Varying Channels", *IEEE Trans. on Neural Networks*, vol. 10, pp. 958–960, Jul. 1999.
86. M.B. Li, G.B. Huang, P. Saratchandran and N. Sundararajan, "Complex-valued growing and pruning RBF neural networks for communication channel equalization", *IEE Proc. Vis. Image Signal Process.*, vol. 153, pp. 411–418, Aug. 2006
87. S. Chen, L. Hanzo and S. Tan, "Symmetric Complex-Valued RBF Receiver for Multiple-Antenna-Aided Wireless Systems", *IEEE Trans. on Neural Networks*, vol. 19, pp. 1658–1663, Sep. 2008.

88. J. M. Shapiro, "Embedded image coding using zerotrees of wavelets coefficients", *IEEE Trans. on Signal Process.*, vol. 41, pp. 3445–3462, Dec. 1993.
89. A. Said, A. A. Pearlman, "A New, Fast, and Efficient Image Codec Based on Set Partitioning in Hierarchical Trees," *IEEE Trans. on Cir. and Syst. for Video Tech.*, vol. 6, pp. 243–250, Jun. 1996.
90. J. Song, K. J. R. Liu, "Robust Progressive Image Transmission over OFDM System Using Space-Time Block Codes," *IEEE Tran. on Multimedia*, vol. 4, pp. 394–406, Sep. 2002.
91. Y. Sun, Z. Xiong, "Progressive Image Transmission over Space-Time Coded OFDM–Based MIMO System with Adaptive Modulation", *IEEE Tran. on Mobile Comp.*, vol. 5, pp. 1016–1028, Aug. 2006.
92. T. Hwang, C. Yang, G. Wu, S. Li and G.Y. Li, "OFDM and its wireless applications: A survey", *IEEE Trans. on Veh. Technol.*, vol. 58, pp. 1673–1694, May 2009.
93. E. Biglieri, R. Calderbank, A. Constantinides, A. Goldsmith, A. Paulraj and H. V. Poor, "MIMO wireless communications", *Camb. Univ. Press*, Cambridge, 2007.
94. J. Mietzner, R. Scobier, L. Lampe, W. H. Gerstacker and P. A. Hoeher, "Multiple antenna techniques for wireless communications–A comprehensive literature survey", *IEEE Commun., Sur., and Tuto.*, vol. 11, Second quarter 2009.
95. B. Lu, G. Yue and X. Wang, "Performance analysis and design optimization of LDPC coded MIMO OFDM systems", *IEEE Trans. on Signal Process.*, vol. 52, pp. 348–361, Feb. 2004.
96. C. Dubuc, D. Starks, T. Creasy and Y. Hou, "A MIMO-OFDM prototype for next-generation wireless WANS", *IEEE Commun. Mag.*, vol. 42, pp. 82–87, Dec. 2004.
97. G. V. Rangaraj, D. Jaliha and K. Giridhar, "Exploiting multipath diversity in multiple antenna OFDM sytems with spatially correlated channels", *IEEE Trans. on Veh. Technol.*, vol. 54, pp. 1372–1378, Jul. 2005.
98. Y. Chen, E. Aktas and U.Tureli, "Optimal space frequency group codes for MIMO–OFDM system", *IEEE Trans. on Commun.*, vol. 54, pp. 553–562, Mar. 2006.
99. S. H. Lee and J. Thompson, "Trade-Off of Multiplexing Streams in MIMO Broadcast Channels", *IEEE Tans. On Commun.*, vol. 14, pp. 115–117, Feb. 2010.
100. C. F. Tsai, C. J. Chang, F. C. Ren and C. M. Yen, "Adaptive radio resource allocation for downlink OFDMA/SDMA system with multimedia traffic", *IEEE Trans. Wireless Commun.*, vol. 7, pp. 1734–1743, May 2008.
101. L. Hanzo, Y. Akhtman, L. Wang and M. Jiang, "MIMO–OFDM for LTE, WiFi and WiMax: coherent verses non-coherent and co-operative turbo transceivers", *IEEE Press/Wiley*, UK, 2011.
102. Y. Isik and N. Taspinar, "Multiuser detection with neuralnetwork and PIC in CDMA systems for AWGN and Raykeugh fading asynchronous channels", *Wireless Pesonal Commun.*, vol. 43, pp. 1185–1194, Dec. 2007.
103. Z. W. Zheng, "Receiver Design for Uplink Multiuser Code Division Multiple Access Communication System Based on Neural Network," *Wireless Pesonal Commun.*, vol. 53, pp. 67–79, 2009.
104. J. Wang, H. Yang, X. Hu and X. Wang, "An adaline neural network based multiuser detector improved by particle swarm optimization in CDMA systems," *Wireless Pesonal Commun.*, vol. 59, pp. 191–203, Jul. 2011.

105. N. Taspinar, and M. Cicek, "Neural Network Based Receiver for Multiuser Detection in MC-CDMA Systems," *Wireless Personal Commun.*, vol. 68, pp. 463–472, Jan. 2013.
106. Y. Okumura, E. Ohmori, T. Kawano and K. Fukua, "Field strength and its variability in UHF and VHF land-mobile radio service," *Rev. Elect. Commun. Lab.*, vol. 16, Sep. 1968.
107. M. Hata, "Empirical formula for propagation loss in land mobile radio services", *IEEE Trans. on Veh. Technol.*, vol. 29, pp. 317–325, Aug. 1980.
108. EURO-COST-231 Revision 2, "Urban transmission loss models for mobile radio in the 900 and 1800 MHz bands," Sep. 1991.
109. F. Ikegami, S. Yoshida, T. Takeuchi and M. Umehira, "Propagation factors controlling mean field strength on urban streets", *IEEE Trans. on Antennas Prop.*, vol. 32, pp. 822–829, Aug. 1984.
110. J. Walfisch and H. L. Bertoni, "A theoretical model of UHF propagation in urban environments", *IEEE Trans. on Antennas and Prop.*, vol. 36, pp. 1788–1796, Dec. 1988.
111. V. Erceg, L. J. Greenstein, S. Y. Tjandra, S. R. Parkoff, A. Gupta, B. Kulic, A. A. Julius and R. Bianchi, "An empirically based path loss model for wireless channels in suburban environments," *IEEE J. Sel. Areas in Commun.*, vol. 17, pp. 1205–1211, Jul. 1999.
112. V. Erceg, K.V.S. Hari, M.S. Smith, D.S. Baum et al, "Channel Models for Fixed Wireless Applications", *Contrib. IEEE 802.16.3c-01/29r1*, Feb. 2001.
113. J. H. Holland, "Adaptation in natural and artificial systems", *Univ. of Mich. Press*, Ann Arbor, USA, 1975.
114. Z. Altman, R. Mittra and A. Boag, "New design of ultra wide-band communication antennas using a genetic algorithm", *IEEE Trans. on Antennas and Prop.*, vol. 45, pp. 1494–1501, Oct. 1997.
115. S. Chen and Y. Wu, "Maximum likelihood joint channel and data estimation using genetic algorithm", *IEEE Trans. on Signal Process.*, vol. 46, pp. 1469–1473, May 1998.
116. X. H. Lin, Y. K. Kwok and V. K. N. Lau, "A genetic algorithm based approach to route selection and capacity flow assignment", *Computer Commun.*, vol. 26, pp. 961 – 974, Jun. 2003.
117. G. Chakraborty, "Genetic algorithm to solve optimum TDMA transmission schedule in broadcast packet radio networks", *IEEE Trans. on Commun.*, vol. 52, pp. 765–777, May 2004.
118. K. P. Ferentinos and T. A. Tsiligiridis, "Adaptive design optimization of wireless sensor network using genetic algorithms", *Computer Netw.*, vol. 51, pp. 1031–1051, Mar. 2007.
119. D. Gozupek and F. Alagoz, "Genetic algorithm based scheduling in cognitive radio networks under interference temperature constraints", *Inter. J. of Commun. Syst.*, vol. 24, pp. 239–257, Feb. 2011.
120. M. Srinivas and L. M. Patnaik, "Adaptive Probabilities of Crossover and Mutation in Genetic Algorithms", *IEEE Trans. Syst. Man, and Cybernetics*, vol. 24, pp. 656–667, Apr. 1994.
121. Q. H. Wu, Y. j. Cao and J. Y. Wen, "Optimal reactive power dispatch using an adaptive genetic algorithm", *Inter. J. of Elect. Pow. and Ener. Syst.*, vol. 20, pp. 563–569, Nov. 1998.
122. K. I. Mak, Y. S. Wong and X. X. Wang, "An adaptive genetic algorithm for manufacturing cell formation", *The Inter. J. of Adv. Manu. Technol.*, vol. 16, pp. 491 – 497, Jun. 2000.
123. S. M. Libelli and P. Alba, "Adaptive mutation in genetic algorithms", *Soft Comp.*, vol. 4, pp. 76–80, 2000.

124. G. Zhang, S. Wang and Y. Li, "A Self-adaptive Genetic algorithm based on the principle of searching for things", *J. of Computing*, vol. 5, pp. 646–653, Apr. 2010.
125. R. Storn, "Differential Evolution, A Simple and Efficient Heuristic Strategy for Global Optimization over Continuous Spaces", *J. of Glob. Optim.*, vol. 11, pp. 341–359, 1997.
126. S. Yang, Y. B. Gan and A. Qing, "Sideband suppression in time modulated linear arrays by the differential evolution algorithm", *IEEE Ant. and Wireless Prop. Lett.*, vol. 1, pp. 173–175, 2002.
127. D.G. Kurup, M. Himdi and A. Rydberg, "Synthesis of uniform amplitude unequally spaced antenna arrays using the differential evolution algorithm", *IEEE Trans. on Antennas and Prop.*, vol. 56, pp. 2210–2217, Sep. 2003.
128. A. Massa, M. Pastorino and A. Randazzo, "Optimization of the directivity of a monopulse antenna with a subarray weighting by a hybrid differential evolution method", *IEEE Ant. and Wireless Prop. Lett.*, vol. 5, pp. 155–158, Dec. 2006.
129. Y. Chen, S. Yang and Z. Nie, "The application of a modified differential evolution strategy to some array pattern synthesis problem", *IEEE Trans. on Antennas and Prop.*, vol. 56, pp. 1919–1927, Jul. 2008.
130. J. Brest, S. Greiner, B. Boskovic, M. Mernik and V. Zumer, "Self adaptive control parameters in differential evolution: A comparative study on numerical benchmark problems", *IEEE Trans. on Evol. Comp.*, vol. 10, pp. 646–657, Dec. 2006.
131. V. L. Huang, A. K. Qin and P.N. Suganthan, "Self adaptive differential algorithm for constrained real parameter optimization", *IEEE Cong. on Evol. Comp.*, pp. 17–24, 2006.
132. A.K. Qin, V. L. Huang and P.N. Suganthan, "Differential evolution algorithm with strategy adaptation for global numerical optimization", *IEEE Trans. on Evol. Comp.*, vol. 13, pp. 398–417, Apr. 2009.
133. J. Zhang and A.C. Sanderson, "JADE: Adaptive differential evolution with optional external archive", *IEEE Trans. on Evol. Comp.*, vol. 13, pp. 945–958, Oct. 2009.
134. J. Brest and M. S. Maucec, "Self adaptive differential evolution algorithm using population size reduction and three strategies", *Soft Computing*, vol. 15, pp. 2157–2174, Nov. 2011.
135. A. R. Mehrabian and C. Lucas, "A novel Numerical Optimization Algorithm Inspired from Weed Colonization", *Elsevier Ecol. Inform.*, vol. 1, pp. 355–366, Dec. 2006.
136. S. Karimkashi, A. A. Kishk, "Invasive Weed Optimization and its Features in Electromagnetics", *IEEE Trans. on Antennas and Prop.*, vol. 58, pp. 1269–1278, Apr. 2010.
137. F. M. Monavar, N. Komjani, P. Mousavi, "Application of Invasive Weed Optimization to Design a Broadband Patch Antenna with Symmetric Radiation Pattern", *IEEE Ant. and Wireless Prop. Lett.*, vol. 10, pp. 1369–1372, 2011.
138. S. Karimkashi, A. A. Kishk, D. Kajfez, "Antenna Array Optimization Using Dipole Models for MIMO Applications", *IEEE Trans. on Antennas and Prop.*, vol. 59, pp. 1312–1316, Aug. 2011.
139. G. G. Roy, S. Das, P. Chakraborty, P. N. Suganthan "Design of Non-Uniform Circular Antenna Arrays Using a Modified Invasive Weed Optimization Algorithm", *IEEE Tran. on Antennas and Prop.*, vol. 59, pp. 110–118, Jan. 2011.

140. Kala Praveen Bagadi and Susmita Das, "Minimum Symbol Error Rate Multiuser Detection Using an Effective Invasive Weed Optimization for MIMO/SDMA – OFDM System", *Inter. J. of Commun. Syst.*, DOI: 10.1002/dac.2579, 2013.
141. Susmita Das, "Performance of fuzzy logic-based slope tuning of neural equaliser for digital communication channel", *Neural Computing and Appl.*, vol. 21, pp. 423–432, Apr. 2012.
142. Susmita Das, "A novel concept of embedding orthogonal basis function expansion block in a neural equalizer structure for digital communication channel", *Neural Computing and Appl.*, vol. 21, pp. 481–488, Apr. 2012.
143. Kala Praveen Bagadi and Susmita Das, "Neural network-based multiuser detection Schemes for SDMA–OFDM system over IEEE 802.11n indoor wireless local area network channel models", *Inter. J. of Elect.*, vol.100, no. 10, pp. 1332–1347, 2013.
144. Kala Praveen Bagadi and Susmita Das, "Neural network-based adaptive multiuser detection Schemes in SDMA–OFDM system for wireless application," *Neural Computing and Appl.*, vol. 23, no. 3–4, pp. 1071–1082, 2013.
145. A. Cichocki and R. Unbehauen, "Neural Networks for solving systems of linear equations and related problems", *IEEE Trans. on Cir. and Syst.*, vol. 39, pp. 124–138, Feb. 1992.
146. Tohru Nitta, "Complex-Valued Neural Networks: Utilizing High-Dimensional Parameters", *Infor. Scien. Ref.*, Hershey, New York, 2009.
147. H. Leung and S. Haykin, "The Complex Backpropagation Algorithm", *IEEE Trans. on Signal Process.*, vol. 39, pp. 2101–2104, Sep. 1991.
148. N. Benvenuto and F. Piazza, "On the Complex Backpropagation Algorithm", *IEEE Trans. on Signal Process.*, vol. 40, pp. 967–969, Apr. 1992.
149. R. Savitha, S.Suresh and N. Sundararajan, "A Full Complex-valued Radial Basis Function Network and its Learning Algorithm", *Inter. J. of Neural Syst.*, vol. 19, pp. 253–267, Aug. 2009.
150. R. Savitha, S. Vigneswaran, S.Suresh and N. Sundararajan, "Adaptive Beamforming using Complex-valued Radial Basis Function Neural Networks," *Proc. of IEEE Reg. Conf. TENCON*, pp. 1–6, 2009.
151. R. Savitha, S.Suresh and N. Sundararajan, "Complex-valued Function Approximation using a fully Complex-valued RBF (FC-RBF) Learning Algorithm", *Proc. of Inter. joint Conf. on Neural Net.*, pp. 2819–2825, 2009.

Appendix

Appendix–A

A. 1. MIMO Rayleigh fading channel model

The MIMO multipath fading channel is modeled as a tapped delay line with 4 taps with non-uniform delays [80, 81]. The gain associated with each tap is characterized by a Rayleigh Distribution and the maximum Doppler frequency. For each tap a set of complex zero-mean Gaussian distributed numbers is generated with a variance of 0.5 for the real and imaginary part, so that the total average power of this distribution is 1. This yields a normalized Rayleigh distribution for the magnitude of the complex coefficients. In a multipath environment, the received power r has a Rayleigh distribution, whose PDF is given by:

$$pdf(r) = \frac{r}{\sigma^2} \exp\left(-\frac{r}{2\sigma^2}\right), \quad 0 \leq r \leq \infty \quad (\text{A. 1})$$

The parameters of MIMO Rayleigh fading channel model is according to Table A. 1. The impulse response of this channel is shown in Figure A. 1.

Table A. 1: MIMO Rayleigh fading Model

Parameters	Value
Number of Propagation Paths	4
Sampling time	3 μ sec
Delays	[0, 1, 2, 3] μ sec.
Average Path Gains	[0, -5, -10, -15] (dB)
Doppler frequency	60 Hz
Antenna correlation	uncorrelated
Doppler spectrum type	Rounded

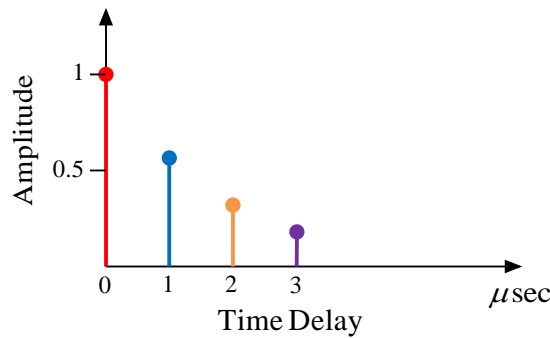


Figure A. 1: Impulse response of MIMO Rayleigh fading channel

A. 2. Stanford University Interim (SUI) channel models:

The SUI channel models for fixed broad band wireless applications are characterized as three models depending on the territorial structures in propagation environment [112]. These channel models are namely A–Category, B–Category and C–Category. The maximum path loss category is the hilly terrain with moderate to heavy tree densities (A–Category). An intermediate path loss condition is the B–Category, which is composition of either high tree density and flat area or low tree density and hilly area. The minimum path loss category is mostly the flat terrain with light tree densities (C–Category). Considering the maximum path loss conditions, SUI–A Category model is chosen here and the associated parameters of the model is summarized in Table A. 2. The impulse response of this channel is shown in Figure A. 2.

Table A. 2: SUI – A Channel Model Parameters

	Tap 1	Tap 2	Tap 3	Units
Delay	0	14	20	μ sec
Power (Omni directional)	0	-10	-14	dB
k- Factor (Omni directional)	1	0	0	
Doppler shift	0.4	0.3	0.5	Hz
Sampling time	5 μ sec			
Antenna correlation	0.3			
RMS delay spread	5.24 μ sec			
Receiver antenna beam width	Omni Directional			
Base station antenna beam width	120 ⁰			

This SUI Channel is modeled as multi-path, frequency selective with non-uniform delays and number of taps used is three. The gain associated with first tap is characterized by a Rician Distribution and the gain associated with remaining two tap is characterized by a Raleigh Distribution. The Rayleigh distribution is according to eq. (A. 1) and the PDF of the Rician distribution with the received power r is given by:

$$pdf(r) = \frac{r}{\sigma^2} \exp\left(-\frac{(r^2 + A^2)}{2\sigma^2}\right) I_0\left(\frac{rA}{\sigma^2}\right), \quad 0 \leq r \leq \infty \quad (\text{A. 2})$$

Here, $I_0(x)$ is the zero ordered modified Bessel function of the first kind. A is zero if there is no line of sight (LOS) component and the PDF of the received power becomes Rayleigh Distribution. The ratio $K = A^2 / (2\sigma^2)$ in the Rician case represents the ratio of LOS component to NLOS component and is called the "K-Factor" or "Rician Factor."

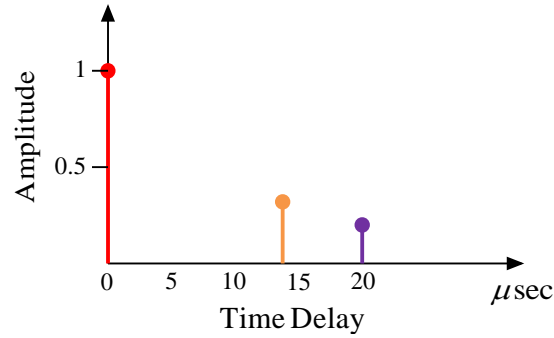


Figure A. 2: Impulse response of SUI channel

A. 3. The Shortened Wireless Asynchronous Transfer Mode (SWATM) channel models

The third channel that considered here is the Shortened Wireless Asynchronous Transfer Mode (SWATM) channel model, which is used for indoor wireless applications [8, 38]. This channel model's parameters are as per the Advanced Communication Technologies and Services (ACTS) Median system specifications. The details of associated parameters of the channel model are summarized in Table A. 3. The resulting impulse response of this channel is shown in Figure A. 3.

Table A. 3: The SWATM Channel Model Parameters

Parameter	Value
Sampling Time	4.44 n sec.
Maximum Delay Spread (τ_{\max})	48.9 n sec.
Delays	[0, 25, 48.93] n sec.
RMS Delay Spread	0.15276 n sec.
Maximum Doppler frequency	2278 Hz
Number of propagation paths	3
Spectrum type	Doppler's rounded

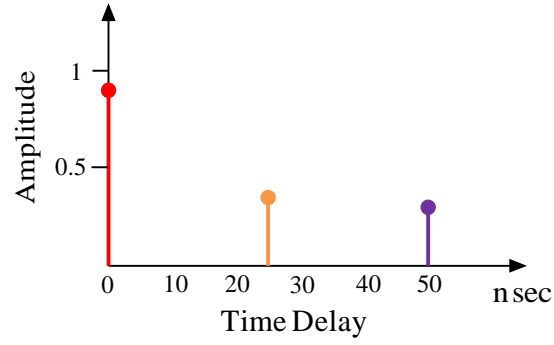


Figure A. 3: Impulse response of SWATM channel

The three tap SWATM channel is a truncated version of the five tap Wireless Asynchronous Transfer Mode (WATM) by retaining only the first three impulses. This reduces the total length of the impulse response, with the last path is arriving at a delay of 48.9 n sec, which correspond to 11 sample period. Each of the three path experiences independent Rayleigh fading having the normalized Doppler frequency of 1.235×10^{-5} .

Appendix–B:

B. Development of Back Propagation (BP) algorithm for MLP network training

The typical training model of MLP is shown in Figure 4.7. This model has Q number of layers each consisting n neurons. Let, g_n^q is the activation output of the n^{th} neuron in the q^{th} layer, then the net activation value of the n^{th} neuron in the q^{th} layer is given by:

$$s_n^q = \sum_{m=0}^{N_{q-1}} W_{nm}^q g_m^{q-1}, \quad n = 1, 2, \dots, N_q, \quad q = 1, 2, \dots, Q$$

Where, $g_n^q = \phi(s_n^q)$ and $n = 0$ refers to the bias input: i.e. $g_0^q = 1$. Also, when $q = 0$, then $g_n^0, n = 1, 2, \dots, N_0$ refers the input signal. The BP algorithm adjusts network weights such that the output error is minimized. Hence, the sum-squared global instantaneous error at the output layer (Q^{th} layer) is expressed as:

$$E = \frac{1}{2} \sum_{n=1}^{N_Q} \|e_n\|^2$$

Where, $e_n = d_n - g_n^Q, n = 1, 2, \dots, N_Q$ and d_n is the desired response. The weight update ΔW_{nm}^q is proportional to the gradient of the error with respect to W_{nm}^q . Hence, the gradient of the error with respect to W_{nm}^q can be expressed using chain rule as:

$$\nabla_{W_{nm}^q} E = \frac{\partial E}{\partial W_{nm}^q} = \frac{\partial E}{\partial e_n^q} \frac{\partial e_n^q}{\partial g_n^q} \frac{\partial g_n^q}{\partial s_n^{qR}} \frac{\partial s_n^{qR}}{\partial W_{nm}^q}$$

In the above equation

$$\frac{\partial E}{\partial e_n^q} = e_n^q;$$

$$\frac{\partial e_n^q}{\partial g_n^q} = -1;$$

$$\frac{\partial g_n^q}{\partial s_n^{qR}} = \phi'(s_n^q);$$

$$\frac{\partial s_n^{qR}}{\partial W_{nm}^q} = g_n^{q-1};$$

The correction ΔW_{nm}^q applied to W_{nm}^q is defined by delta rule as:

$$\Delta W_{nm}^q = -\mu \nabla_{W_{nm}^q} E \quad (\text{B.1})$$

Where, μ weight learning parameter. The use of minus sign is accounts for gradient descent in weight space. Accordingly, the use of eq. (B.1) yields:

$$\Delta W_{nm}^q = \mu \delta_n^q g_n^{q-1} \quad (\text{B.2})$$

Where, the local gradient δ_n^q is defined by:

$$\begin{aligned} \delta_n^q &= -\frac{\partial E}{\partial s_n^q} = -\frac{\partial E}{\partial e_n^q} \frac{\partial e_n^q}{\partial g_n^q} \frac{\partial g_n^q}{\partial s_n^{qR}} \\ &= e_n^q \phi'(s_n^q) \end{aligned}$$

The generalized error gradient for $q = Q, Q-1, \dots, 1$ and $n = 1, 2, \dots, N_q$ as:

$$e_n^q = \begin{cases} e_n, & \text{for } q = Q \\ \sum_{r=1}^{N_{q+1}} W_{rn}^{(q+1)} \delta_r^{q+1}, & \text{for } q = Q-1, \dots, 1 \end{cases} \quad (\text{B.3})$$

$$\delta_n^q = e_n^q \phi'(s_n^q) \quad (\text{B.4})$$

Appendix–C:**C. k-means clustering algorithm for center selection of RBF network**

The modeling of RBF network mainly depends on selection of centers and proper approximation of connection weights. During network training, it is essential to fix the centers of hidden neurons before updating connection weights. The k -means clustering algorithm is one of efficient technique used to fix centers [85]. Let $C_h(n)$, $h = 1, 2, \dots, H_N$ denote the center vectors of RBF at an iteration i of the algorithm. Then, the k -means clustering algorithm proceeds as follows:

- a. Initialize $C_j(i)$ with some random values.
- b. Generate a possible input vector y^t randomly.
- c. Find $h(y^t)$, which denote the index of the nearest center for input vector y^t using Euclidean criterion as follows:

$$h(y^t) = \arg \min_h \|y^t(i) - C_h(i)\|, \quad h = 1, 2, \dots, H_N$$

- d. Adjust the centers of the RBF using

$$C_h(i+1) = \begin{cases} C_h(i) + \mu_c [y^t(i) - C_h(i)], & \text{if } h = h(y^t) \\ C_h(i), & \text{otherwise} \end{cases}$$

Where μ_c is learning rate parameter that lies between zero and one.

- e. Increment i by 1, go back to step b, and continue the procedure until no noticeable changes are observed in the centers C_h .

Appendix–D:**D. Development of Gradient Descent (GD) algorithm for RBF network training**

During RBF network training, the GD algorithm updates all free parameters at a time based on error obtained. The GD algorithm computes the instantaneous gradient of the squared error and updates the network free parameters in the opposite direction of their respective gradients. The sum squared error is defined as:

$$E = \frac{1}{2} \sum_{l=1}^L \|e_l\|^2, \text{ where } e_l = d_l - x_l^t$$

Here, d_l represent desired response and x_l^t , $l = 1, 2, \dots, L$ is the RBF network output for training vector y_p^t , $p = 1, 2, \dots, P$. The gradient of the weight vector can be obtained by calculating the gradient of the error with respect to W_{lh} according to:

$$\nabla_{W_{lh}} E = \frac{\partial E}{\partial W_{lh}}$$

Using chain rule

$$\frac{\partial E}{\partial W_{lh}} = \frac{\partial E}{\partial x_l^t} \frac{\partial x_l^t}{\partial W_{lh}}$$

In the above equations

$$\frac{\partial E}{\partial x_l^t} = -e; \quad \frac{\partial x_l^t}{\partial W_{lh}} = z_h \tag{D.1}$$

From eq. (4.21) and (D.1), the update of weight can obtain as:

$$\Delta W_{lh} = -\mu_w \nabla_{W_{lh}} E$$

$$\Delta W_{lh} = \mu_w z_h e_l \tag{D.2}$$

Where, μ_w is the weight learning parameter. Among the three control parameters (W , C and σ), the center control parameter is in complex form. Therefore, the update of C_h require gradient of error with respect to real and imaginary components of C_h .

$$\nabla_{C_h} E = \frac{\partial E}{\partial C_h} = \frac{\partial E}{\partial C_h^R} + j \frac{\partial E}{\partial C_h^I}$$

using chain rule,

$$\begin{aligned} \frac{\partial E}{\partial C_h^R} &= \frac{\partial E}{\partial x_l^t} \frac{\partial x_l^t}{\partial C_h^R}, \quad \frac{\partial E}{\partial C_h^I} = \frac{\partial E}{\partial x_l^t} \frac{\partial x_l^t}{\partial C_h^I} \\ \frac{\partial x_l^t}{\partial C_h^R} &= \frac{W_{lh} z_h}{\sigma_h^2} \sum_{p=1}^P (y_p^t - C_h)^R; \quad \frac{\partial x_l^t}{\partial C_h^I} = \frac{W_{lh} z_h}{\sigma_h^2} \sum_{p=1}^P (y_p^t - C_h)^I \\ \nabla_{C_h} E &= -e \frac{W_{lh} z_h}{\sigma_h^2} \left(\sum_{p=1}^P (y_p^t - C_h)^R + j \sum_{p=1}^P (y_p^t - C_h)^I \right) \end{aligned} \quad (D.3)$$

From eq. (4.21) and (D.3), the update of center can obtain as:

$$\begin{aligned} \Delta C_h &= -\mu_c \nabla_{C_h} E \\ \Delta C_h &= \mu_c e \frac{W_{lh} z_h}{\sigma_h^2} \left(\sum_{p=1}^P (y_p^t - C_h)^R + j \sum_{p=1}^P (y_p^t - C_h)^I \right) \end{aligned} \quad (D.4)$$

Where, μ_c is center learning parameter. Finally, the update of σ_h require gradient of error with respect to σ_h , which is defined as follows:

$$\nabla_{\sigma_h} E = \frac{\partial E}{\partial \sigma_h}$$

Using chain rule,

$$\frac{\partial E}{\partial \sigma_h} = \frac{\partial E}{\partial x_l^t} \frac{\partial x_l^t}{\partial \sigma_h}$$

$$\frac{\partial x_l^t}{\partial \sigma_h} = W_{lh} z_h \frac{\|y^t - C_h\|^2}{\sigma_h^3}$$

$$\nabla_{\sigma_h} E = -\mu_\sigma e W_{lh} z_h \frac{\|y^t - C_h\|^2}{\sigma_h^3} \quad (\text{D.5})$$

From eq. (4.21) and (D.5), we can obtain the update of spread as:

$$\Delta \sigma_h = -\mu_c \nabla_{C_h} E$$

$$\Delta \sigma_h = \mu_s e W_{lh} z_h \frac{\|y^t - C_h\|^2}{\sigma_h^3} \quad (\text{D.6})$$

Where, μ_s is the spread learning parameter. Once all these updates are found, all these free parameters are updated iteratively.

BIO-DATA

Name : Kala Praveen Bagadi
Date of Birth : 18th Jul., 1985
Permanent Address : Kalaparthi (PSSK), Amadalavalasa,
Srikakulam, Andhra Pradesh,
India, Pin: 532185.
Address for Communication : Assistant Professor (SG), SENSE,
VIT University, Vellore,
India, Pin: 632014.
Email : kalapraveen.bagadi@gmail.com

Academic Qualification

- M. Tech in Electrical Engineering with specialization in Electronics System and Communication, National Institute of Technology Rourkela, Odisha, India.
- B. E. in Electronics and Communication Engineering from Andhra University, Andhra Pradesh, India.

Professional Experience:

Joined as Assistant Professor (Selection Grade) in the School of Electronics (SENSE), VIT University, Vellore in January 2013.

Major Research Areas:

Wireless communications, 3G and 4G Systems, MIMO-OFDM, Multiuser Detection, Optimization Techniques, Neural Networks Applications.

Publications:

- 07 Journal Articles
- 06 Conference Papers